NASA CR-2181

# LARGE SCALE STATIC TESTS OF A TILT-NACELLE V/STOL PROPULSION/ATTITUDE CONTROL SYSTEM

July 1978





Prepared by

Grumman Aerospace Corporation
Bethpage, New York

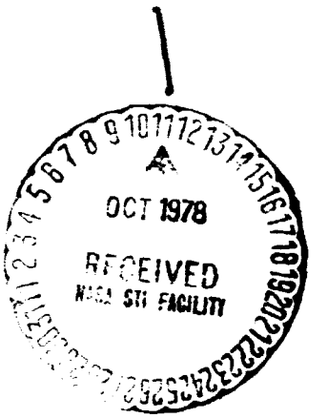


for

AMES RESEARCH CENTER
NATIONAL AERONAUTICS AND SPACE ADMINISTRATION

# LARGE SCALE STATIC TESTS OF A TILT-NACELLE V/STOL PROPULSION/ATTITUDE CONTROL SYSTEM

Prepared by

GRUMMAN AEROSPACE CORPORATION
BETHPAGE, NEW YORK 11714

PDR 698-8

JULY 1978

CONTENTS

CONTENTS (Contd)

## ILLUSTRATIONS

ILLUSTRATIONS (Contd)

ILLUSTRATIONS (Contd)

ILLUSTRATIONS (Contd)

ILLUSTRATIONS (Contd)

ILLUSTRATIONS (Contd)

## LIST OF SYMBOLS

| | |
|---|---|
| $A$ | area, sq ft |
| $AF_B$ | axial force component measured by vane force balance, lb |
| $AF_L$ | axial component of load in vane gearing link, lb |
| $AF_V$ | total axial component of force experienced by vane, lb |
| $C$ | vane chord, (30.4 in.) |
| $C_{F_X}$ | vane drag coefficient, $\frac{\text{drag}}{\text{installed gross thrust}}$ |
| $C_{F_Z}$ | vane lift coefficient, $\frac{\text{lift}}{\text{installed gross thrust}}$ |
| $C_{m_{.45}}$ | vane pitching moment coefficient about pivot axis located at 45% of vane chord, $\frac{\text{pitching moment}}{\text{installed gross thrust x vane chord}}$ |
| $C_p$ | specific heat, BTU/LB $^oF$ |
| $d$ | density, lb/cu ft |
| dB | decibels re $2 \times 10^{-5}$ Newtons/sq meter |
| $D_N$ | fan nozzle exit diameter, (57.1 in.) |
| $C_{P_e}$ | static pressure coefficient at engine nozzle exit plane, $\frac{P_{S_e} - P_{S_o}}{q_f}$ |
| $C_{P_f}$ | static pressure coefficient in fan nozzle, $\frac{P_{S_f} - P_{S_o}}{q_f}$ |
| $f$ | frequency Hz |
| $F_g$ | gross thrust, lb |
| $F_L$ | load in flap gearing link, lb |
| $h$ | skin film heat transfer coefficient, BTU/hr sq ft $^oF$ |
| $m$ | local skin mass, lb |
| $N_1$ | rotational speed of gas producer, rpm |
| $N_2$ | rotational speed of power turbine, rpm |

| | |
|---|---|
| $NF_B$ | normal force component measured by vane force balance, lb |
| $NF_\ell$ | normal component of load in vane gearing link, lb |
| $NF_V$ | total normal component of force experienced by vane, lb |
| $N_{STR}$ | Strouhal number, $\frac{D_N \cdot f}{u_f}$ |
| $PM_B$ | pitching moment measured by vane force balance, in. lb |
| $PM_V$ | total pitching moment experienced by vane, in. lb |
| $P_S$ | static pressure, lb/sq in. |
| $P_{S_e}$ | static pressure at engine nozzle exit plane, lb/sq in. |
| $P_{S_f}$ | static pressure in fan nozzle, lb/sq in. |
| $P_{S_o}$ | ambient static pressure, lb/sq in. |
| $P_{rms}$ | root-mean-square value of fluctuating component of surface pressure, lb/sq in. |
| $P_T$ | stagnation pressure, lb/sq in. |
| $q_f$ | dynamic pressure at fan nozzle exit plane, $\frac{\rho_e \cdot u_f^2}{288}$, lb/sq in. |
| SPL | sound pressure level, dB or lb/sq ft |
| $u_F$ | fan nozzle exit velocity, ft/sec |
| $t$ | thickness of skin, ft |
| $T_g$ | local gas temperature, $^oF$ |
| $T_s$ | skin temperature, $^oF$ |
| $\overline{T}_s$ | mean skin temperature over designated time interval, $^oF$ |
| $T_T$ | stagnation temperature, $^oR$ |
| X | axial distance, in. |
| Y | distance measured perpendicular to X, in. |
| $\beta_L$ | angle between flap gearing link and vane chord line, degrees |
| $\delta$ | ratio of absolute ambient air temperature to standard sea level value of 518 $^oR$ |

| | |
|---|---|
| $\delta_V$ | vane deflection angle, degrees |
| $\theta$ | nacelle pitch angle, degrees |
| $\frac{\Pi(N_{STR})}{q_F^2}$ | one-third octave band power spectrum |
| $\rho_e$ | density of fan exhaust at nozzle exit plane, slugs/cu ft |
| $\tau$ | time, sec |
| $\phi$ | nacelle bank angle, degrees |

# 1 - INTRODUCTION

Grumman is currently involved in the development of a "Type A" V/STOL aircraft. The design (698) concept is based on the use of a V/STOL nacelle which embodies both the powerplant and control vanes immersed in the fan stream of a high bypass ratio turbofan. The twin tilting nacelles contain all the VTOL functions - propulsive thrust, thrust modulation, and control about all three axes - without the need for additional lift fans or other devices.

A test program was conducted using a 55 inch Hamilton Standard "Q-Fan" (fan pressure ratio of 1.135) powered by a Lycoming T55 turboshaft engine (6500 lb thrust) to: demonstrate the control forces and moments inherent in this approach; identify and investigate potential problem areas which might arise when operating the engine/control surface in close proximity to the ground and; provide design data on thermal and acoustic loads.

The T55 engine and nacelle assembly were loaned to Grumman by NASA Ames Research Center under terms of NASA/GAC bailment agreement dated Jan. 20, 1977. The Q-Fan and technical support for the testing were supplied by Hamilton Standard Division of United Technologies.

## 2 - SUMMARY

The concept of a combined V/STOL propulsion and aircraft attitude control system was subjected to large scale engine tests at the Grumman Bethpage V/STOL Static Test Facility. The tilt nacelle/attitude control vane package consisted of the T55 powered Hamilton Standard Q-Fan demonstrator, a NASA Ames/Boeing V/STOL inlet and fan exhaust nozzle and a boom-mounted attitude control vane assembly. Vane forces, moments, thermal and acoustic characteristics as well as the effects on propulsion system performance were measured under conditions simulating hover in and out of ground effect. The principal conclusions are:

- Large values of vane control force were obtained at maximum vane deflection (vane lift approaches 40% total thrust)
- Losses in Q-fan and T55 engine thrust and power levels due to vane and ground proximity effects were negligible and within the accuracy band of the measurements taken
- Structural temperature levels, distributions and differentials and the measured average heat transfer film coefficients were tolerable
- The acoustic environment which the vane experienced was found to be no more severe than that measured on sections of structure of existing turbojet powered aircraft
- Dynamic strain measurements taken at key points in the vane structure showed very low strain levels
- Post test inspection of the vane assembly revealed no evidence of structural damage or thermal distress.

# 3 - TEST PROGRAM

## 3.1 OBJECTIVES

The primary objectives of the test program were to:

- Determine vane control power at different vane locations, deflection angles, and ground-vane separation distances
- Obtain design data based on measured
  - Steady state vane surface pressure distributions
  - Acoustic and thermal inputs to the vane
  - Vane drag losses
  - Engine backpressure losses caused by the vane and ground
  - Vane hinge moments.

## 3.2 FACILITY AND EQUIPMENT DESCRIPTION

The tests were conducted at Grumman's test site in Bethpage, N.Y. Figure 3.2-1 shows the test setup. Hamilton Standard's Q-Fan demonstrator was mounted on a thrust measuring table on top of the test stand. Fan centerline was 15 ft above the ground. The test vane was mounted between booms which were in turn mounted on the test stand. The boom support allowed horizontal and vertical variations of vane position relative to the engine/fan. A 20 ft x 20 ft simulated ground plane was attached to a movable frame which allowed variation of vane/ground plane separation, and relative pitch and roll attitudes. A chute was added to the lower edge of the ground plane which forced the impinging flow to turn under the plane and exhaust to the rear. This was done to eliminate non-representative recirculation which might degrade fan or engine performance or generate spurious airloads on the nacelle.

### 3.2.1 Propulsion Unit

The Hamilton Standard Q-Fan Demonstrator is a 13-bladed, variable-pitch 55 inch diameter fan powered by a Lycoming T55-L-11A, 3750 hp, turbo shaft engine. The fan has a bypass ratio of 17:1 and is driven through a 4.75:1 reduction gear box. Fan maximum speed is 3365 rpm. Details of the Q-Fan Demonstrator are contained in Reference 1.

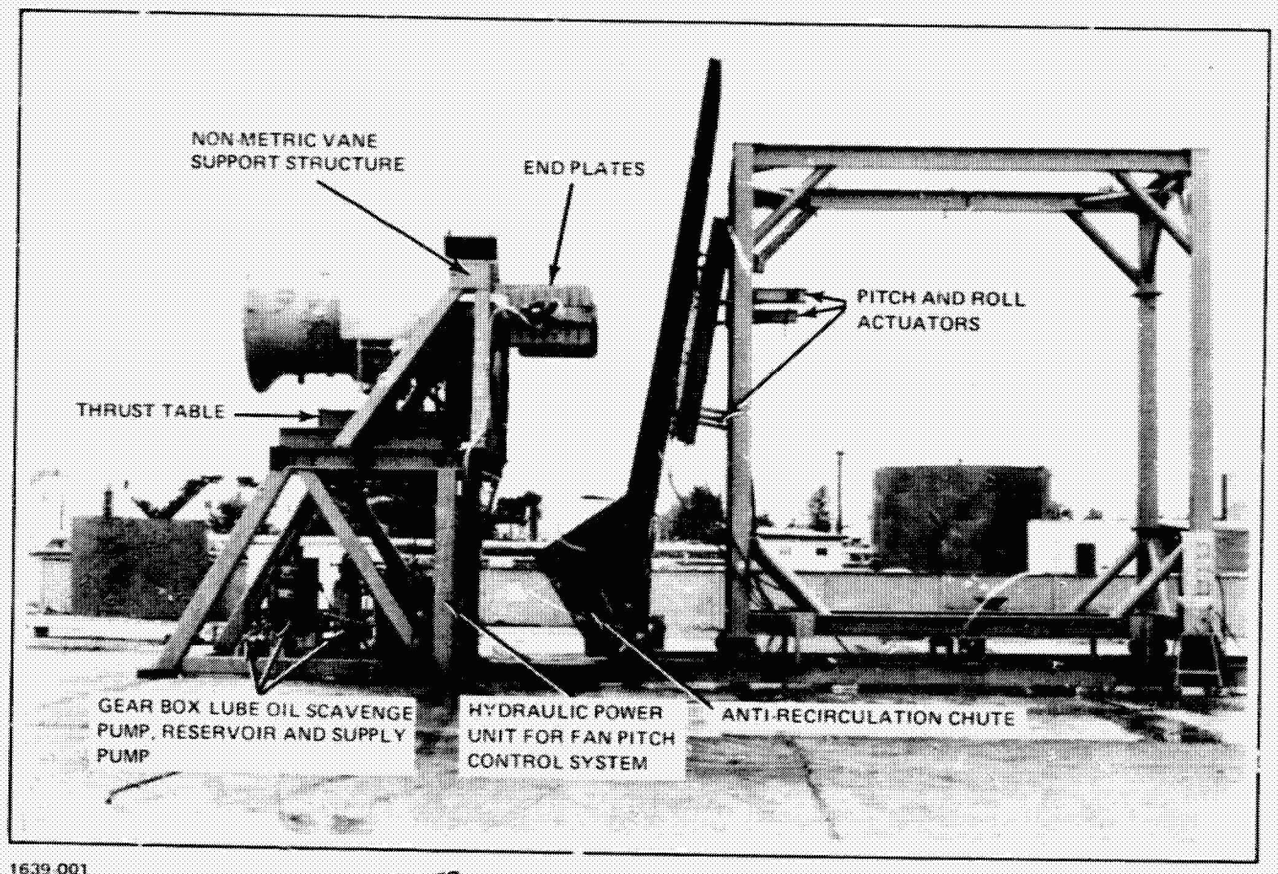


1639-001



Fig. 3.2-1 Q-Fan/Control Vane Test Facility

Consistent with helicopter turboshaft engine practice, the T55-L-11A engine is fitted with a divergent exhaust nozzle which reduces the core exhaust velocity to 340 ft/sec at maximum power. In contrast, the fan exit velocity is 459 ft/sec. With the fan flow rate at 450 lb/sec and the engine airflow rate 26.6 lb/sec, it is evident that the fan flow is the predominant contributor to the fluid dynamic characteristics of the combined exhaust stream. Consequently, the dynamic pressure at the fan exit rather than at the engine exhaust outlet is used to non-dimensionalize the data where appropriate. Figure 3.2-1 shows the test installation during a test with the vane in the centerline position and the ground plane mounted at an angle close to the vane structure. Figure 3.2-2 depicts the vane at the offset position 3. Only the centerline and the number 3 positions were used in this program. Pertinent dimensions are given in Figure 3.2-3.

At the outset the fan/engine unit was equipped with a fan inlet and exhaust nozzle assembly supplied by Boeing Military Aircraft Development, Seattle. This assembly is shown schematically in Fig. 3.2-3 and described in detail in Reference 2. The fan speed hunting problem described in Subsection 4.3.3 led to replacement of the Boeing inlet with the Hamilton Standard bellmouth assembly. This bellmouth was used for all vane performance tests (Fig. 3.2-1).

### 3.2.2 Control Vane Design

The control vane is a two-dimensional airfoil panel having a 30.4 in. chord, 63.75 in. span and a 10% thickness-to-chord ratio. It incorporates a geared trailing edge flap which pivots about the 70% chord station. Flap deflection is controlled by two outboard links which are grounded to the boom supports. These links provide a flap-to-vane deflection ratio of 1.0 and are strain gage instrumented to derive component load corrections to vane force balance measurements.

Two force balances are mounted to either side of the vane at the 45 percent chord station and are the main structural members supporting the vane in the boom assembly. The balances measure vane lift force (max 6000 lb), drag force (max 3000 lb) and pitching moment (max 36,000 in. lb) about the vane pivot axis (0.45 c). A model schematic presented as Fig. 3.2-3 shows the location of the vane pivot axis relative to the nacelle.

An electrical actuator mounted on the left boom is used to vary vane deflection. A cardion cam type potentiometer fixed to the right boom provides a direct measurement of vane angle.

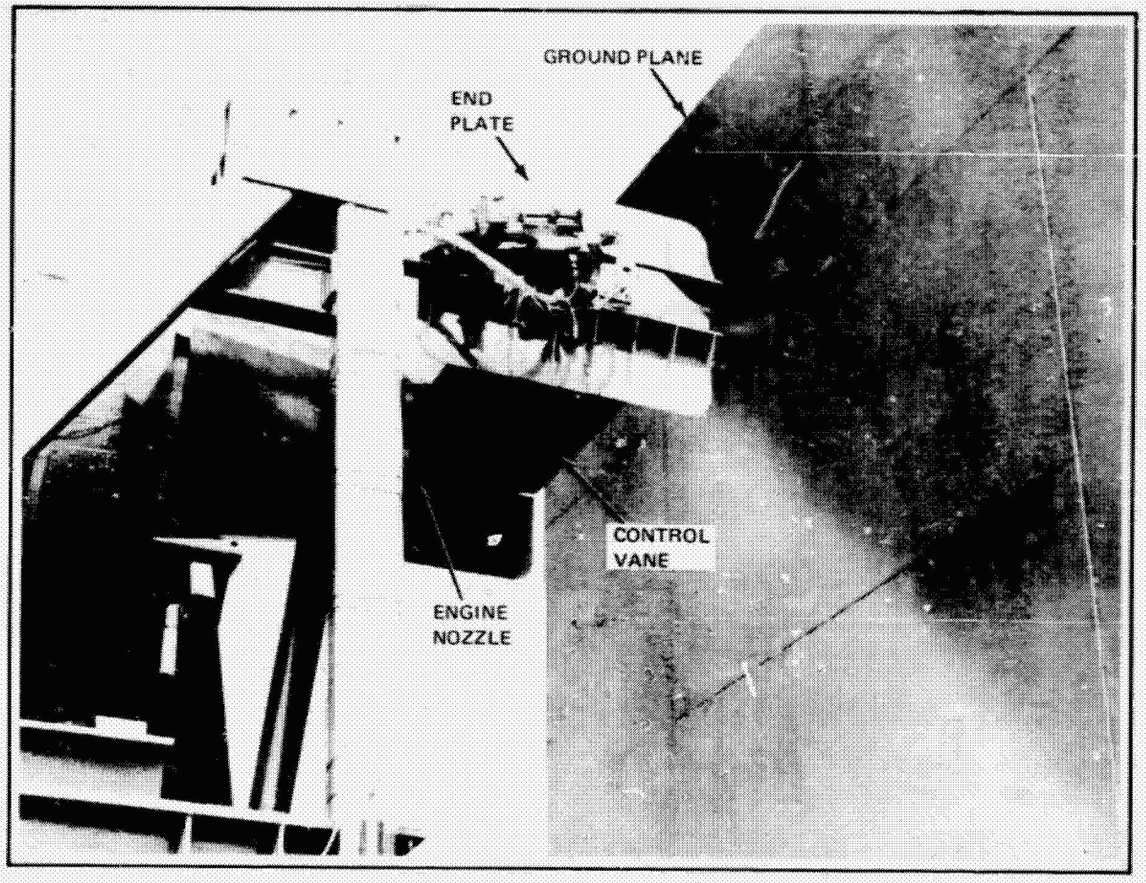


Fig. 3.2-2 Control Vane in Offset Position No. 3

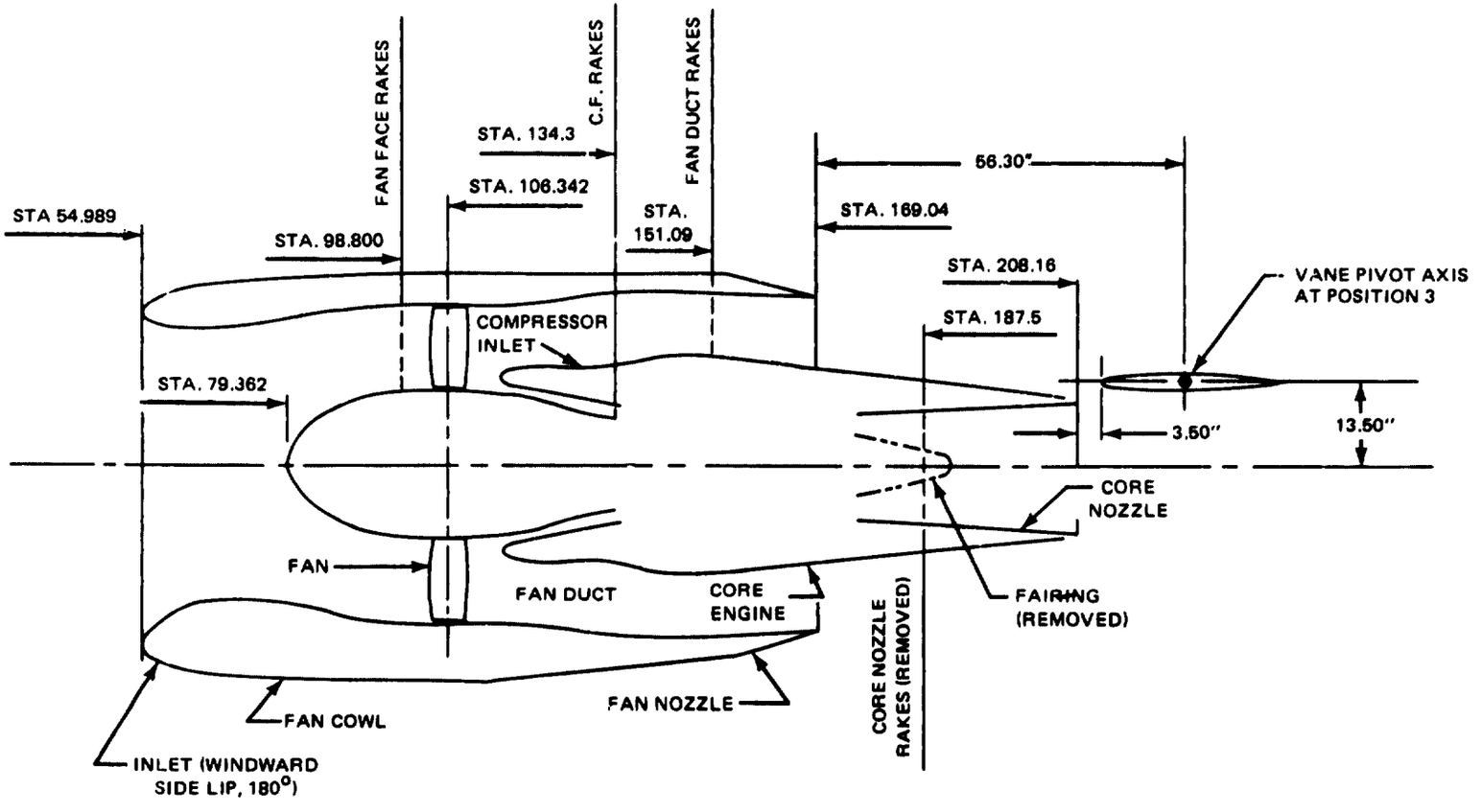


Fig. 3.2-3 Nacelle & Vane Schematic

3.2.2.1 Loads and Criteria - The critical design load for the control vane occurs at the maximum deflected position, 30 degrees nose up to 30 degrees nose down. Measurements made during small scale wind tunnel tests indicated that the maximum control vane is about 40% of the maximum engine thrust. Since the maximum thrust of the Q-Fan engine is about 6500 lb, the design limit load for the control vane is conservatively assumed to be 3000 lb. The chordwise pressure distribution for the design limit load is presented in Fig. 3.2-4.

Proof of structural strength by static test was not included in the program; therefore a design ultimate factor of safety of 2.0 was used. Since the total test time was not expected to exceed 100 hours, fatigue life was not a design consideration except in the case of sonic fatigue. Sonic fatigue analyses were conducted, as discussed in Subsection 3.2.2.2, to ensure survival in the severe sonic environment. Compression buckling of the skin could degrade the sonic fatigue life, although data supporting this opinion is very limited. Therefore, it was decided to design the structure so that the skins would not buckle at limit load.

3.2.2.2 Sonic Fatigue - The control vane is subjected to high intensity noise levels produced by the direct impingement of the Q-Fan engine exhaust flow. Sound pressure levels on the structure were predicted for the maximum thrust condition using procedures of Reference 3. Stress levels resulting from excitation of the structure by the noise field generated at maximum thrust were predicted by analytical techniques presented in Reference 4.

The stress prediction procedures of Reference 4 are based on data derived from analysis and tests of skin stringer panels. The control vane design consists of a box type construction of two skins with interconnecting ribs. Reference 5 states that analysis procedures for skin stringer construction will over estimate the stresses in box type structures by a factor of 2. Based on this data, the stress predictions on the control vane were reduced in half.

In addition, adjustments were made to account for the presence of stress concentrations. These adjustments consisted of increasing the stress predictions by a factor of 3.

Prediction of fatigue life of an acoustically excited structure requires the use of random SN data for the material used. Such data was derived from SN curves based on constant amplitude and constant frequency loading. A computer program, "RNDSN," was used to derive the necessary curves. The curves and predicted stresses were used to determine the number of cycles to failure of the structure.

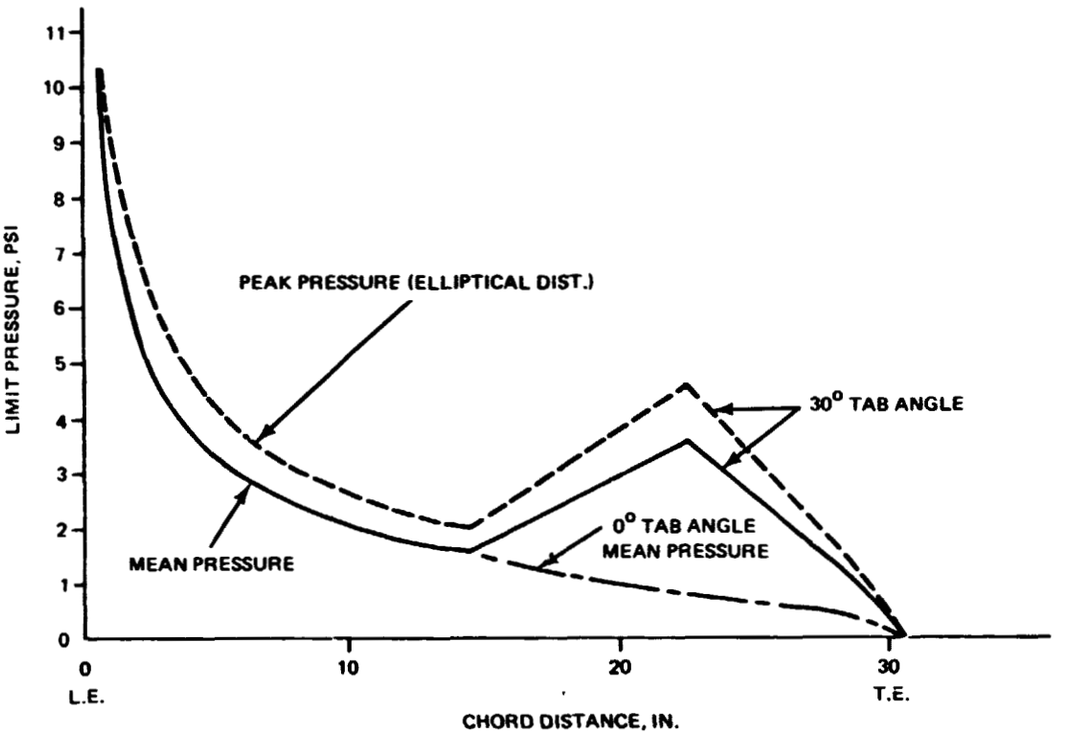


Fig. 3.2-4 Q-Fan Contol Vane Limit Chordwise Pressure Distribution

The required fatigue life was based on: the exposure time, the fundamental resonant frequency of the structure and a scatter factor of 5. Comparison of the predicted with the required fatigue life was used to determine if the design was acceptable.

The analysis procedure yielded a minimum acceptable skin gauge of 0.080 in. Based on this skin gauge and design techniques of Reference 4, an allowable minimum rib gauge of 0.090 in. was obtained.

3.2.2.3 Structural Description - For this test it was not necessary to provide a structural arrangement representative of a flight worthy control vane. The design objective was to conservatively design a vane to withstand the combination of airload, high engine core exhaust temperatures and severe acoustic environment, and which could also be manufactured inexpensively in a short period of time. That is, weight was not a design consideration. Essentially, the control vane was considered to be a prototype to be used for obtaining design data (i.e., air loads, vibration, acoustic environment, temperatures).

The general structural arrangement and dimensions of the test vane are shown in Fig. 3.2-5. The construction is conventional sheet/stringer with front and rear beam and chordwise ribs. The trailing edge tab is supported off the rear beam by three hinges. The material selected for the skins is a titanium alloy, 6Al-2Sn-4Zr-2Mo, which has improved elevated temperature performance. It is creep resistant and relatively stable to about 1050° F. Titanium was the choice over steel because the thermal coefficient of expansion and the modulus of elasticity of titanium alloys are one-half of the corresponding values for steel. Since thermal stresses are a direct function of these two parameters the thermal stresses in Titanium are one-fourth the thermal stresses in steel. The skin thickness is .112 inches.

The chordwise ribs are fabricated from 0.090 in. A286 stainless steel sheet. For minimizing thermal stresses, it would have been preferable to use a titanium alloy for the ribs but the stainless steel was selected for fabrication convenience. Stainless steel sheet can be cold formed to much smaller bend radii than titanium alloy sheet and it was undesirable, for reasons of cost and schedule, to resort to hot forming. The ribs are used to stabilize the skins and distribute airloads to the front and rear beams. As mentioned earlier, the spacing of the ribs was selected to preclude compression buckling of the skins at limit load. The fasteners are made of A-286 stainless steel. The vane pivots about a shaft attached at each end of the vane to two support ribs. The support ribs transfer the pivot shaft shear loads and bending reactions to the vane structure. The shafts are supported by two bearings mounted in the test fixture booms. All lateral loads are resisted by the

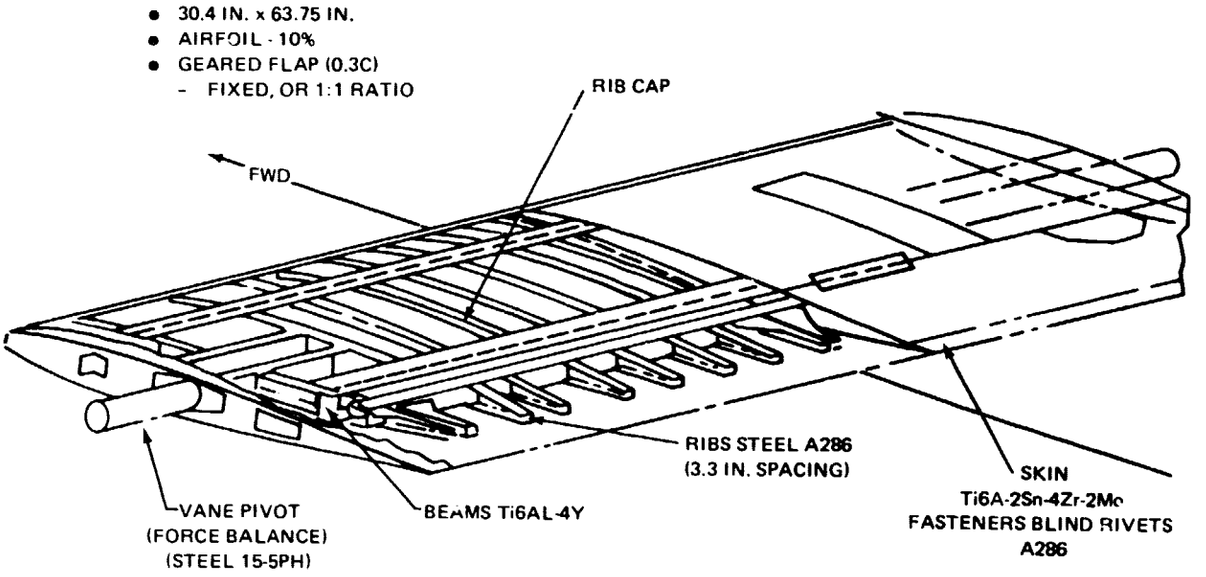


Fig. 3.2-5 Test Vane

left side spherical bearing. The control vane actuator load is applied to a torque arm bolted to the end of the left pivot shaft.

3.2.2.1 Stress and Thermal Analyses - The control vane structure carries the air loads as a beam, simply supported at both ends. The shear loads are resisted in the front and rear beam while most of the bending moment is sustained by spanwise tension and compression stresses in the upper and lower skins. Due to the non-buckling criteria, the skin stresses are quite low (about 20,000 psi at limit load).

The vane design thermal environment, presented in Fig. 3.2-6 creates two basic thermal gradient patterns. The first is due to the external skins heating up more rapidly than the sub-structure, particularly during the initial transient at start up. This gradient induces compression thermal stresses in the skins. The second thermal stress condition is the result of the spanwise temperature variation along the vane surface. The portions of the surface skin immersed in the center of the core exhaust plume were estimated to be 500° F to 900° F hotter than the area on either side of the heated portion. The hot portion of the skin expands and is constrained by the cooler portions, causing significant chordwise thermal stresses in the transition zone between the hot and cooler areas.

Thermal stresses were analytically determined for the thermal gradients to verify the structural integrity of the vane. The stress pattern associated with the first gradient (between the skin and sub-structure) was compounded by material dissimilarity. The thermal coefficient of expansion of the titanium skins is half that of the underlying steel ribs. Analysis indicated that the unequal expansion resulted in excessive attachment loads. To alleviate this situation the rib caps were notched between every third rivet. This reduced the attachment loads to tolerable levels. To assess the thermal stresses induced by the spanwise temperature variations, an elastic analysis was performed. The maximum thermal stress calculated was a chordwise compressive stress of 36,000 psi in the hot portion of the titanium skin. The compression yield strength of Ti-6-2-4-2 at 900° F is 72,000 psi so the desired factor of safety of 2.0 was maintained.

3.2.3 Instrumentation

The data acquisition, recording and reduction equipment used in this program are described in the following subsections.

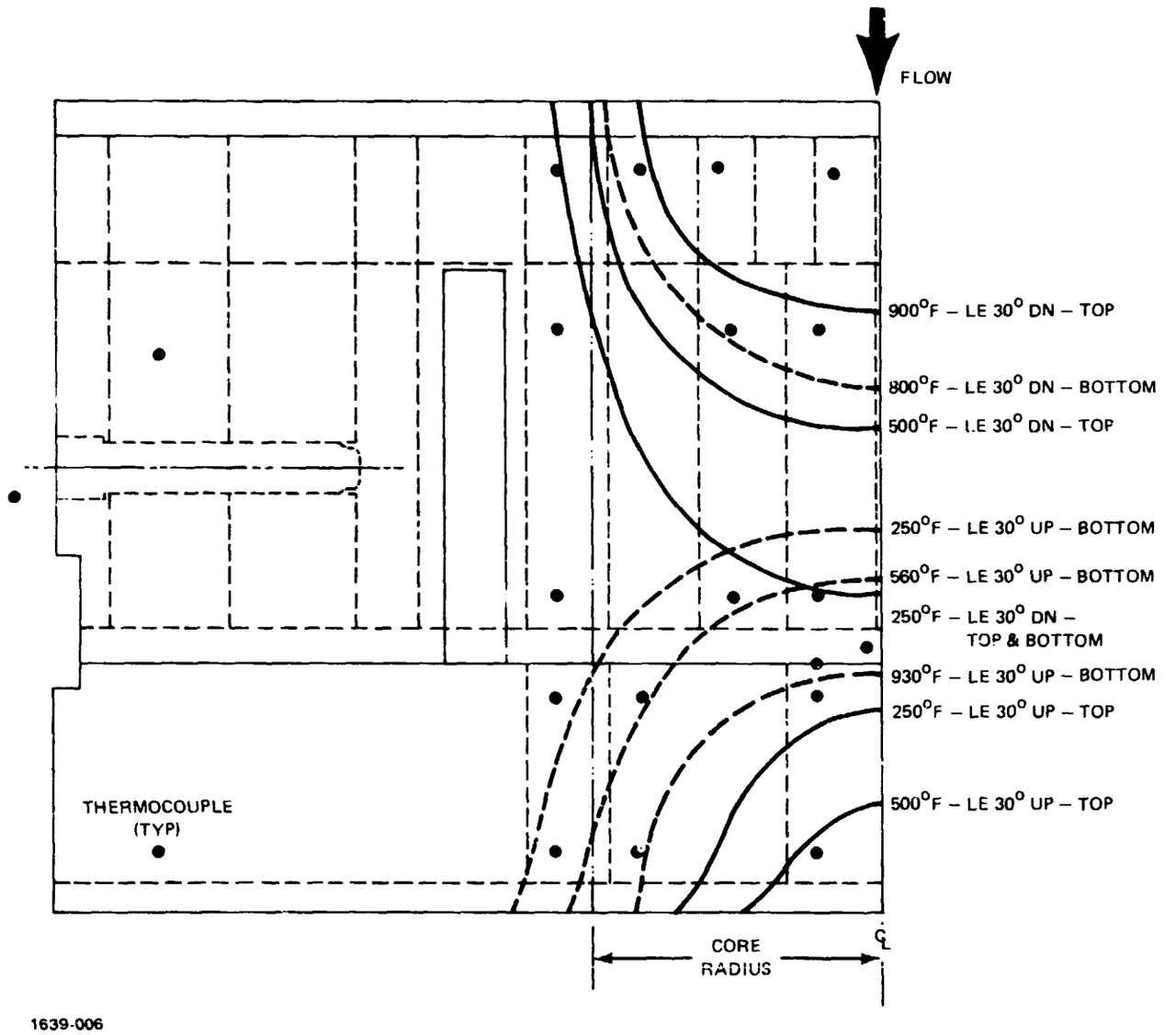


**Fig. 3.2-6 Vane Design Thermal Environment**

3.2.3.1 Vane Aerodynamic Performance Characteristics - Vane lift, drag and pitching moment, in the vane body axis system, were measured with multicomponent force balances mounted in the left and right vane pivots and with strain gages on the flap gearing links (Fig. 3.2-7). The forces and moments were summed vectorially with the equations shown on this figure. The vane force balances and the lower ends of the flap gearing links were attached to non-metric support structure that bypassed the table of the nacelle thrust stand (Fig. 3.2-1). Vane surface pressures were measured with chordwise surface pressure tap arrays on the upper and lower surfaces located at 6%, 36% and 83% of the left hand semi-span (Fig. 3.2-8). These 39 channels of pressure data were acquired with a Scani-valve located within the vane structure.

3.2.3.2 Fan and Engine Performance - Table 3.2-1 lists the instrumentation used for operation and control of the fan/engine combination, for monitoring and recording stresses, temperatures, displacements and accelerations of critical components of the fan/gearbox assembly, and those associated with the automatic shutdown and the various warning systems.

The entire nacelle assembly, except for the vane and its support system, was mounted on a thrust table (Fig. 3.2-1) which measured total installed thrust. For correlation and diagnostic purposes, fan gross thrust was calculated from the fan nozzle exit properties measured with the pair of pressure and temperature rakes shown in Fig. 3.2-9. Engine gross thrust, which constituted only 4% of the total nacelle thrust, was determined from the engine manufacturer's specification, using measured shaft horsepower as the independent variable.

For assessment of back pressure effects, the average engine nozzle exit static pressure was determined with the four static pressure taps at the nozzle exit plane (Fig. 3.2-10). Fan nozzle exit pressures were measured by the static pressure probes of the rakes shown in Fig. 3.2-9.

3.2.3.3 Structural Dynamic Measurements - The dynamic components of the stresses induced at various points in the vane structure by the turbulent coaxial fan and engine exhaust streams were measured by 12 high-frequency single-arm axial-strain gages (Fig. 3.2-11). Sound pressure levels felt by the vane were measured by five high intensity microphones (Kulite pressure transducers) mounted flush in the upper and lower vane skins at a chordwise station located $15\frac{1}{2}$ in. from the vane centerline (Fig. 3.2-8 and 3.2-11). Assessment was made of the effect of the ground plane on the sound pressure levels that would be felt by aircraft structure adjacent to the nacelle via

NOTES:
1) $\beta_L$ & ALL FORCES SHOWN ARE RELATIVE TO VANE BODY AXIS SYSTEM.
2) TENSION IN FLAP GEARING LINK IS REACTION TO POSITIVE (+) LOADS $NF_L$ & $AF_L$.
3) $F_L$ = LINK TENSION
4) $\beta_L$ STAYS WITHIN $0° \leq \beta_L \leq 90°$ FOR VANE DEFLECTIONS WITHIN $-30° \leq \delta_V \leq +30°$
5) PITCHING MOMENT MEASURED BY LEFT HAND FORCE BALANCE ONLY.

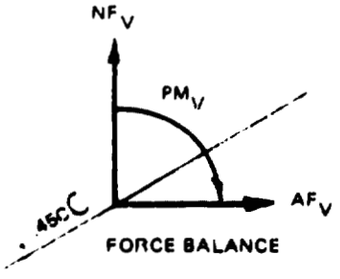

FORCE BALANCE

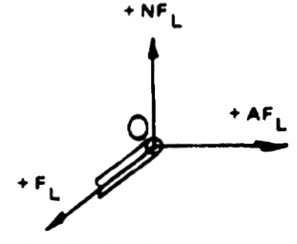

LINK-TO-FLAP
CONNECTION

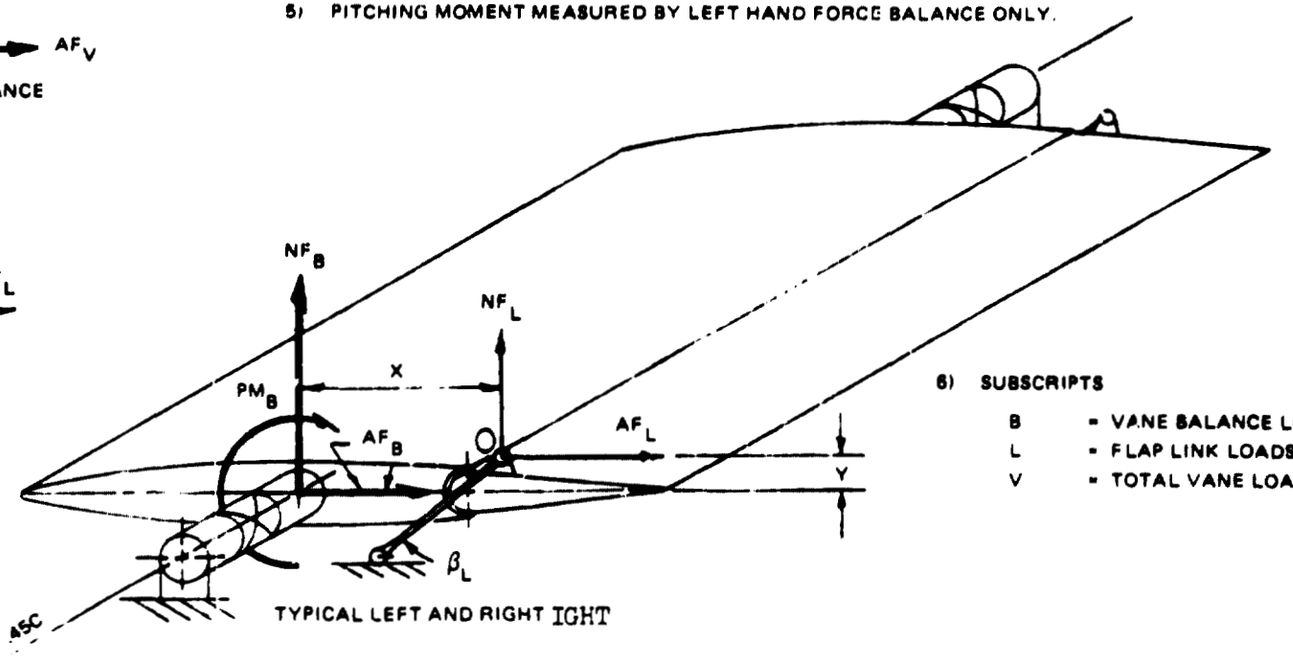

TYPICAL LEFT AND RIGHT IGHT

6) SUBSCRIPTS
- B = VANE BALANCE LOADS
- L = FLAP LINK LOADS
- V = TOTAL VANE LOADS

7) COMPONENT LINK LOADS

$NF_L = (F_L) \sin \beta_L$

$AF_L = (F_L) \cos \beta_L$

8) TOTAL VANE LOADS

$NF_V = NF_B + NF_L$

$AF_V = AF_B + AF_L$

$PM_V = PM_B + F_L [(Y) \cos \beta_L - (X) \sin \beta_L]$

1639-007

**Fig. 3.2-7 Left & Right Hand Vane Force Balances & Flap Gearing Links**

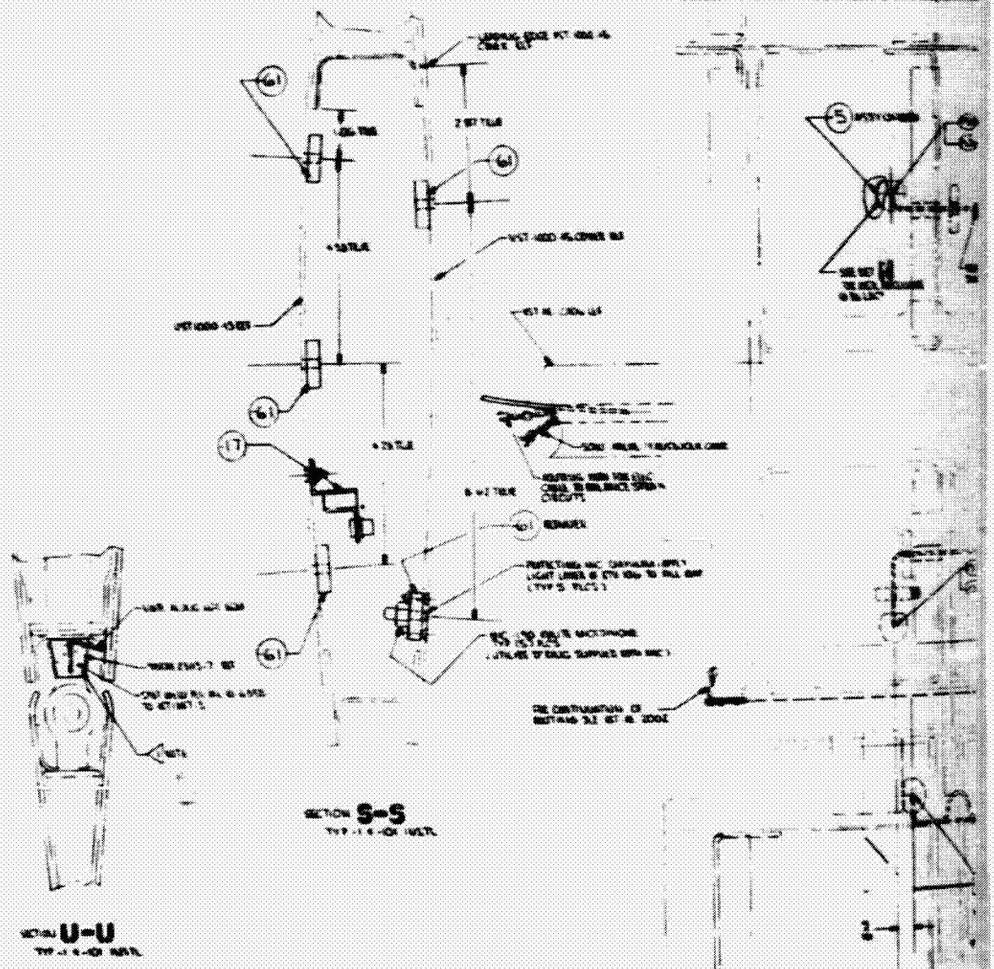


FOLDOUT FRAME

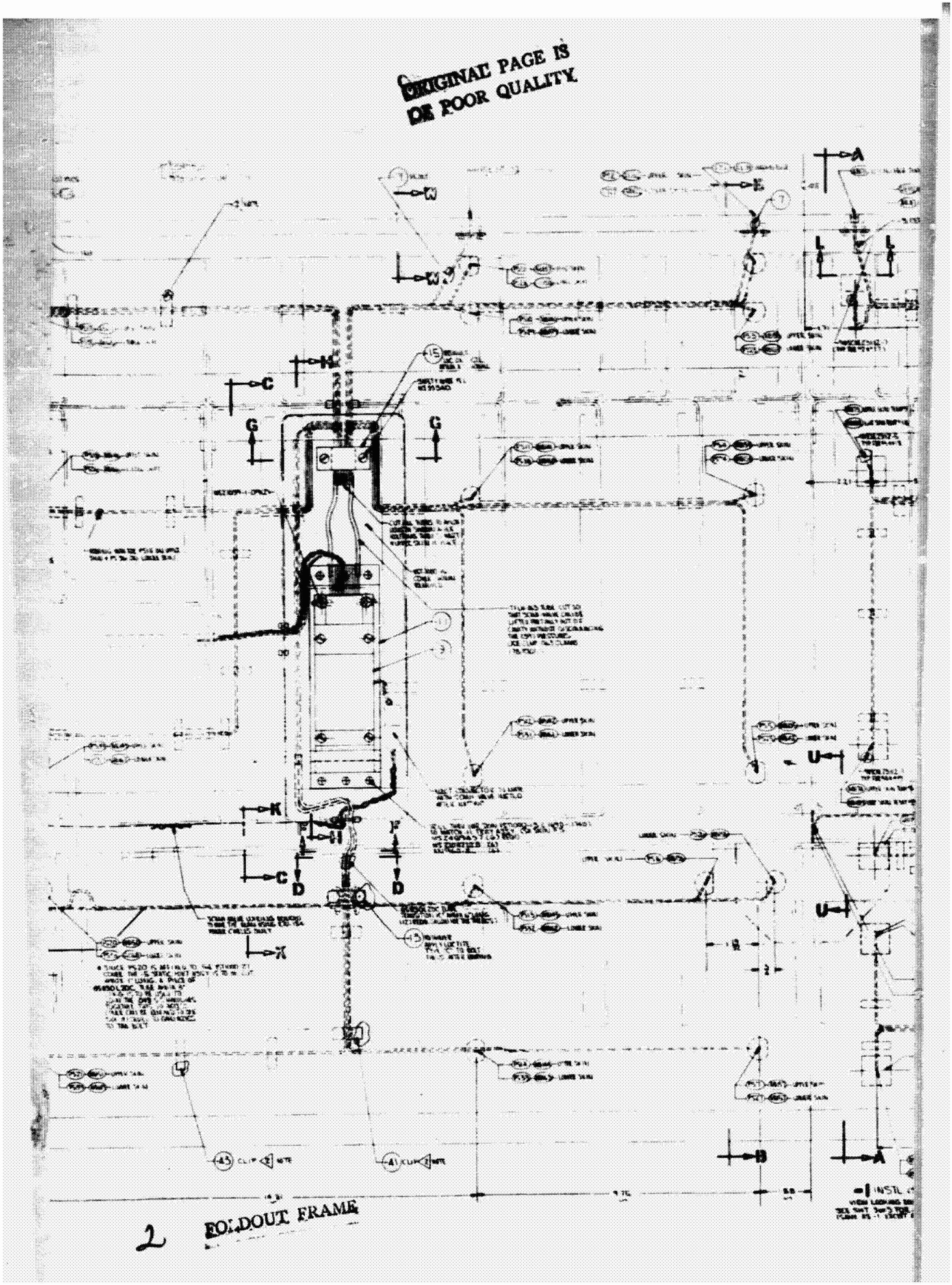

2 FOLDOUT FRAME

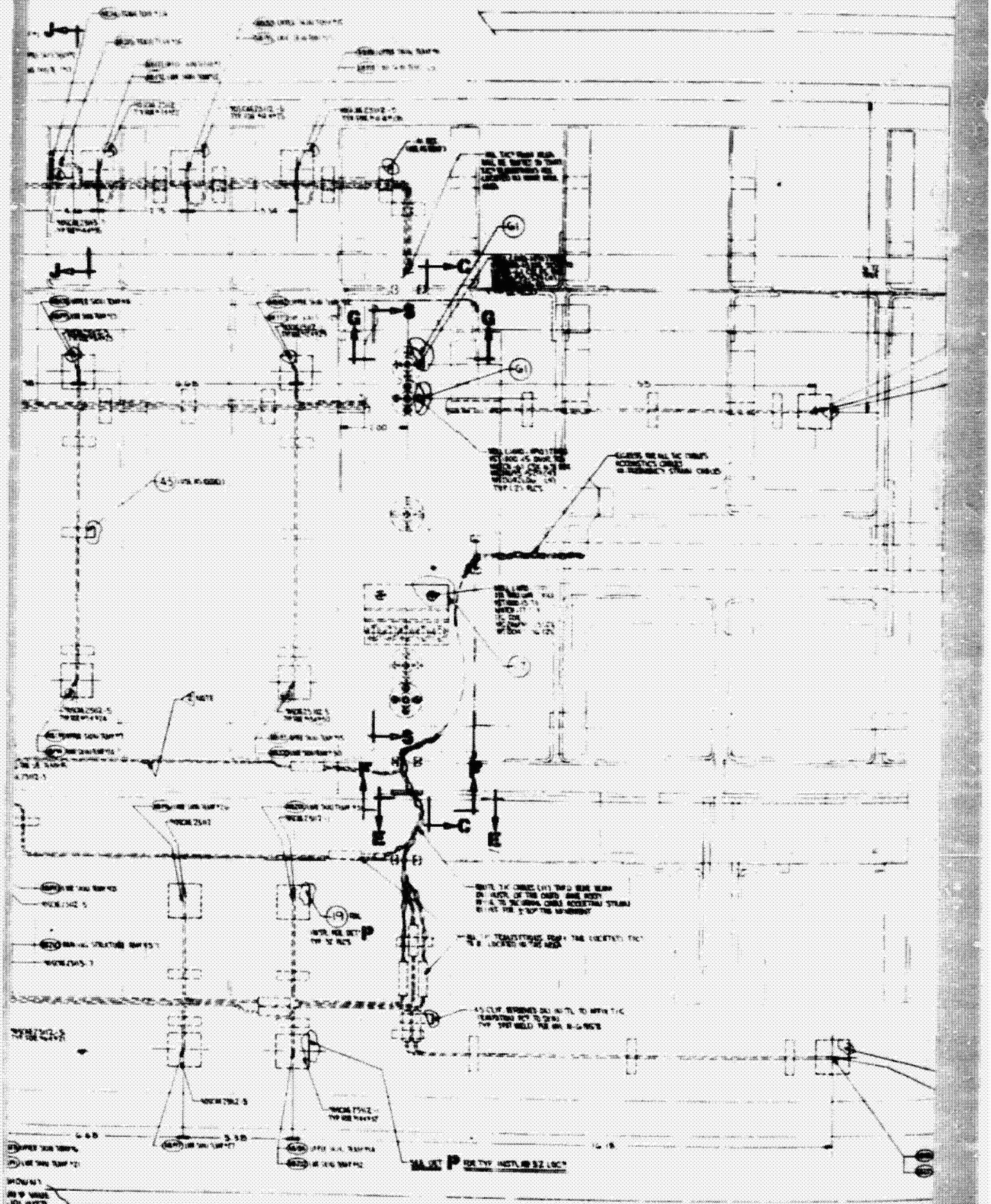

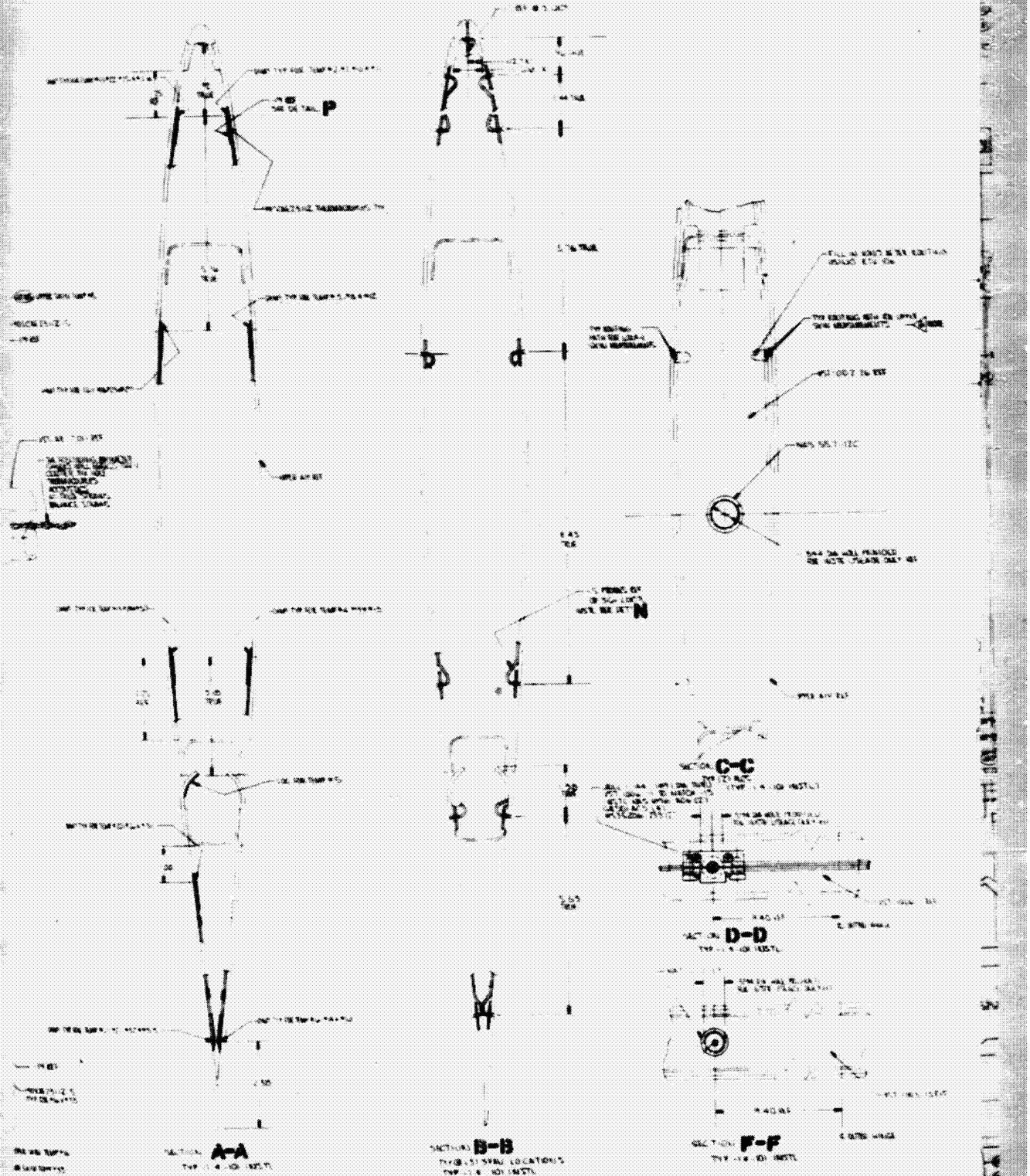

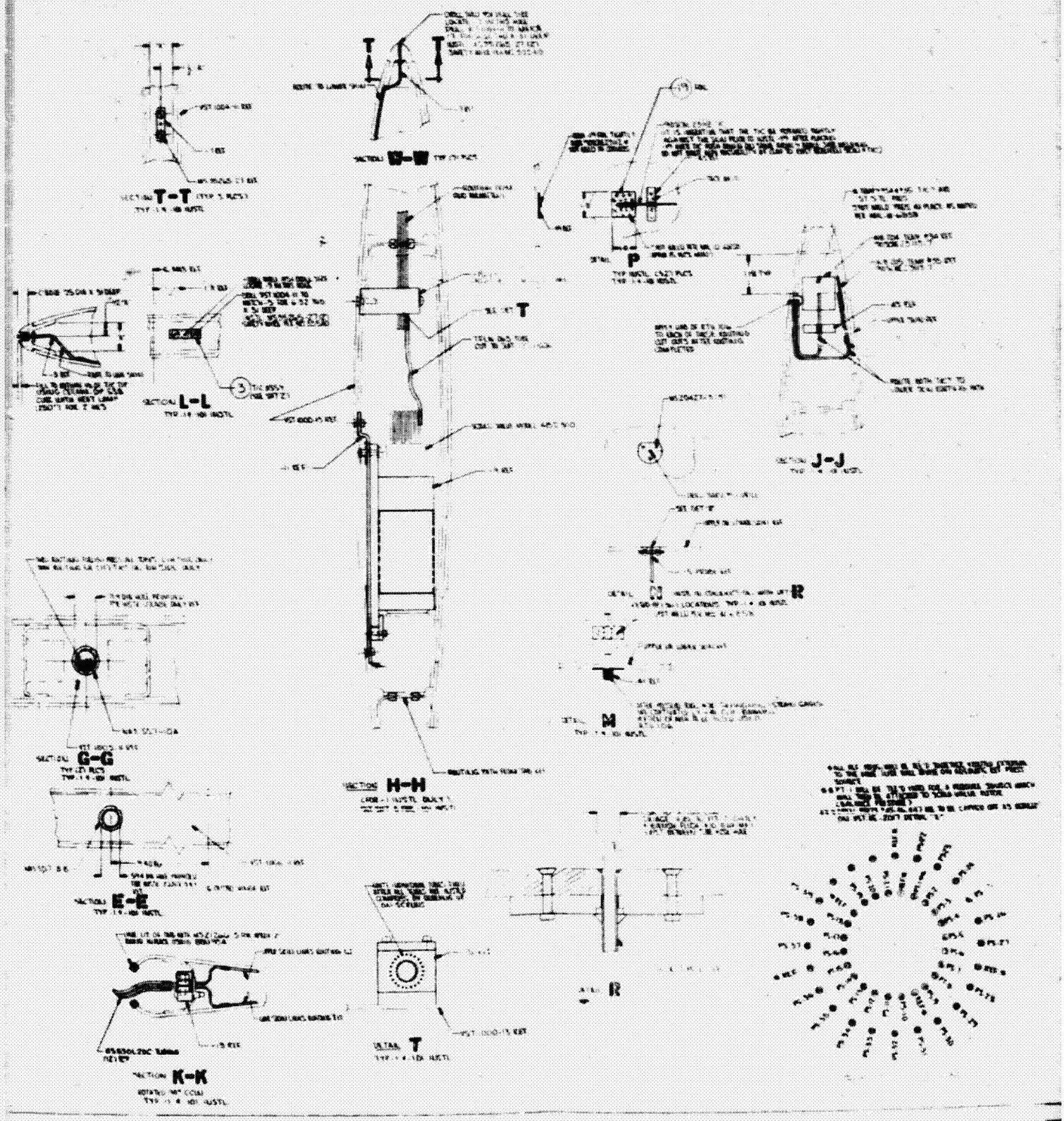

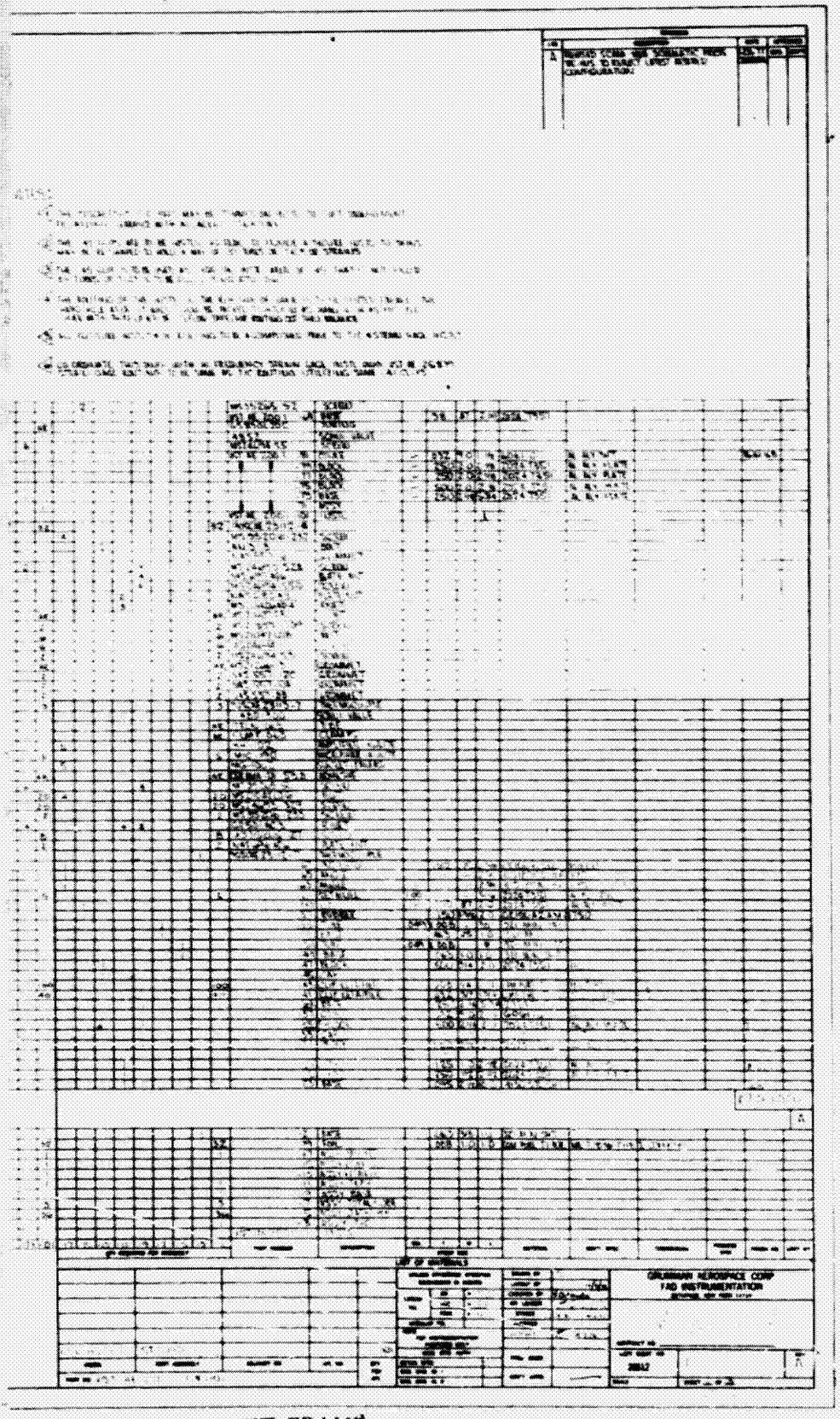

FOLDOUT FRAME

Fig. 3.2-g Installation Vane Instrumentation Pressures, Temperatures & Acoustics (Sheet 1 of 3)

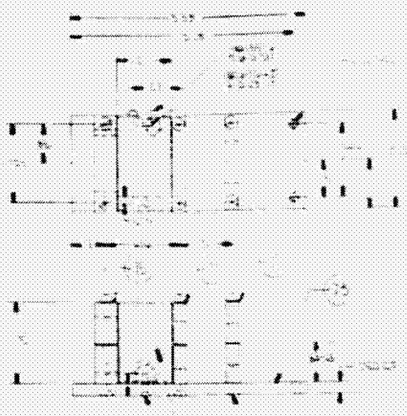

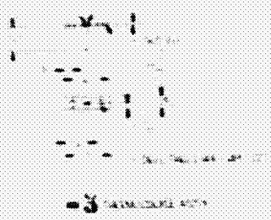

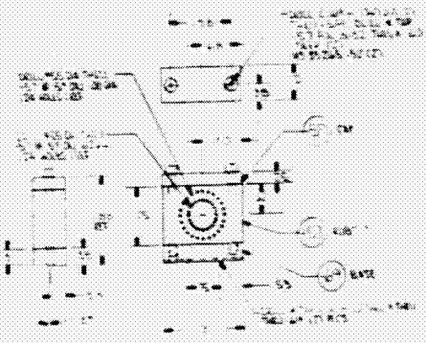

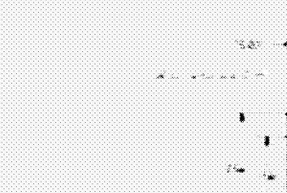

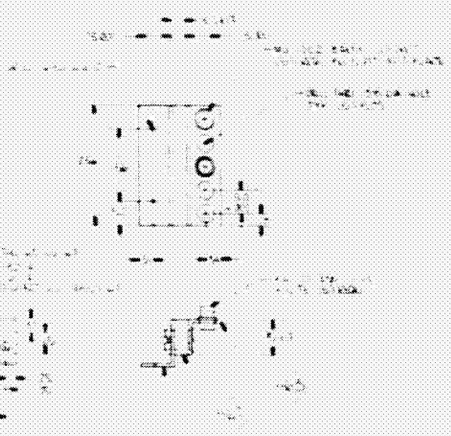

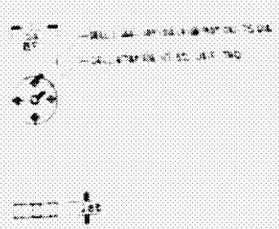

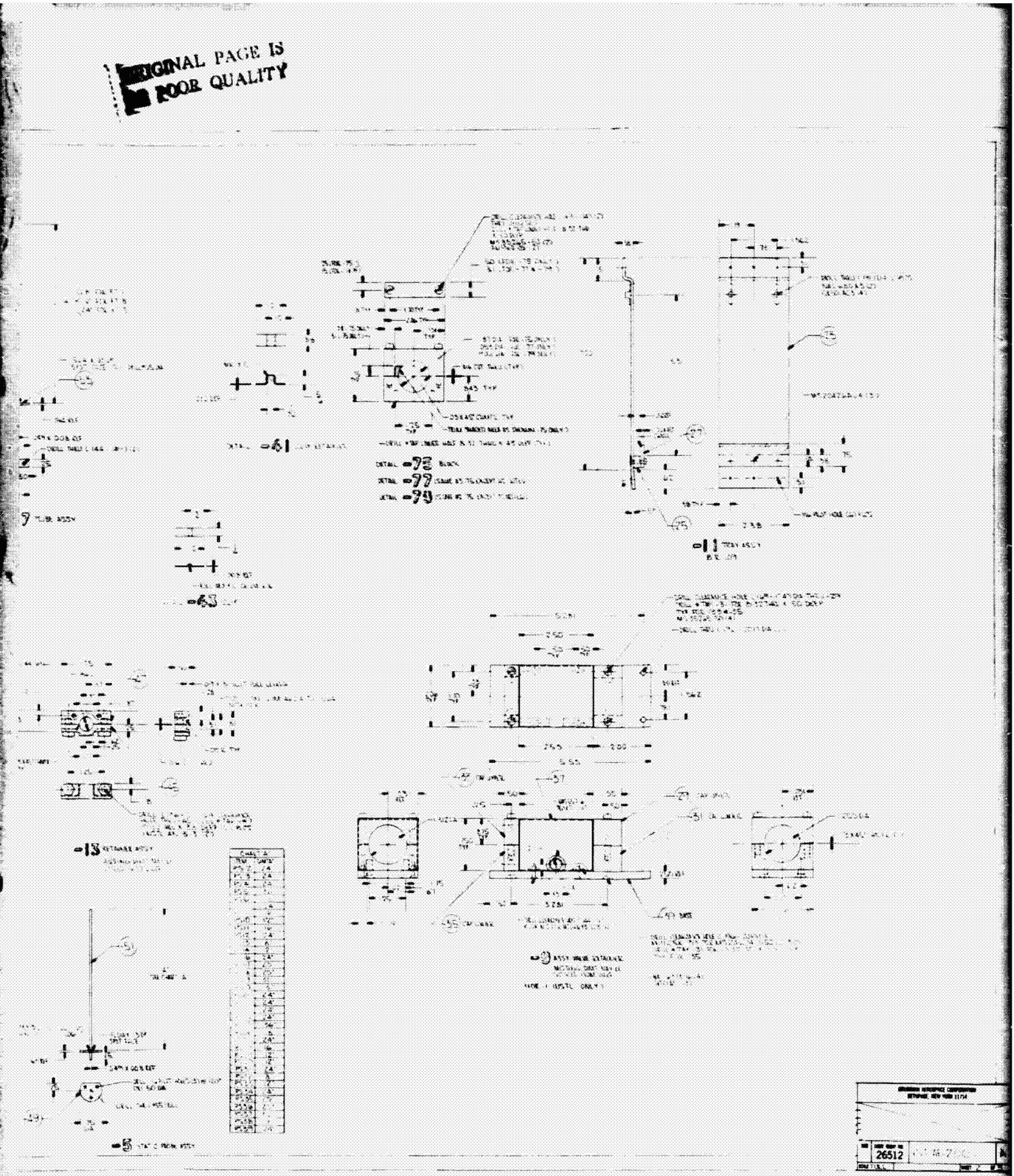

FOLDOUT FRAME

Fig. 3.2-8 Installation Vane Instrumentation Pressures, Temperatures & Acoustics (Sheet 2 of 3)

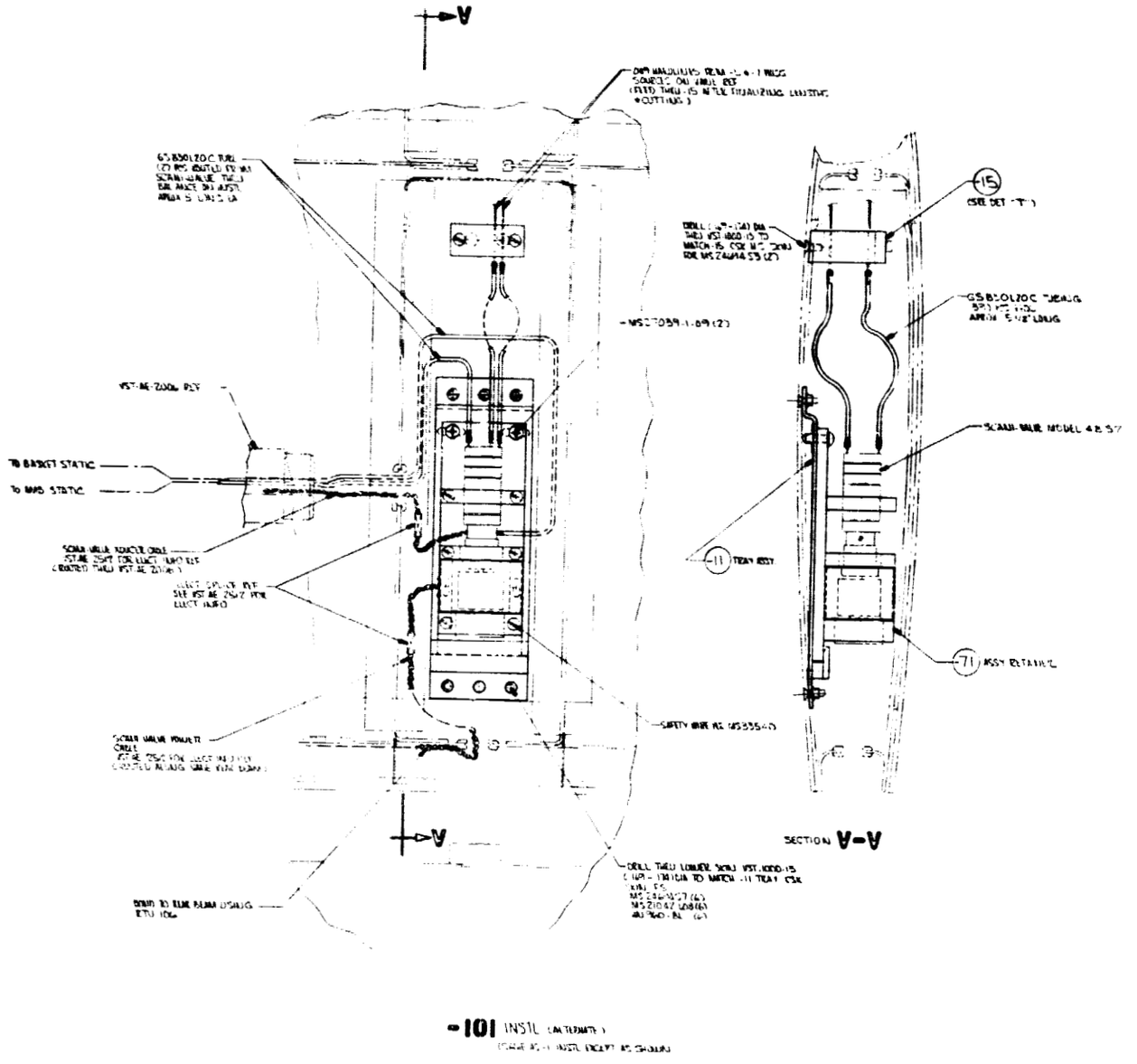


ORIGINAL PAGE IS
OF POOR QUALITY

**Fig. 3.2-8 Installation Vane Instrumentation Pressures, Temperatures & Acoustics (Sheet 3 of 3)**

**Table 3.2-1 Fan-Engine Instrumentation**

**1. CONTINUOUSLY MONITORED (Hand Recorded as Required)**

- Gas Producer Speed, $N_1$
- Power Turbine Speed, $N_2$
- Power Turbine Inlet Temp., $T_{T_7}$
- Fan Blade Angle
- Power Lever Angle
- Engine Oil Pressure
- Engine Oil Temperature
- Engine Drive Shaft Torque
- Fuel Pressure
- Lube Oil Temperature (in/out)
- Lube Oil Flow
- Lube Oil Pressure
- Engine Vibration (3)
- Inlet Vibration (2)
- Gearbox Vibration (2)
- Engine Temperature (8)
- Nacelle Cavity Temperature (2)
- Wind Direction
- Wind Velocity
- Ambient Air Temperature
- Ambient Air Pressure

**2. RECORDED BY HAMILTON-STANDARD**

- Ring Gear Proximeters (4)
- Sun Gear Proximeters (2)
- Retaining Nut Proximeters (2)
- Blade Bending Stress (3)
- Torque
- Fan Speed
- Blade Angle
- Gas Producer Speed
- Sun Gear Stress (7)
- Idler Carrier Acceleration (4)
- Inlet Acceleration (2)
- Gearbox Acceleration (2)

**3. AUTOMATIC SHUTDOWN & WARNING SYSTEMS**

- $N_2$ Overspeed Shutdown (2)
- Overtorque Shutdown
- Gearbox and Engine Chip Detector Warning
- Engine Low Oil Level Warning
- Gearbox Low Oil Pressure Warning
- Temperature (Engine Case and Cowl) Warning
- Engine Fuel Filter Pressure Warning
- Chip Detector – Fan Gearbox
- Chip Detector – Engine Gearbox

1629-145

| 0° PROBES | 180° PROBES | RADIUS $R/R_{FAN}$ | $\Delta A/AR$ |
|---|---|---|---|
| NOZZLE WALL | NOZZLE WALL | 1.0676 | |
| PM1 | PM3 | 1.0640 | |
| PTM1 | PTM11 | 1.0447 | .142 |
| PTM2 | PTM12 | .9964 | .134 |
| TTM1 | TTM4 | .9738 | |
| PTM3 | PTM13 | .9513 | .121 |
| PTM4 | PTM14 | .9084 | .110 |
| PTM5 | PTM15 | .8676 | .100 |
| PTM6 | PTM16 | .8287 | .091 |
| TTM2 | TTM5 | .8102 | |
| PTM7 | PTM17 | .7916 | .083 |
| PTM8 | PTM18 | .7555 | .077 |
| PTM9 | PTM19 | .7211 | .071 |
| TTM3 | TTM6 | .7044 | |
| PTM10 | PTM20 | .6876 | .073 |
| PM2 | PM4 | .6767 | |
| CORE CASE | CORE CASE | .6676 | |

$\Delta A$: AREA ASSIGNED TO TOTAL PRESSURE PROBE
AR: FLOW AREA AT RAKE FACE = 1.064 $m^2$

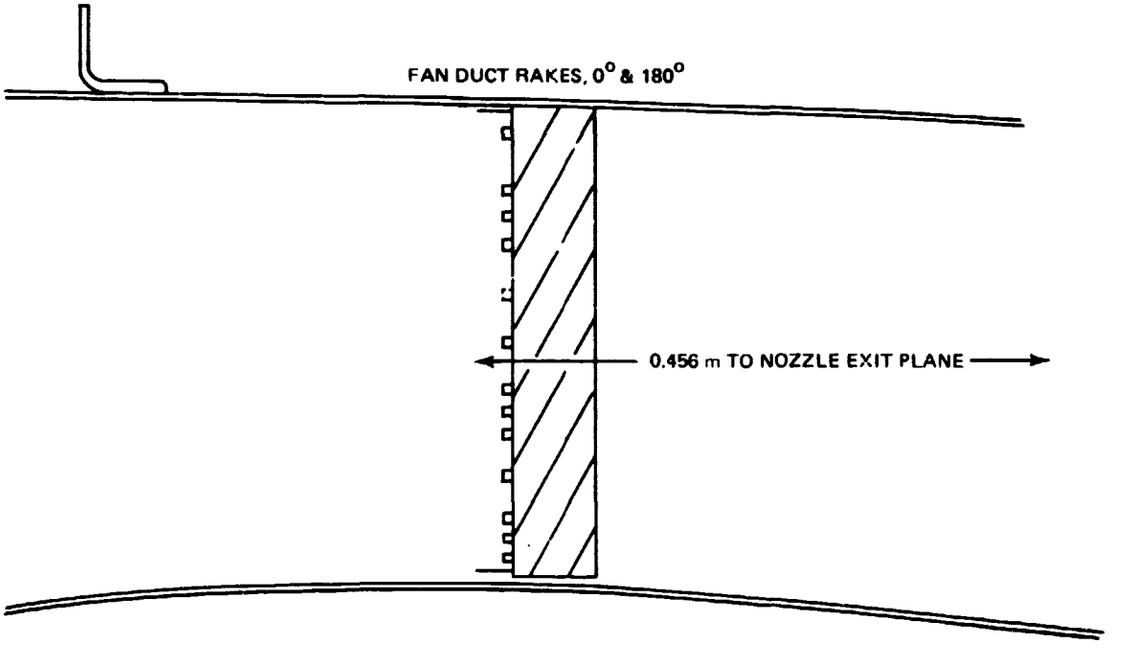


**Fig. 3.2-9 Fan Duct Instrumentation**

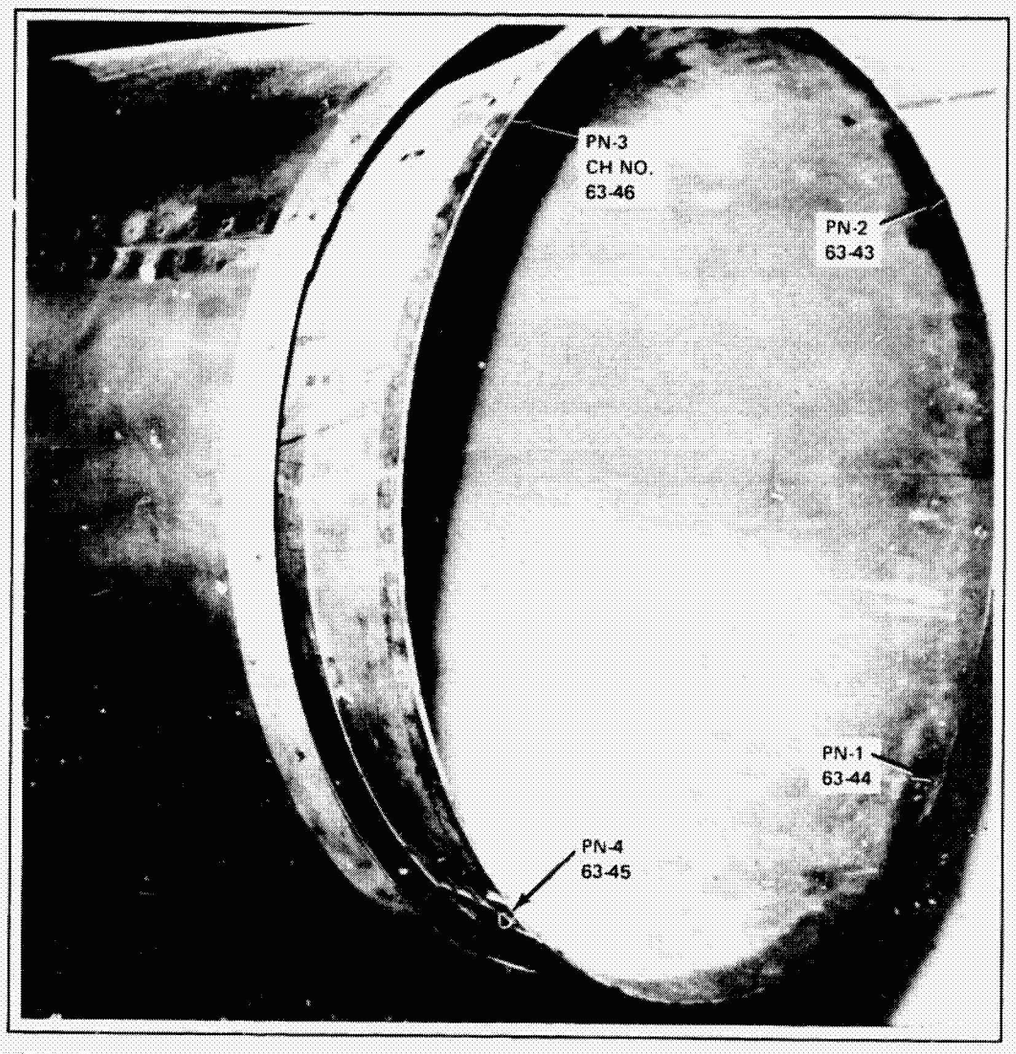


1639-010



**Fig. 3.2-10 Internal Static Pressure Taps at Engine Nozzle Exit Plane**

NOTE: MICROPHONE 1.2.3, ON LOWER SKIN (0)
MICROPHONE 4.5, ON UPPER SKIN (Δ)

| MIC NO. | LOC. AFT OF L.E. |
|---|---|
| 1 | 8.2 INCHES |
| 4 | 9.2 INCHES |
| 2 | 12.5 INCHES |
| 5 | 18.0 INCHES |
| 3 | 17.0 INCHES |

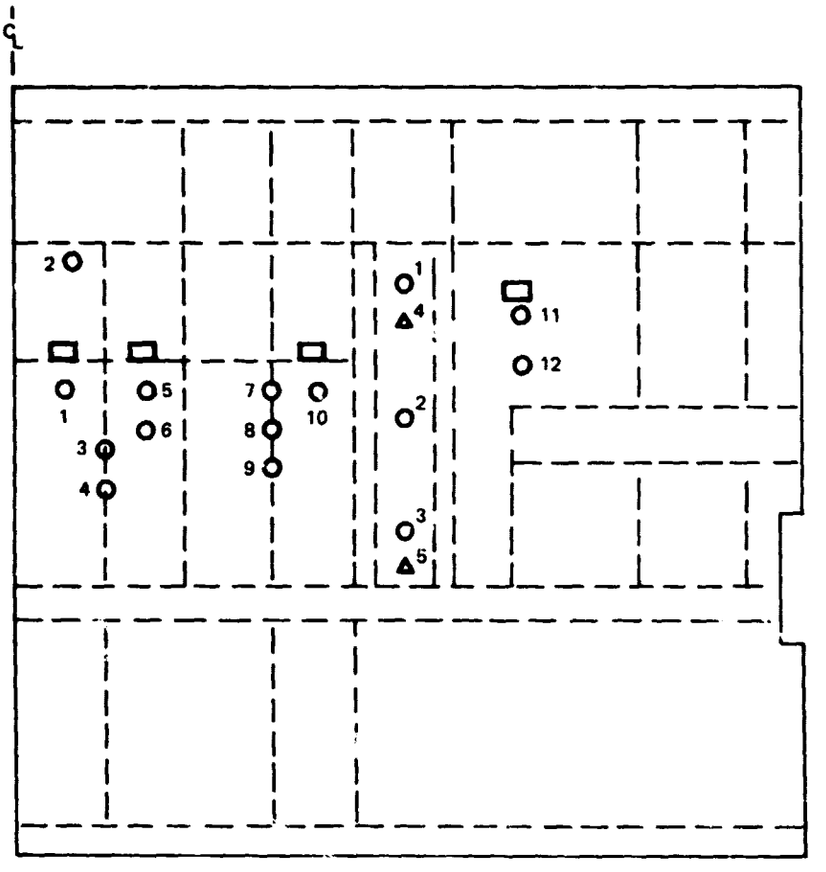


VANE STARBOARD SIDE – LOOKING DOWN

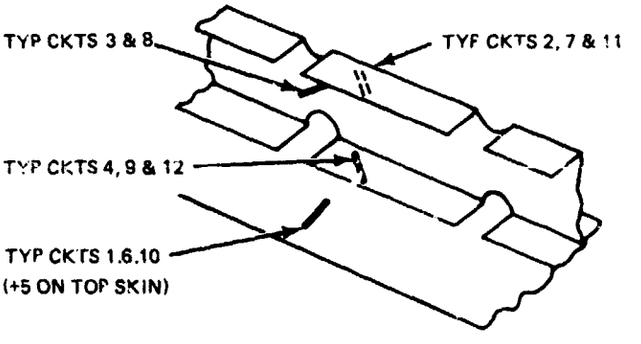


1639-011

**Fig. 3.2-11 Location of Microphones & Strain Gages on Vane**

measurements taken with a single high intensity condenser microphone mounted on test stand structure $4\frac{1}{2}$ ft to the right of the nacelle and 2 ft above the engine centerline.

3.2.3.4 Structural Temperatures - Thermocouples were used to measure temperatures of the inner surfaces of the upper and lower vane skins at 32 locations, the center flap bearing structure and the actuator motor surface (Fig. 3.2-8).

3.2.3.5 Data Recording and Processing Equipment - The data recording equipment used for all steady-state measurements consists of a 64-channel SEL 600 digital data acquisition system controlled by a SEL 810 A general purpose computer. The data were recorded in digital form on magnetic tape for off-line reduction to engineering units. During each test selected critical channels were printed out in real time for operational monitoring purposes. Final engineering data was printed out on a Gould 4800 printer/plotter.

The channel designations and the units of each measurement are shown in Table 3.2-2. It should be noted that the last three of the 64-channels were used for the pressure data acquired by the three Scani-valves.

The vane force and moment data measured by the balances and drag links were reduced to coefficient form and transformed to the nacelle body axis system with a Hewlett Packard 8930 computer. This computer was also used to reduce all of the engine power output and fan performance data. The tabular outputs of both computers for all of the tests are presented in Appendix A.

The acoustic and dynamic structural stress data and a time code signal were recorded on a multi-channel tape recorder system and subsequently were reduced by a one-third octave band real time analyzer and plotted by an X-Y recorder.

3.2.4 Test Procedure

Vane, fan and engine performance data were measured over a series of discrete vane deflection angles for each vane/ground plane configuration tested. Engine power and fan blade angle were held constant while data were being recorded at each deflection angle. A typical run consisted of one minute of operation at constant thrust level for each vane deflection angle in the sequence of 0, +10, +20, +25, +30, 0, -10, -20, -25, -30, 0 degrees. The majority of the data were taken at maximum attainable thrust and with a nacelle configuration consisting of the Hamilton Standard bellmouth inlet and the Boeing fan nozzle and engine cowling.

Table 3.2-2 SEL 600 Data Acquisition System Channel Assignments & Units of Measurement
(Sheet 1 of 3)

| Channel No. | Name of Measurement | Channel No. | Name of Measurement |
|---|---|---|---|
| 1 | Engine Thrust, lb | 44 | Vane Skin Temp No. 19, °F. |
| 2 | N-2, RPM | 45 | Vane Skin Temp No. 20, °F. |
| 3 | N-1, RPM | 46 | Vane Skin Temp No. 21, °F. |
| 4 | Engine Torque, % Max (1300 ft lb) | 47 | Vane Skin Temp No. 22, °F. |
| 5 | Engine TT7 Temp, °F. | 48 | Vane Skin Temp No. 23, °F. |
| 6 | Engine Fuel Flow, gal./min. | 49 | Vane Skin Temp No. 24, °F. |
| 7 | Engine Fuel Temp, °F. | 50 | Vane Skin Temp No. 25, °F. |
| 8 | Engine Fuel Press., psi | 51 | Vane Skin Temp No. 26, °F. |
| 9 | Air Temp Ambient, °F. | 52 | Vane Skin Temp No. 27, °F. |
| 10 | Fan Exhaust TT-101 TTM1, °F. | 53 | Vane Skin Temp No. 28, °F. |
| 11 | Fan Exhaust TT-102 TTM3, °F. | 54 | Vane Skin Temp No. 29, °F. |
| 12 | Fan Exhaust TT-103 TTM4, °F. | 55 | Vane Skin Temp No. 30, °F. |
| 13 | Fan Exhaust TT-104 TTM6, °F. | 56 | Vane Skin Temp No. 31, °F. |
| 14 | Engine Comp TT-110 TTC, °F. | 57 | Vane Skin Temp No. 32, °F. |
| 15 | Engine Thrust (Second Circuit), lb | 58 | Vane Skin Temp No. 33, °F. |
| 16 | RT. Vane Normal Force, (Second Circuit), micro in./in. | 59 | Vane Skin Temp No. 34, °F. |
| | | 60 | Vane Skin Temp No. 35, °F. |
| 17 | Flap Control Link L, lb | 61 | Vane Bearing Temp, °F. |
| 17 | Flap Control Link L, lb | 62-1 | Fan Inlet Rake PTF-1 |
| 18 | Flap Control Link R, lb | 62-2 | Fan Inlet Rake PTF-3 |
| 18 | Flap Control Link R, lb | 62-3 | Fan Inlet Rake PTF-5 |
| 20 | Vane Angle, Deg. | 62-4 | Fan Inlet Rake PTF-7 |
| 21 | Lt Vane Normal Force, micro in./in. | 62-5 | Fan Inlet Rake PP-1 Static |
| 22 | Lt Vane Axial Force, micro in./in. | 62-6 | Fan Inlet Rake PTF-10 |
| 23 | Vane Pitching Moment, micro in./in. | 62-7 | Fan Inlet Rake PTF-11 |
| 24 | Rt Vane Normal Force, micro in./in. | 62-8 | Fan Inlet Rake PTF-13 |
| 25 | Rt Vane Axial Force, micro in./in. | 62-9 | Fan Inlet Rake PTF-15 |
| 26 | Vane Skin Temp No 1, °F. | 62-10 | Fan Inlet Rake PTF-17 |
| 27 | Vane Skin Temp No. 2, °F. | 62-11 | Fan Inlet Rake PP-2 Static |
| 28 | Vane Skin Temp No. 3, °F. | 62-12 | Fan Inlet Rake PTF-20 |
| 29 | Vane Skin Temp No. 4, °F. | 62-13 | Fan Face Cowl Static Press., PC-39 |
| 30 | Vane Skin Temp No. 5, °F. | 62-14 | Fan Face Cowl Static Press., PC-41 |
| 31 | Vane Skin Temp No. 6, °F. | 62-15 | Fan Inlet Rake PTF-21 |
| 32 | Vane Skin Temp No. 7, °F. | 62-16 | Fan Inlet Rake PTF-23 |
| 33 | Vane Skin Temp No. 8, °F. | 62-17 | Fan Inlet Rake PTF-25 |
| 34 | Vane Skin Temp No. 9, °F. | 62-18 | Fan Inlet Rake PTF-27 |
| 35 | Vane Skin Temp No. 10, °F. | 62-19 | Fan Inlet Rake PP-3 Static |
| 36 | Vane Skin Temp No. 11, °F. | 62-20 | Fan Inlet Rake PTF-30 |
| 37 | Vane Skin Temp No. 12, °F. | 62-21 | Fan Inlet Rake PTF-31 |
| 38 | Vane Skin Temp No. 13, °F. | 62-22 | Fan Inlet Rake PTF-33 |
| 39 | Vane Skin Temp No. 14, °F. | 62-23 | Fan Inlet Rake PTF-35 |
| 40 | Vane Skin Temp No. 15, °F. | 62-24 | Fan Inlet Rake PTF-37 |
| 41 | Vane Skin Temp No. 16, °F. | 62-25 | Fan Inlet Rake PP-4 Static |
| 42 | Vane Skin Temp No. 17, °F. | 62-26 | Fan Inlet Rake PTF-40 |
| 43 | Vane Skin Temp No. 18, °F. | 62-27 | Fan Face Cowl Static Press., PC-43 |

Table 3.2-2 SEL 600 Data Acquisition System Channel Assignments & Units of Measurement
(Sheet 2 of 3)

| Channel No. | Name of Measurement | Channel No. | Name of Measurement |
|---|---|---|---|
| 62-28 | Fan Face Cowl Static Press., PC-45 | 63-25 | Fan Exhaust Rake PTM-16 |
| 62-29 | Fan Inlet Rake PTF-41 | 63-26 | Fan Exhaust Rake PTM-17 |
| 62-30 | Fan Inlet Rake PTF-43 | 63-27 | Fan Exhaust Rake PTM-18 |
| 62-31 | Fan Inlet Rake PTF-45 | 63-28 | Fan Exhaust Rake PTM-19 |
| 62-32 | Fan Inlet Rake PTF-47 | 63-29 | Fan Exhaust Rake PTM-20 |
| 62-33 | Fan Inlet Rake PP-5 Static | 63-30 | Fan Exhaust Rake PM-4 (Inoperative) |
| 62-34 | Fan Inlet Rake PTF-50 | 63-31 | Ref Press. |
| 62-35 | Fan Inlet Rake PTF-51 | 63-32 | Inlet Throat Static Press., PC-38 |
| 62-36 | Fan Inlet Rake PTF-53 | 63-33 | Eng Comp Face Rake PTC-10 |
| 62-37 | Fan Inlet Rake PTF-55 | 63-34 | Eng Comp Face Rake PTC-22 |
| 62-38 | Fan Inlet Rake PTF-57 | 63-35 | Eng Comp Face Rake PTC-34 |
| 62-39 | Fan Inlet Rake PP-6 Static | 63-36 | Eng Comp Face Rake PTC-46 |
| 62-40 | Fan Inlet Rake PTF-60 | 63-37 | Eng Comp Face Rake PSC-2 |
| 62-41 | Ref Press. | 63-38 | Eng Comp Face Rake PSC-4 |
| 62-42 | Fan Inlet Rake PTF-61 | 63-39 | Eng Comp Face Rake PSC-6 |
| 62-43 | Fan Inlet Rake PTF-63 | 63-40 | Eng Comp Face Rake PSC-8 |
| 62-44 | Fan Inlet Rake PTF-65 | 63-41 | Ref Press. |
| 62-45 | Fan Inlet Rake PTF-67 | 63-42 | Ref Press. |
| 62-46 | Fan Inlet Rake PP-7 Static | 63-43 | Eng Exhaust PN-2 |
| 62-47 | Fan Inlet Rake PTF-70 | 63-44 | Eng Exhaust PN-1 |
| 62-48 | Ref Press. | 63-45 | Eng Exhaust PN-4 |
| 63-1 | Fan Exhaust Rake PM-1 | 63-46 | Eng Exhaust PN-3 |
| 63-2 | Fan Exhaust Rake PTM-1 | 63-47 | Ref Press. |
| 63-3 | Fan Exhaust Rake PTM-2 | 63-48 | Ref Press. |
| 63-4 | Fan Exhaust Rake PTM-3 | 64-1 | Ref Press. |
| 63-5 | Fan Exhaust Rake PTM-4 | 64-2 | Vane Press. PT-1 |
| 63-6 | Fan Exhaust Rake PTM-5 | 64-3 | Vane Press. PS-2 |
| 63-7 | Ref Press. | 64-4 | Vane Press. PS-3 |
| 63-8 | Inlet Throat Static Press., PC-13 | 64-5 | Vane Press. PS-4 |
| 63-9 | Fan Exhaust Rake PTM-6 | 64-6 | Vane Press. PS-5 |
| 63-10 | Fan Exhaust Rake PTM-7 | 64-7 | Vane Press. PS-6 |
| 63-11 | Fan Exhaust Rake PTM-8 | 64-8 | Vane Press. PS-7 |
| 63-12 | Fan Exhaust Rake PTM-9 | 64-9 | Vane Press. PT-8 |
| 63-13 | Fan Exhaust Rake PTM-10 | 64-10 | Vane Press. PS-9 |
| 63-14 | Fan Exhaust Rake PM-2 | 64-11 | Ref Press. |
| 63-15 | Ref Press. | 64-12 | Vane Press. PS-10 |
| 63-16 | Inlet Throat Static Press., PC-33 | 64-13 | Vane Press. PS-11 |
| 63-17 | Fan Exhaust Rake PM-3 | 64-14 | Vane Press. PS-12 |
| 63-18 | Fan Exhaust Rake PTM-11 | 64-15 | Vane Press. PS-13 |
| 63-19 | Fan Exhaust Rake PTM-12 | 64-16 | Vane Press. PS-14 |
| 63-20 | Fan Exhaust Rake PTM-13 | 64-17 | Vane Press. PT-15 |
| 63-21 | Fan Exhaust Rake PTM-14 | 64-18 | Vane Press. PS-16 |
| 63-22 | Fan Exhaust Rake PTM-15 | 64-19 | Vane Press. PS-17 |
| 63-23 | Ref Press. (4.5 $psi_g$) | 64-20 | Vane Press. PS-18 |
| 63-24 | Inlet Throat Static Press. PC-37 | 64-21 | Ref Press. |

Table 3.2-2 SEL 600 Data Acquisition System Channel Assignments & Units of Measurement
(Sheet 3 of 3)

| Channel No. | Name of Measurement | Channel No. | Name of Measurement |
|---|---|---|---|
| 64-22 | Vane Press. PS-19 | 64-36 | Vane Press. PS-32 |
| 64-23 | Vane Press. PS-20 | 64-37 | Vane Press. PS-33 |
| 64-24 | Vane Press. PS-21 | 64-38 | Vane Press. PS-34 |
| 64-25 | Vane Press. PS-22 | 64-39 | Vane Press. PS-35 |
| 64-26 | Vane Press. PS-23 | 64-40 | Vane Press. PS-36 |
| 64-27 | Vane Press. PS-24 | 64-41 | Ref Press. |
| 64-28 | Vane Press. PS-25 | 64-42 | Vane Press. PS-37 |
| 64-29 | Vane Press. PS-26 | 64-43 | Vane Press. PS-38 |
| 64-30 | Vane Press. PS-27 | 64-44 | Vane Press. PS-39 |
| 64-31 | Ref Press. | 64-45 | Open |
| 64-32 | Vane Press. PS-28 | 64-46 | Open |
| 64-33 | Vane Press. PS-29 | 64-47 | Open |
| 64-34 | Vane Press. PS-30 | 64-48 | Open |
| 64-35 | Vane Press. PS-31 | | |

NOTE: All pressures are in PSI gage. Inlet rakes were removed prior to test no. 101

It should be noted that the one-minute run duration, which was dictated by the commutation cycle of the data acquisition system, exceeds the anticipated full scale values of immersion time. The temperatures of the vane structure near mid-span were monitored in real time during these runs to guard against damage of the instrumentation equipment mounted within the vane.

# 4 - TEST RESULTS

## 4.1 SUMMARY OF TEST PROGRAM

The sequence of tests run, the configurations tested and the power settings used are summarized in Table 4.1-1. The test conductor's log sheets and the computer printouts of the data acquired are contained in Appendix A. Analyses of the important test results are presented in the following subsections.

## 4.2 AERODYNAMIC PERFORMANCE

The primary objective of the test program was to obtain control vane forces and moments from a large scale model of the Grumman V/STOL nacelle. Additional data, related to the effects of height above ground, power setting, and nacelle pitch and roll attitudes in ground proximity, were also obtained for different vane locations. Analyses of the test data indicated that:

- The centerline vane location results in higher levels of vane control effectiveness than the off-center location when operating out of ground effect.
- The centerline vane location is more sensitive to the presence of ground than the off-center location.
- There is no effect of power setting on the levels of vane force and moment coefficients for the off-center location operating out of ground effect.
- Pitch and bank angle have no major effect on the levels of vane effectiveness.
- Subscale test results obtained to date correlate well with those of the full scale test article both with respect to data magnitude and trends.

### 4.2.1 Test Configuration and Data Reduction

The T-55/Q-Fan Vane Test Article is of unswept rectangular planform with an aspect ratio of 2.097 (chord = 30.4 in., span = 63.75 in.) and 64A010 airfoil section. A plain trailing edge flap (hinged at 0.70c) is provided to augment the effectiveness of the basic surface. The deflection of the flap is geared to that of the unflapped vane surface in a 1:1 ratio. The entire vane surface is pivoted about its 0.45c point and is mounted between two booms extending from the fan cowl. Other pertinent geometric information for the two vane configurations tested appears in Fig. 4.2-1.

Forces and moments generated by the vane are presented in non-dimensionalized coefficient form:

$$\text{Vane Lift Coefficient, } C_{F_z} = \frac{\text{Lift}}{\text{Installed Gross Thrust}}$$

$$\text{Vane Drag Coefficient, } C_{F_x} = \frac{\text{Drag}}{\text{Installed Gross Thrust}}$$

$$\text{Vane Pitching Moment Coefficient, } C_m = \frac{\text{Pitching Moment}}{\text{Installed Gross Thrust x Vane Chord}}$$

Pitching moments are referenced to the vane pivot point (0.45c); sign convention and reference axis system used to define vane forces and moments are depicted in Fig. 4.2-2.

The majority of the vane effectiveness tests were performed at the maximum thrust setting available which corresponds to a fan pressure ratio of about 1.135. The fan-to-core dynamic pressure ratio at this condition is between 6 and 7.

### 4.2.2 Effect of Vane Location

The effect of vane location is presented in Fig. 4.2-3 and 4.2-4 for the out-of-ground effect and in-ground effect conditions, respectively. For the out-of-ground effect case, the centerline vane location results in symmetrical and higher levels of control effectiveness (Fig. 4.2-3). With the off-center location (designated position 3), effectiveness is not symmetric with respect to deflection. Stall occurs in the vicinity of 25 degrees deflection. For the configuration of Fig. 4.2-4, which represents the aircraft at rest on the deck, the centerline vane location exhibits a more non-linear variation of effectiveness with deflection than the off-center position.

### 4.2.3 Effect of Boom Endplates

An earlier series of subscale vane configuration development tests had indicated the desirability of adding endplates in order to increase levels of vane effectiveness. In view of this, the T-55/Q-Fan static test article was equipped with endplates for the majority of tests. The incremental effects due to the endplates were ascertained by conducting one test run with the endplates removed; the resulting data being shown in Fig. 4.2-5. Although some increase in vane effectiveness is present especially at negative vane deflection angles, it is conjectured that the full benefit of endplating was not realized due to leakage through a gap of 3/8 in. between the vane tip chords and the endplates. This gap allowed flow between the upper and lower vane surfaces, somewhat negating the effectiveness of the endplates.

### 4.2.4 Effect of Power Setting

For the configuration tested (off-center vane location operating out of ground effect) there is no effect of power setting on the levels of vane effectiveness coefficients as may be observed from the data presented in Fig. 4.2-6. This is consistent with subscale test results and demonstrates the utility of normalizing the vane forces with gross thrust.

### 4.2.5 Effect of Ground Proximity

The effect of proximity to ground on the levels of vane control effectiveness coefficients is shown in Fig. 4.2-7 and 4.2-8 for the off-center and centerline vane positions, respectively. For both vane positions tested, ground effects were evident at a ground plane distance of 40 in. from the vane trailing edge. At 60 in. groundplane distance only the off-center location displays a difference in data from the free-air case. The centerline position possesses a more non-linear variation in effectiveness due to the presence of ground than the off-center location (which basically displays zero-lift angle and lift curve slope shifts).

### 4.2.6 Effect of Pitch Attitude

Pitch attitude (in ground effect) has no effect on the levels of vane control effectiveness for the off-center location (Fig. 4.2-9) and only minor effect on the levels for the centerline location (Fig. 4.2-10).

### 4.2.7 Effect of Bank Attitude

Control vane effectiveness is essentially independent of vehicle bank attitude (Fig. 4.2-11 thru 4.2-14). The only differences in effectiveness displayed by the data are minor ones which appeared for the centerline vane position when bank was combined with a pitch attitude of 10° (Fig. 4.2-14).

### 4.2.8 Comparison of Vane Force Balance Measurements and Pressure Measurement For Determination of Vane Forces and Moments

The test vane was instrumented to provide direct strain gauge measurement of the forces and moments as well as spanwise and chordwise pressure measurements which could be integrated to determine the forces and moments.

Thirty nine pressure taps located at three semi-span stations (6%, 36% and 83% of the vane semi-span) measured the pressure distribution across the vane. The chordwise pressures were measured by taps at the leading edge, 5%, 10%, 60%, 72% and 90% of the chord on both upper and lower surfaces. Flap pressures were measured by taps at 72% and 90% of the vane chord.

The results obtained by chordwise and spanwise integrations of the pressure data closely match the force and pitching moment characteristics obtained from direct balance measurements as shown in Table 4.2-1 and illustrated in Fig. 4.2-15 (for run 110). The figure shows that the close correlation is obtained for all vane deflections.

### 4.2.9 Comparison of T-55/Q-Fan and Subscale Test Results

Comparison of an 8 in. fan exit subscale test with results from the T-55/Q-Fan program are shown in Fig. 4.2-16. Considering that data taken at higher deflection angles results in vane stall which is scale sensitive, very reasonable correlation is obtained. Also, subscale data was obtained at a somewhat different value of vane-to-flap gearing ratio. Additional data which more accurately duplicates the vane-to-flap gearing duplicates the data trends at lower values of vane deflection displayed by the T-55/Q-Fan test data.

Table 4.1-1 Summary of Test Program

| TEST NO. | VANE CONFIGURATION | | POWER TURBINE | FAN BLADE | GROUND PLANE CONFIGURATION | | | REMARKS |
|---|---|---|---|---|---|---|---|---|
| | POSITION | DEFL RANGE | SPEED RANGE | ANGLE | DIST FROM VANE T.E. | PITCH ANGLE | ROLL ANGLE | |
| 101-23 | VANE | REMOVED | 15,980, 15,200, 14,400, 12,000 | 52° | 342 IN. | 0° | 0° | BASELINE DATA WITH BOEING INLET |
| 104 | 3 | -30° TO +30° | 15,000 | 56° | 342 IN. | 0° | 0° | ACOUSTIC & STRUCTURAL DYNAMIC DATA ONLY |
| 110 | 3 | -30° TO +30° | 15,000, 13,400 11,400 | 56° | GROUND PLANE REMOVED | -- | -- | HAMILTON STANDARD BELLMOUTH INSTALLED FOR REMAINDER OF PROGRAM |
| 111 | 3 | -30° TO +30° | 15,000 | 56° | 120 IN. | 0° | 0° | |
| 112 | 3 | -30° TO +30° | 15,000 | 56° | 60 IN. | 0° | 0° | CHIP DETECTOR LIGHT-PLANETARY GEAR SYSTEM OVERHEATED |
| 113 | 3 | -30° TO +30° | 15,000 | 56° | 40 IN. | 0° | 0° | |
| 114 | 3 | -30° TO +30° | 15,000 | 56° | 40 IN. | 10° | 0° | |
| 115 | 3 | -30° TO +30° | 15,000 | 56° | 40 IN. | 0° | 7° | |
| 116 | 3 | -30° TO +30° | 15,000 | 56° | 40 IN. | 10° | 7° | |
| 117 | 3 | -30° TO +30° | 15,000 | 56° | 342 IN. | 0° | 0° | END PLATES REMOVED |
| 118 | ℄ | -30° TO +30° | 15,000 | 56° | 342 IN. | 0° | 0° | END PLATES REPLACED |
| 119 | ℄ | -30° TO +30° | 15,000 | 56° | 60 IN. | 0° | 0° | |
| 120-02 | ℄ | -30° TO +30° | 15,000 | 56° | 40 IN. | 0° | 0° | |
| 121 | ℄ | -30° TO +30° | 15,000 | 56° | 40 IN. | 10° | 0° | |
| 122 | ℄ | -30° TO +30° | 15,000 | 56° | 40 IN. | 0° | 7° | SOME FAN SPEED HUNTING & INLET VORTICES SEEN |
| 123 | ℄ | -30° TO +30° | 15,000 | 56° | 40 IN. | 10° | 7° | CONSIDERABLE FAN SPEED HUNTING & INLET VORTEX ACTIVITY |

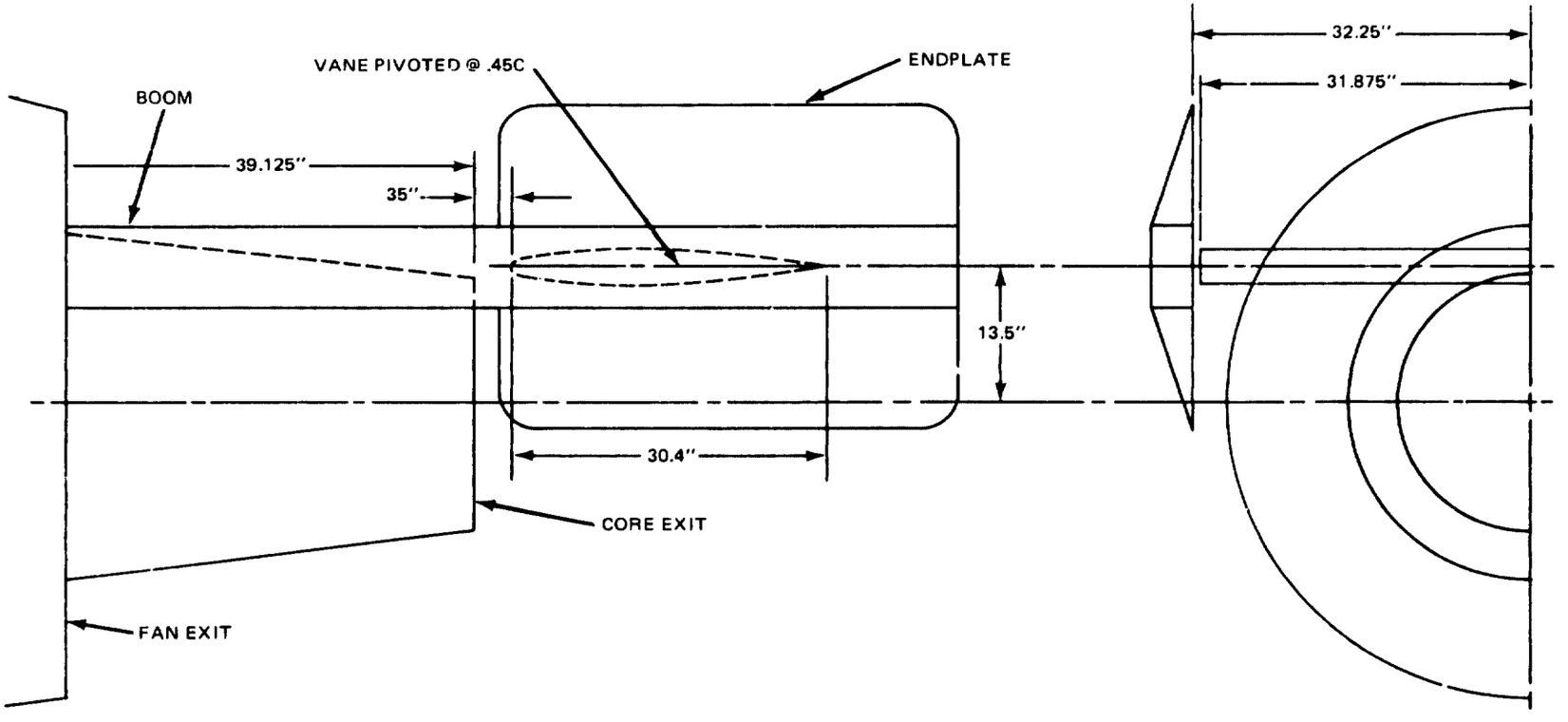


NOTE: ONLY OFF-CENTER (POSITION 3) LOCATION SHOWN FOR CLARITY, FOR CENTERLINE LOCATION VANE, BOOM AND ENDPLATE LOWERED 13.5 INCHES

**Fig. 4.2-1 Test Article Geometry**

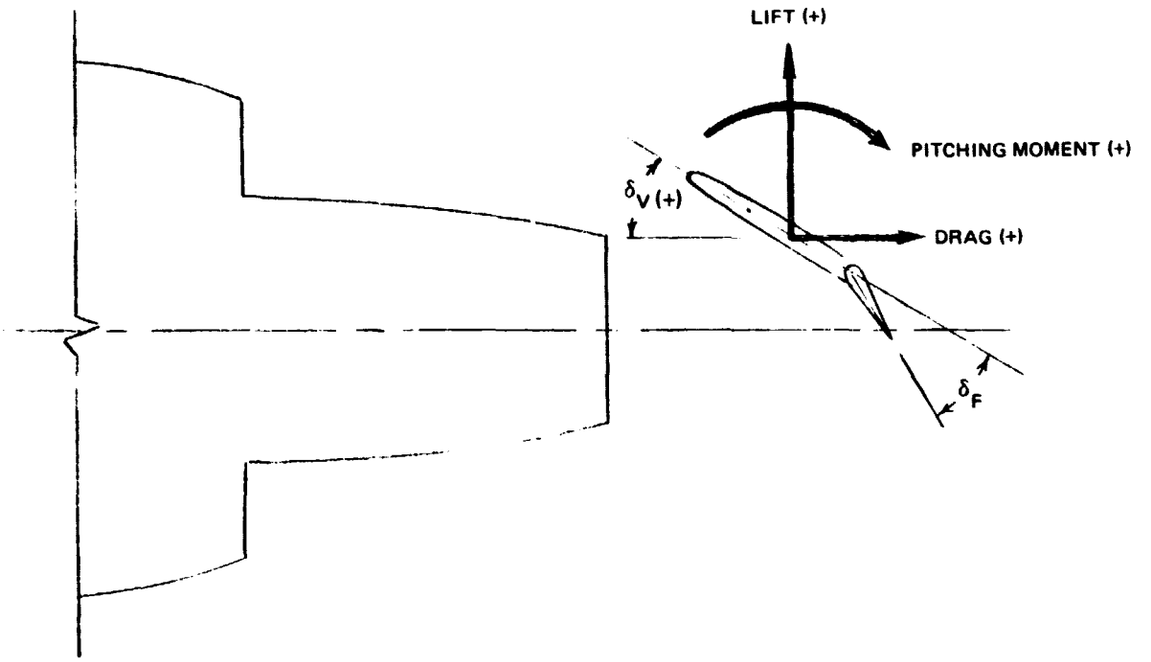


**Fig. 4.2-2 Control Vane Force & Moment Definition**

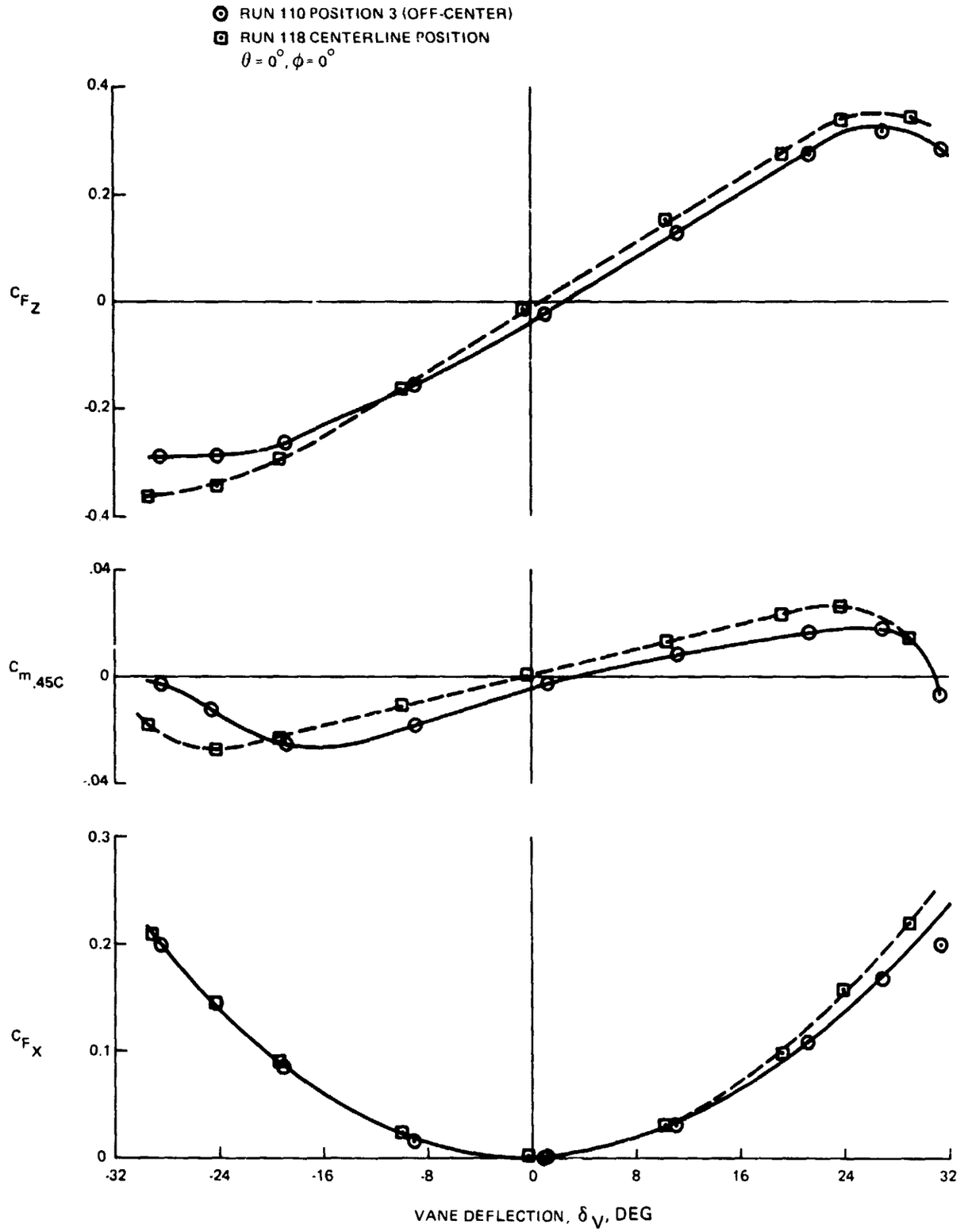


1639-015

**Fig. 4.2-3 Effect of Vane Location Out of Ground Effects**

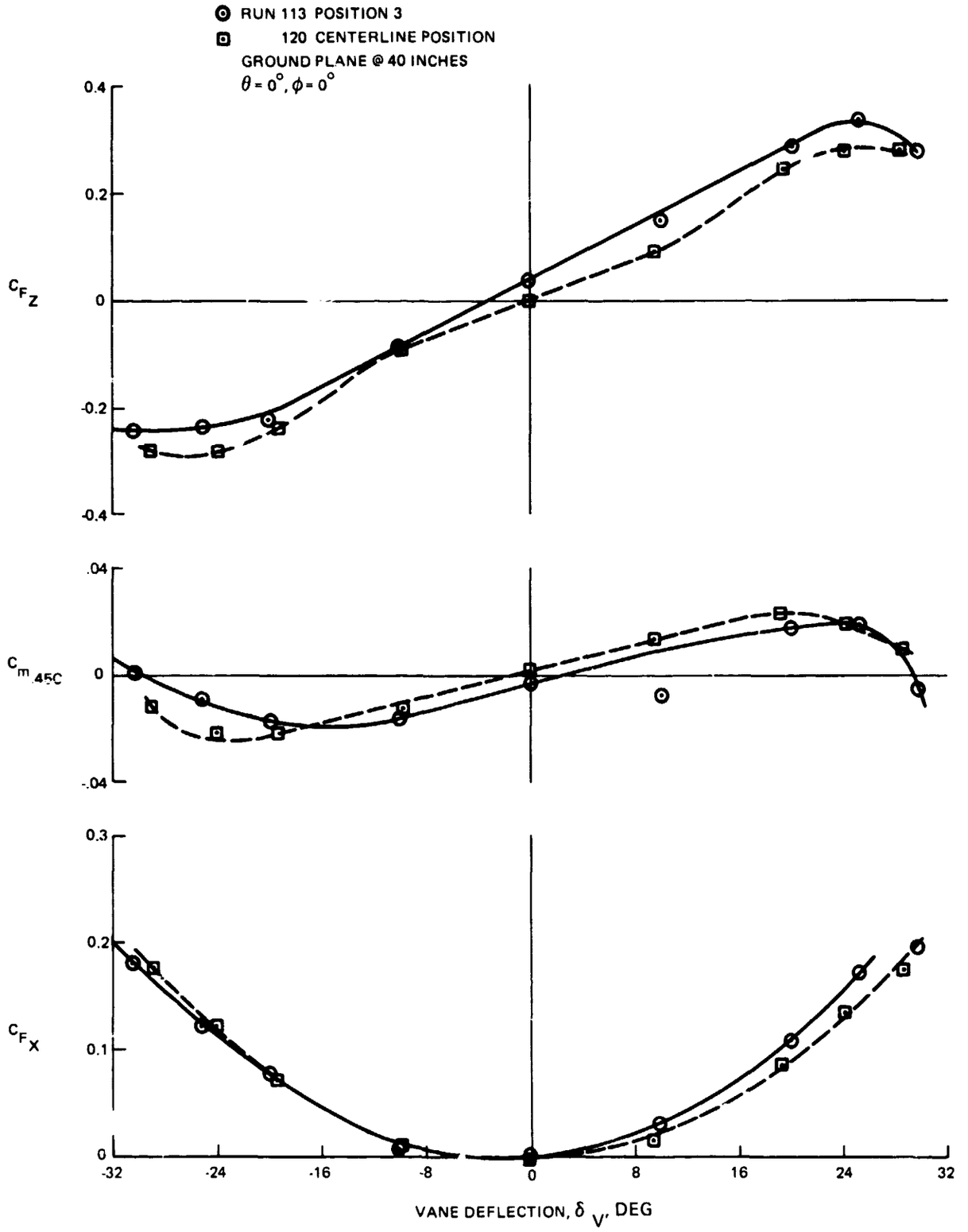


Fig. 4.2-4 Effect of Vane Location in Ground Effect

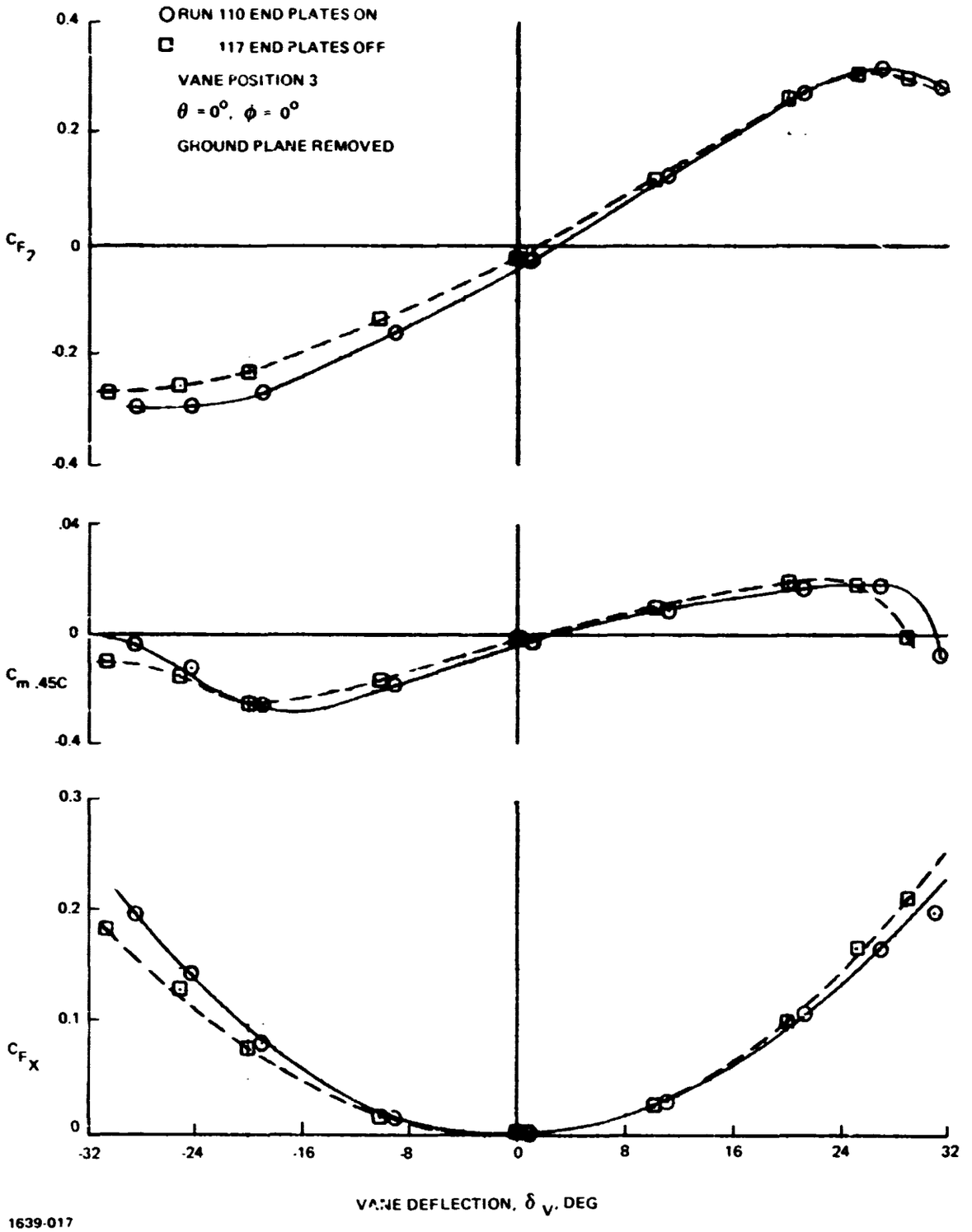


Fig. 4.2-5 Effect of Boom Endplates Off-Center Vane Position.

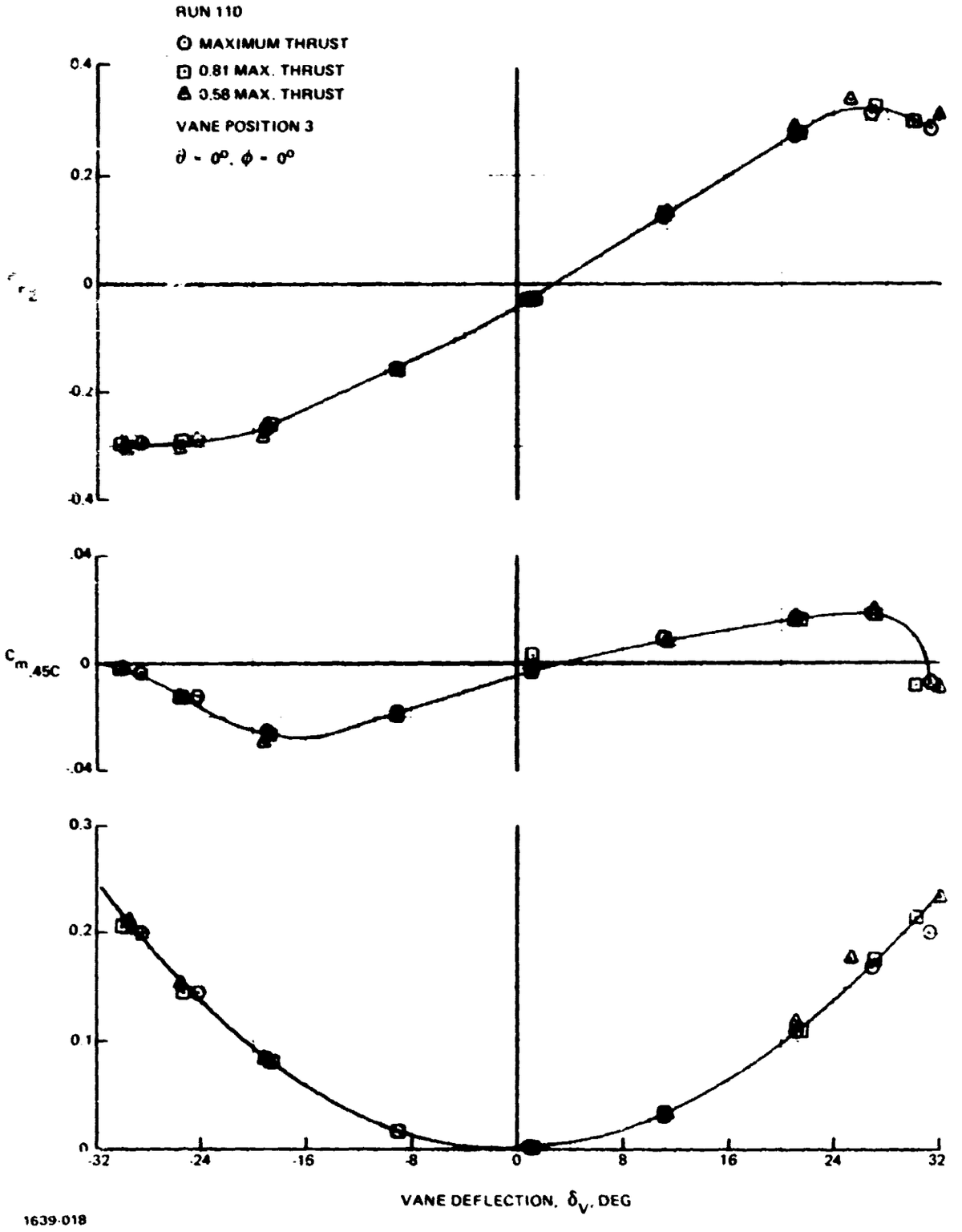


Fig. 4.2-6 Effect of Power Setting Off-Center Vane Position

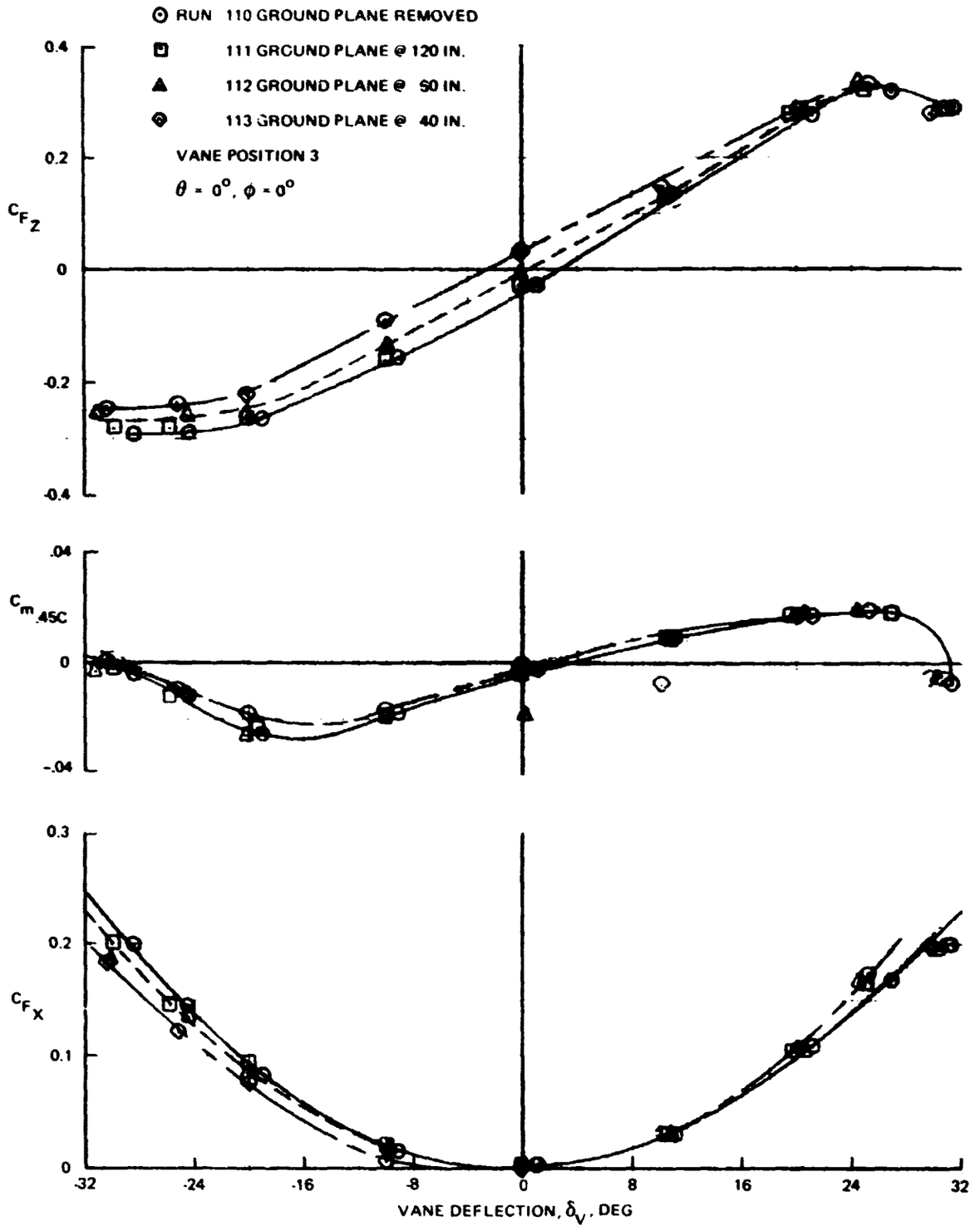


1639-019

**Fig. 4.2-7 Effect of Ground Proximity Off-Center Vane Position**

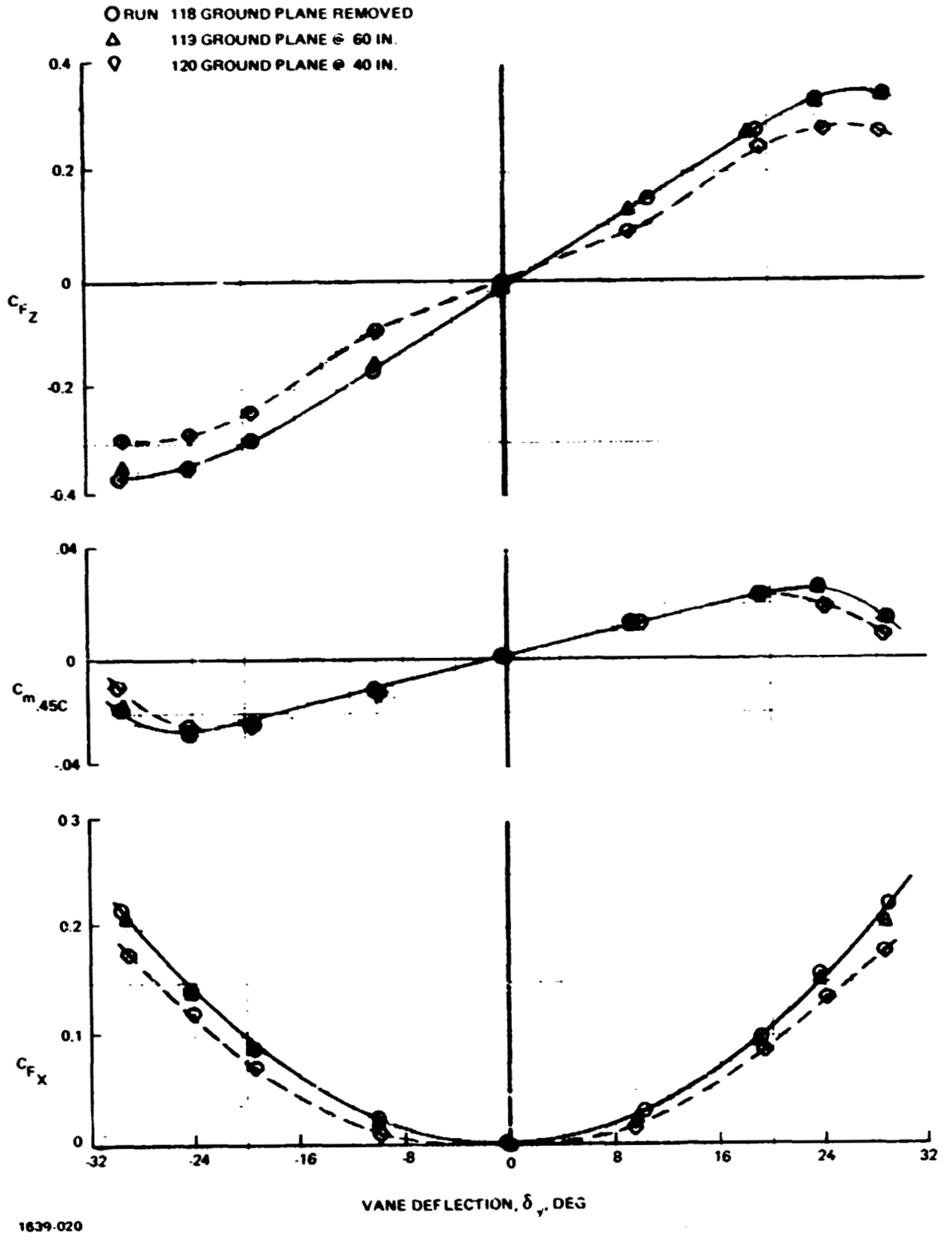


Fig. 4.2-8 Effect of Ground Proximity Center Line Vane Position

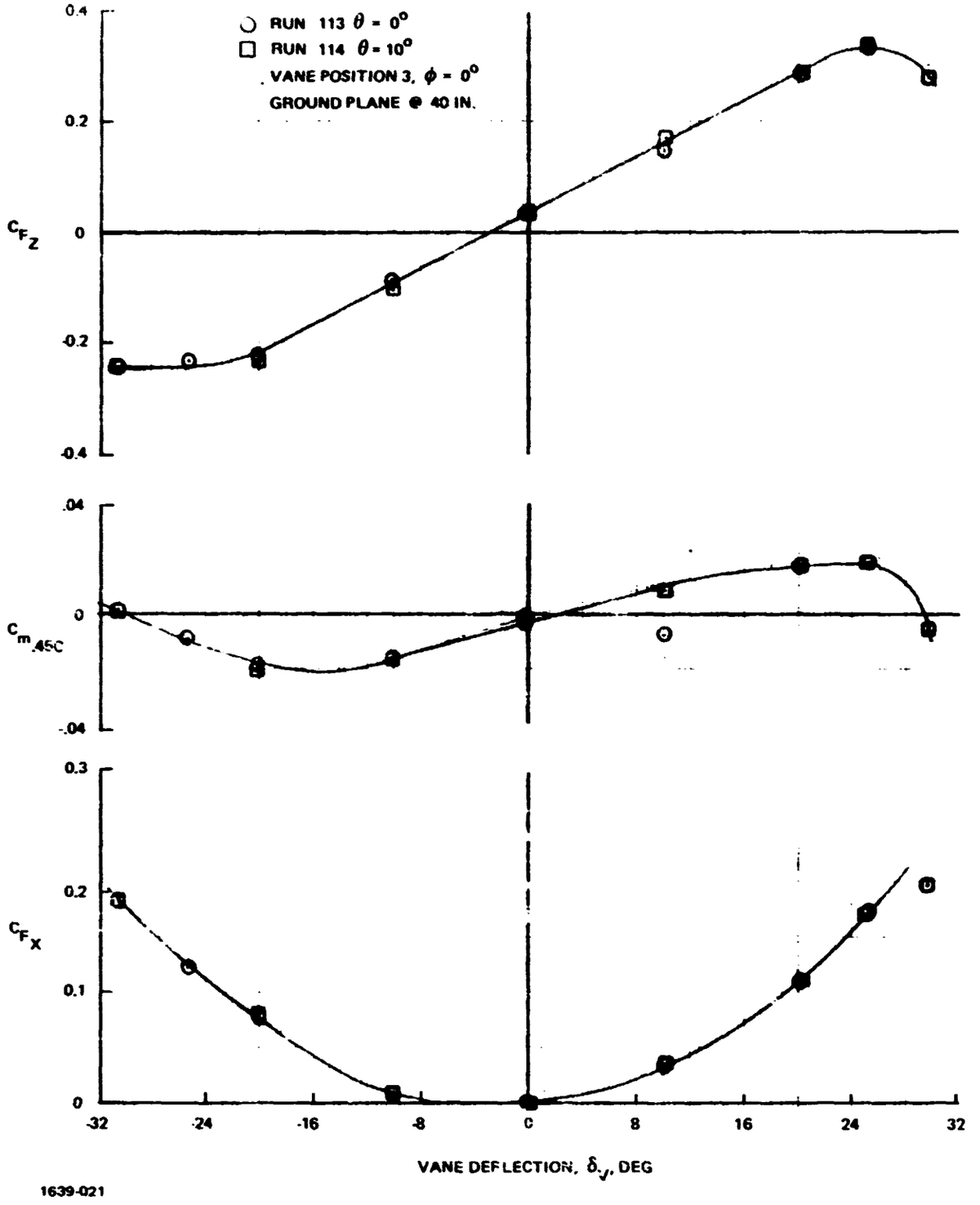


Fig. 4.2-9 Effect of Pitch Attitude Off-Center Vane Position

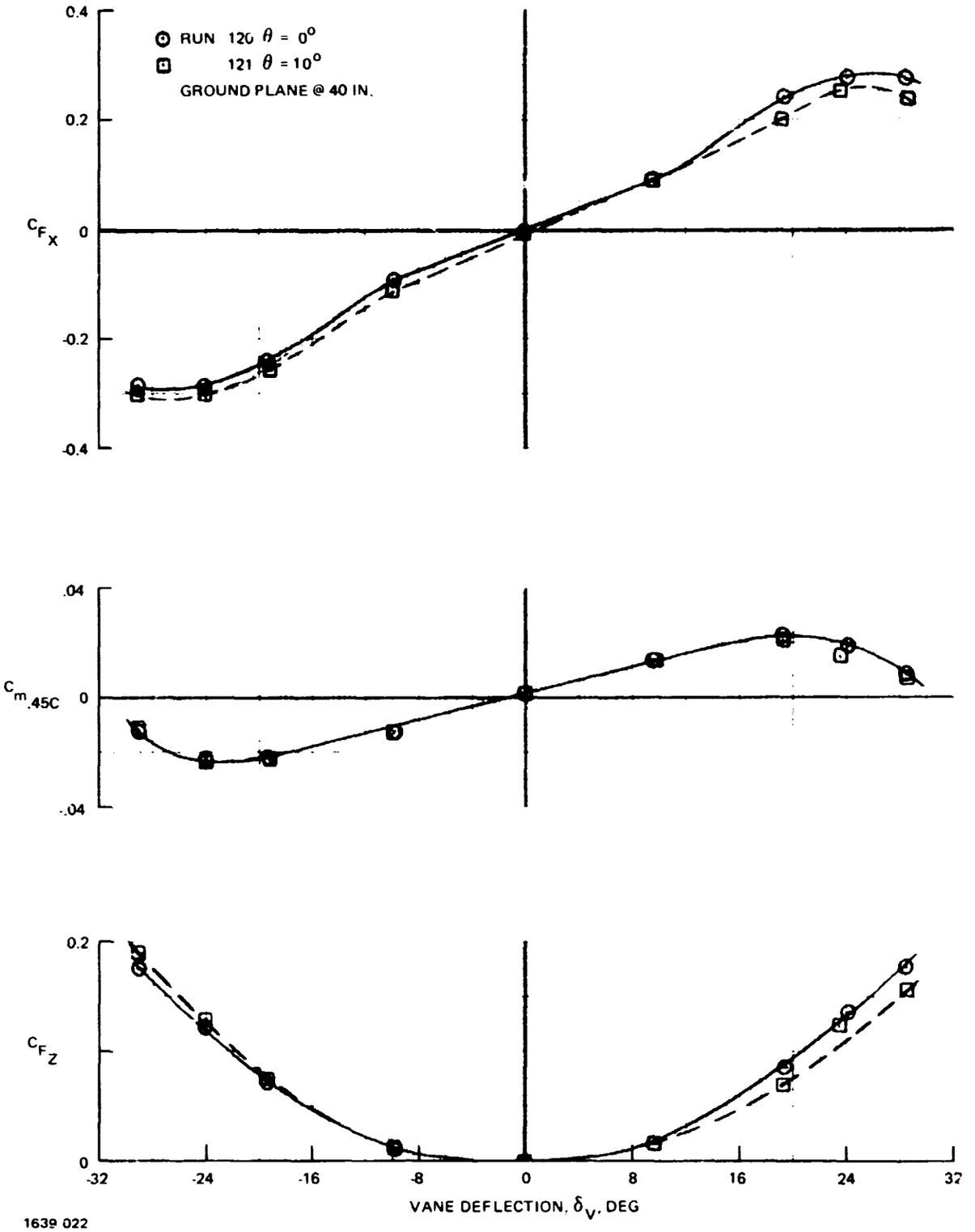


Fig. 4.2-10 Effect of Pitch Attitude Center Line Vane Position

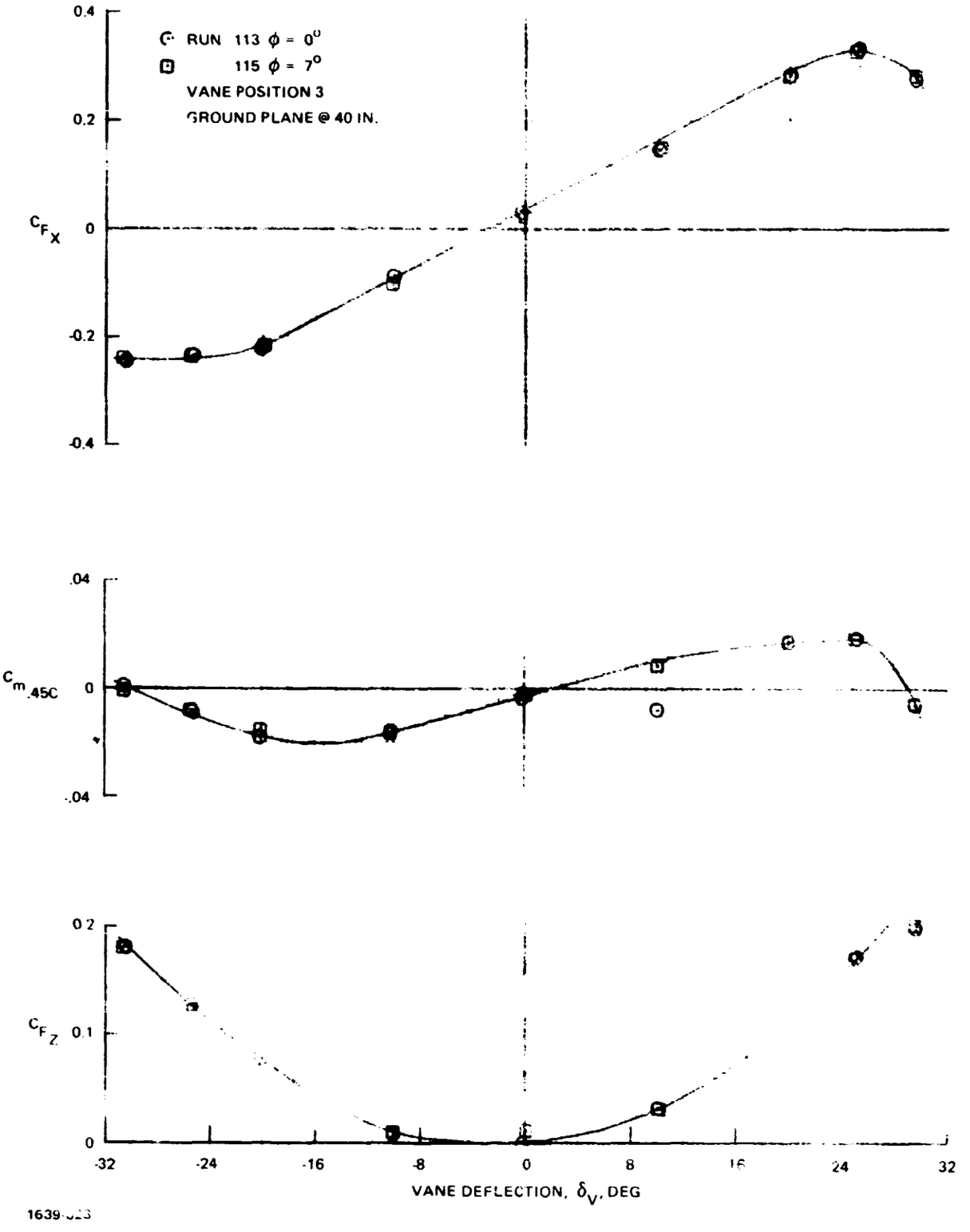


Fig. 4.2-11 Effect of Bank Attitude at $\theta = 0^{\circ}$ Off-Center Vane Position

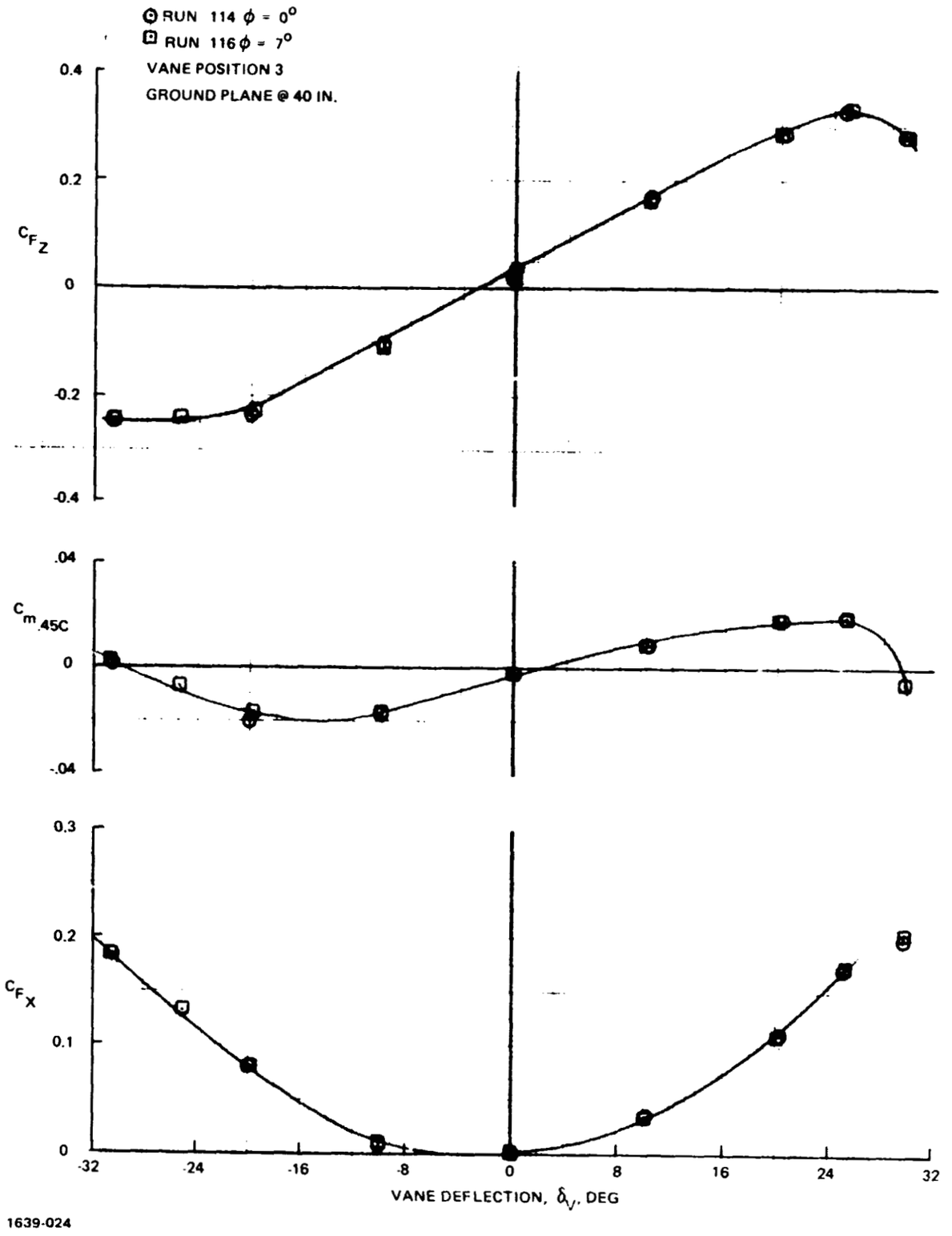


Fig. 4.2-12 Effect of Bank Attitude at $\theta$ = 10° Off-Center Vane Position

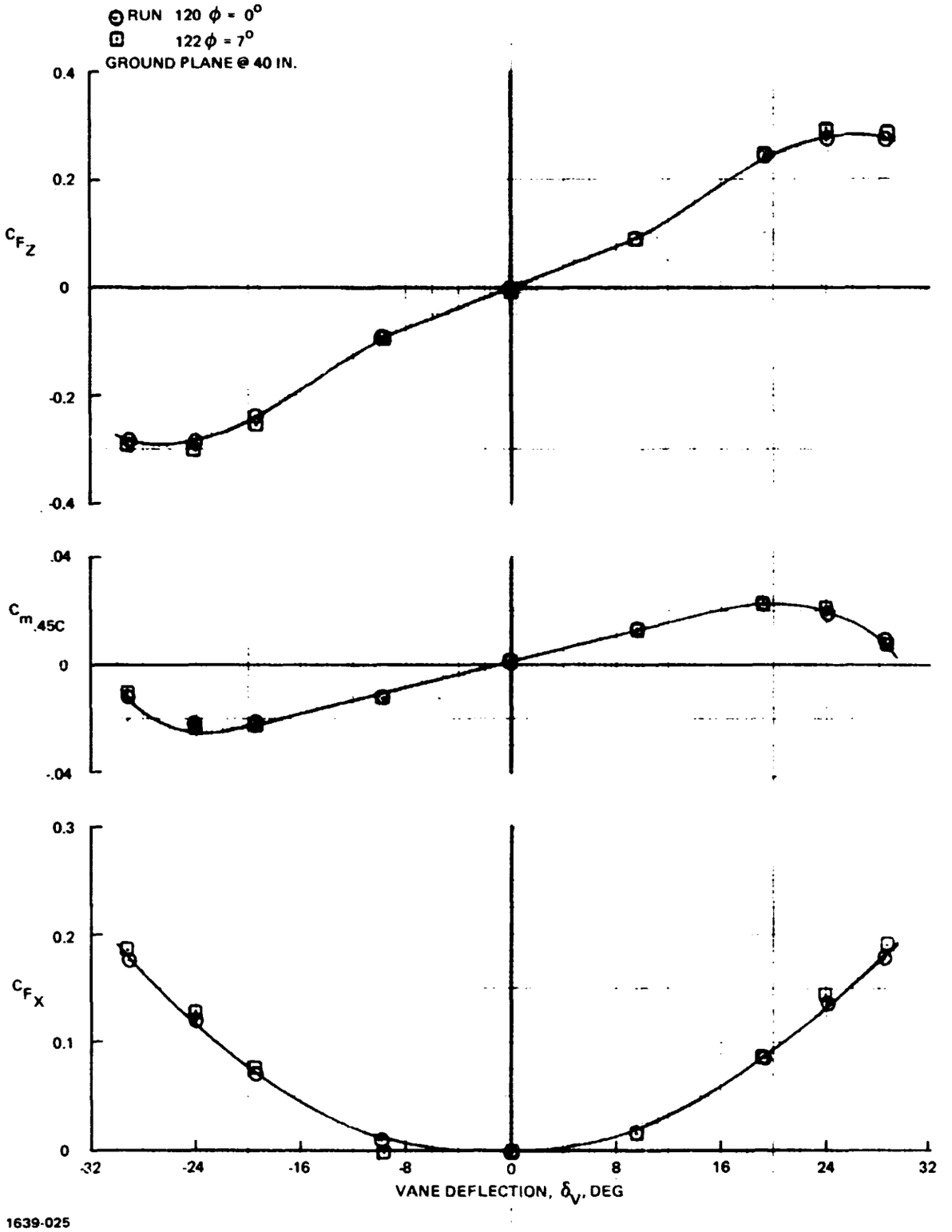


**Fig. 4.2-13 Effect of Bank Attitude at $\theta = 0^\circ$ Centerline Vane Position**

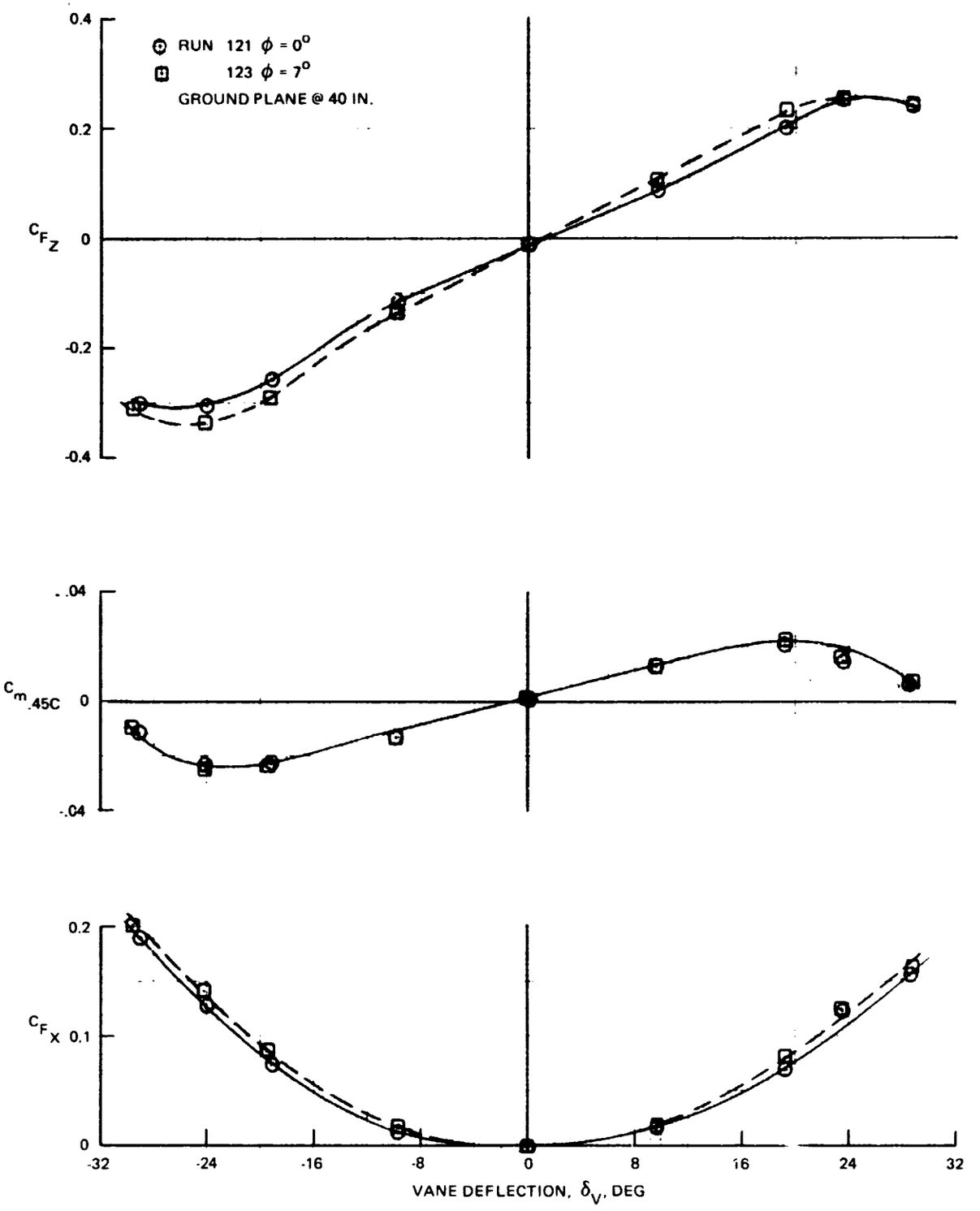


**Fig. 4.2-14 Effect of Bank Attitude at $\theta$ = 10° Centerline Vane Position**

**Table 4.2-1 T55/Q-Fan Vane Characteristics, Comparison of Force & Moment Coefficients Obtained from Pressure & Force Measurements**

| RUN NO. | VANE DEF, DEG | VANE POS | END PLATES | GROUND PLANE, IN. | $C_{FZ}$ | | $C_{FX}$ | | $C_{M.45}$ | |
|---|---|---|---|---|---|---|---|---|---|---|
| | | | | | PRESS | BAL | PRESS. | BAL | PRESS | BAL |
| 110 | 11 | 3 | ON | 324 | 0.1127 | 0.125 | 0.0298 | 0.0310 | 0.0024 | 0.0092 |
| 110 | 21 | 3 | ON | 324 | 0.257 | 0.275 | 0.1317 | 0.110 | 0.0098 | 0.017 |
| 110 | 26 | 3 | ON | 324 | 0.305 | 0.317 | 0.1951 | 0.168 | 0.0144 | 0.018 |
| 110 | 31 | 3 | ON | 324 | 0.251 | 0.285 | 0.2181 | 0.201 | -0.0057 | -0.007 |
| 117 | 20 | 3 | OFF | 324 | 0.264 | 0.264 | 0.1252 | 0.1031 | 0.0128 | 0.0197 |
| 118 | 19 | ℄ | OFF | 324 | 0.271 | 0.277 | 0.1196 | 0.0985 | 0.0208 | 0.0235 |

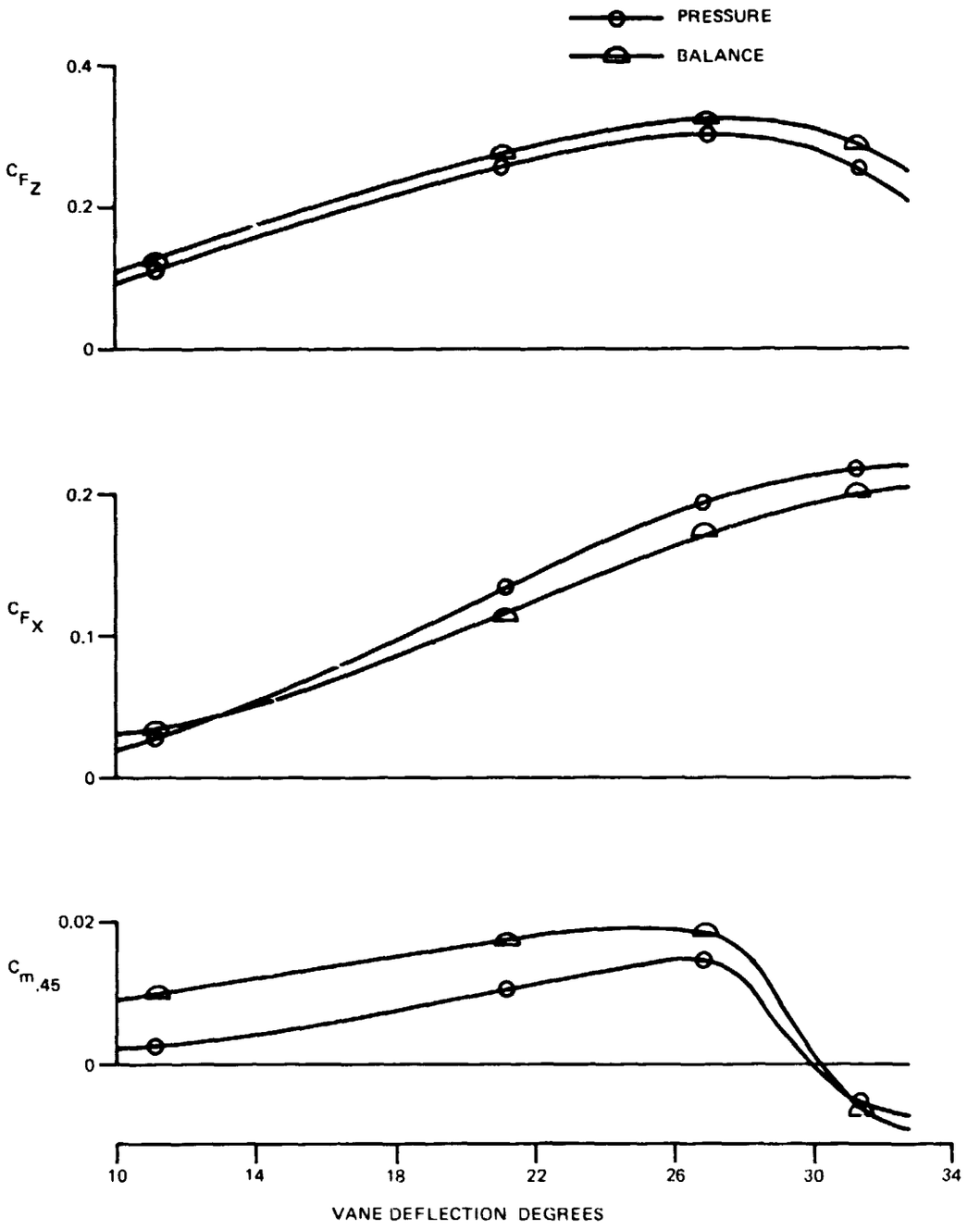


1639-027

**Fig. 4.2-15 VSTOL Q-Fan Vane Characteristics Pressure Integration vs Balance, Run 110**

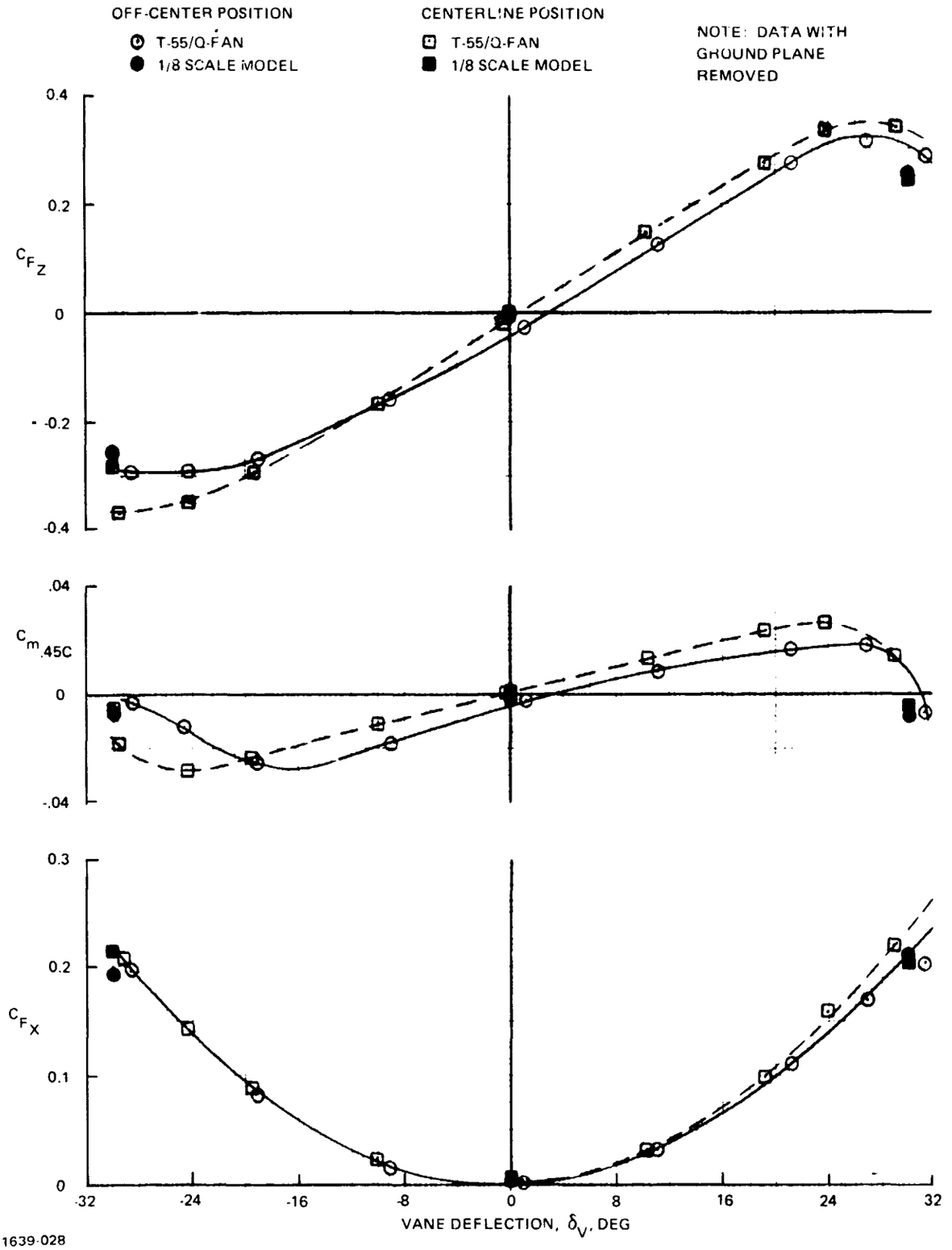


**Fig. 4.2-16 Comparison With 1/8 Scale Model Test Data**

## 4.3 PROPULSION ANALYSES

### 4.3.1 Effects of Vane and Ground Plane on Exhaust Nozzle Exit Pressures

An objective of the test was to determine the effects of vane orientation and ground plane separation distance on fan and engine nozzle exit pressures. A back pressure imposed upon the exit plane of either the fan or engine exhaust nozzle may degrade fan gross thrust, and will reduce turbine output power. Measurements of fan and engine nozzle exit static pressures were taken to determine the magnitudes of the back pressures felt by the nozzles due to the presence of the vane at various deflection angles and to ground plane proximity. The data show that no adverse effects on engine power output or measured total thrust are discernible over the full range of back pressures that were generated by the slipstreams flowing over the vane and ground plane. The highlights of these measurements are presented in the following paragraphs. The pressures are presented in the form of a coefficient consisting of the average pressure rise above ambient non-dimensionalized by fan nozzle exit dynamic pressure.

4.3.1.1 Effect of Vane Proximity and Deflection Angle - Nozzle exit pressure coefficients measured with the vane removed and the ground plane at maximum separation distance (6.0 fan nozzle exit diameters downstream of the vane trailing edge) were as follows:

| Total Thrust, lb | | Fan Nozzle Exit Press Coef, $C_{p_f}$ | Engine Nozzle Exit Press Coef, $C_{p_f}$ |
|---|---|---|---|
| 6912 | | 0.159 | 0 |
| 6018 | | 0.153 | 0 |
| 5524 | | 0.134 | 0 |
| 5515 | | 0.149 | 0 |
| 4871 | | 0.152 | 0 |
| 3375 | | 0.160 | 0 |
| | Average = | 0.151 | |

Within data accuracy both coefficients have constrant values over the full range of thrust. The fan nozzle exit pressure coefficient is positive because the fan exit static pressures were measured by the fan nozzle exit rake which, with the Boeing fan nozzle in place, is located $1\frac{1}{2}$ ft upstream of the nozzle exit plane.

Figure 4.3-1 presents fan nozzle exit pressure coefficient as a function of vane deflection angle with the vane in the offset position 3 and the ground plane removed. The measurements cover a thrust range of 58% to 100% of maximum attainable. The coefficient is independent of thrust level and vane deflection angle and is of the same level as that measured with the vane removed. Figure 4.3-2 shows the same type of results obtained with the vane on the center line position, the ground plane at the maximum separation distance ($x/D_N = 6.0$) and with the engine running at maximum thrust. It is seen that the fan nozzle exit pressure is unaffected by vane proximity, location or deflection angle.

Figure 4.3-3 and 4.3-4 present the engine nozzle exit pressure coefficients in the same format and for the same power levels and vane and ground plane geometries. The coefficient is seen to non-dimensionalize well with fan nozzle dynamic pressure over the range of thrust levels tested (Fig. 4.3-3). The engine nozzle exit pressure, unlike that of the fan nozzle, is seen to be significantly influenced by vane position and deflection angle. The offset vane position 3 produces an unsymmetric curve of $C_{p_e}$ vs. vane deflection angle with $C_{p_e} = 0$ at 2.5° deflection (where the force data shows zero vane lift; (Fig. 4.2-3) and again at -22°. The coefficient is negative in the range of deflection angles of +2.5° to -22°, suggesting a small increase in power turbine output power and fan and engine gross thrust in this range.

With the vane in the centerline position the coefficient is always positive and varies symmetrically with vane deflection angle. At zero deflection, the vane produces a back pressure of approximately 4% of the dynamic pressure at the fan nozzle exit.

4.3.1.2 Effect of Ground Plane Proximity - The combined effects of ground plane proximity, vane position and vane deflection angle on the fan nozzle exit pressure coefficient are shown in Fig. 4.3-5 and 4.3-6. The coefficient is presented as a function of ground plane-to-vane trailing edge separation distance ($X/D_N$) for both the offset and center line vane positions and for vane deflection angles of 0° and +30°. The data were taken at max. thrust and the ground plane was at 0° pitch and roll angles. The coefficient is seen to be constant for all situations and at the same value as that obtained with the vane removed and the ground plane at max. separation distance. Consequently it may be concluded that the fan nozzle experienced no measurable back pressure with any combination of vane position, deflection angle and ground plane separation distance within the ranges tested.

Figures 4.3-7 and 4.3-8 show the effect of the same variations of vane and ground plane geometries on the engine nozzle exit pressure coefficient. These data were also taken at maximum thrust level and with the ground plane at roll and pitch angles of 0°.

With vane deflection angles of 0° and 30°, the contribution to nozzle back pressure due to ground plane proximity vanishes at a separation distance of $X/D_N > 3.0$. These data also show that vane deflection angle is a more powerful contributor to engine-nozzle back pressure than ground plane proximity because the increment in back pressure due to maximum change in vane deflection is $(\Delta C_{p_e})_{\delta V_{max.}} \approx 0.25$ (Fig. 4.3-3 and 4.3-4) while the increment due to maximum change in separation distance is $(\Delta C_{p_e})_{X/D_{N_{max.}}}$ 0.1 (Fig. 4.3-7).

Figure 4.3-9 shows that the back pressure produced by vane deflection had no discernible effect on fan or engine performance. It treats the worst back pressure situation encountered, i.e., the vane located on the engine centerline and the ground plane located at minimum separation distance ($X/D_N$ 0.70). These data show that within experimental accuracy, total thrust measured by the thrust stand, shaft horsepower and power turbine inlet temperature all remained constant over the full range of vane deflection angles and resulting engine nozzle exit pressure coefficients.

4.3.2 Comparison of Thrust Measurement Results

Analysis and application of the measured values of the forces and moments acting upon the attitude control vane require that these measurements be converted to coefficient form by non-dimensionalizing the forces with measured gross thrust and the moments with the product of measured thrust and vane chord length. The Q-Fan T55 nacelle (but not the vane) was mounted on a thrust measurement stand and the fan and engine nozzles were equipped with pressure and temperature rakes, therefore two methods for measuring total nacelle thrust were available. The thrust measured by the thrust stand was used to non-dimensionalize the vane data because it was considered to be the more accurate method and because it was the easiest to apply. The total gross thrust values obtained with the two techniques are compared in Fig. 4.3-10 and 4.3-11.

The total thrust measured with the thrust stand and corrected to standard day ($F_{g_{total}}$ $\delta$) is compared with the sum of the corrected fan and engine gross thrusts. The corrected fan gross thrust was determined analytically from the pressure and temperature measurements obtained with the two fan nozzle exit rakes. The engine gross thrust was determined from the engine manufacturer's performance specification (Reference 6) because the engine nozzle rakes failed early in the test program.

Figure 4.3-10 compares the corrected thrustmeter and calculated values of corrected total thrust obtained with the Boeing inlet, the vane removed and the ground plane at the maximum attainable separation distance of $X/D_N$ 6.0. The data points for the four thrust levels tested are within ±2% of the true thrust level.

Figure 4.3-11 shows the same type of data obtained with the Hamilton Standard bell mouth in place of the Boeing inlet, the vane in position 3 and the ground plane removed. The majority of the data points fall within the ±2.0% error band and the scatter pattern suggests random error in both methods of determining thrust rather than consistent bias in either.

4.3.3 Effect of Inlet Vortex on Fan Speed at Constant Power

A unique combination of ambient air conditions coupled with operation without benefit of a governor controlling fan speed caused an intermittent fan speed hunting problem that is worthy of mention.

The photograph of Fig. 4.3-12 shows the core of an extremely transient vortex that sprung into the inlet from a point at the base of the test stand. This fortuitous picture, which was obtained during the very last run of the program, provides a qualitative explanation for the fan speed hunting problem that defied explanation throughout the program, despite the expenditure of a good deal of diagnostic measurement effort.

The core of the votex was made visible by ambient water vapor that condensed when the adiabatic expansion within the core produced the required super-saturation temperature level. This condensation phenomenon, which commonly occurs in transonic atmospheric wind tunnels, requires a local Mach number in excess of 0.8 when the ambient relative humidity is at a typical value of 60% (Reference 7). In this light, it is apparent that the overall diameter of the vortex was considerably larger than the visible portion of the core and the vortex therefore influenced the flow field over a significant portion of the fan face area. The onset and duration of a single vortex were very fleeting, requiring a sharp eye and a fast shutter speed to discern it. Its net effect was to cause a momentary change in fan loading and a consequent short duration excursion in fan speed.

Fan speed excursions put in an appearance early in the program. Oscillograph data showed that the excursions, which were of approximately ±2.5%, occurred at a somewhat irregular low frequency (approximately 10 to 20 cycles per minute) and were not caused by variations in fan blade angle or input shaft horsepower. Furthermore, the phenomenon seemed to occur only on certain days.

A conference with Hamilton Standard personnel lead to the conclusions that ingestion of ambient turbulence shed from nearby buildings might be the cause and that the high throat velocity of the Boeing inlet might be an aggravating factor. The Boeing inlet was replaced by a Hamilton Standard bellmouth and a smoke generator was used in an

attempt to monitor the inlet flow field. From this point until the very last hour of testing the watched pot did not boil - fan speed remained constant, the inlet flow field appeared to be undisturbed (Fig. 4.3-13) and the desired steady-state data reported herein were acquired. At the last hour, fleeting inlet vortex activity became visible and fan speed hunting returned.

Review of the data in light of the correlation of fan speed hunting with the presence of inlet vortex activity revealed that the hunting only occurred while running with a tail wind. This leads to the inference that turbulence shed by the test stand support structure was the triggering mechanism for the sporadic formation of the vortices which in turn caused corresponding excursions in fan loading and hence fan speed.

It should be noted that all testing was done with fixed blade angle and with no automatic control of fan speed. If blade angle had been under control of a governor, the 100° /sec blade slewing rate capability of the Q-Fan very likely would have reduced the fan speed excursions to an insignificant level. Furthermore, if the inlet vortex should produce objectionable blade stress levels on a future installation, the vortex can be readily destroyed as is done on the Boeing 737 when fitted for operation from unpaved runways (Reference 8).

4.3.4 Q-Fan Blade Stress Measurements

Blade numbers 1, 6 and 7 were instrumented with strain gages which measured bending stresses continuously. Hamilton Standard personnel recorded these measurements on magnetic tape and also monitored them on an oscillograph during each test. The following summary of the post test analysis of these data is quoted from Hamilton Standard's letter report to Grumman of 25 July, 1977.

"At no time during the acquisition of data for the Grumman test were the vibratory blade stress limits of ±5500 psi exceeded. During some of the testing, there appeared to be points where blade overstress may have occurred. However, when this data was played back on a spectrum analyzer, it was obvious that electrical interference caused the spiking indications. Inspection of the data tabulated from the stress recordings allows the following conclusions:

1. Throughout the test, blade stresses ranged from 400-2100 psi
2. Blade stresses were generally 300-400 psi lower with the Hamilton Standard Bellmouth vs the Boeing/Ames fixed lip inlet

3. Ground effect location or pitching and rolling of the ground plane did not influence blade stressing

4. Stress components were mostly 1P, 2P, and 3P which is typical for this propulsor

5. The first flatwise blade mode occurred at approximately 112 Hz, again typical for the fan

6. Votices which were visible during the final day of testing increased the blade stresses generally 1000 psi above those reported in item 1 above.

Inspection of the blades following the test revealed no structural abnormalities."

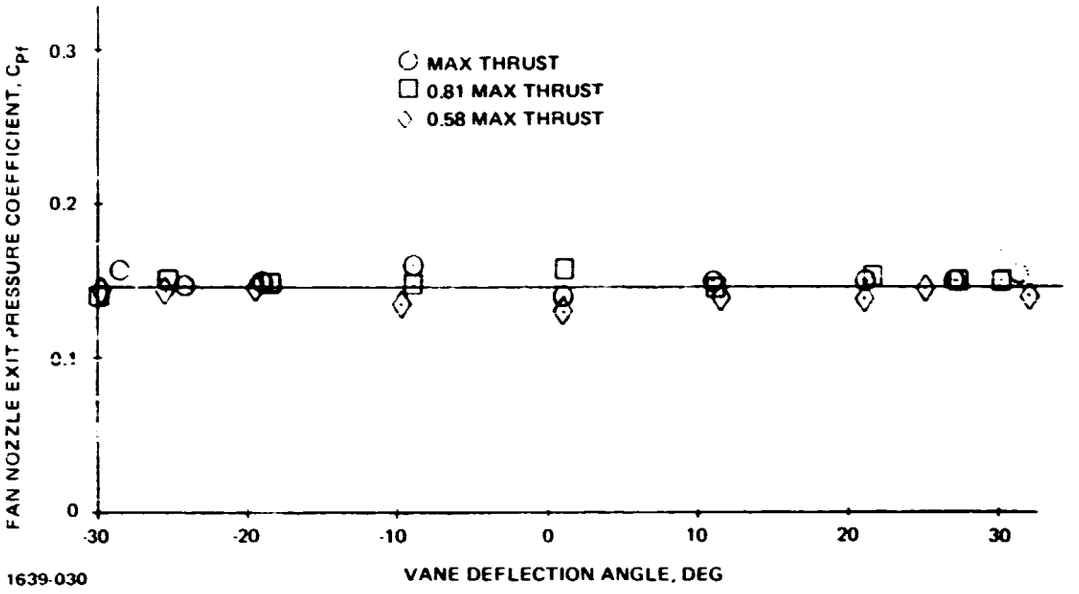


**Fig. 4.3-1 Effects of Vane Deflection on Fan Nozzle Exit Pressure Coefficient , Vane Position 3, Ground Plane Removed**

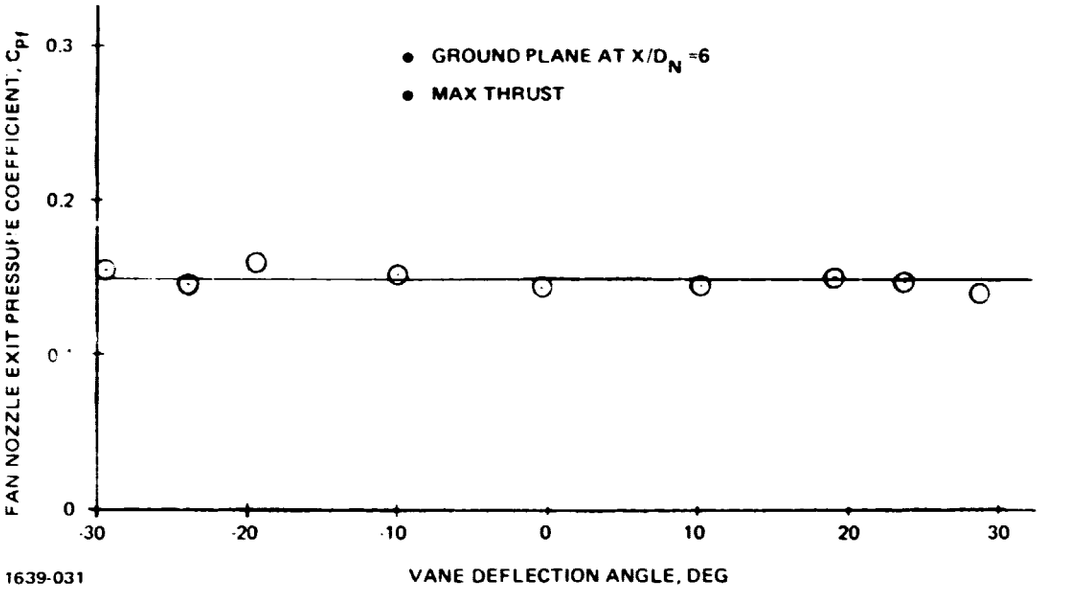


**Fig. 4.3-2 Effect of Vane Deflection on Fan Nozzle Exit Pressure Coefficient, Vane Position Centerline**

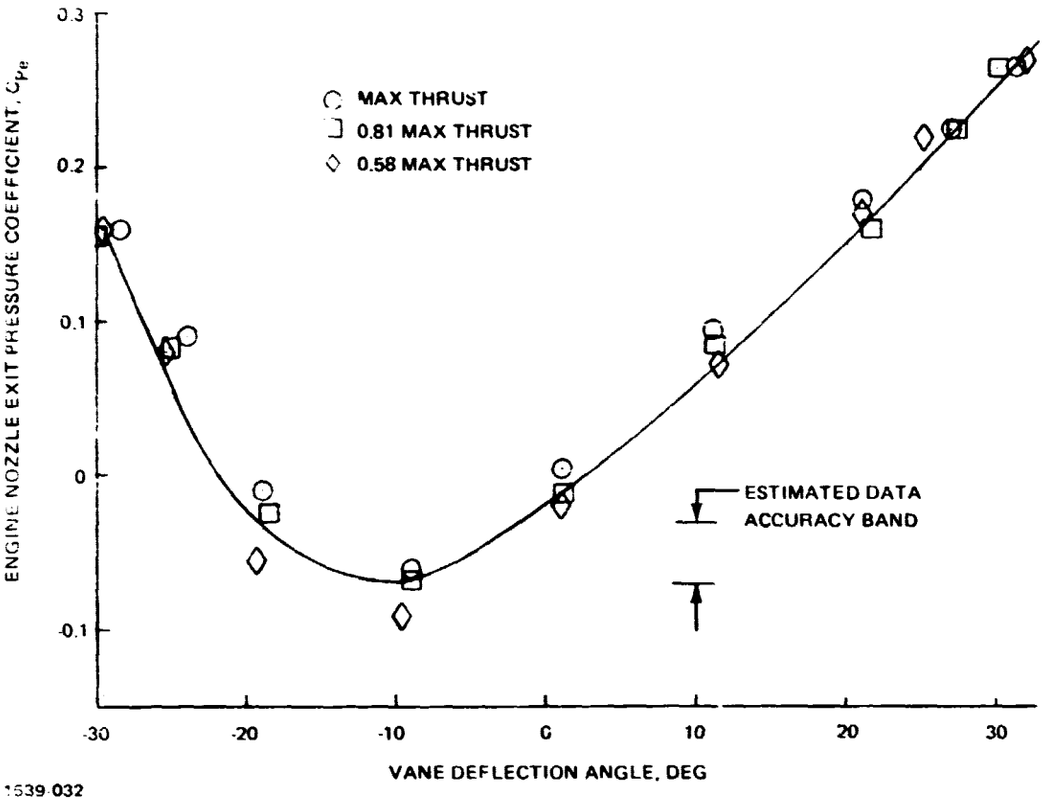


**Fig. 4.3-3 Effect of Vane Deflection on Engine Nozzle Exit Pressure Coefficient, Vane Position 3, Ground Plane Removed**

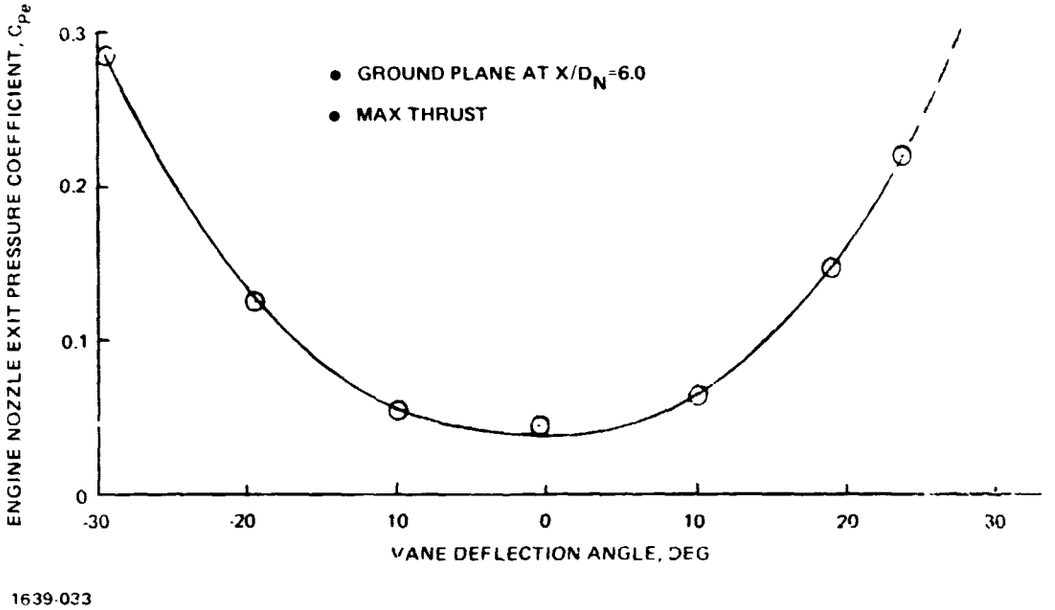


**Fig. 4.3-4 Effect of Vane Deflection on Engine Nozzle Exit Pressure Coefficient, Vane Position Centerline**

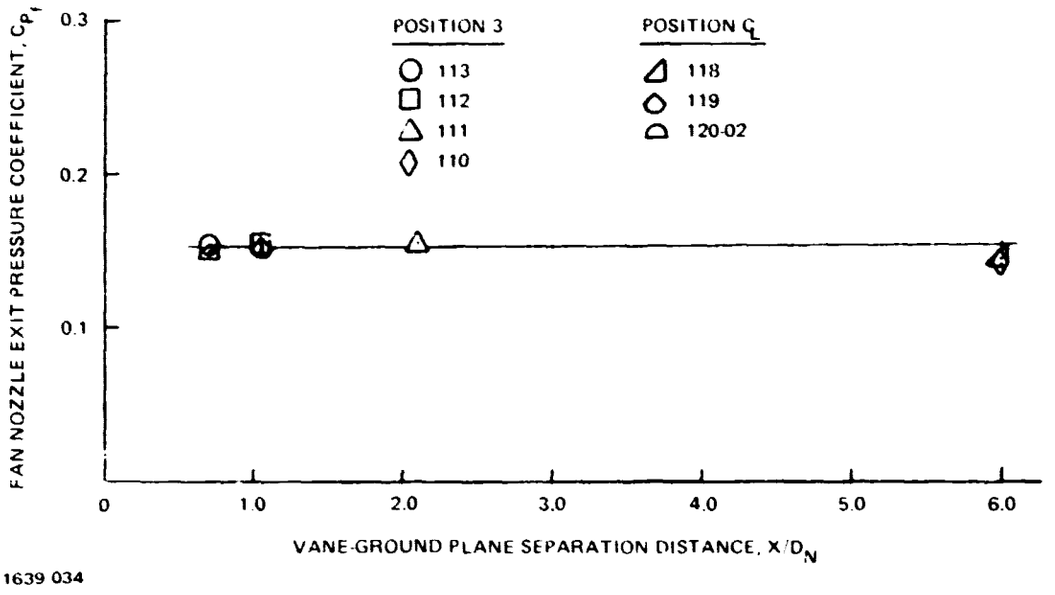


**Fig. 4.3-5 Effect of Ground Plane Separation Distance on Fan Nozzle Exit Pressure Coefficient, Vane Deflection Angle = $0^o$**

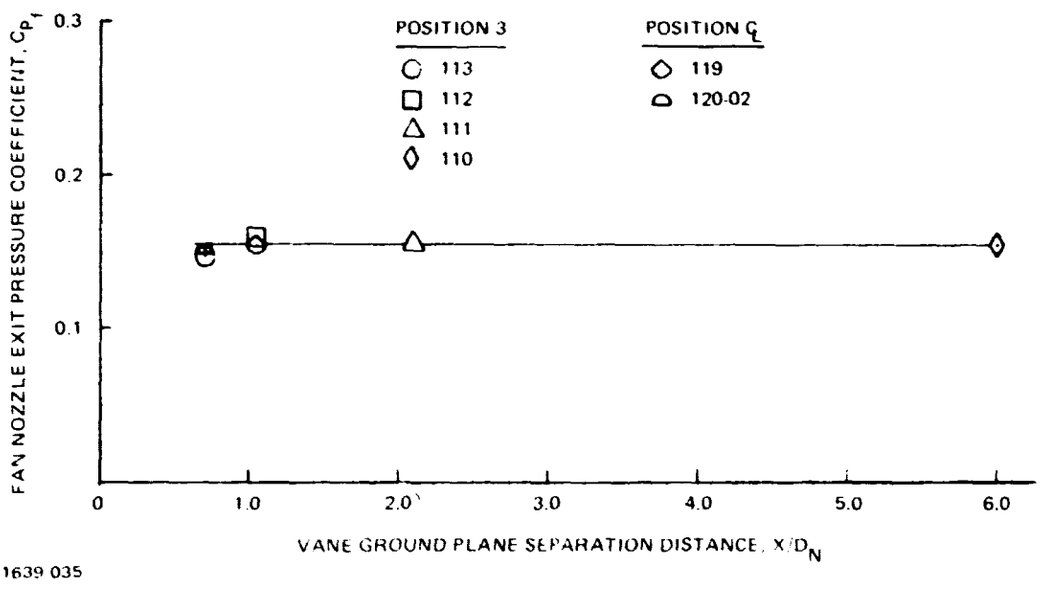


**Fig. 4.3-6 Effect of Ground Plane Separation Distance on Fan Nozzle Exit Pressure Coefficient, Vane Deflection Angle = $30^C$**

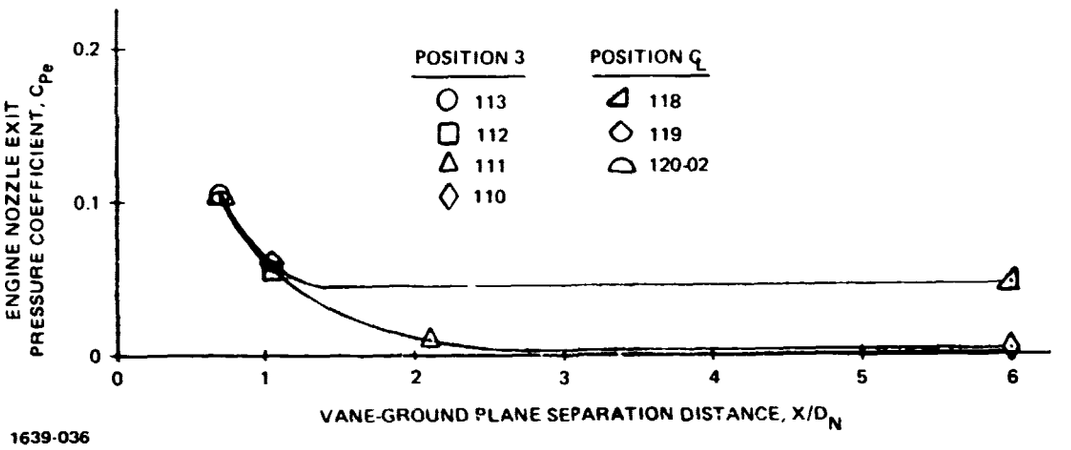


**Fig. 4.3-7 Effect of Ground Plane Separation Distance on Engine Nozzle Exit Pressure Coefficient, Vane Deflection Angle = 0°**

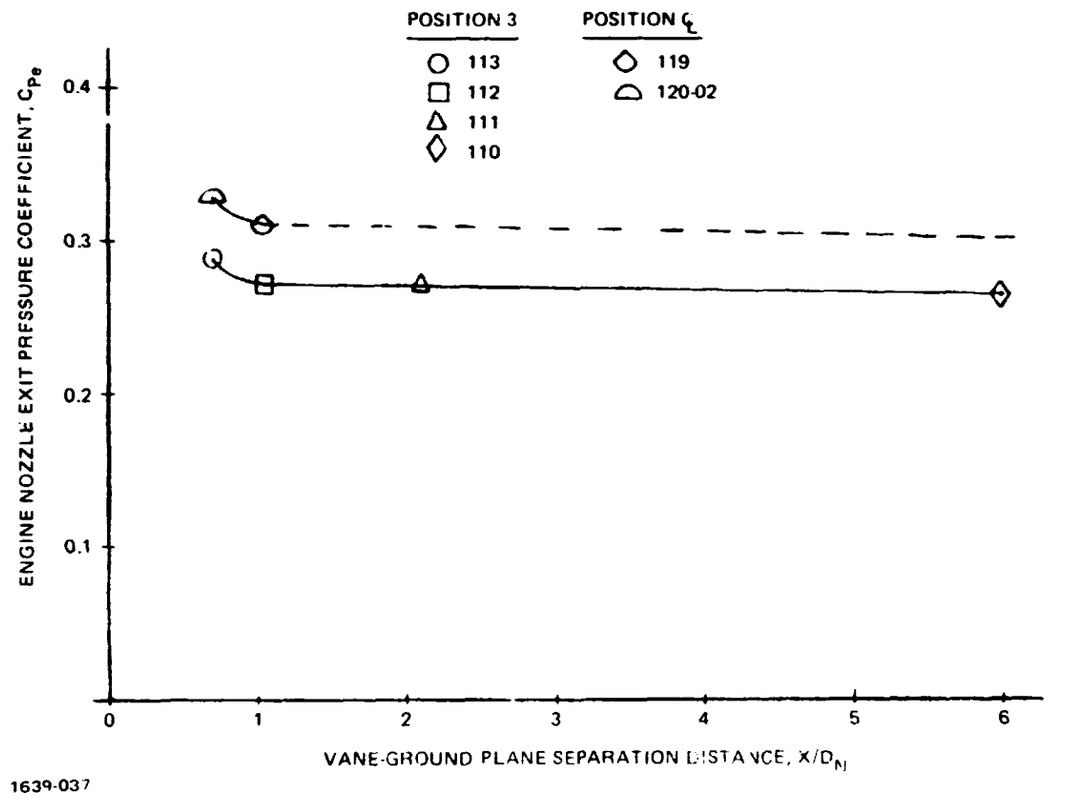


**Fig. 4.3-8 Effect of Ground Plane Separation Distance on Engine Nozzle Exit Pressure Coefficient, Vane Deflection Angle = 30°**

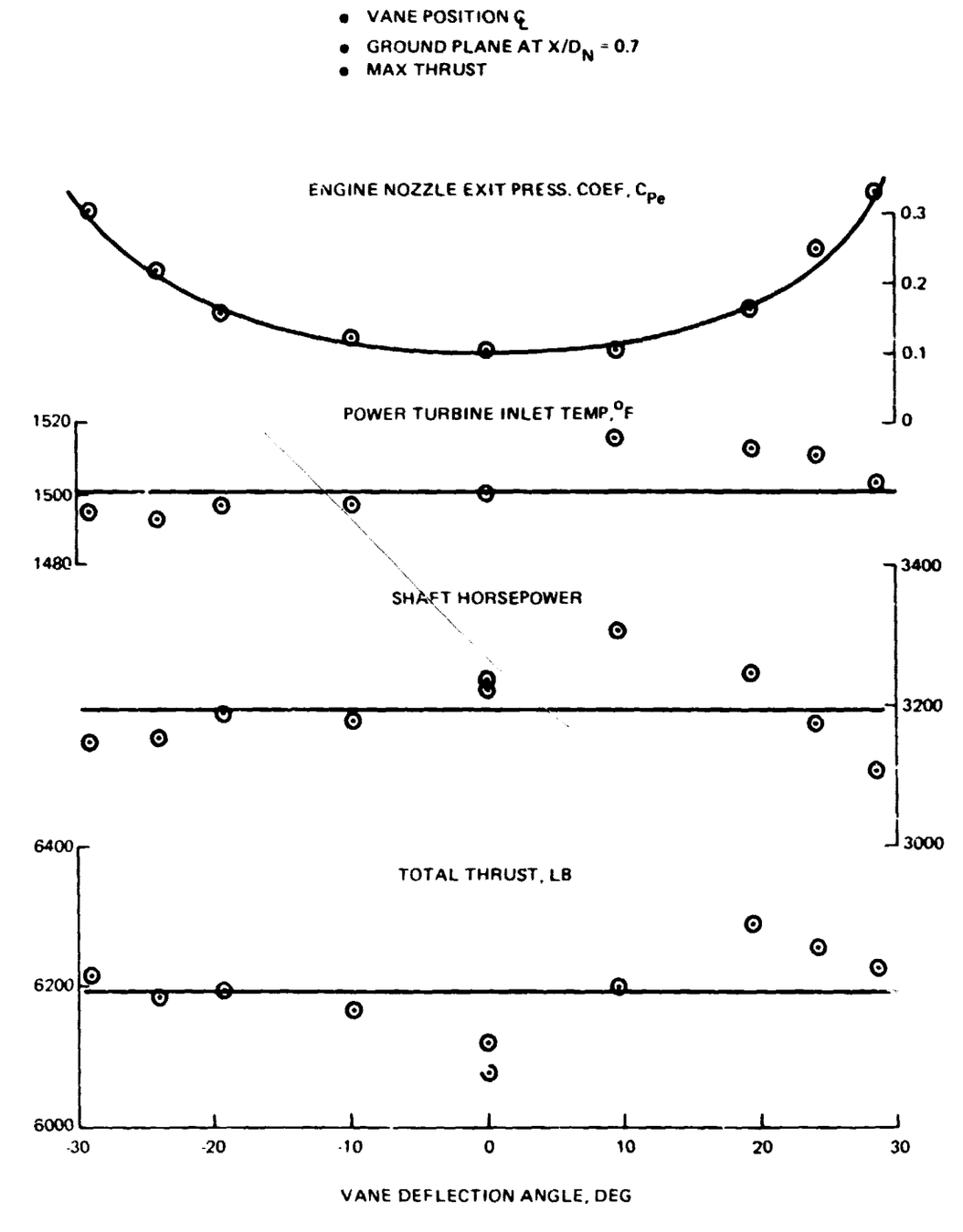


**Fig. 4.3-9 Effect of Engine Nozzle Back Pressure on Engine and Fan Performance Characterisitcs**

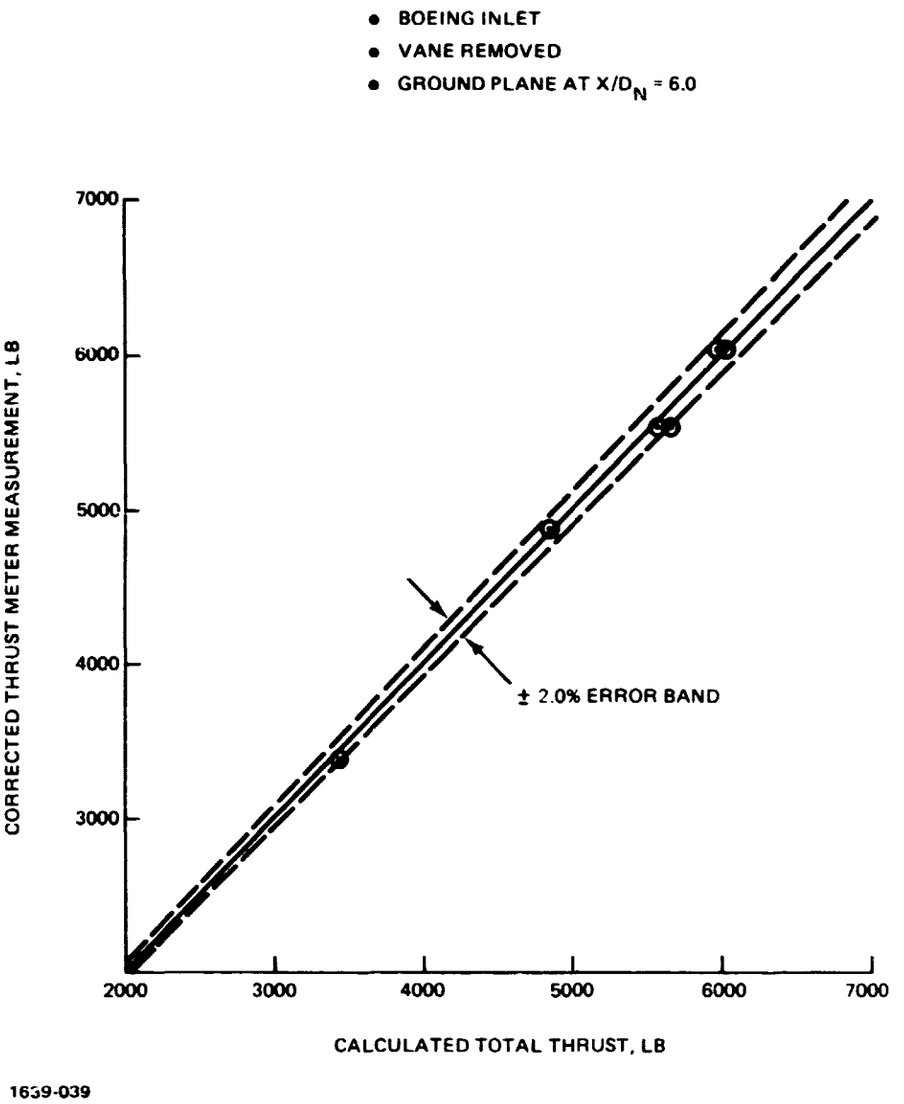


**Fig. 4.3-10 Comparison of Thrusts Determined by Thrust Meter and by Reduction of Pressure Data**

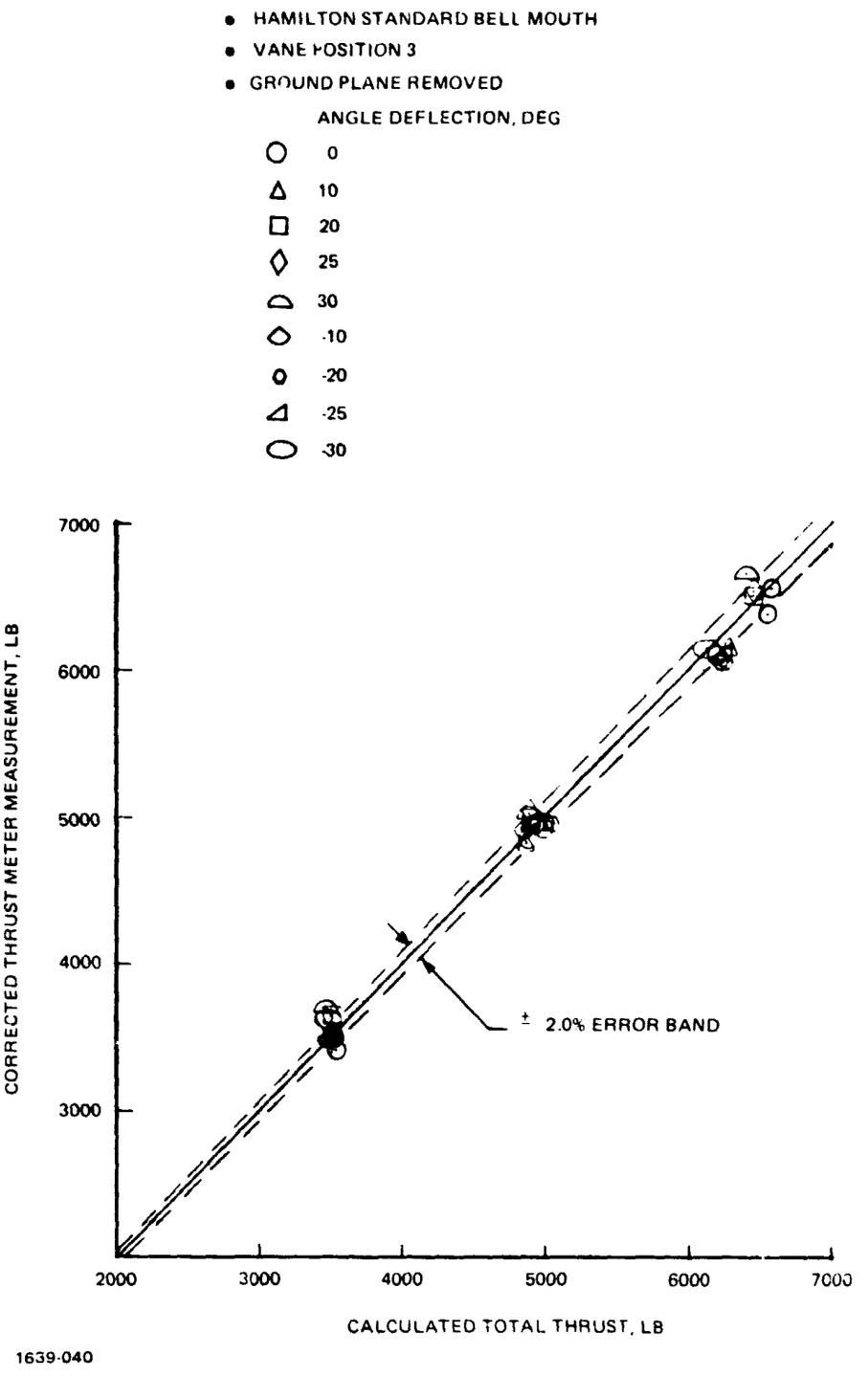


**Fig. 4.3-11 Comparison of Thrusts Determined by Thrust Meter and by Reduction of Pressure Data**

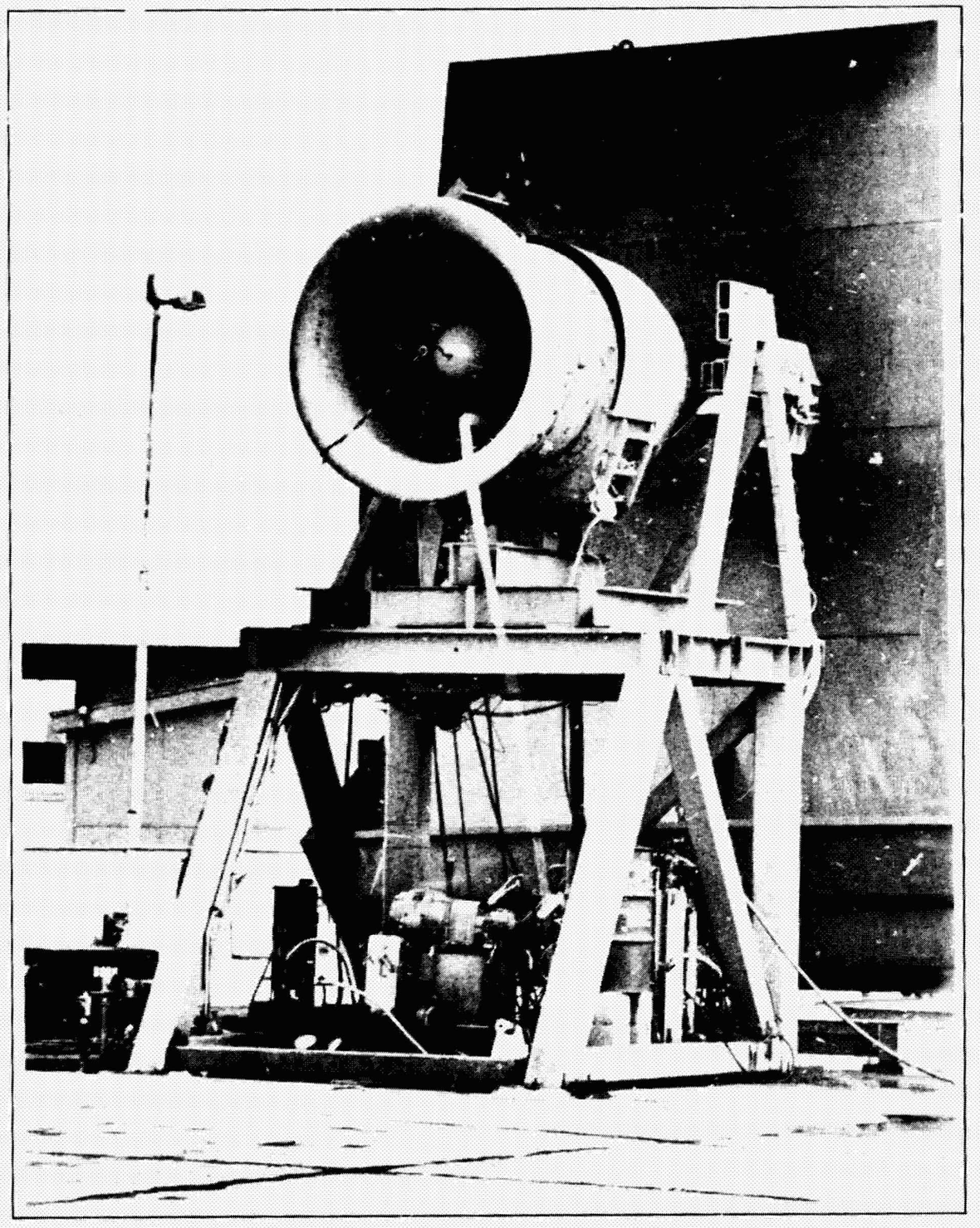

1639-041

Fig. 4.3-12 Core of Ingested Vortex Made Visible by Condensation of Atmospheric Water Vapor

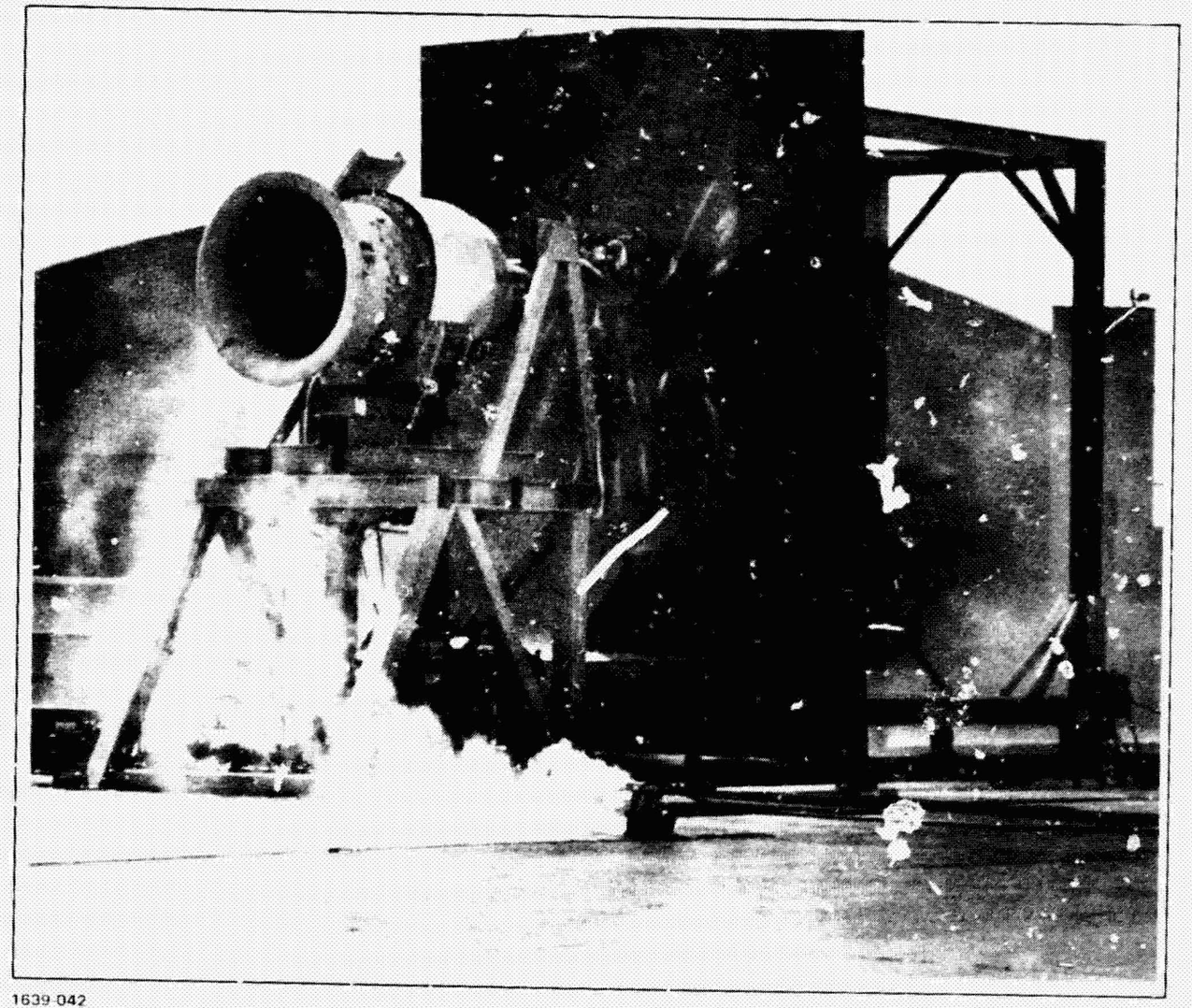

1639-042

Fig. 4.3-13 Vortex-Free Operation at Maximum Thrust

## 4.4 THERMAL ANALYSIS

The purpose of the thermodynamic portion of the test was to determine local mixed gas temperatures and local skin film coefficients from measured values of local skin temperature. These parameters will assist in the thermal design of a full scale vane. Since the recorded skin temperatures were all transient values, and since the vane was held at a particular angular position for a much longer period than would actually occur during flight, the overall skin temperature changes recorded were larger than would actually occur on a flight article.

Results of the analysis of the recorded test data are presented in charts of the local average gas temperature and film coefficient (h) and the maximum vane temperatures as functions of vane angle and position. The data show that, as expected, the film coefficient is more nearly functions of vane position and angle than of the gas temperature.

### 4.4.1 Local Gas Temperature/Film Coefficient Analysis

The thermodynamic data obtained during the tests representing the four most critical operating conditions were analyzed in detail. These tests were:

| Test No. | Vane Position | Ground Plane Distance, in. |
|---|---|---|
| 110 | Offset (3) | 342 |
| 113 | Offset (3) | 40 |
| 118 | Centerline | 342 |
| 120 | Centerline | 40 |

The local gas temperature and skin film coefficient were calculated from the measured rate of change of skin temperature that was obtained with a particular thermocouple while vane deflection angle and engine power were held constant.

An analysis was performed to estimate the heat leak from the skins (upper and lower) to the internal structure (ribs, opposite skin). This analysis indicated that the heat leak would be considerably less ($< 3\%$) than the energy radiatively and conductively exchanged with the gas stream or stored in the local mass (node) surrounding the thermocouple; also the convective film coefficient is large enough that radiation to the surroundings can be neglected. Based on this conclusion:

Heat input rate = heat storage rate

$$hA\,(T_g - \overline{T}_s) = (mC_p)_{skin}\,(\Delta T/\Delta \tau) = (dA\ t\ C_p)\,(\Delta T/\Delta \tau)$$

where:

h = local skin film coefficient, btu/hr $ft^2$ $^oF$

A = local area surrounding thermocouple, sq ft

$T_g$ = local gas temperature, $^oF$

m = local skin mass, lb

$C_p$ = specific heat, 0.16 btu/lb $^oF$

$\bar{T}_s$ = mean skin temperature over time interval, $^oF$

$\Delta T$ = skin temperature increase (decrease) over time interval, $^oF$

$\tau$ = time, seconds

d = density of skin material, lb/cu ft

t = thickness of skin, ft

Denoting the slope, $\Delta T/\Delta\tau$ as S, then for two consecutive time intervals:

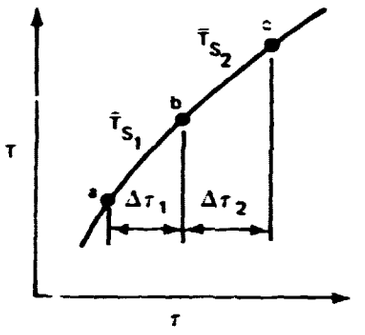


$$(hA)_1 (\bar{T}_{g1} - \bar{T}_{s1}) = (m C_p)S_1$$

$$(hA)_2 (\bar{T}_{g2} - \bar{T}_{s2}) = (m C_p)S_2$$

where:

$$\bar{T}_{S1} = \frac{Ta + Tb}{2}$$

$$\bar{T}_{S2} = \frac{Tb + Tc}{2}$$

Assuming that over each interval, the local gas temperature and film coefficient essentially will be constant, one of these parameters can be eliminated to solve for the other based on the recorded data; i.e., since

$$h_1 = h_2, \quad \bar{T}_{g1} = \bar{T}_{g2}$$

$$\bar{T}_g = (S_1 \bar{T}_{S2} - S_2 \bar{T}_{S1})/(S_1 - S_2)$$

$$h = \frac{d\,t\,C_p S_1}{\bar{T}_g - \bar{T}_{S1}} = \frac{d\,t\,C_p S_2}{\bar{T}_g - \bar{T}_{S2}}$$

Hence, local gas temperatures and skin film coefficients can be determined based on the recorded data, providing that the vane setting is held constant long enough for the data acquisition system to obtain data defining two successive time increments.

### 4.4.2 Data Compilation/Analysis

In order to use this predictive method, two consecutive time increments had to be selected for each vane setting interval to be analyzed. During each vane/ground plane test sequence, the angular position of the vane was stepped over the complete deflection range and the time of arrival at each new vane setting was recorded. An interval (~ 10-20 seconds) existed during which the vane was moving from one angular position to another. Therefore, some engineering judgement was required to select the appropriate end points for each case. In order to select appropriate data points for analysis, time history plots of representative skin temperature measurements were prepared from the recorded data. For example, Fig. 4.4-1 presents the plot which was used to select the appropriate time increments (data points) for the 110 test sequence. The time recorded during testing, at which a particular vane setting was achieved is indicated. Based on the slope of the plot, the "apparent" time at which the vane began moving is indicated. Over each of these intervals the tabulated data was reviewed to see if at least three data points could be extracted. The analysis assumes a linear temperature change over each of these increments. Since the time increment for each data collection was brief (~20 seconds) this is a reasonable approximation.

### 4.4.3 Data Evaluation

Figures 4.4-2 through 4.4-23 present a summary of the calculated local gas temperatures and film coefficients and the maximum temperature recorded for each test and vane setting. Figure 4.4-24 presents the thermocouple map that was used to compile this information. Computed results have only been presented for those locations where sufficient measured data existed for analytical purposes. With the vane in the offset position, the upper surface thermocouples showed little response and remained at about the same temperature as the fan exhaust (~100° F). Therefore, since the recorded temperatures were essentially constant, it was not possible to calculate a reasonable film coefficient for this situation. Gas and film coefficients could be determined, however, for the vane lower surface.

In general, as would be expected, the gas temperatures are higher for the cases where the ground plane is present (112, 120) than when it is not (110, 118). This is due to stronger recirculation of the hot gases in the wake region as a result of the ground plane's presence. Local film coefficients on the other hand appear to be affected only slightly (if at all) by the presence of the ground plane. This also appears reasonable, suggesting that the local film coefficient is more a function of vane setting (and the resulting flow

pattern), than gas temperature (since film coefficient is in general a weak function of bulk gas temperature).

Although not rigorously justifiable, the calculated gas temperature and film coefficient data were numerically averaged to see if any trends could be observed. As noted, the analytical procedure required a significant level of $\Delta T/\Delta \tau$ to be productive, therefore, these averages only include data from portions of the vane surface that underwent significant heating.

Table 4.4-1 presents a summary of the average gas and film coefficients calculated for each test and vane angle. As shown, the average film coefficient on the vane varies from about 40 to 60 btu/hr $ft^2$ $^o$ F, depending on the vane angle. Looking at the 110 and 113 test sequences (offset vane position), a good agreement between average film coefficient and vane setting is seen at each angular position. Similarly, the average gas temperature recorded was in general higher for the 113 (with the ground plane) than the 110 test.

Figure 4.4-25 presents a direct comparison of gas temperatures and film coefficients calculated for each thermocouple location for a vane setting of -20° for test numbers 110 and 113. The same level of agreement exists for each location on the vane as the numerical averaged data indicates, implying that the average data may be used to evaluate vane performance.

The tabulated averaged data of Table 4.4-1 indicates that for each case a change in the flow condition appears to have occurred at vane deflections between -20 and -25°. In each run, the maximum gas temperature and skin temperatures are observed in this range. An examination of the 110 run indicates that the average gas temperature increases from about 100 to 450° F as the vane angle shifts from 0 to -20°, and then decreases from about 450 to 200° F as the vane angle shifts from -20 to -30°. Similar results are observed in each of the other cases. This observation correlates well with the aerodynamic force data which indicate the onset of the stall in this range and the acoustic data which show a sharp rise in overall sound pressure level at these angles.

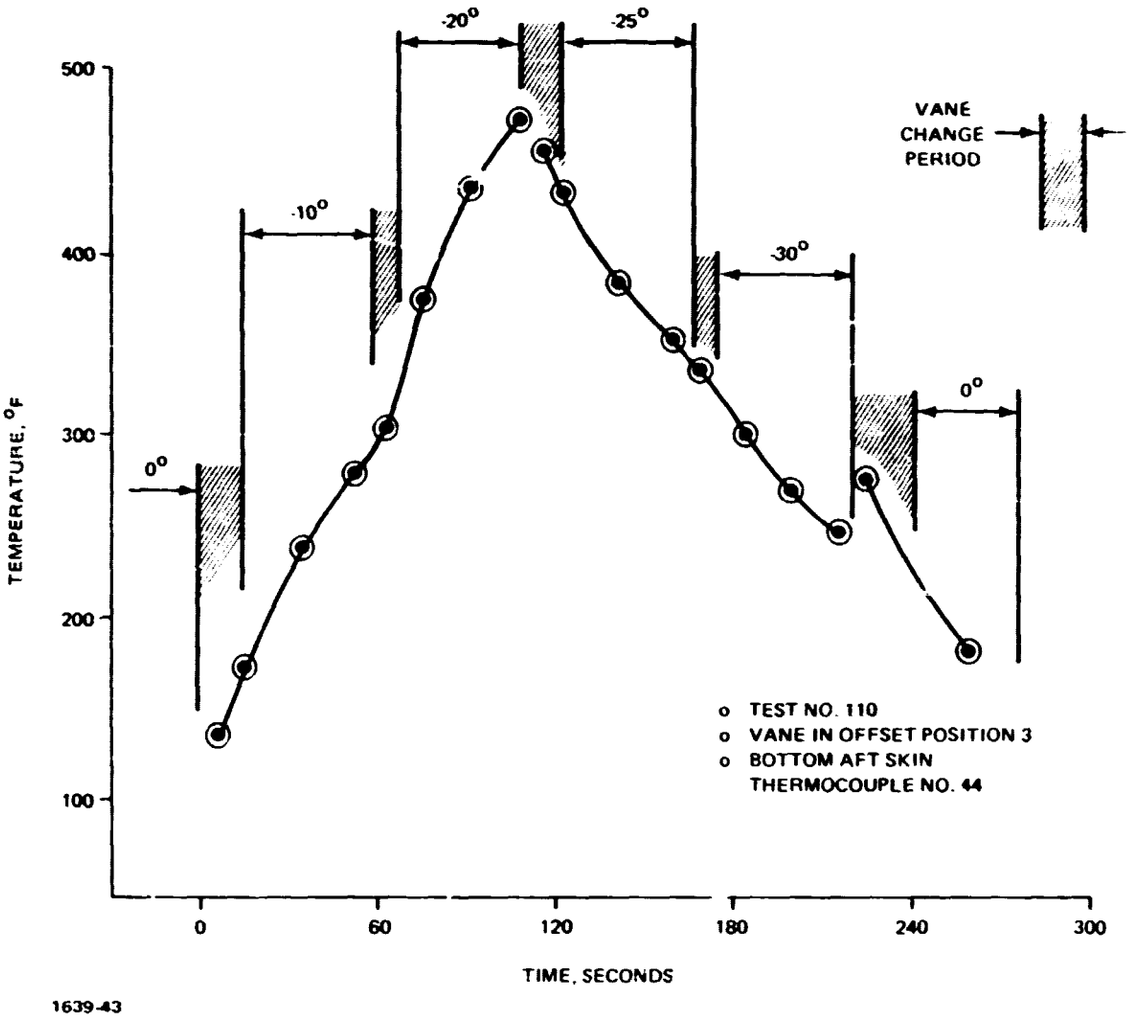


Fig. 4.4-1 Measured Skin Temperatures

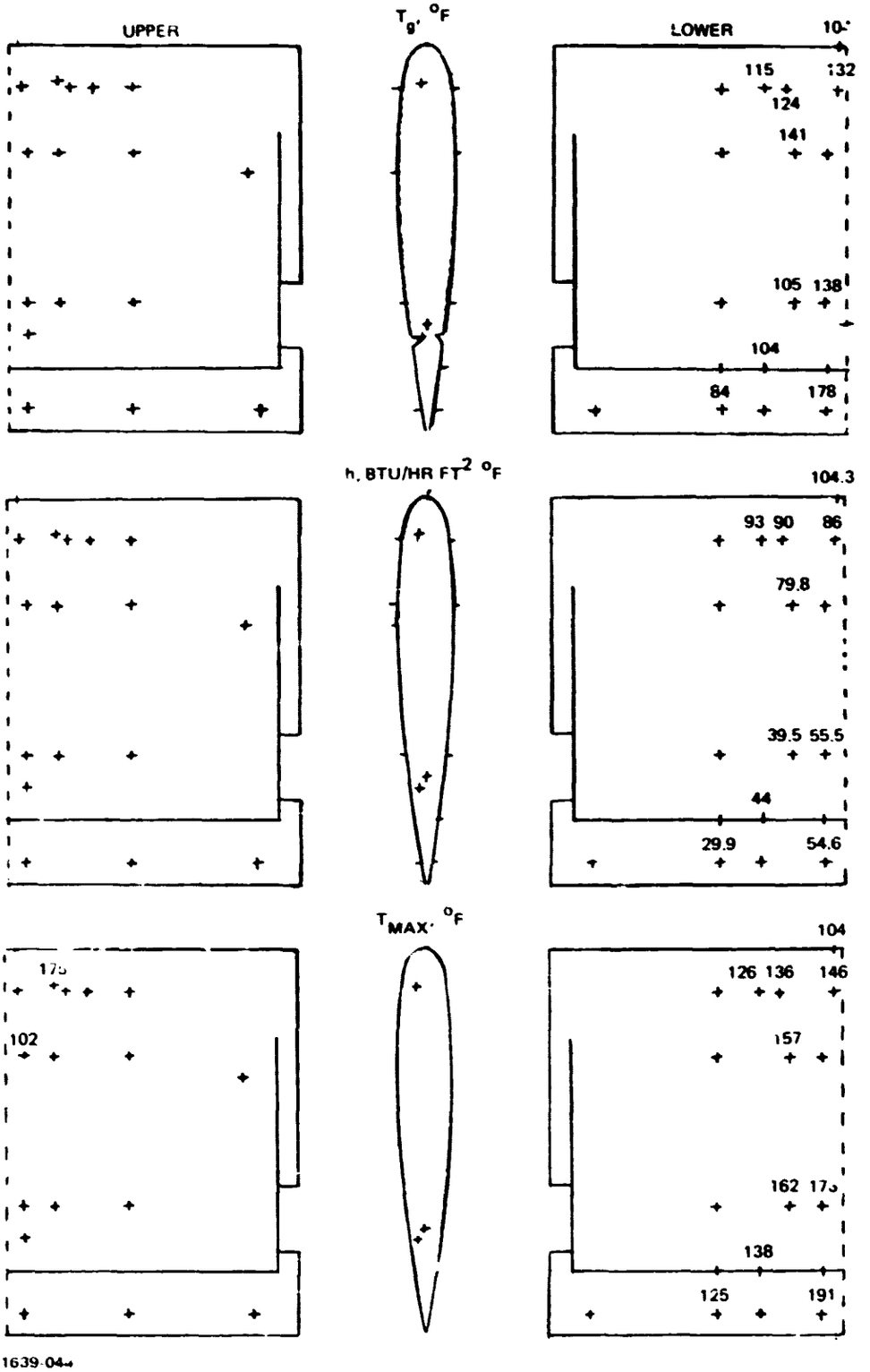


Fig. 4.4-2 110-01 Test Results, 0°

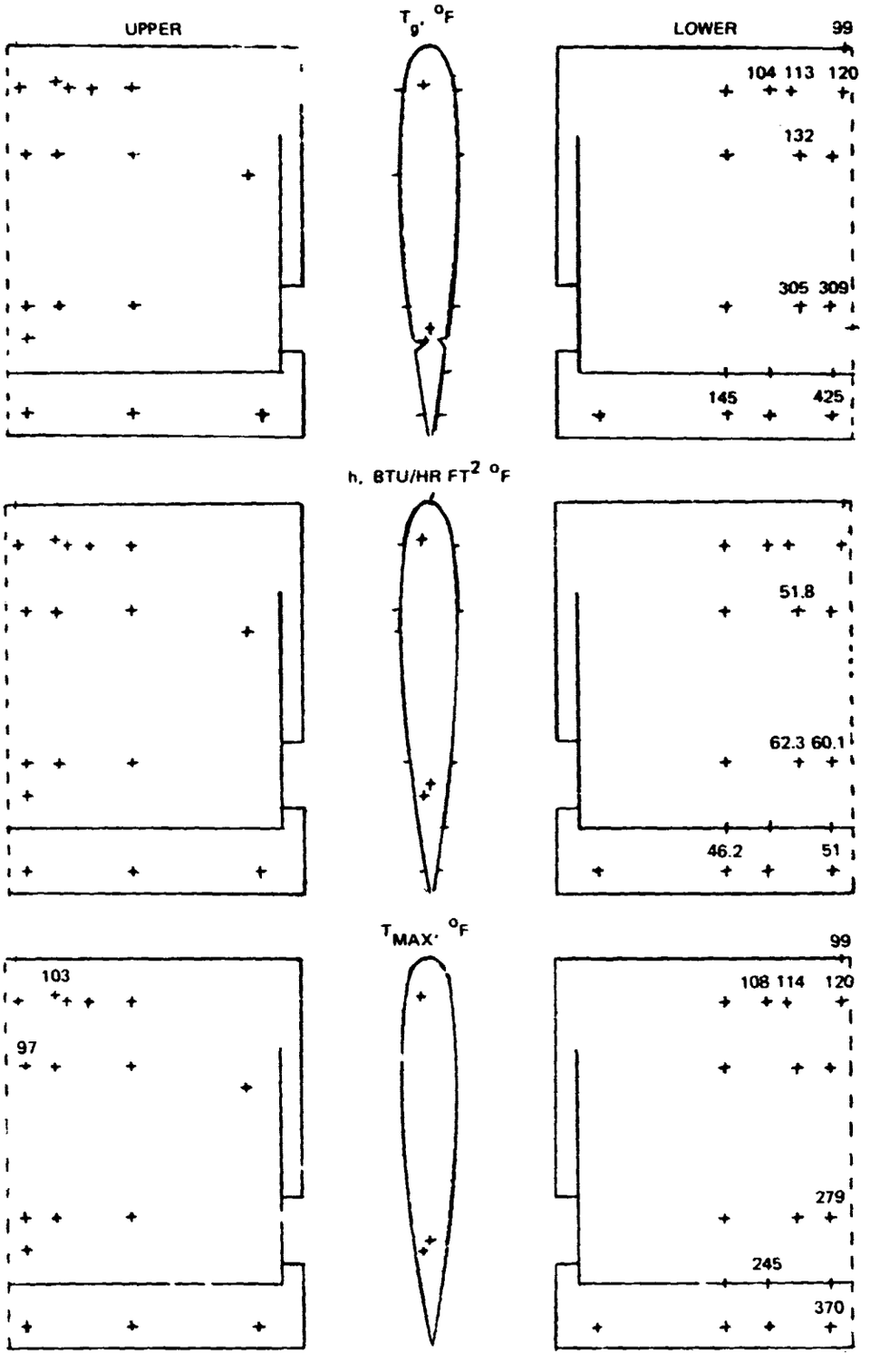


Fig. 4.4-3 110-01 Test Results, -10°

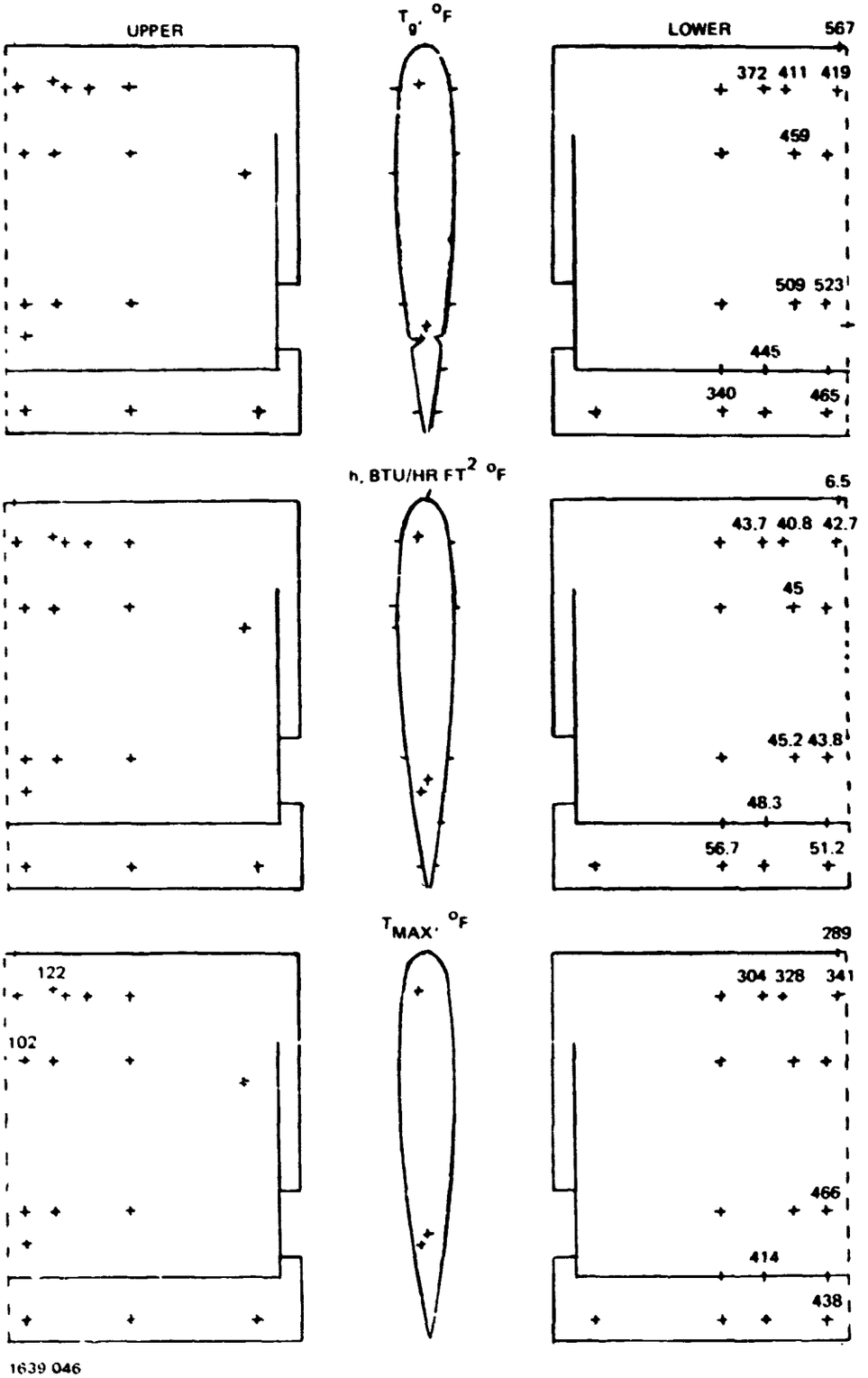


Fig. 4.4-4 110-01 Test Results, -20°

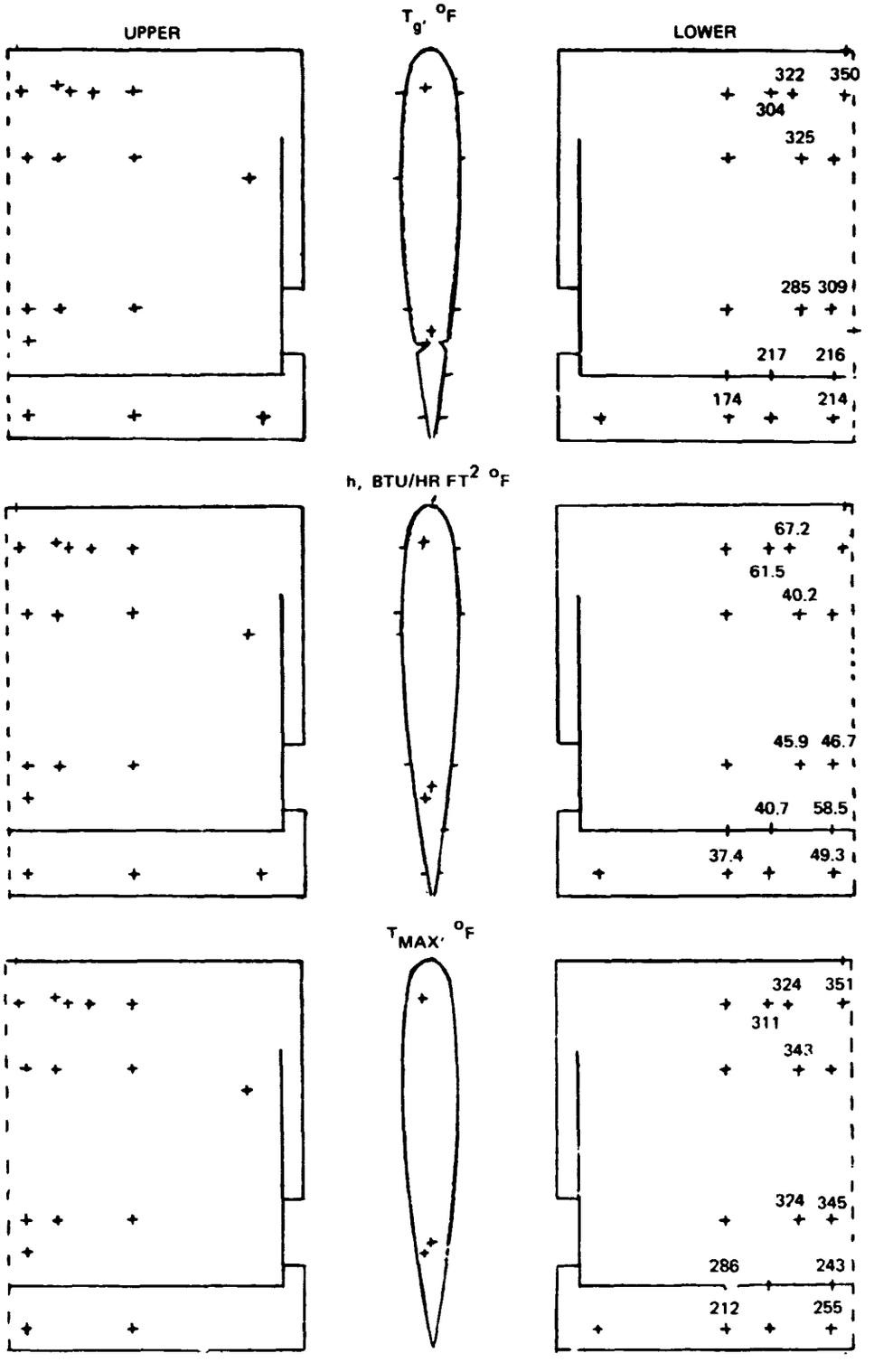


Fig. 4.4-5 110-31 Test Results, -25°

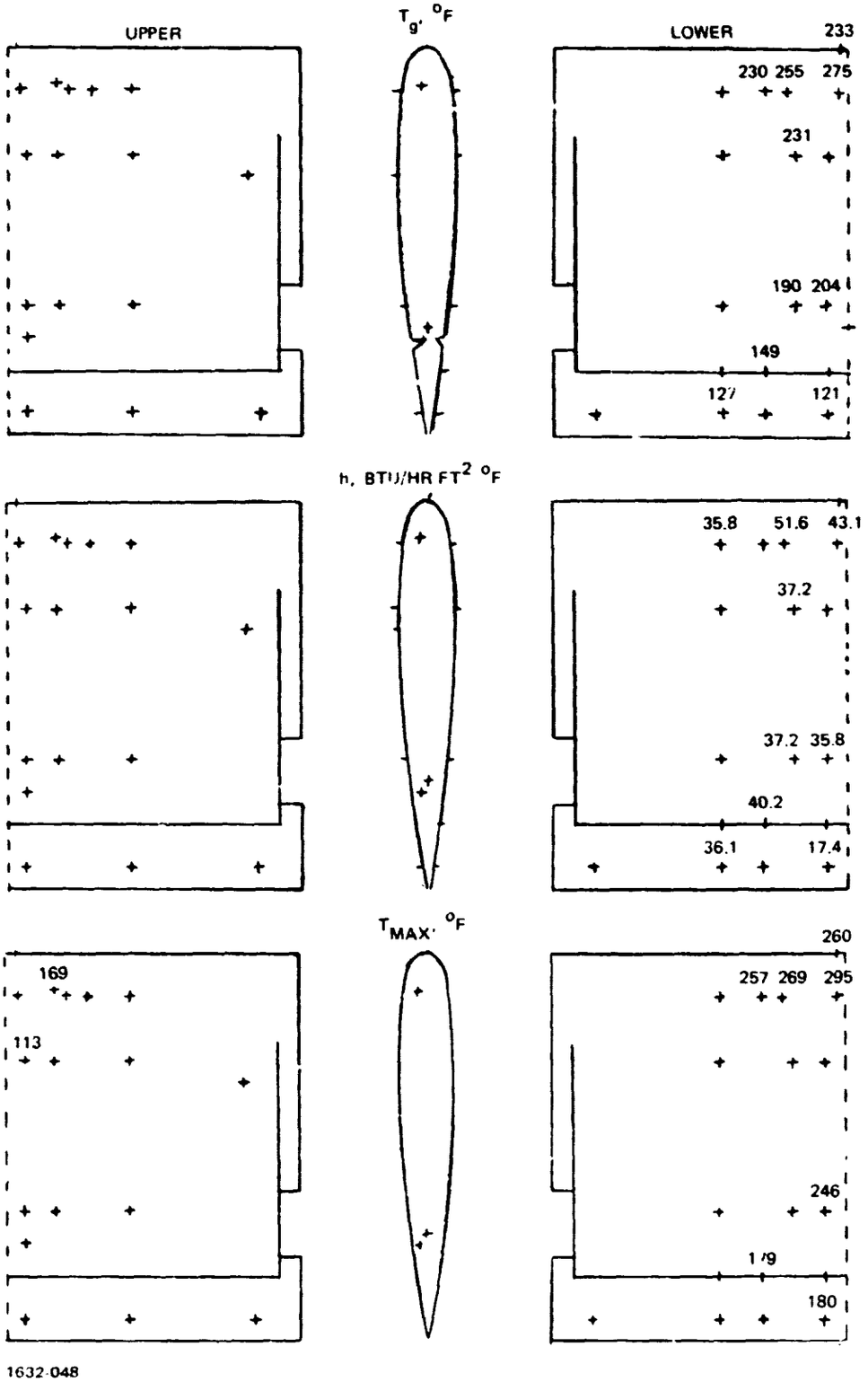


Fig. 4.4-6 110-01 Test Results, -30°

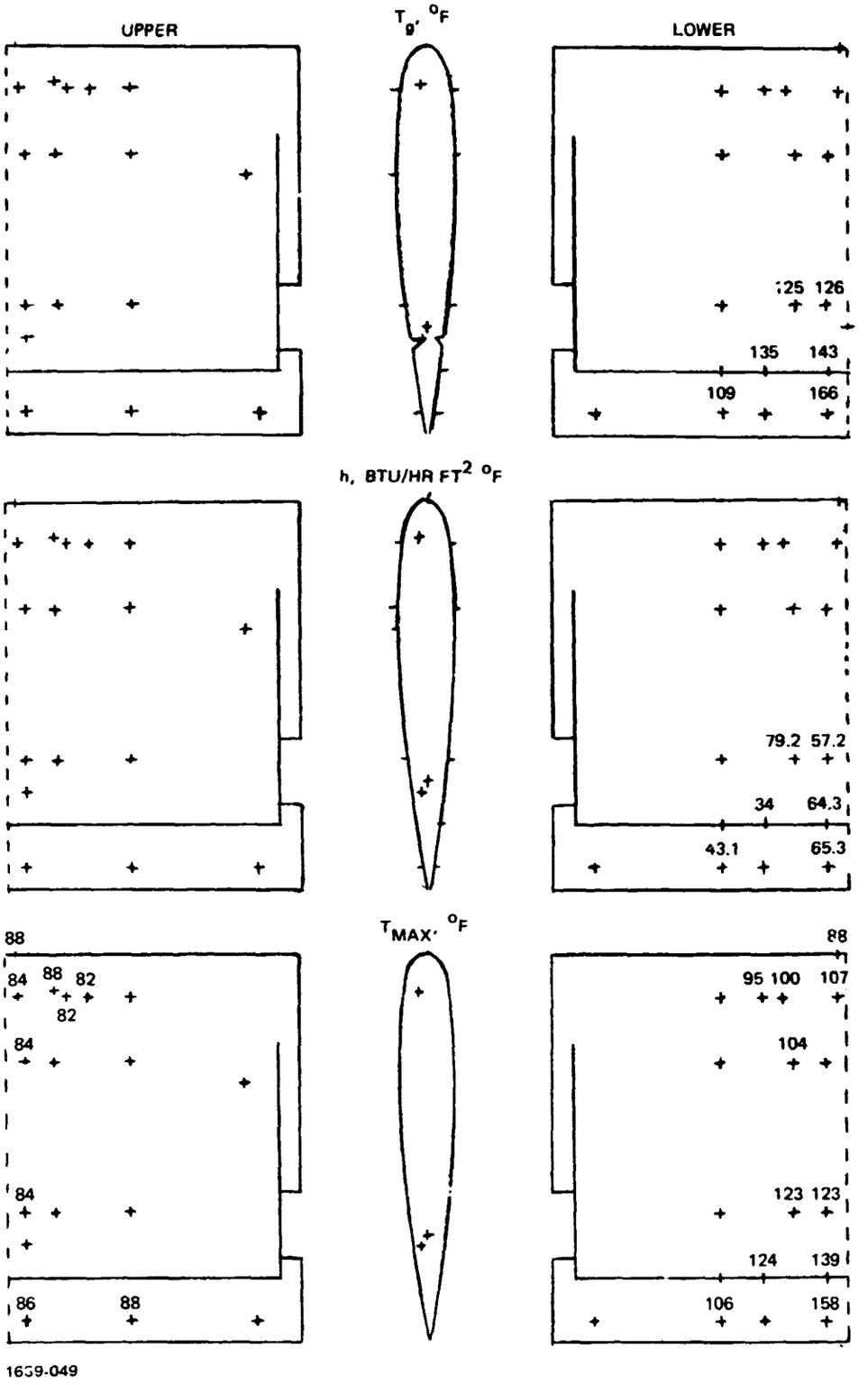


Fig. 4.4-7 113-01 Test Results, 0°

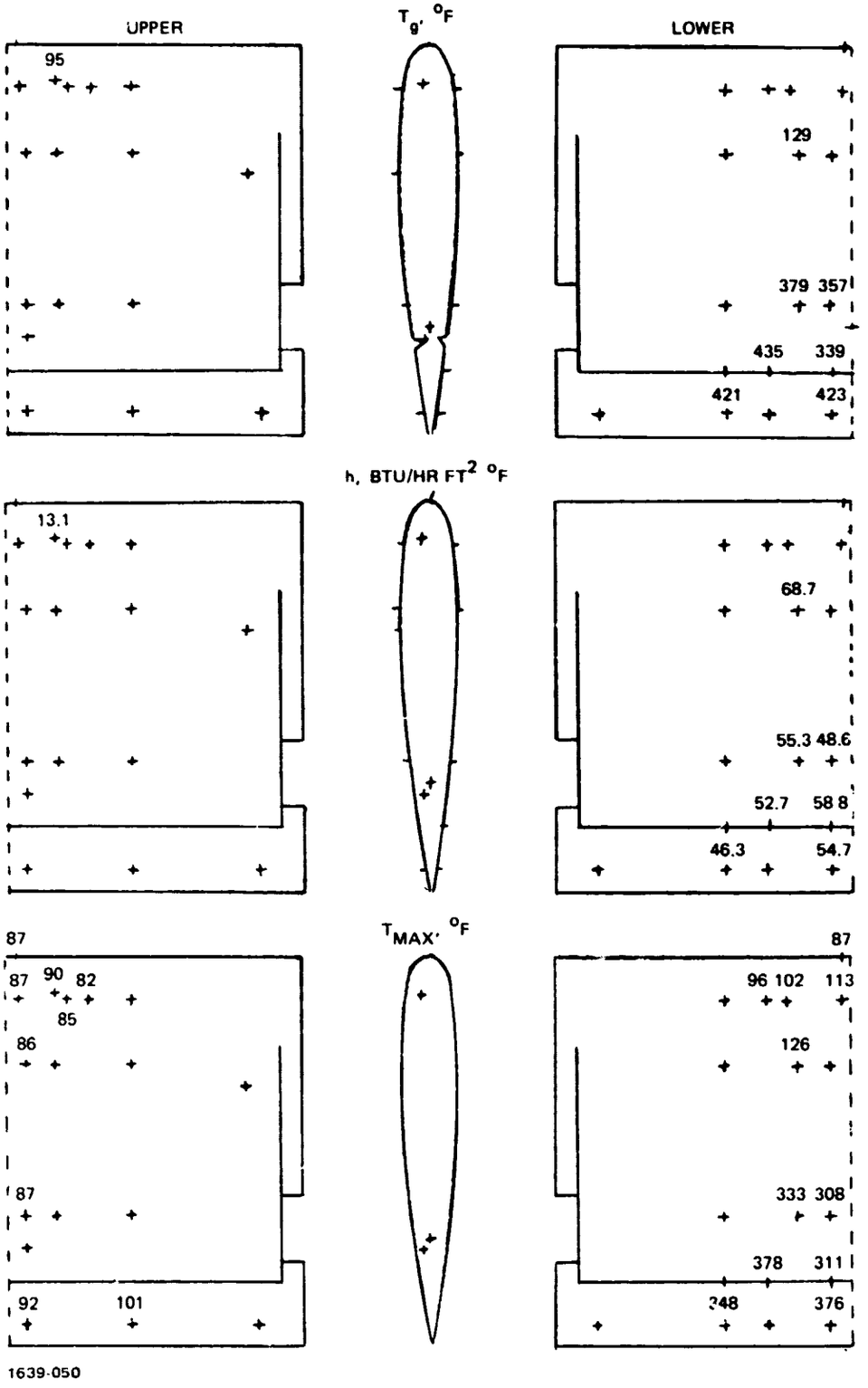


Fig. 4.4-8 113-01 Test Results, -10°

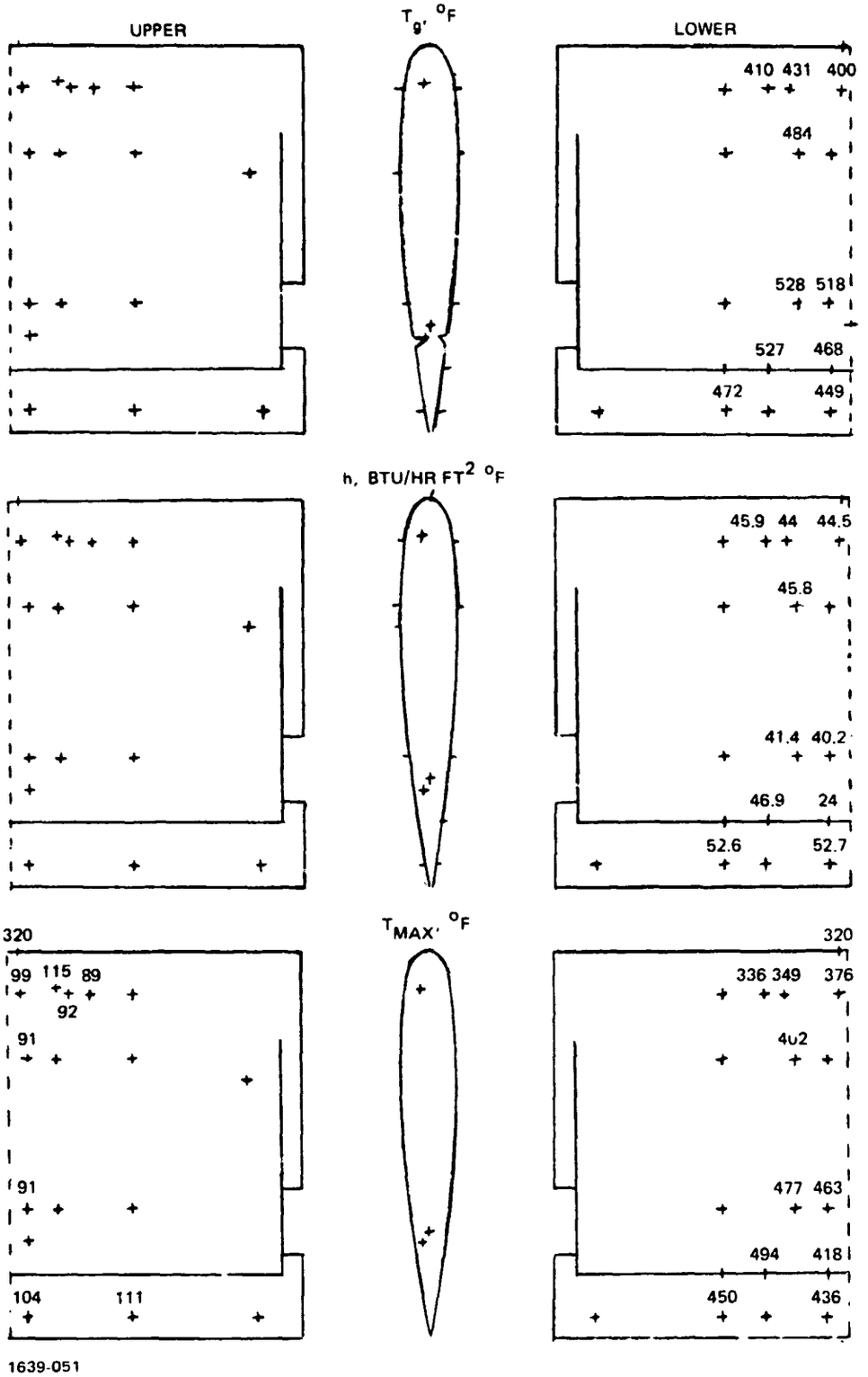


Fig. 4.4-9 113-01 Test Results, -20°

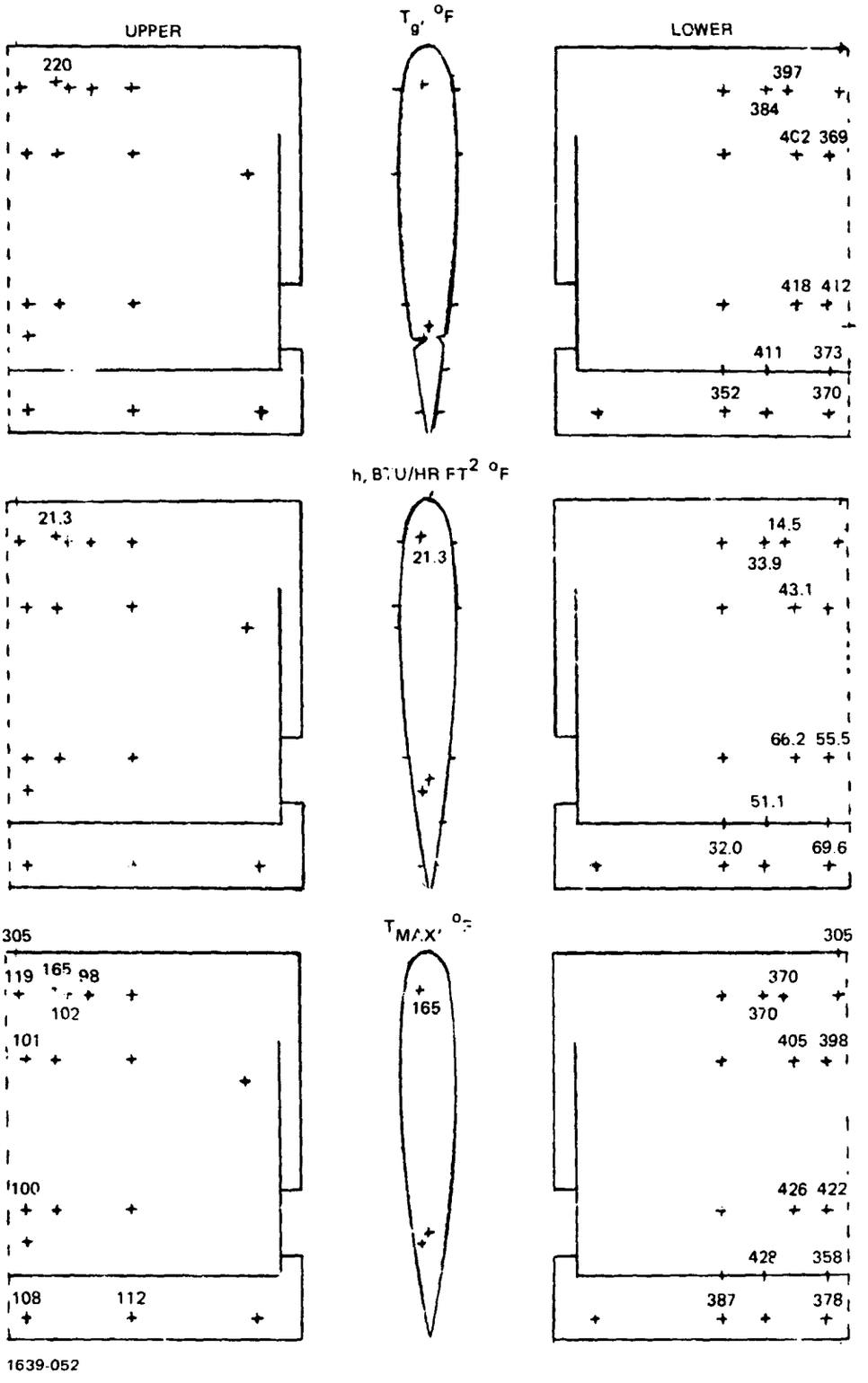


Fig. 4.4-10 113-01 Test Results, -25°

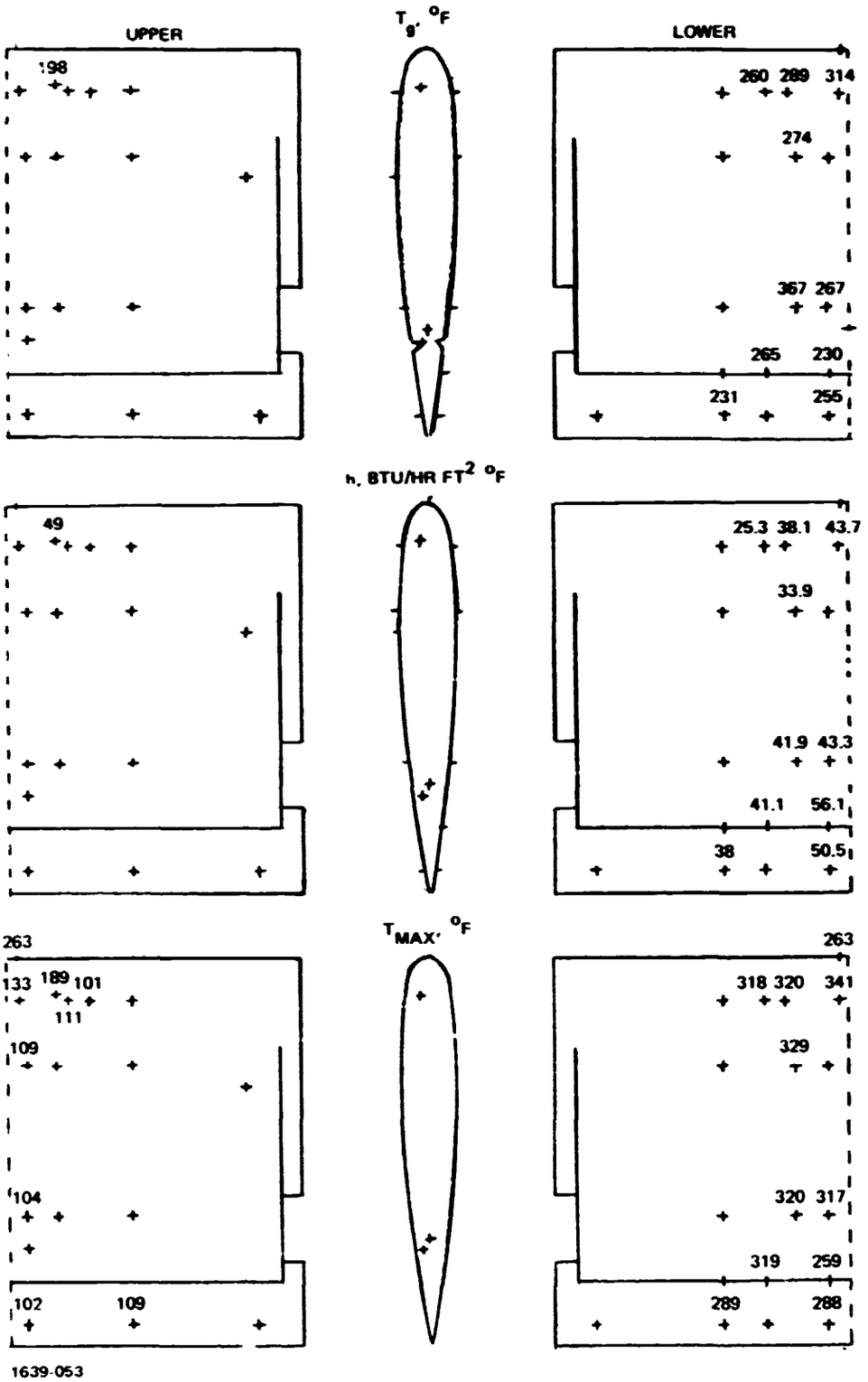


Fig. 4.4-11 113-01 Test Results, -30°

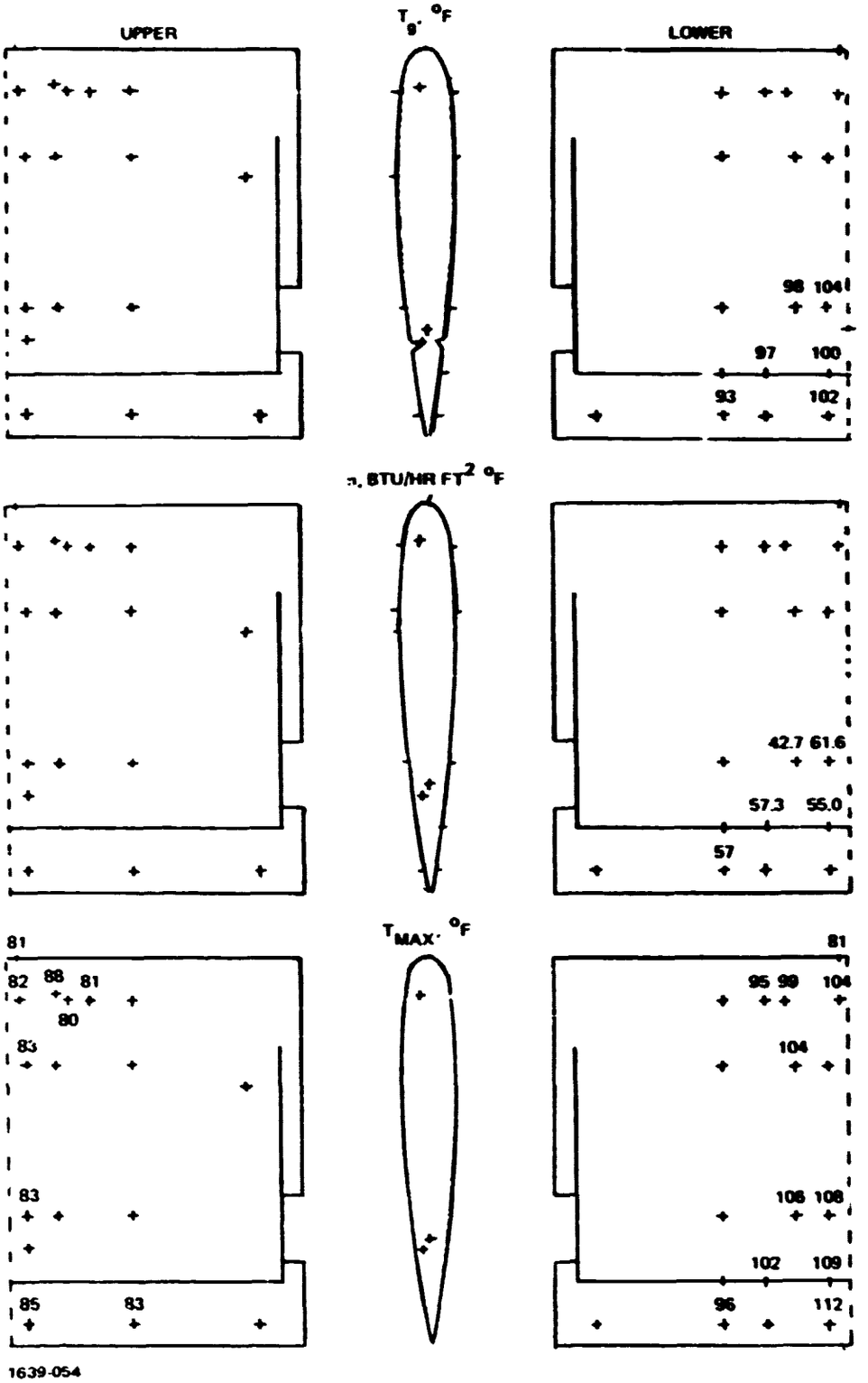


Fig. 4.4-12 118-01 Test Results, +10°

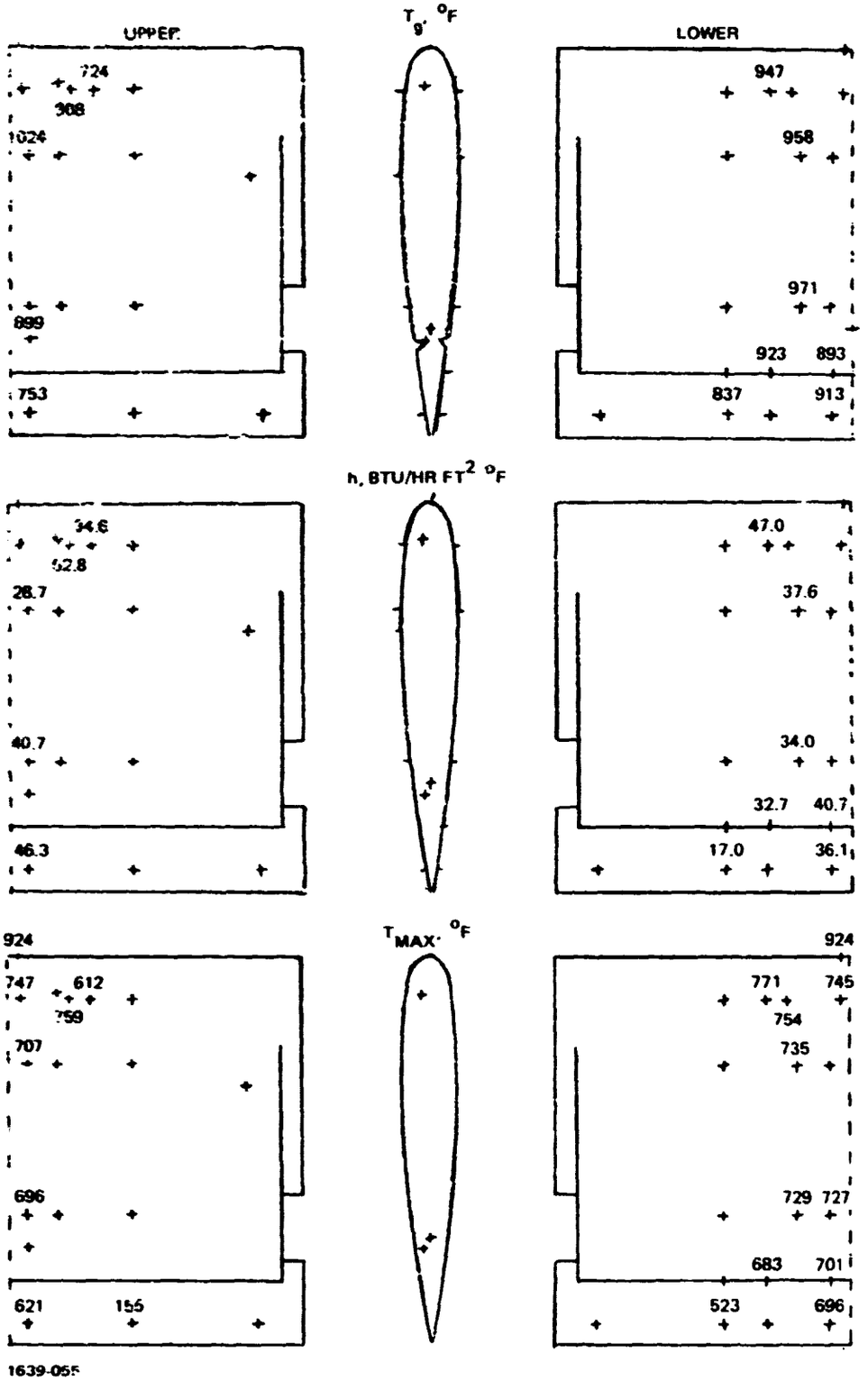


Fig. 4.4-13 118-01 Test Results, 0°

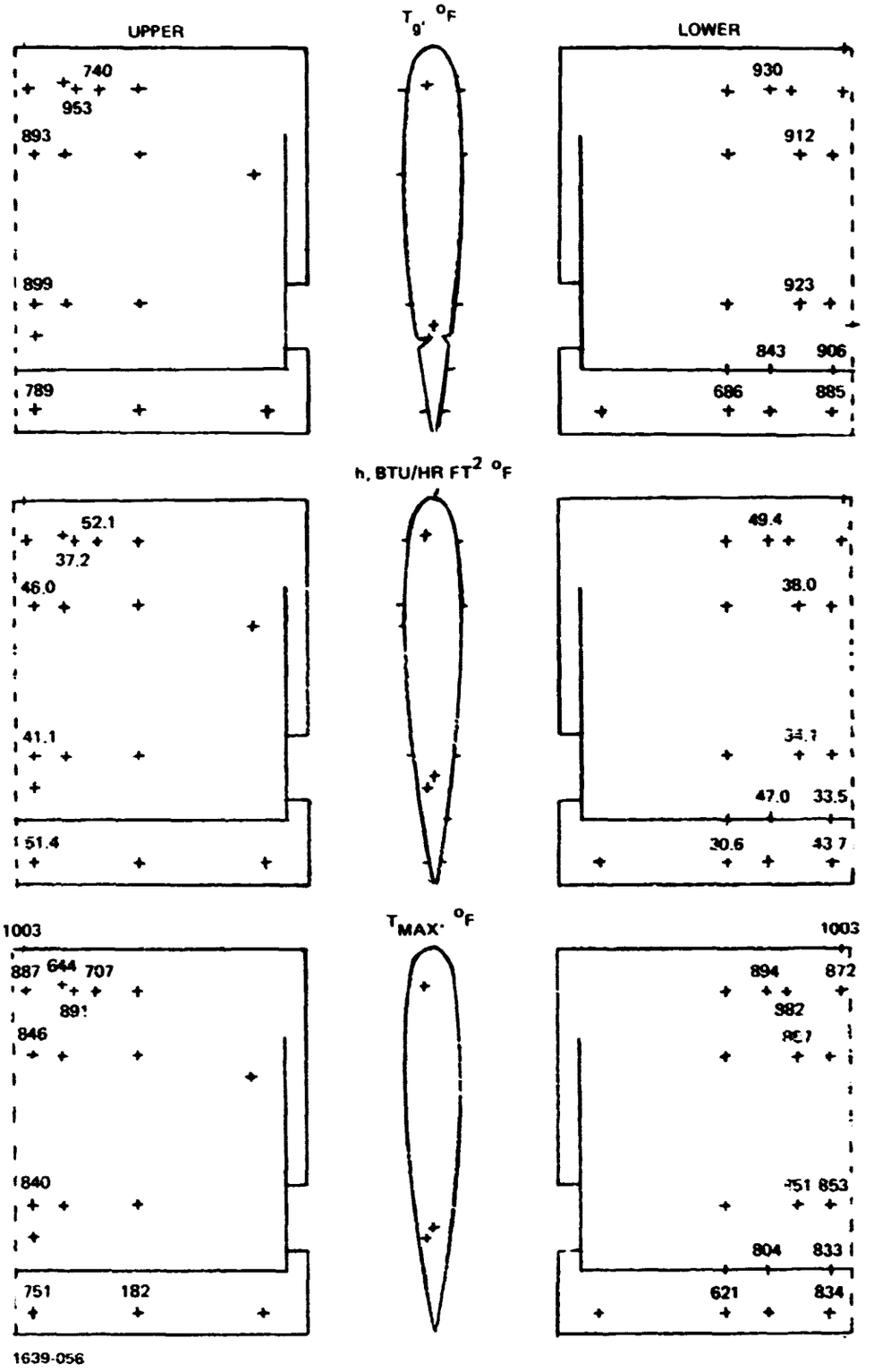


Fig. 4.4-14 118-01 Test Results, +10°

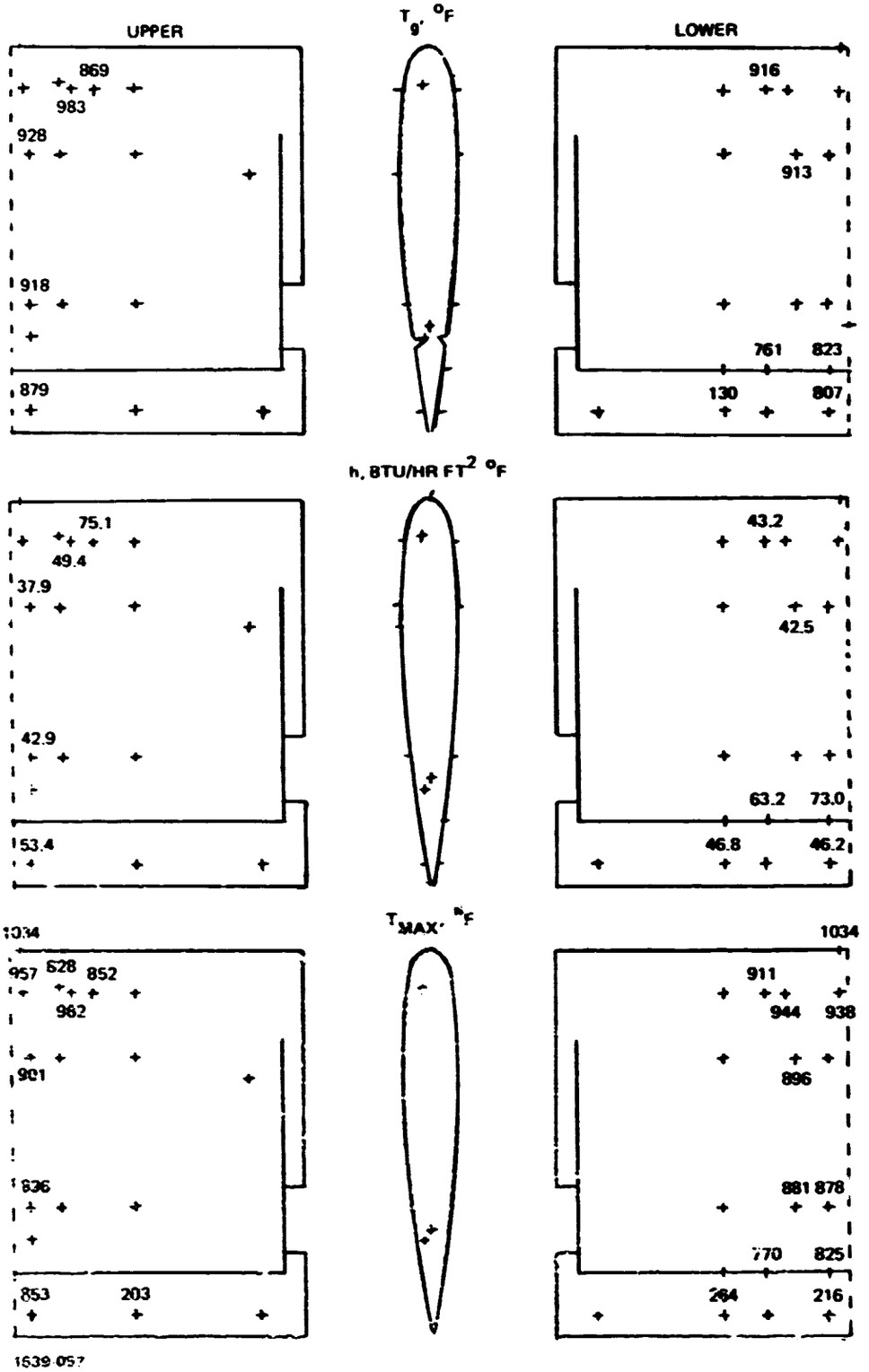


Fig. 4.4-15 118-01 Test Results, +20°

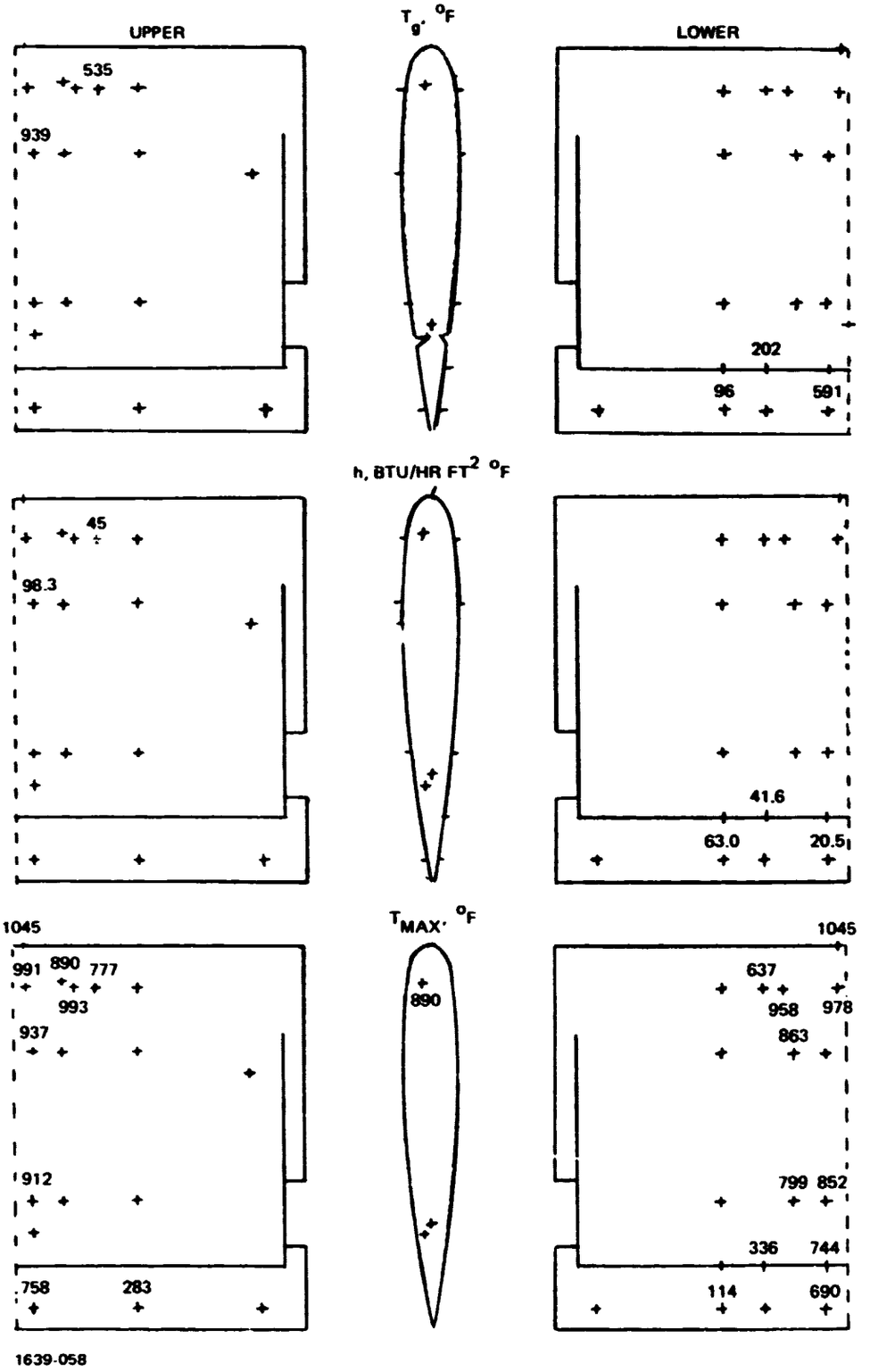


Fig. 4.4-16 118-01 Test Results, +25°

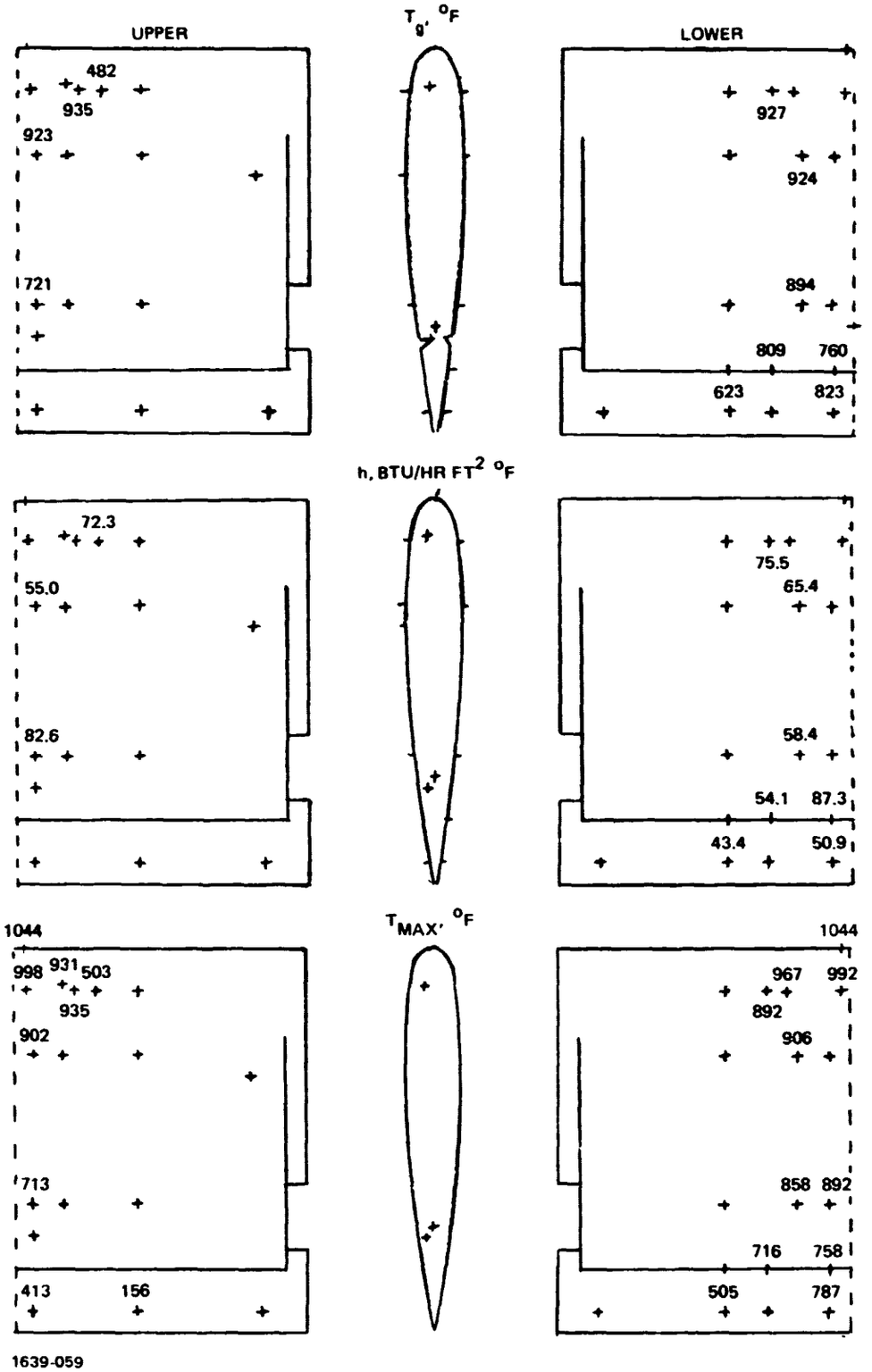


Fig. 4.4-17 118-01 Test Results, -10°

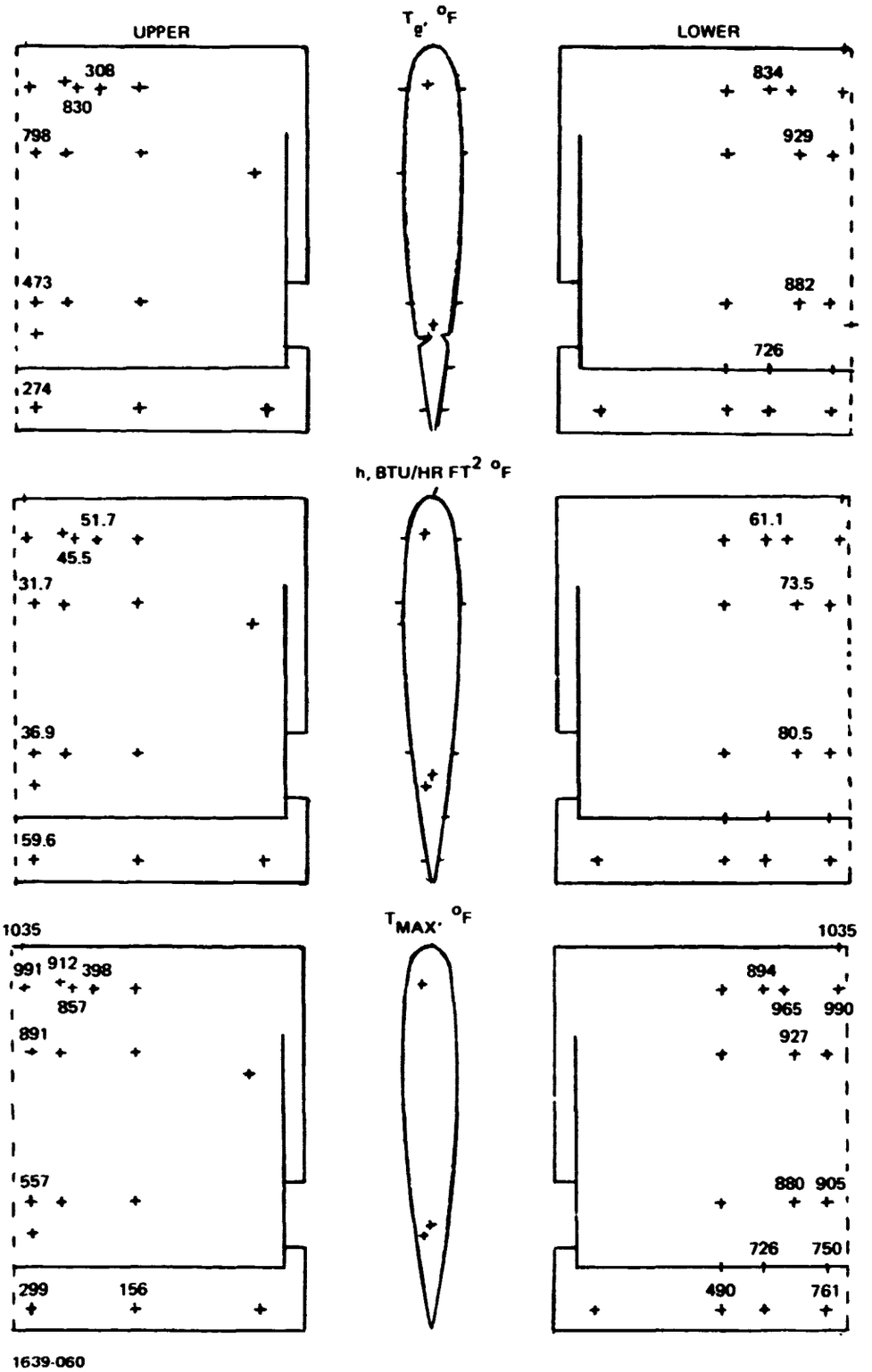


Fig. 4.4-18 118-01 Test Results, -20°

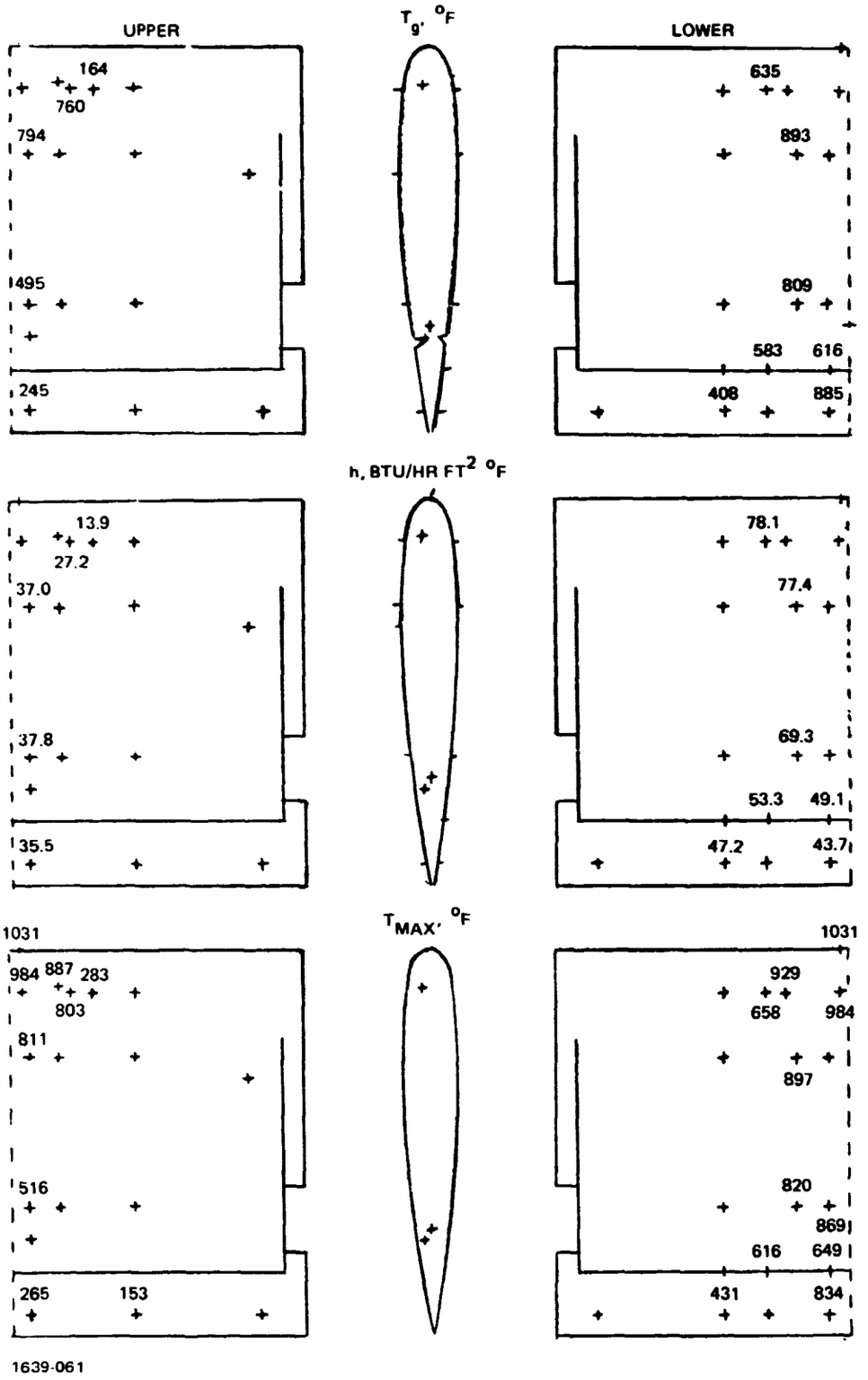


Fig. 4.4-19 118-01 Test Results, -25°

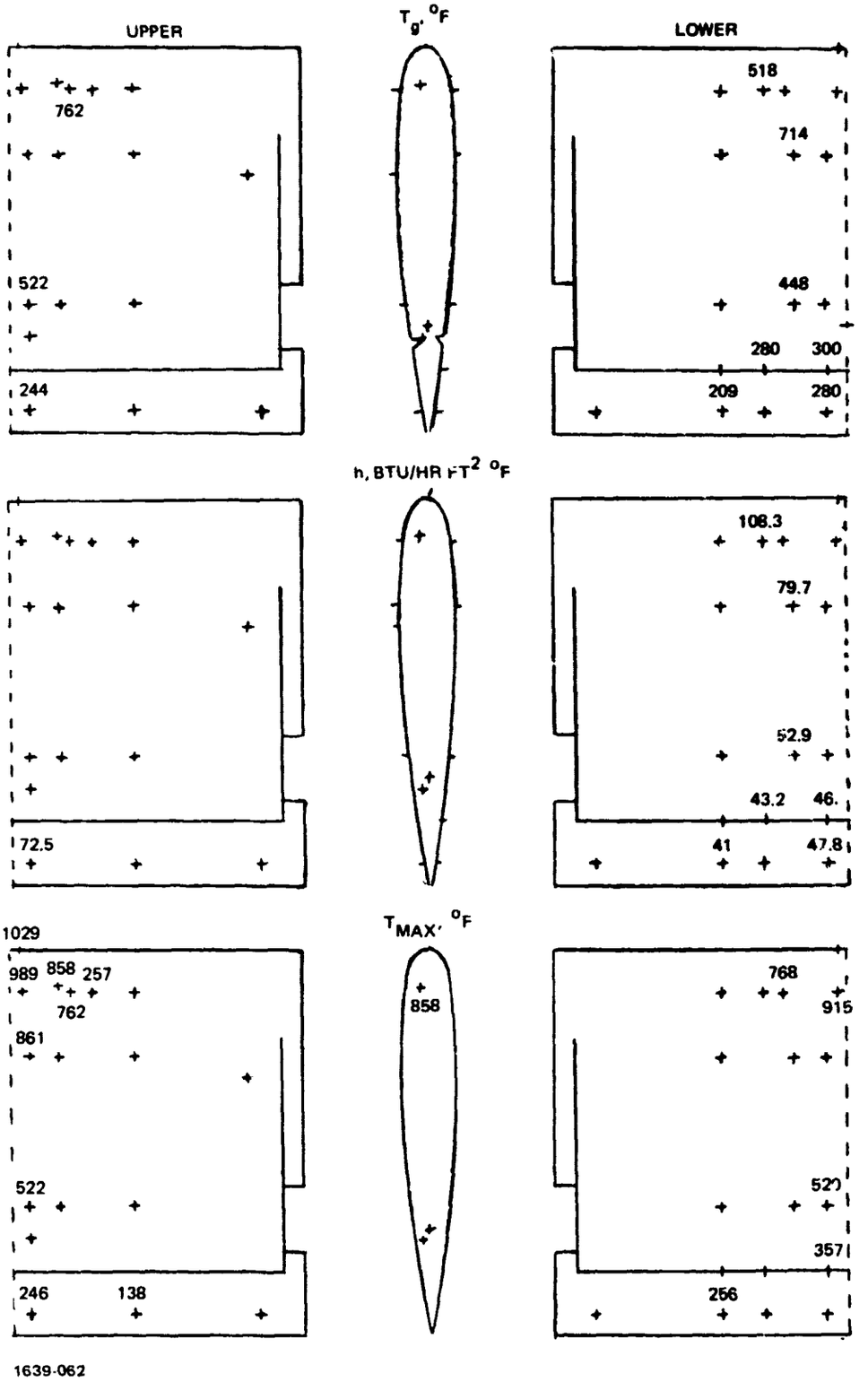


Fig. 4.4-20 118-01 Test Results, -30°

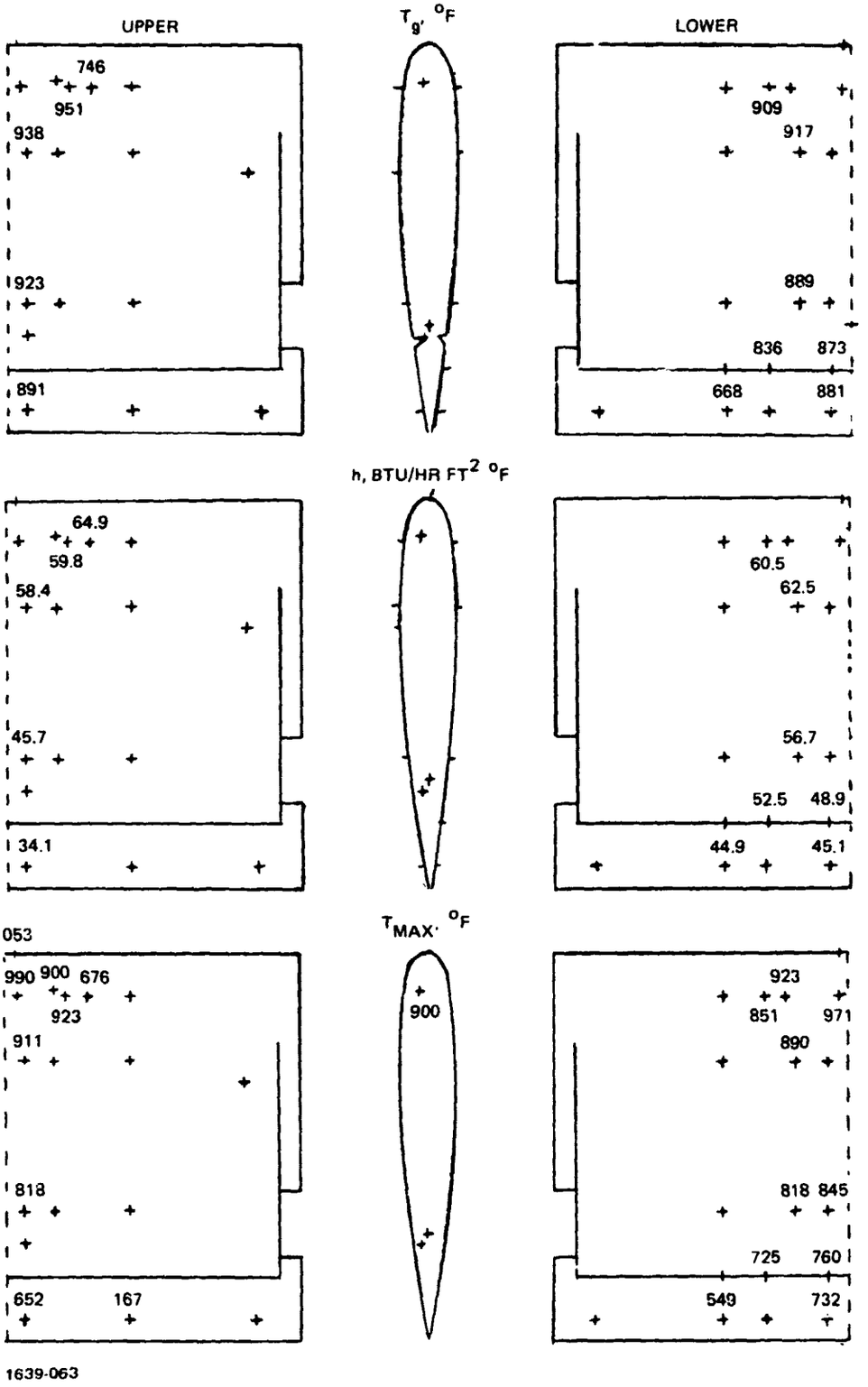


Fig. 4.4-21 118-01 Test Results, -0°

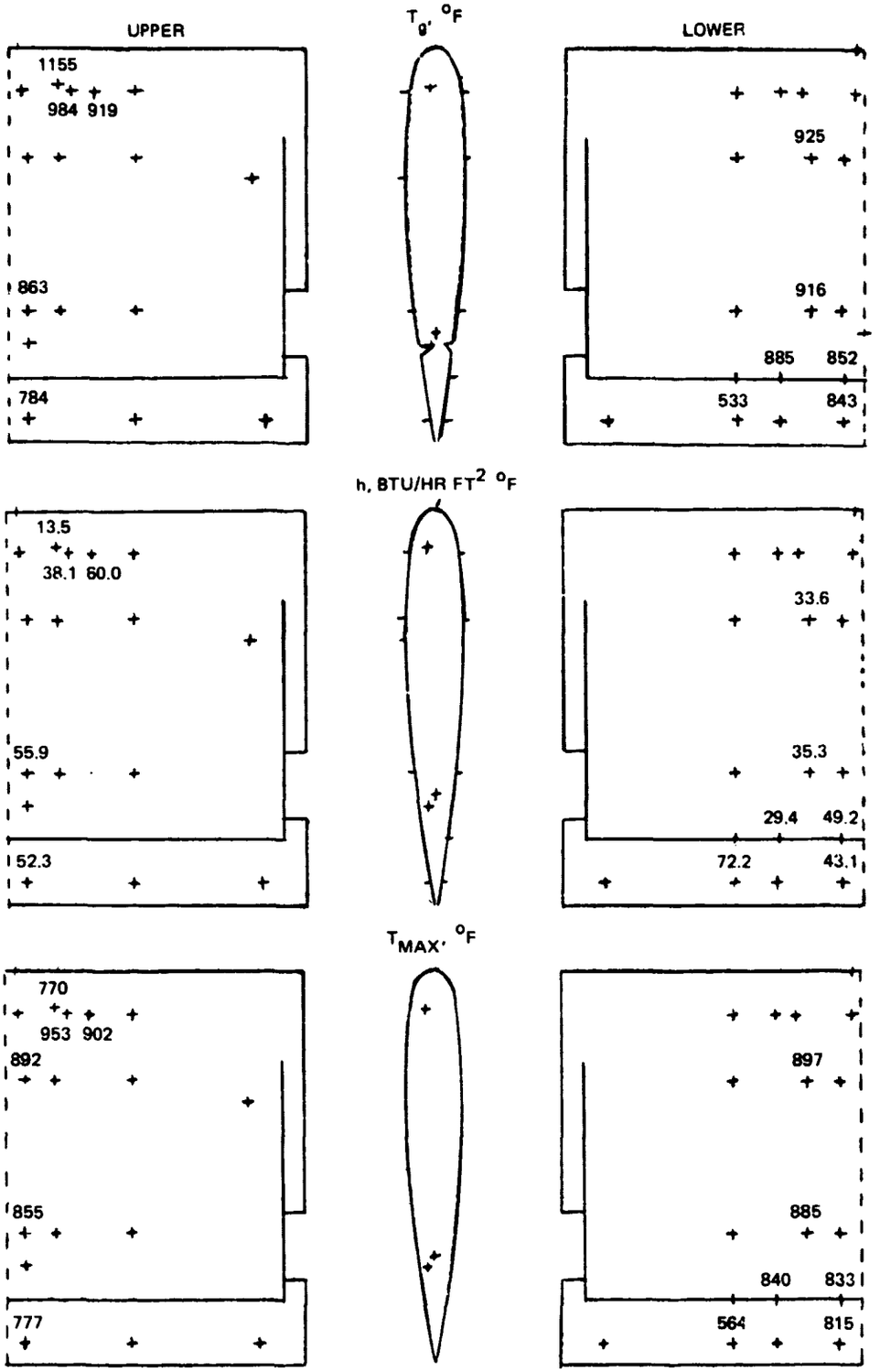


Fig. 4.4-22 120-01 Test Results +10°

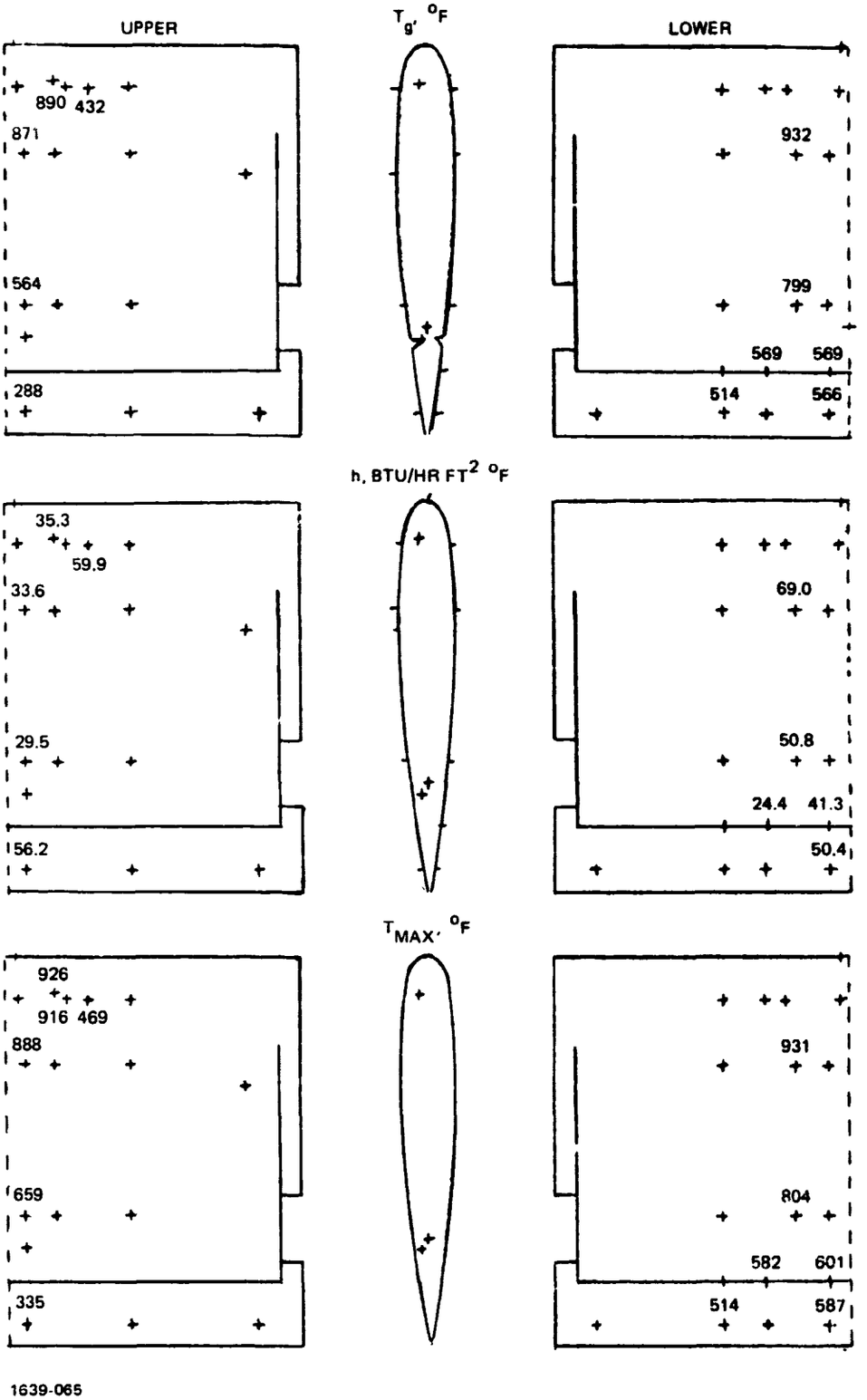


**Fig. 4.4-23 120-01 Test Results, -20°**

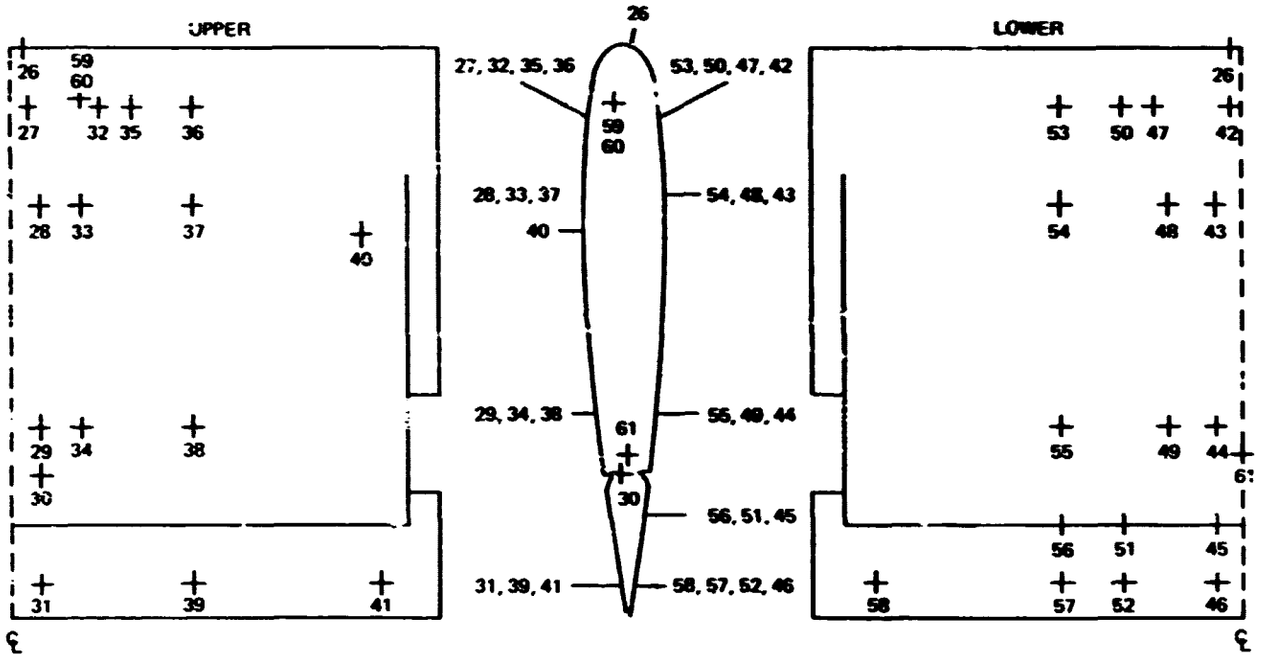


Fig. 4.4-24 Vane T/C Locations

Table 4.4-1 Average Gas ($\bar{T}_g$) & Film Coefficient ($\bar{h}$) Data

| VANE ANGLE, DEG | RUN NO. 110 | 113 | 118 | 120 |
|---|---|---|---|---|
| | $\bar{T}_g$, °F | | | |
| -30 | 202 | 265 | 393 | – |
| -25 | 389 | 389 | 690 | – |
| -20 | 451 | 475 | 843 | 636 |
| -10 | 195 | 355 | 823 | – |
| 0 | 95 | 134 | 920 | – |
| 10 | – | 99 | 869 | 881 |
| 20 | – | – | 844 | – |
| 25 | – | – | INSUF. DATA | – |
| 30 | – | – | – | – |
| | $\bar{h}$, BTU/HR FT$^2$ °F | | | |
| -30 | 37 | 41 | 40 | – |
| -25 | 50 | 46 | 60 | – |
| -20 | 44 | 44 | 72 | 45 |
| -10 | 54 | 55 | 62 | – |
| 0 | 64 | 57 | 35 | – |
| 10 | – | 55 | 40 | 43 |
| 20 | – | – | 54 | – |
| 25 | – | – | INSUF. DATA | – |
| 30 | – | – | – | – |

1639-68

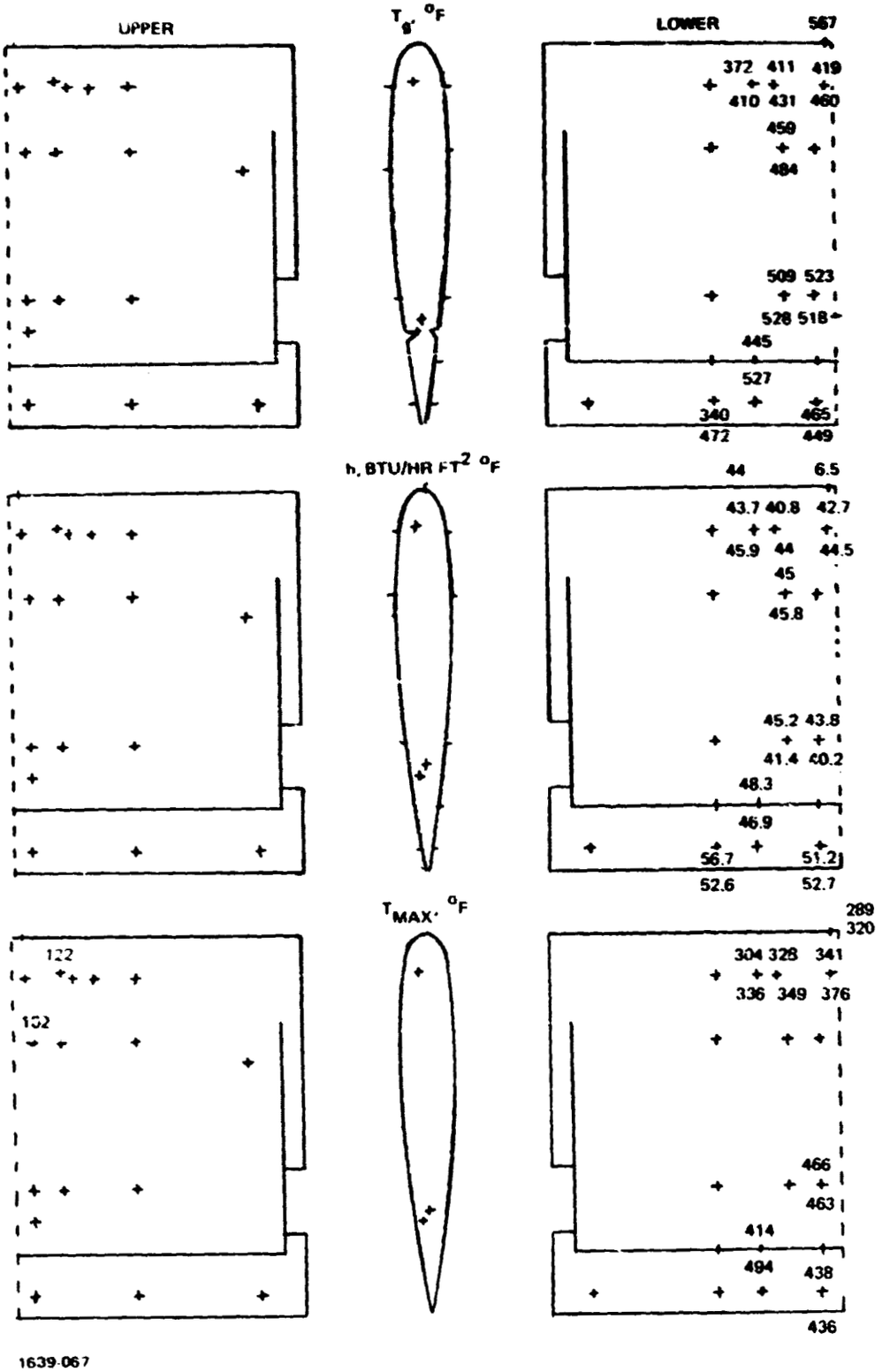


Fig. 4.4-25 Comparison of 110-01 Test Results (-20°) and 113-01 Test Results (-20°)

## 4.5 DYNAMIC ANALYSIS

The location of a control vane in close proximity to the exhaust of a turbofan engine subjects the vane to high intensity fluctuating loads which have the potential for inducing high vibration levels and sonic fatigue. An objective of the test was to define the environment and the resulting vibration levels induced in a test vane. Dynamic measurements were made to determine noise level profiles for different vane positions, angles of attack, and vane/ground separation distances.

Pressure and strain measurements obtained during the test did not reveal any prohibitively difficult problems associated with this control vane concept.

Pressure data indicated that abrupt increases in level can be expected at vane angles equal to or in excess of ±20 degrees.

Peaks occurred on the suction side of the vane and are probably due to separation of flow from the vane. Deflections of the control vane in these high positive and negative angles will be of short duration for control during take off/landing operations.

In particular, the pressure data indicated that the highest levels do not occur on the jet centerline. These results showed the highest levels occurred during operation of the vane above the centerline. Non-similarity of spectral shapes is also evident for these two vane locations.

Strain levels were lower than expected and never exceeded 30 $\mu$ in./in. rms overall. This is attributed to the heavy skin gage and small rib spacing.

Scaling the pressure data to a larger fan/higher thrust engine is feasible with this data using the Strouhal scaling relationship illustrated herein.

### 4.5.1 Vane Microphone Measurements

Vane Microphones 1 and 4, located on the lower and upper skins respectively are the primary microphones for this test. These are the forward most microphones, located just aft of the leading edge structure (Fig. 4.5-1).

The base line data was the information obtained with the ground plane placed at infinity which defines a nonreflective barrier placement. Figure 4.5-2 is a comparison of the overall levels for these two microphones during nine vane angles of attack and two vane positions. The upper plot is data obtained with the vane in Position 3 (See Fig. 4.5-3). The lower microphone does not experience significant increases in overall level in the positive direction but does exhibit an abrupt 15 decibel increase in amplitude as the vane

changes from -10° to -20°. This sharp increase is followed by a decrease to the maximum negative angle.

The upper microphone peaks at a positive vane angle of 25 degrees. The jump in amplitude from +20 to +25 degrees is 7 decibels. All other angles for this microphone indicate small changes in amplitude.

As seen on the lower plot, both microphones indicate similar amplitudes encompassing the angles +10 and -20 degrees with the vane located at the centerline position. A peak for the lower microphone occurs at -25° while the peak for the upper microphone remains at +25°. The lower microphone experiences a 9 decibel jump while the upper microphone increases by 15 decibels.

A composite of one-third octave band data for the lower microphone for vane position 3 is presented in Fig. 4.5-4. In general all data exclusive of the -20, -25 and -30 degree angles fall within an envelope of ±3 decibels. These data indicate a broadband response from 40 to 1250 Hz. The sharp change in amplitude for the -20 degree angle appears for all bands with the maximum amplitude occurring at 80 Hz.

Comparisons between 0 degrees and -20 degrees for the remaining Position 3 runs are presented in Fig. 4.5-5 thru 4.5-11. The peak amplitudes normally occur between 50 and 100 Hz. The spectrum decays in the high frequency at about 4 dB/octave. The proximity of the ground plane appears to suppress the high frequency levels and slightly increase the low frequency levels.

Vane end plates were removed for run 117 and their removal appeared to have no change on the vane noise levels.

A composite of one-third octave band data for the upper microphone for vane position 3 is presented in Fig. 4.5-12. With the exception of the peak spectrum (+25 degrees) the data appears more widely scattered when compared with the lower microphone. These data peak at about 100 Hz and exhibits a typical "hay stack" spectrum. The spectrum levels at a +25 degree vane angle are broad band containing more energy at higher frequencies than does the data for the lower microphone. The fall-off in the high frequency is about 2 decibels per octave band. Data for the remaining test runs for vane Position 3, comparing the 0 degree angle with the +25 degree angle, is presented in Fig. 4.5-13 thru 4.5-19. Note that negative angles result in lower levels than the 0° angle.

Q-Fan operation with the vane located at the centerline position produces somewhat different results when compared with Position 3 (Fig. 4.5-2). Microphone 1 does not experience a peak spectrum until a vane angle of -25° is reached.

The peak in this spectrum now occurs at a higher frequency (200 to 500 Hz) and at a lower amplitude (Fig. 4.5-20.) Reduction in ground plane longitudinal distance results in lower high frequency amplitudes (spectra start to fall at 315 to 400 Hz) while a small increase in the lower frequency amplitude (25 to 40 Hz) occurs. This data is presented in Fig. 4.5-20 thru 4.5-25.

Upper microphone data for this series of runs is presented in Fig. 4.5-26 through 31. The peak spectrum occurs at a vane angle of +25 degrees. Negative 25 degrees results in an increase in level when compared with the 0 degree position. This is contrary to the lower microphone where the spectrum stays essentially the same at 0° and +25°.

Comparisons of the results for the two vane positions are presented in Fig. 4.5-32 and 4.5-33. Lower surface exposures at 0° vane positions are very similar but peak spectrum results at the negative vane angles are quite different in the 50 to 160 Hz frequency range. A significant increase in energy results for vane position 3.

The upper microphone yields higher amplitudes at the centerline position for the positive 25 degree vane angle. Levels for vane angle at 0° and vane position 3 are several decibels higher in the 50 to 500 Hz range.

Microphones 1 and 4 are approximately opposite each other on the lower and upper surfaces of the vane. Figures 4.5-34 through 4.5-41 present comparisons of spectra for the same angle and for the highest amplitudes. At vane position 3 the largest variation of spectra occurs. The lower microphone has a higher amplitude spectrum with a peak. The upper microphone exhibits a broad-band spectrum.

The spectra are similar at both the positive and negative angle with the exception of amplitude. The vane centerline position produces very similar results for the 0 degree angle.

Examples of one-third octave power spectra of the surface pressures discussed above are shown in Fig. 4.5-42 through 4.5-51. The spectra are divided by the square of the fan jet dynamic pressure and are plotted against the Strouhal number $N_{STR} = \frac{D_N \cdot f}{u_F}$ based on fan nozzle diameter $D_N$ and the fan exit velocity $u_F$.

The lower microphone peaks at a Strouhal number of 0.6 to 0.9 for vane position 3. The upper microphone produces a broader spectrum with peaks occuring at Strouhal numbers of 1 to 2.

Zero degree angle runs with the vane in position 3 produce peaked spectrums at Strouhal numbers of 1.

Operation in the centerline location yields peaks at higher Strouhal numbers and higher power spectra.

The variation of this data may be seen in Fig. 4.5-52 through 4.5-55. These plots are summarized further in Fig. 4.5-56 and 4.5-57. Vane position 3 produces the greatest variation in amplitudes and spectrums while very similar data is obtained for the centerline location. The high frequency portion of the lower surface spectra falls off at about the inverse 1.38 to 1.45 power of the Strouhal number. This is a simple approximation of the decay which could be useful for analytical purposes.

### 4.5.2 Vane Dynamic Strain Measurements

Strain gages were located on the internal skin and rib flanges. The high thermal exposure anticipated resulted in relatively heavy vane structure and as a consequence the combination of this plus small panel sizes resulted in very low amplitude dynamic strain responses. During these tests the overall RMS strain level never exceeded 30 $\mu$ in/in on any strain gage. Figure 4.5-58 is an overall strain level plot for several selected runs at the various angles of incidence. One-third octave strain level spectra are presented for two strain gages in Fig. 4.5-59 thru 4.5-67. These strain results all indicate the same spectrum trend demonstrated by higher amplitudes at low frequencies then falling off to 500 Hz followed by a second peak occuring at about 1250 Hz. Angle of incidence increases result in changes in amplitude but not as dramatic as would be expected when compared with pressure data. Figure 4.5-63 compares the two vane positions tested. The centerline position yields slightly higher results.

### 4.5.3 External Microphone

A single high intensity microphone was mounted on the engine stand framework to determine the effect of ground plane longitudinal changes. The reflections off the vane and the location of the vane relative to the exhaust appear to have small effects on this microphone when compared to overall radiated noise. The results with the ground plane at infinity for both vane positions are presented in Fig. 4.5-68. The centerline position appears to yield higher low-frequency results at this microphone position. The results for vane position 3 are complied in Fig. 4.5-69. The effect of the ground plane reflections is large from 25 through 100 Hz while smaller increases occur through 2.5 KHz. The results for the vane centerline position (Fig. 4.5-70) are similar, however, the spectra do not change significantly as the barrier longitudinal distance is decreased.

The effect of vane angle is presented in Fig. 4.5-71 through 4.5-74. Negative vane angles tend to increase the noise levels at this microphone position for both vane positions.

4.5.4 Dynamic Pressure Coefficients

The range of values of the dynamic pressure coefficient, for a representative run, are plotted against angle of attack in Fig. 4.5-75. The dynamic pressure coefficient is the ratio of $P_{rms}$, the root-mean-square value of the fluctuating component of the surface pressure, to the dynamic pressure at the fan nozzle exit, $q_F$. The highest values occur at -20° and +25° (the vane stall angles) while the majority of the data fall in the range of .02 to .06.

4.5.5 Scaling to Other Fan/Engine Configurations

The normalized one-third octave power spectra plots obtained in this test program may be used to estimate surface sound pressure levels for larger configurations operating at higher thrust levels. The following paragraphs illustrate the procedure with an example using a fan pressure ratio of 1.3, a fan nozzle exit diameter of 78 inches and the most critical acoustic situation encountered in this program, i.e., the lower surface of the vane in the offset position and at a -20° setting.

In hover at sea level on a tropical day, the fan pressure ratio of 1.3 will produce a fan nozzle velocity of approximately 686 ft/sec and a dynamic pressure of 530 lb/sq ft.

At a one-third octave band having a center frequency of 100 Hz, the Strouhal number for the new configuration is:

$$N_{STR} = \frac{D_N \cdot f}{u_F} = \frac{78 \times 100}{12 \times 686} = 9.5 \times 10^{-1}$$

From Fig. 4.5-42, the normalized one-third octave power level at this Strouhal number is:

$$\frac{\Pi(N_{STR})}{q_F^2} = 3 \times 10^{-3}$$

The one-third octave sound pressure level for the larger configuration at the 100 Hz center frequency is:

$$\text{One-third octave } SPL_{100\text{ Hz}} = \left[\frac{\Pi(N_{STR}) \cdot q_F^2}{q_r^2}\right]^{\frac{1}{2}}$$

$$= \left[(3 \times 10^{-3}) \times (530)^2\right]^{\frac{1}{2}}$$

$$= 29.03 \text{ lb/sq ft}$$

Converting to decibels:

$$SPL_{100\text{ Hz}} = 20 (\log SPL - \log SPL_{ref.})$$

$$= 20 (\log 29.03 - \log 4.18 \times 10^{-7})$$

$$= 156.8 \text{ dB}$$

Application of this procedure to the overall spectrum yields the results shown in Fig. 4.5-76.

The calculated curve is similar in shape to the measured data in this case. This results because the ratio of $D_N/u_F$ in the Strouhal formula are approximately the same for both the test and the new configuration. Other examples might result in the spectra peaking at different frequencies.

The overall sound pressure level for this new curve is obtained by standard procedures and yields a value of 166.5 dB, an increase of 5 decibels over the value for the test configuration.

When applying this method for other locations and operating angles the data will yield somewhat lower noise spectra. Selection of operating conditions and durations is important in determining the overall lifetime exposure to acoustic energy.

NOTE: MICROPHONE 1.2.3, ON LOWER SKIN (0)
MICROPHONE 4.5, ON UPPER SKIN (Δ)

| MIC NO. | LOC. AFT OF L.E. |
|---|---|
| 1 | 8.2 INCHES |
| 4 | 9.2 INCHES |
| 2 | 12.5 INCHES |
| 5 | 13.0 INCHES |
| 3 | 17.0 INCHES |

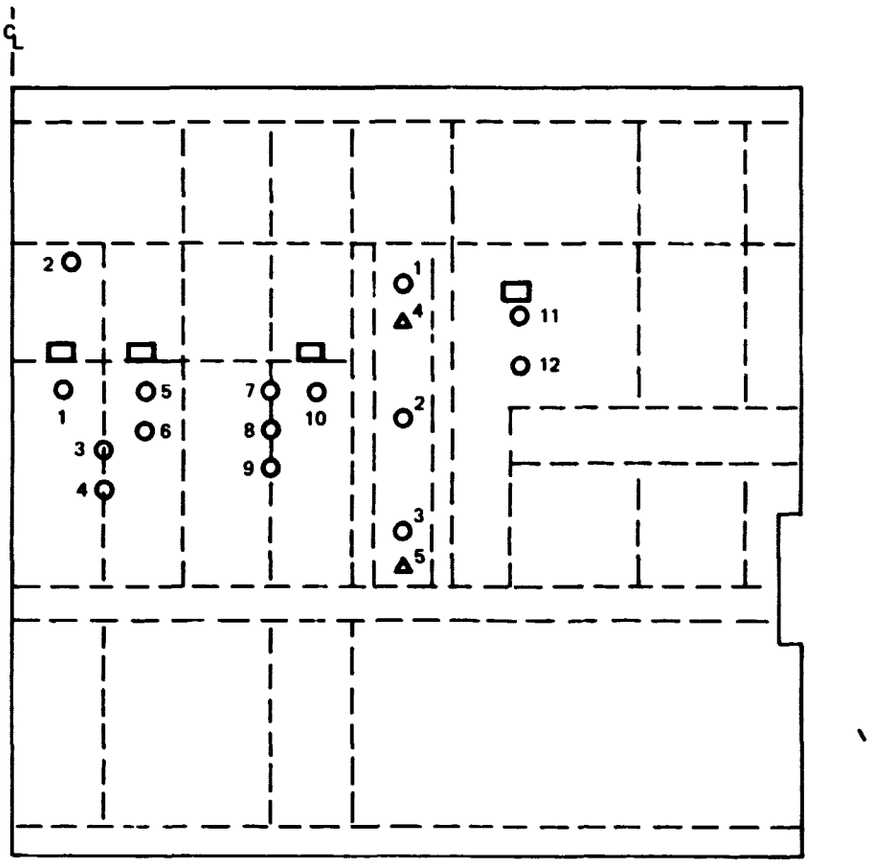


VANE STARBOARD SIDE – LOOKING DOWN

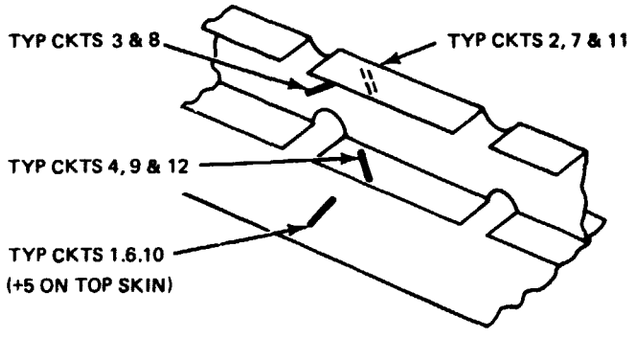


1639-069

**Fig. 4.5-1 Location of Microphones & Strain Gages on Vane**

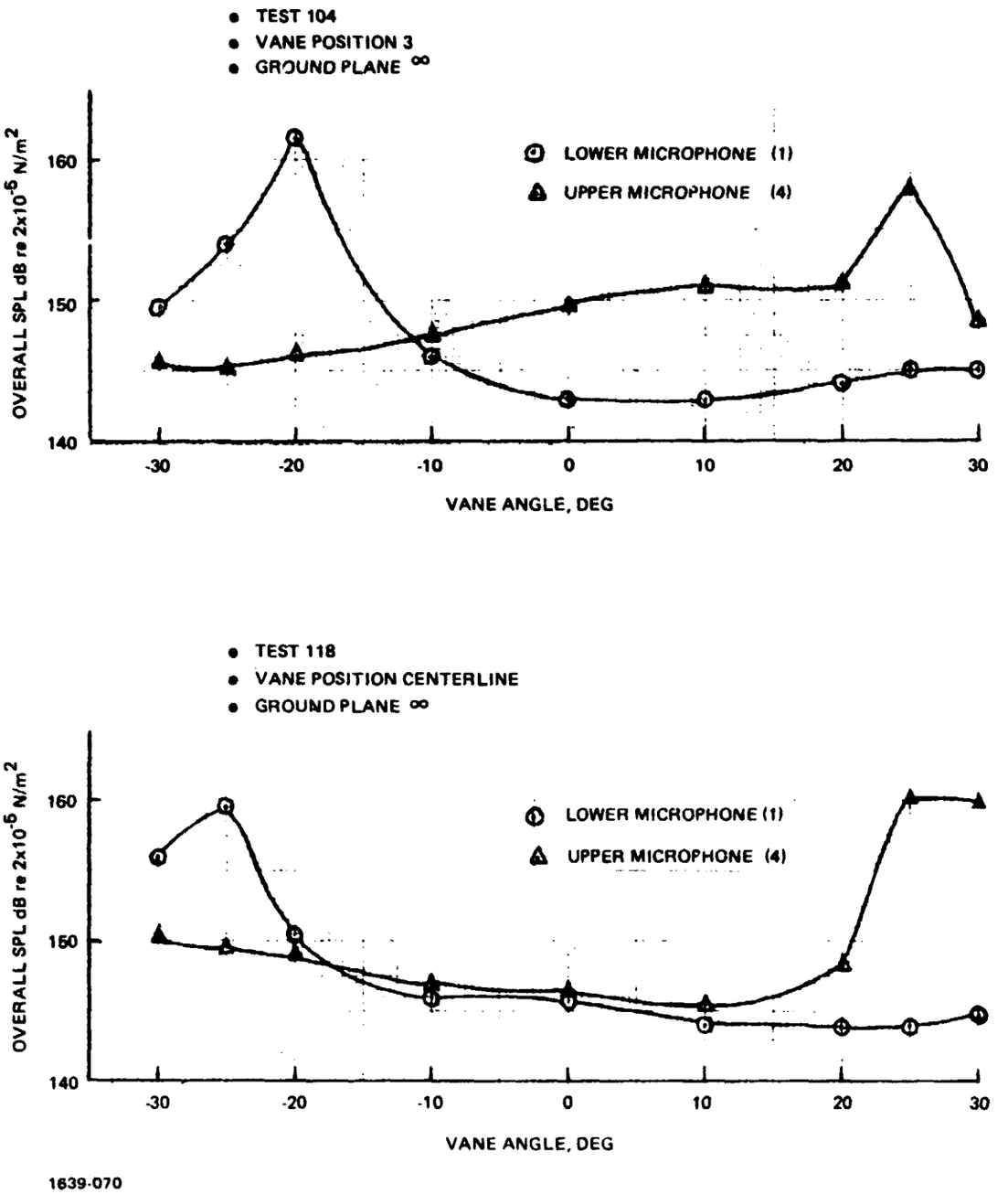


**Fig. 4.5-2 Overall SPL vs Vane Angle for Two Vane Positions**

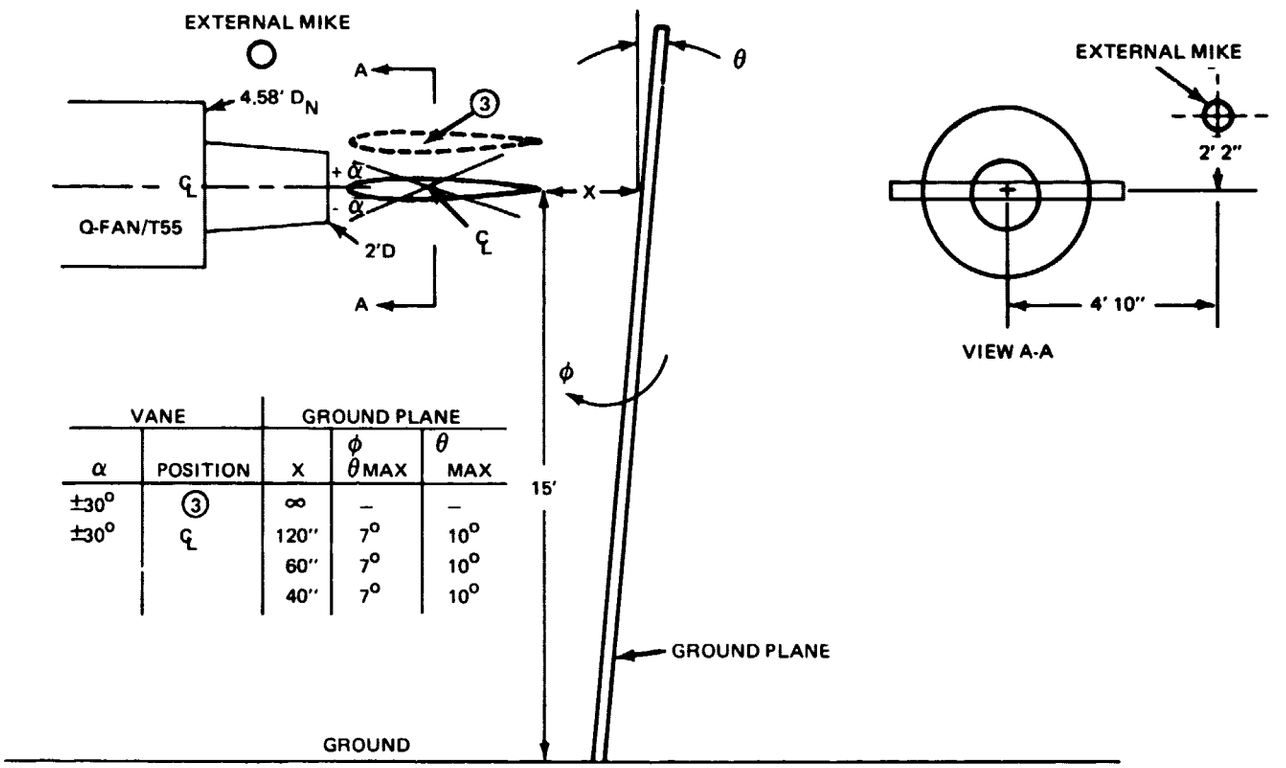


| VANE | | GROUND PLANE | | |
|---|---|---|---|---|
| α | POSITION | X | ϕ θMAX | θ MAX |
| ±30° | ③ | ∞ | – | – |
| ±30° | ℄ | 120" | 7° | 10° |
| | | 60" | 7° | 10° |
| | | 40" | 7° | 10° |

1639-71

**Fig. 4.5-3 Engine/Vane/Ground Plane Configuration**

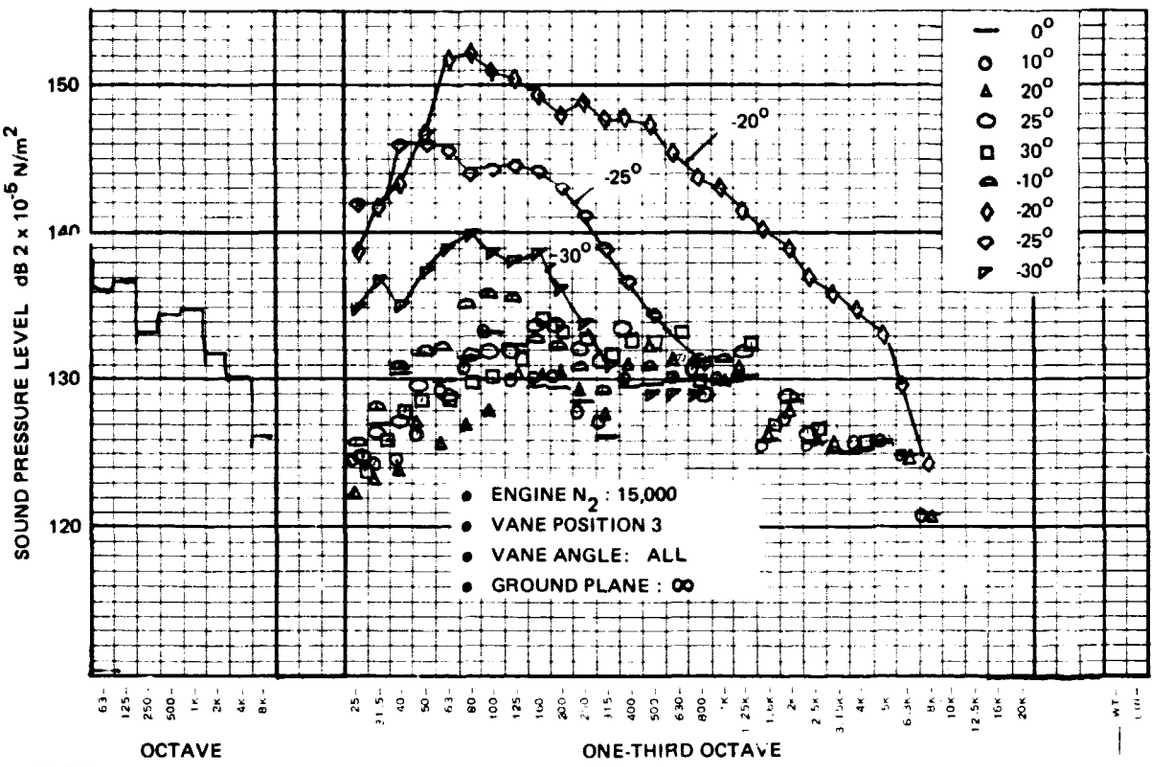


1639-072

**Fig. 4.5-4 Vane Microphone Measurement, Microphone No. 1, Test No. 104**

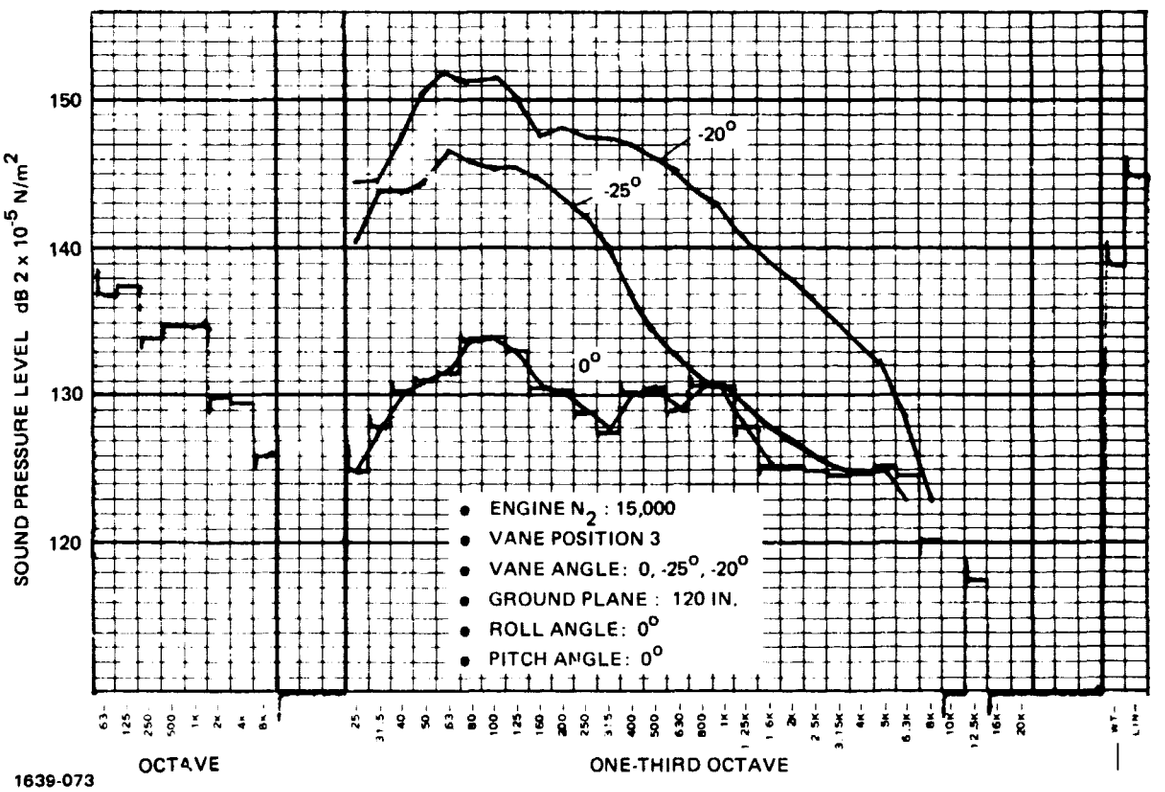


1639-073

**Fig. 4.5-5 Vane Microphone Measurement, Microphone No. 1, Test No. 111**

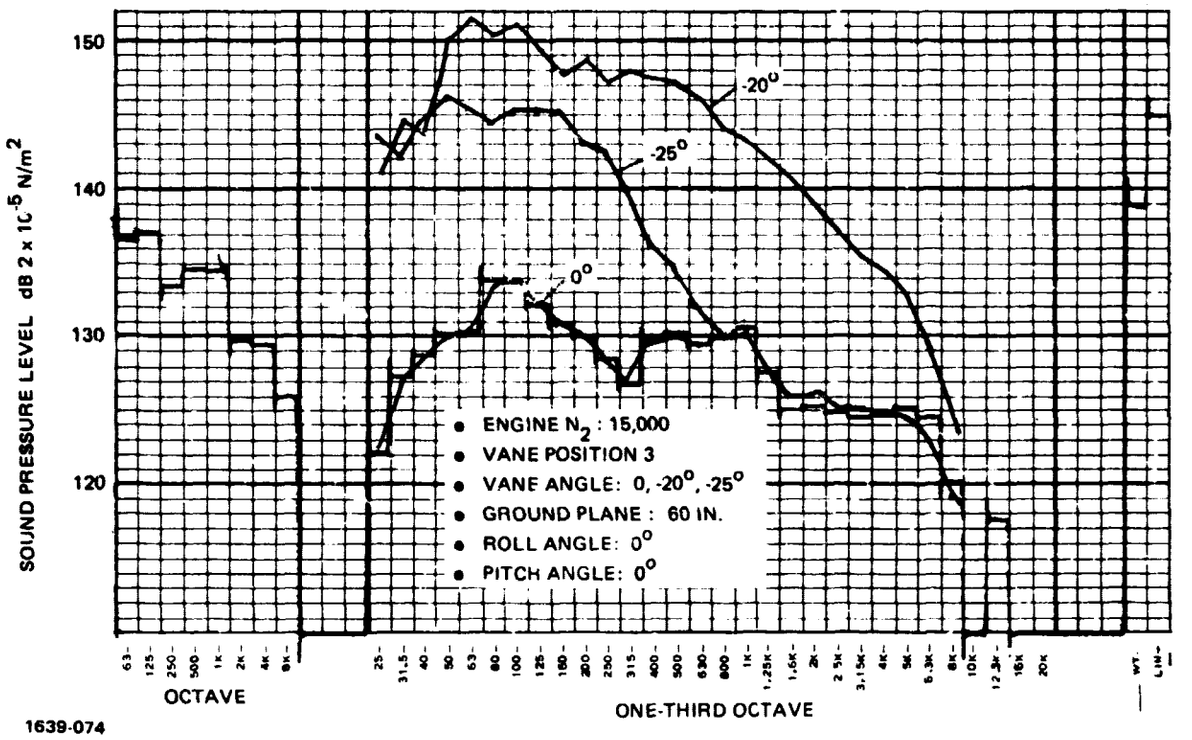


Fig. 4.5-6 Vane Microphone Measurement, Microphone No. 1, Test No. 112

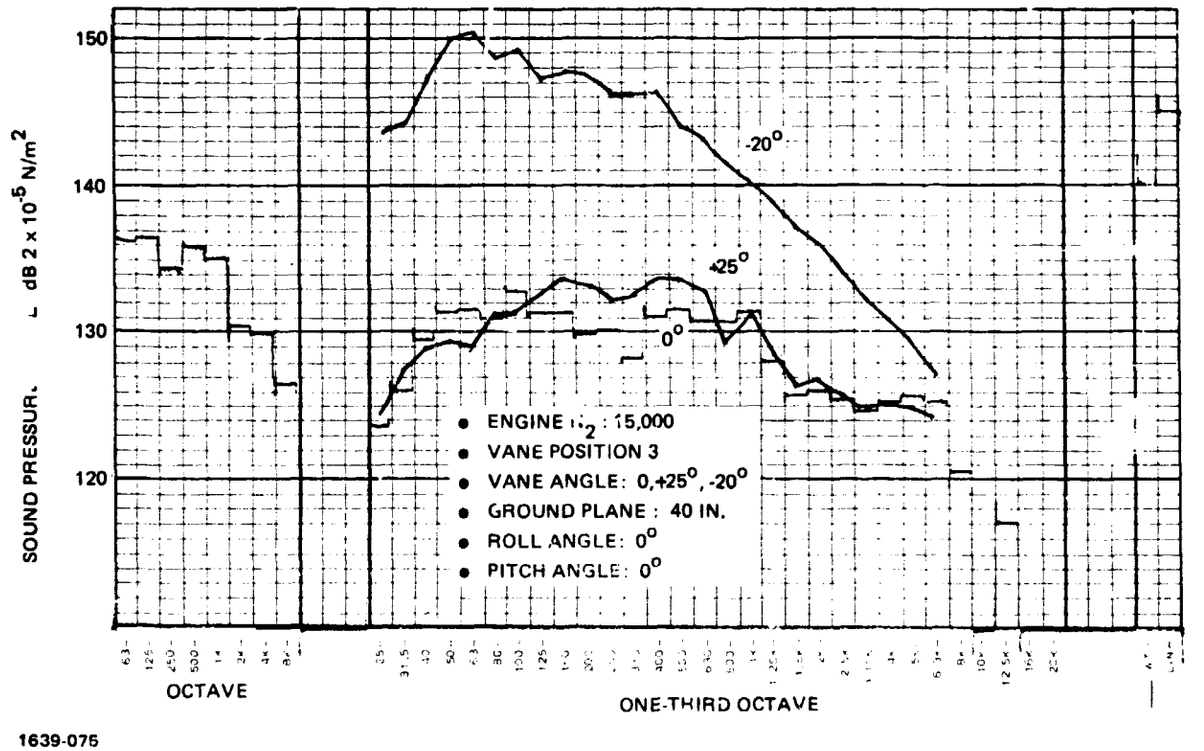


Fig. 4.5-7 Vane Microphone Measurement, Microphone No. 1, Test No. 113

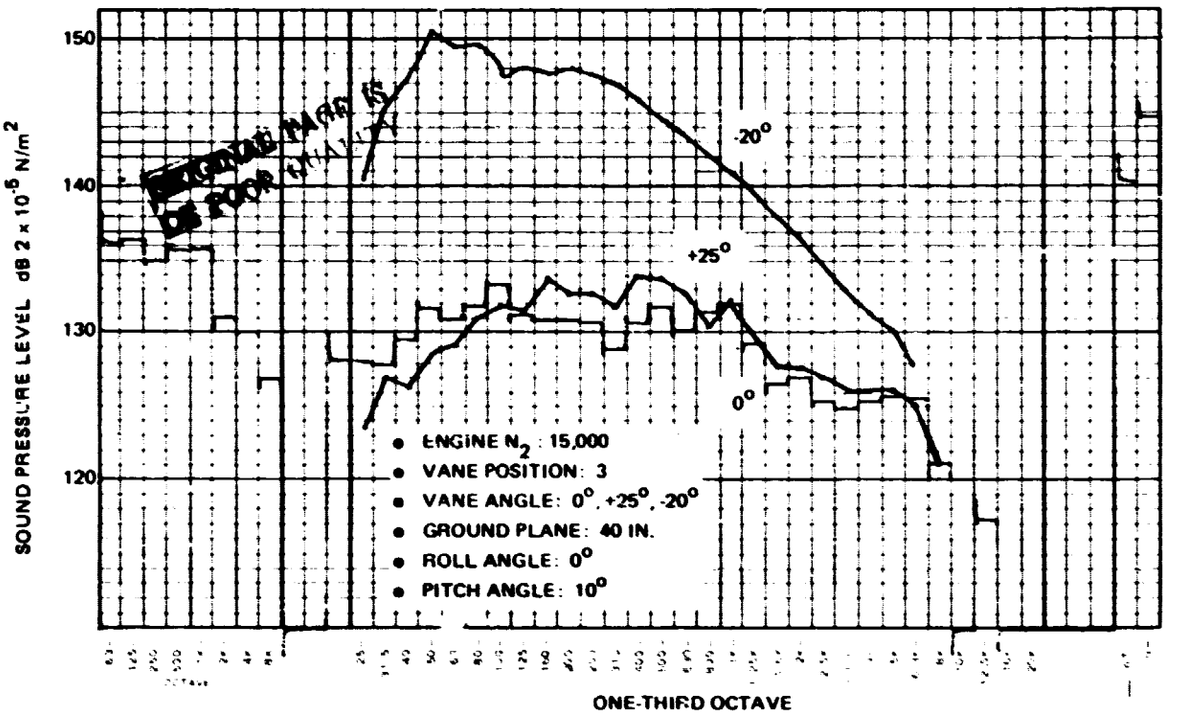


1639-076

**Fig. 4.5-8 Vane Microphone Measurement, Microphone No. 1, Test No. 114**

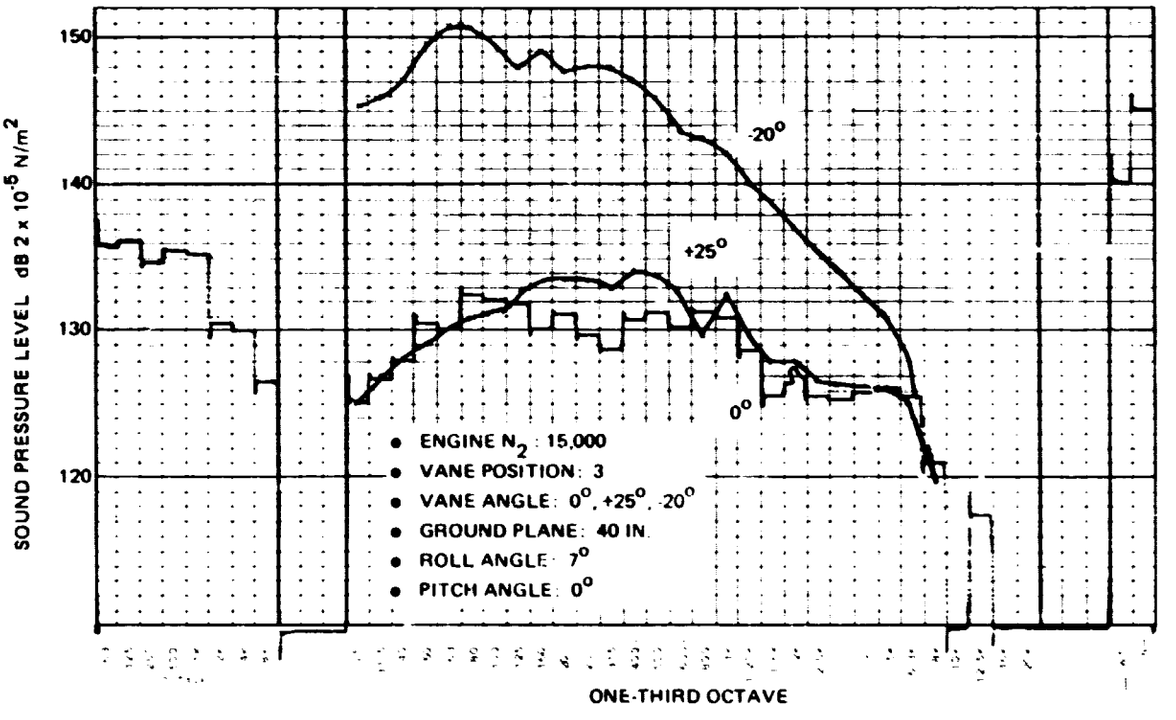


1639-077

**Fig. 4.5-9 Vane Microphone Measurement, Microphone No. 1, Test No. 115**

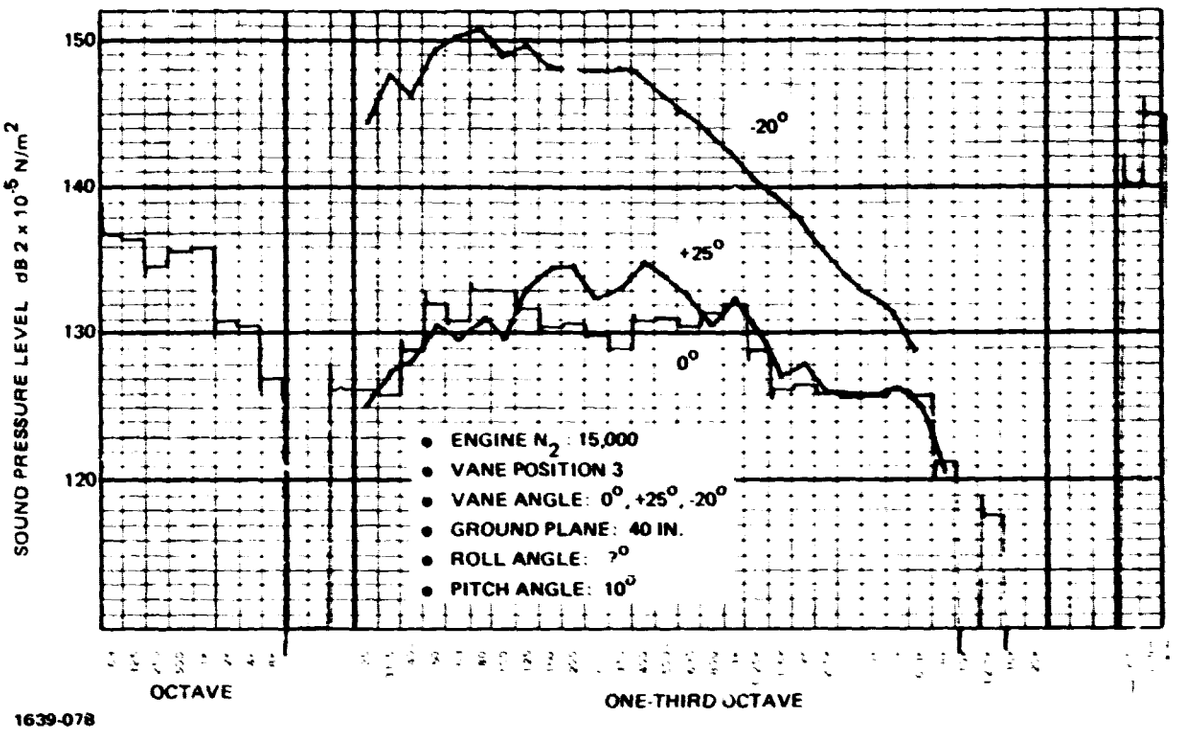


Fig. 4.5-10 Vane Microphone Measurement, Microphone No. 1, Test No. 116

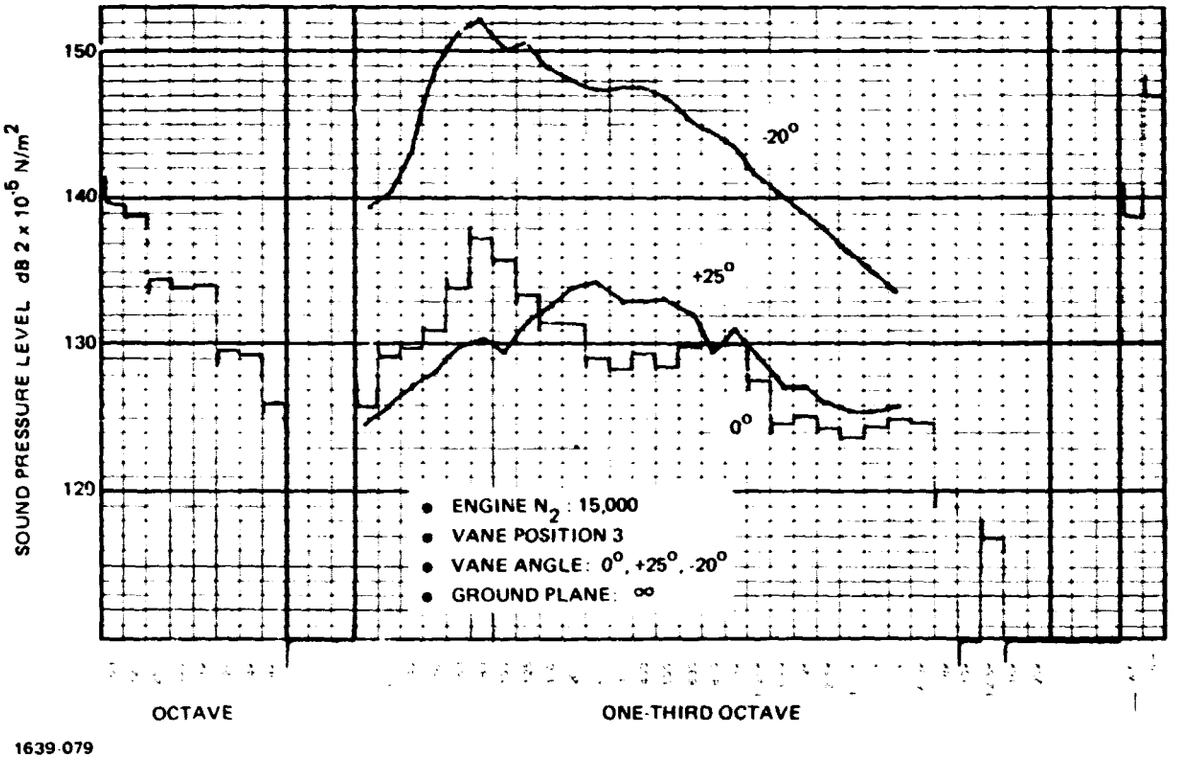


Fig. 4.5-11 Vane Microphone Measurement, Microphone No. 1, Test No. 117

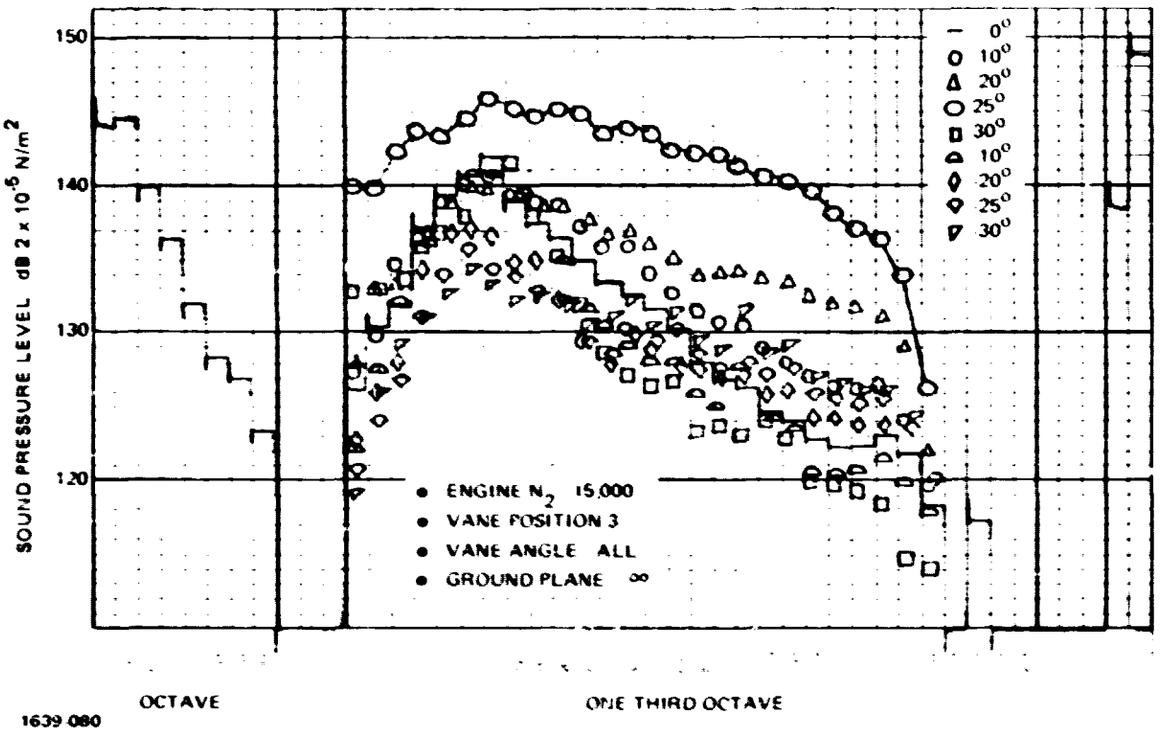


Fig. 4.5-12 Vane Microphone Measurement, Microphone No. 4, Test No. 104

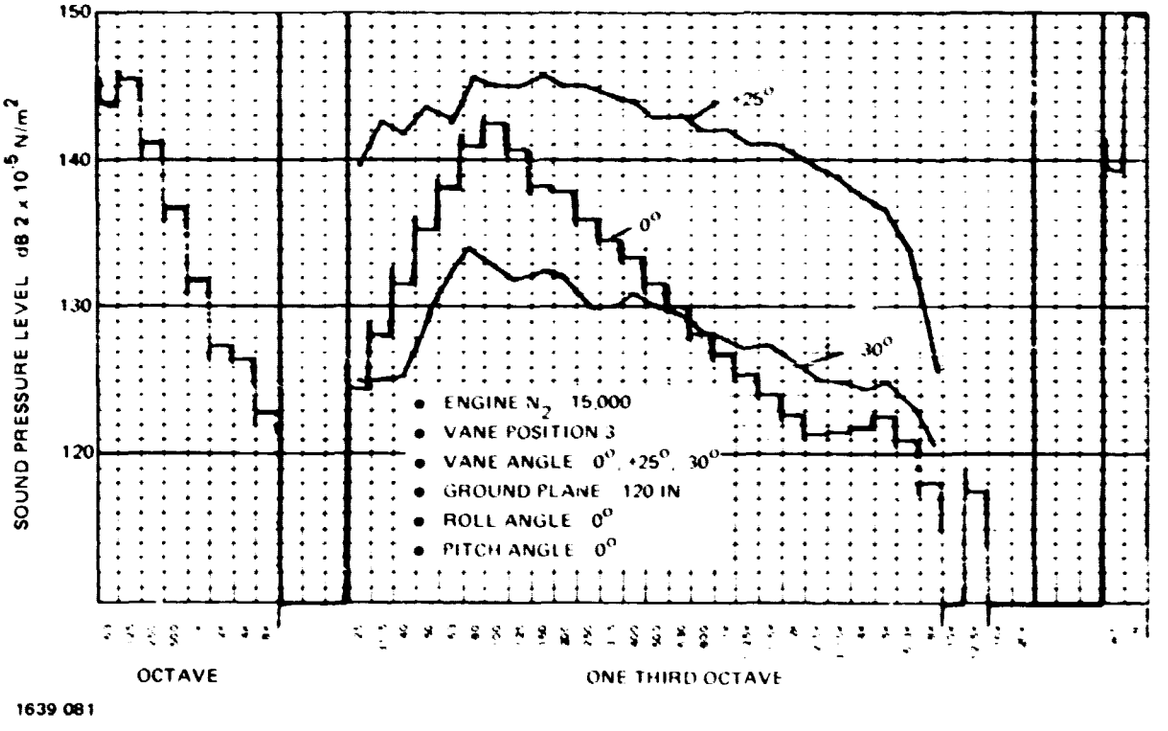


Fig. 4.5-13 Vane Microphone Measurement, Microphone No. 4, Test No. 111

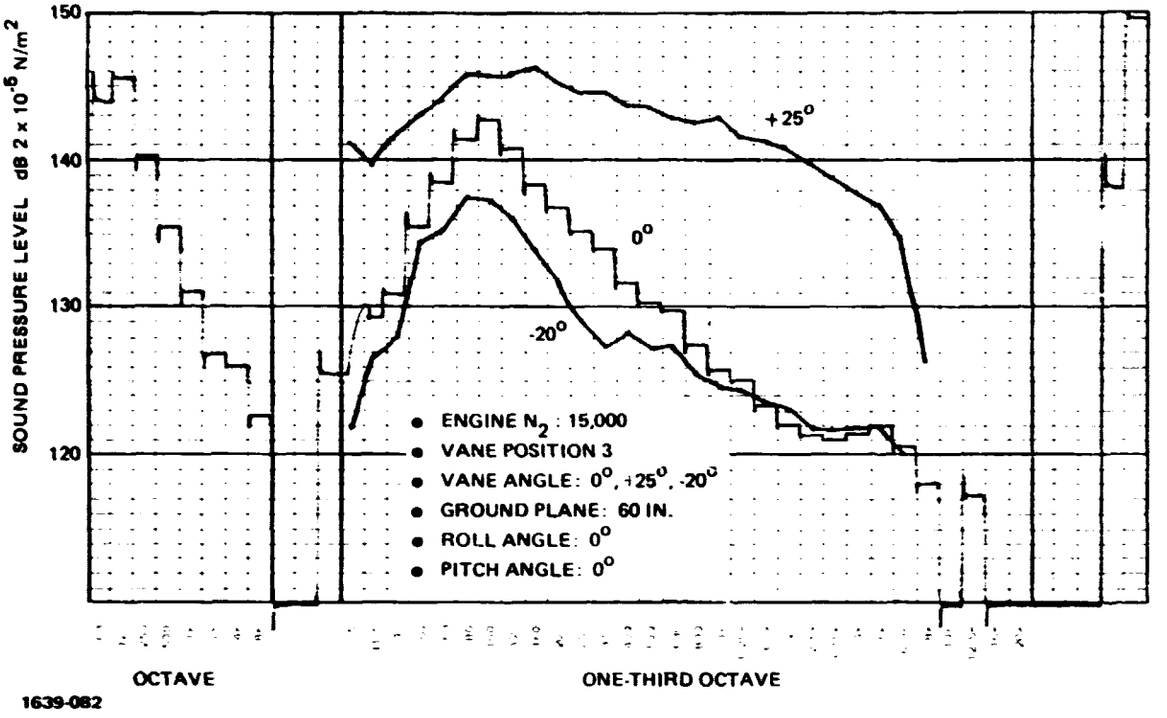


Fig. 4.5-14 Vane Microphone Measurement, Microphone No. 4, Test No. 112

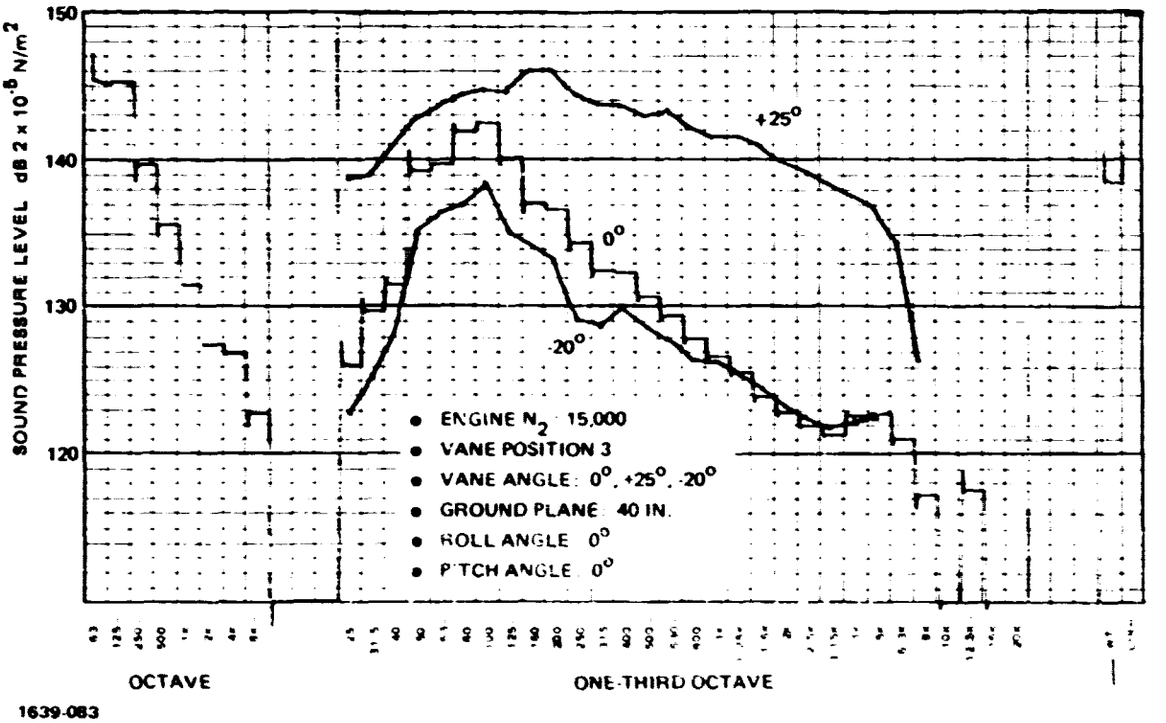


Fig. 4.5-15 Vane Microphone Measurement, Microphone No. 4, Test No. 113

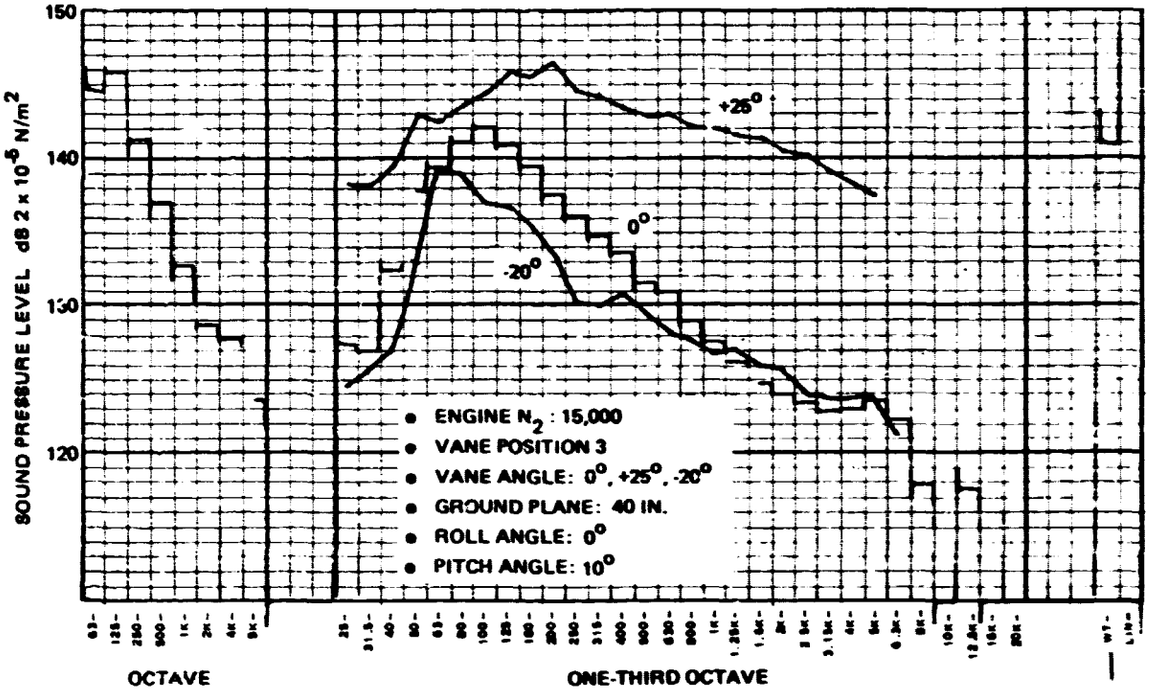


1639-084

Fig. 4.5-16 Vane Microphone Measurement, Microphone No. 4, Test No. 114

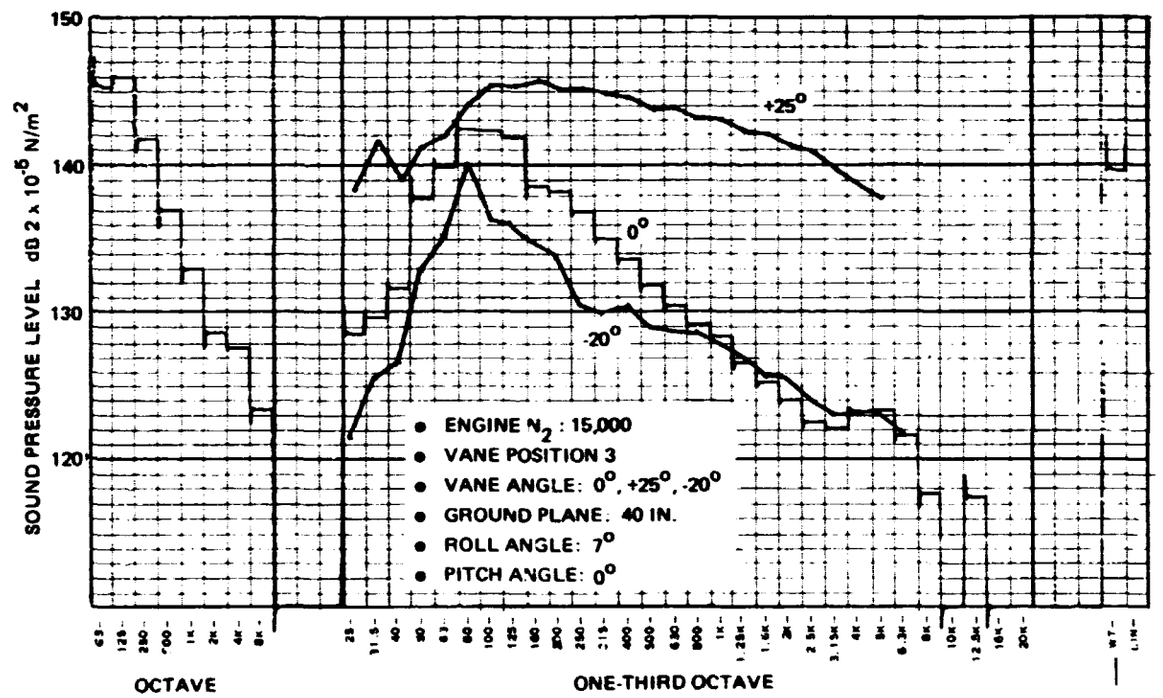


1639-085

Fig. 4.5-17 Vane Microphone Measurement, Microphone No. 4, Test No. 115

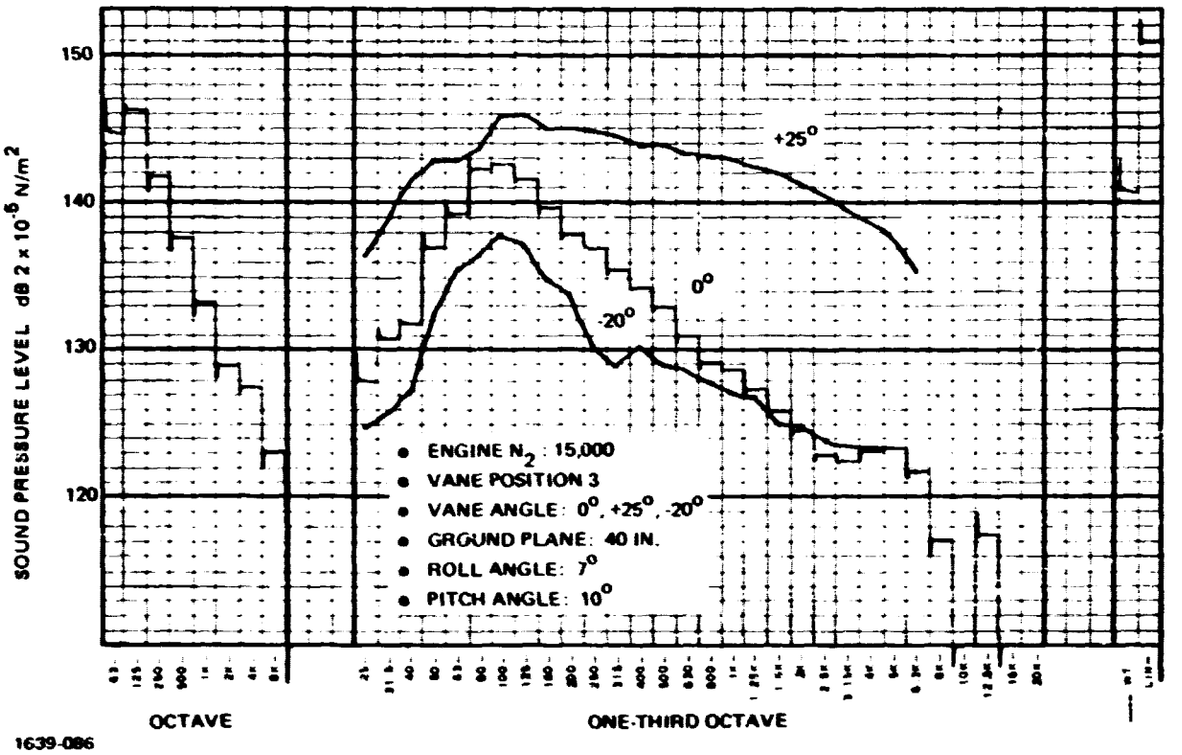


Fig. 4.5-18 Vane Microphone Measurement, Microphone No. 4, Test No. 116

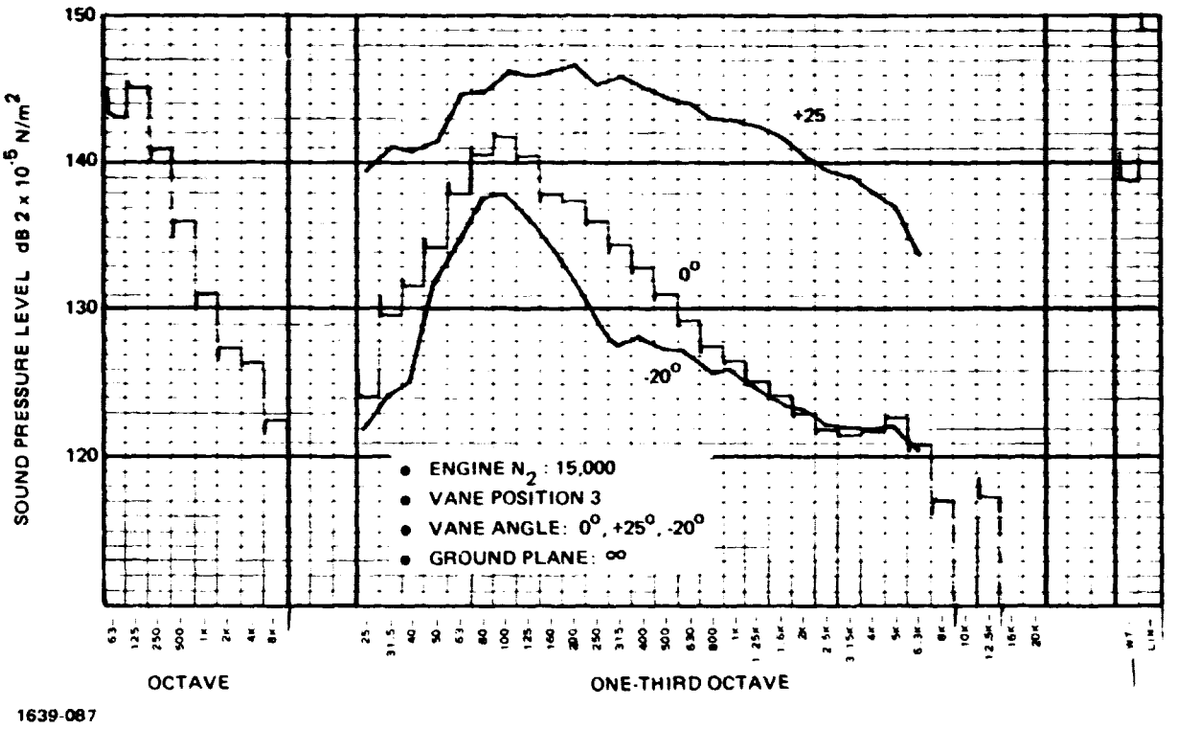


Fig. 4.5-19 Vane Microphone Measurement, Microphone No. 4, Test No. 117

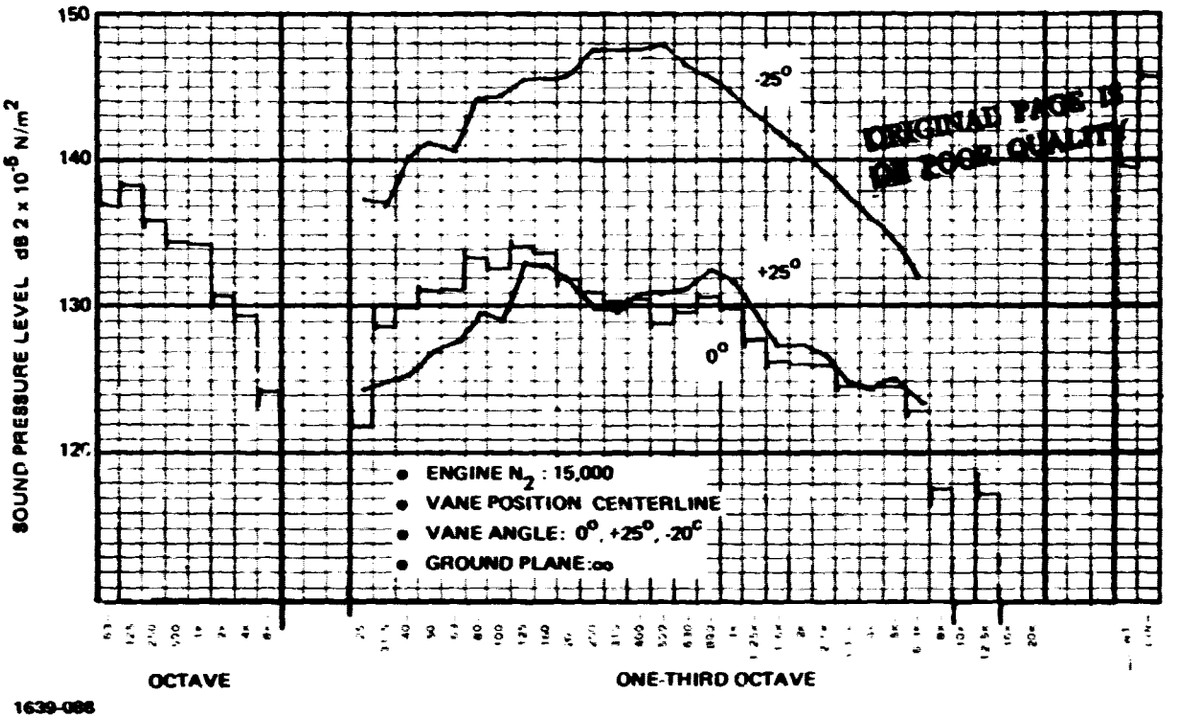


Fig. 4.5-20 Vane Microphone Measurement, Microphone No. 1, Test No. 118

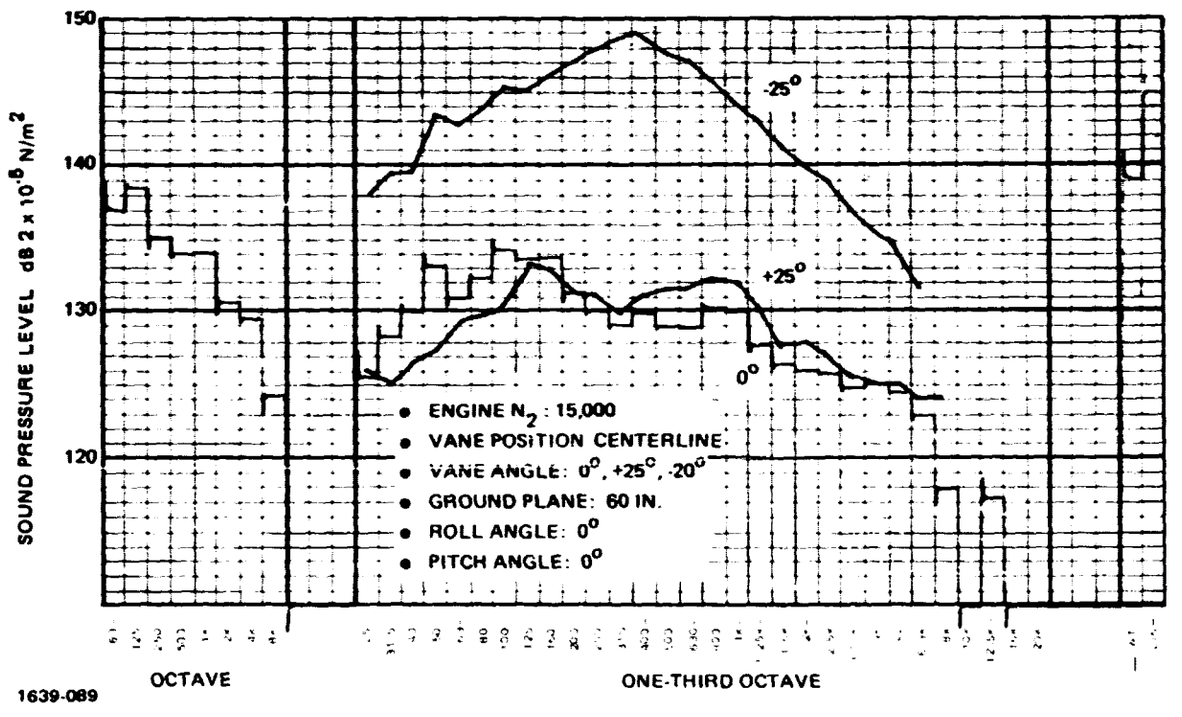


Fig. 4.5-21 Vane Microphone Measurement, Microphone No. 1, Test No. 119

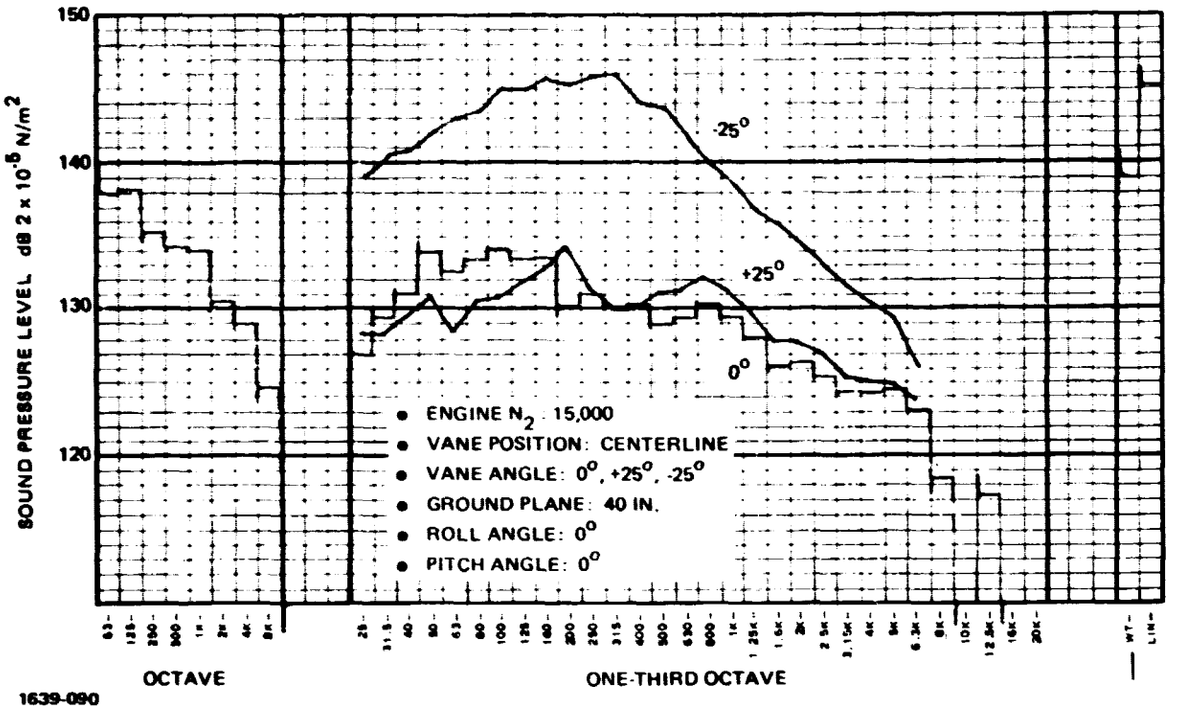


Fig. 4.5-22 Vane Microphone Measurement, Microphone No. 1, Test No. 120

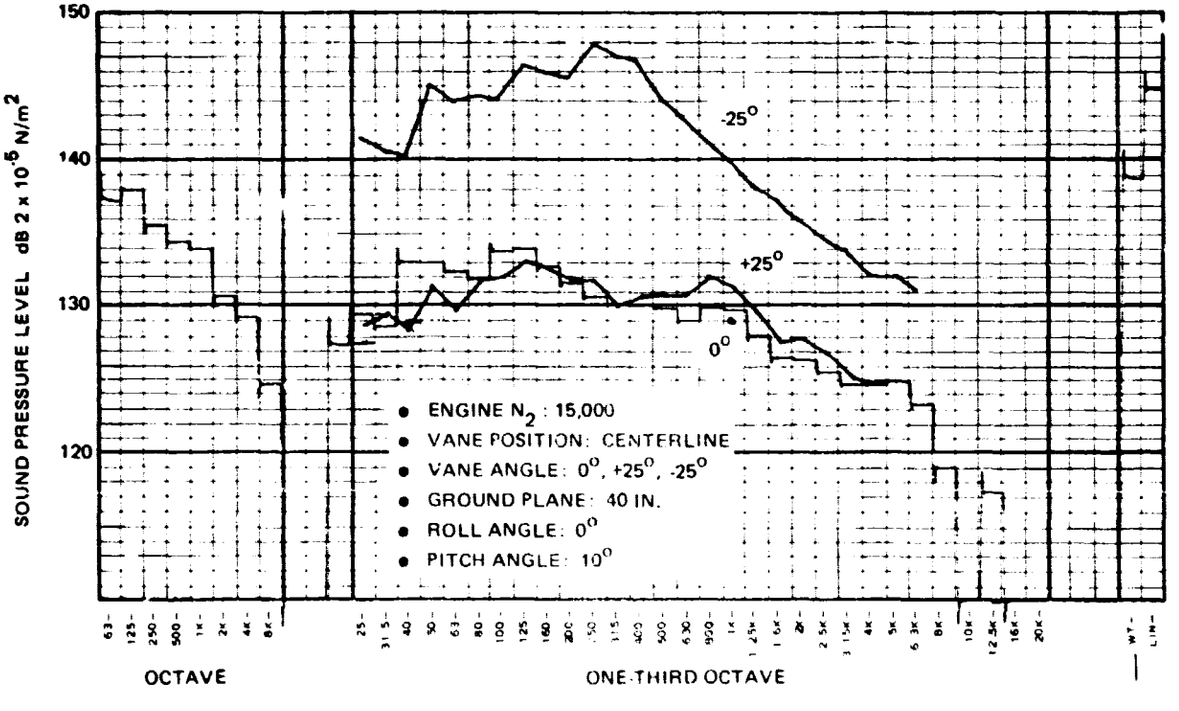


Fig. 4.5-23 Vane Microphone Measurement, Microphone No. 1, Test No. 121

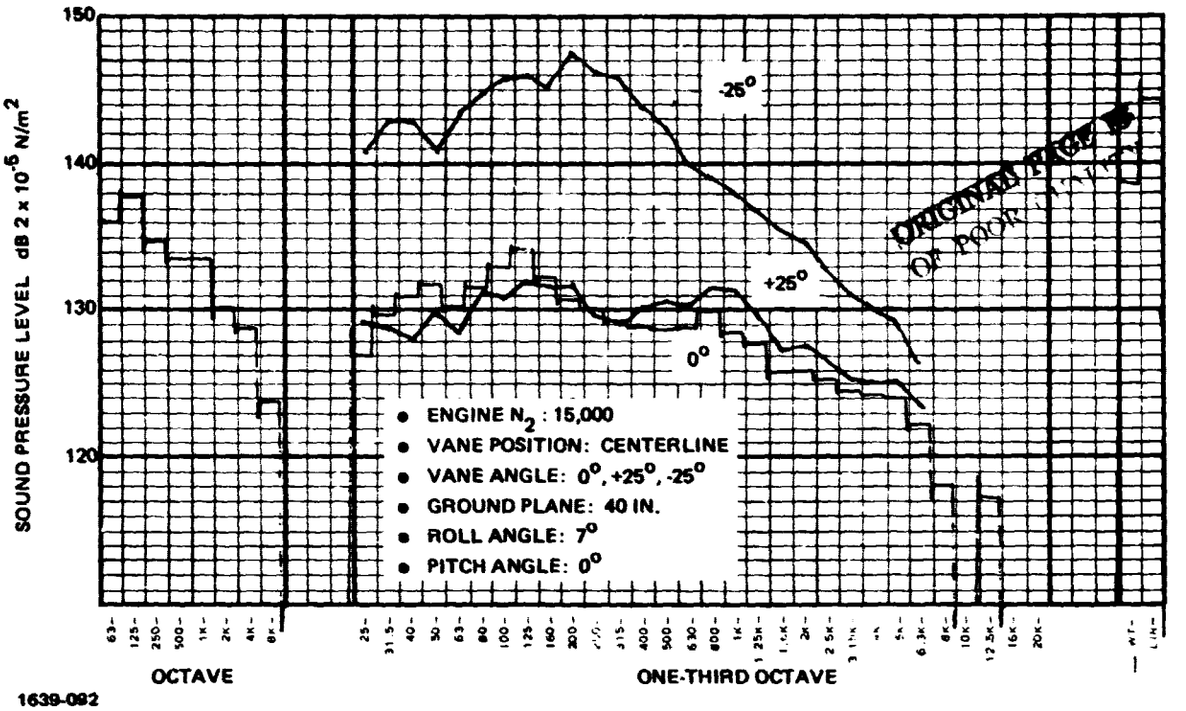


Fig. 4.5-24 Vane Microphone Measurement, Microphone No. 1, Test No. 122

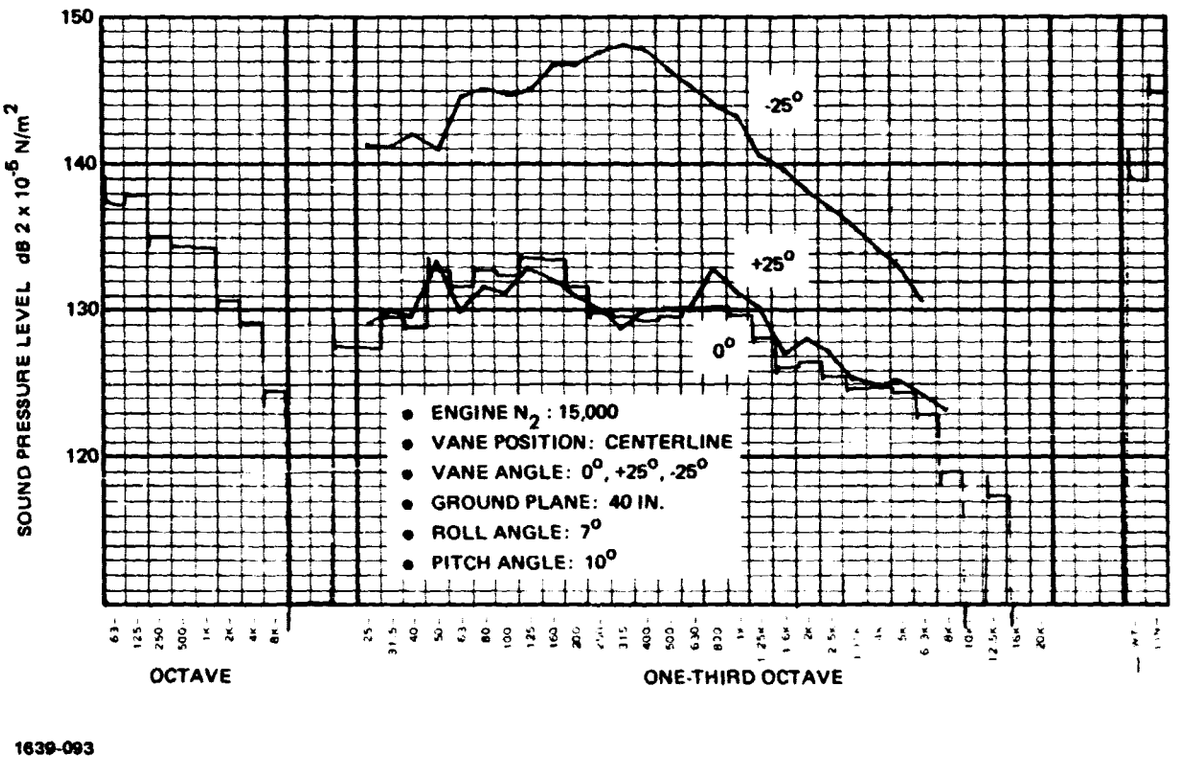


Fig. 4.5-25 Vane Microphone Measurement, Microphone No. 1, Test No. 123

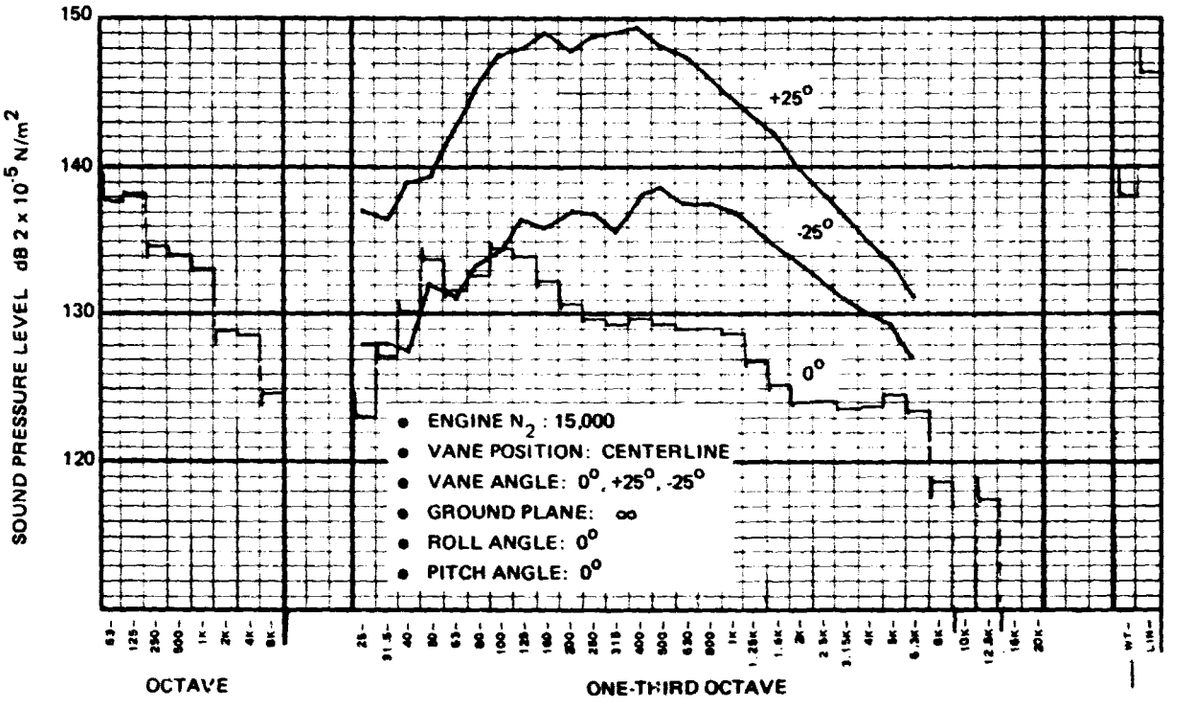


1639-094

Fig. 4.5-26 Vane Microphone Measurement, Microphone No. 4, Test No. 118

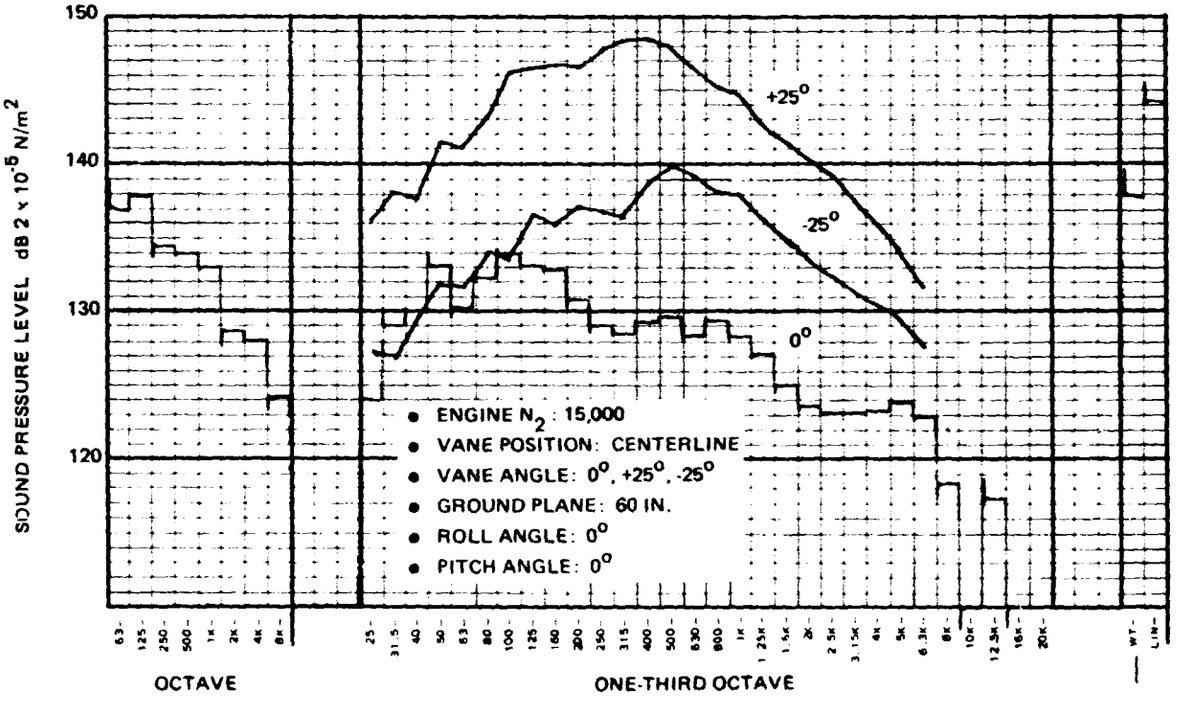


1639-095

Fig. 4.5-27 Vane Microphone Measurements, Microphone No. 4, Test No. 119

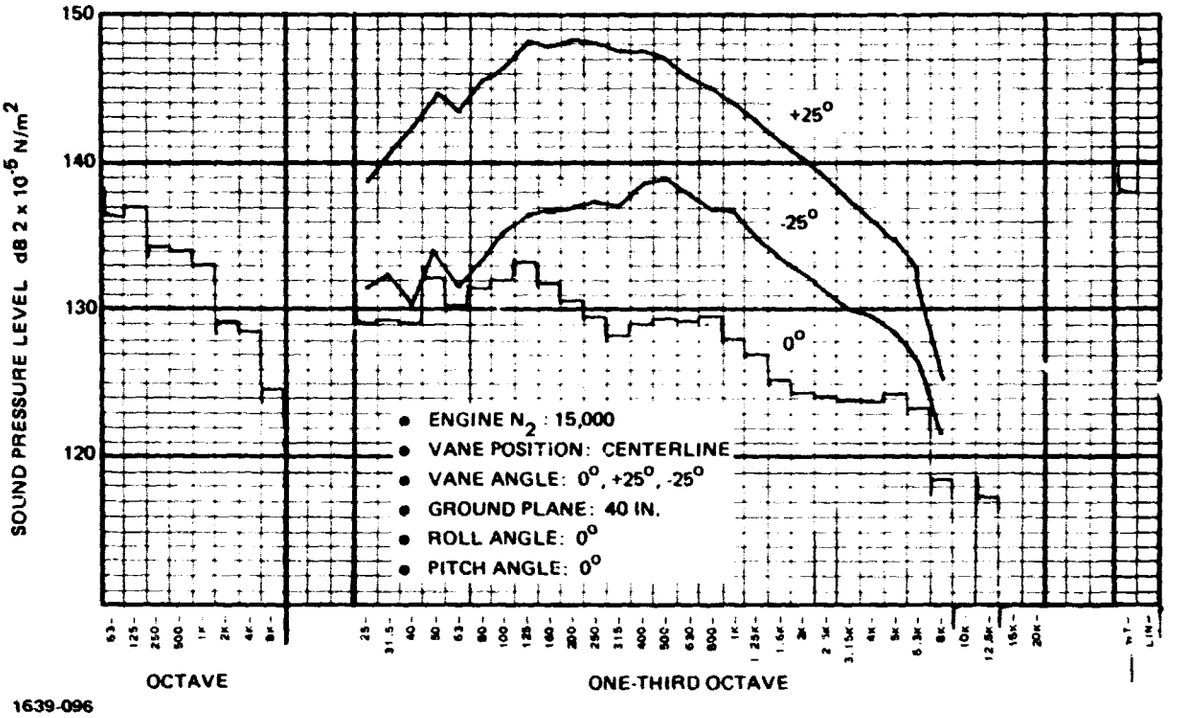


Fig. 4.5-28 Vane Microphone Measurement, Microphone No. 4, Test No. 120

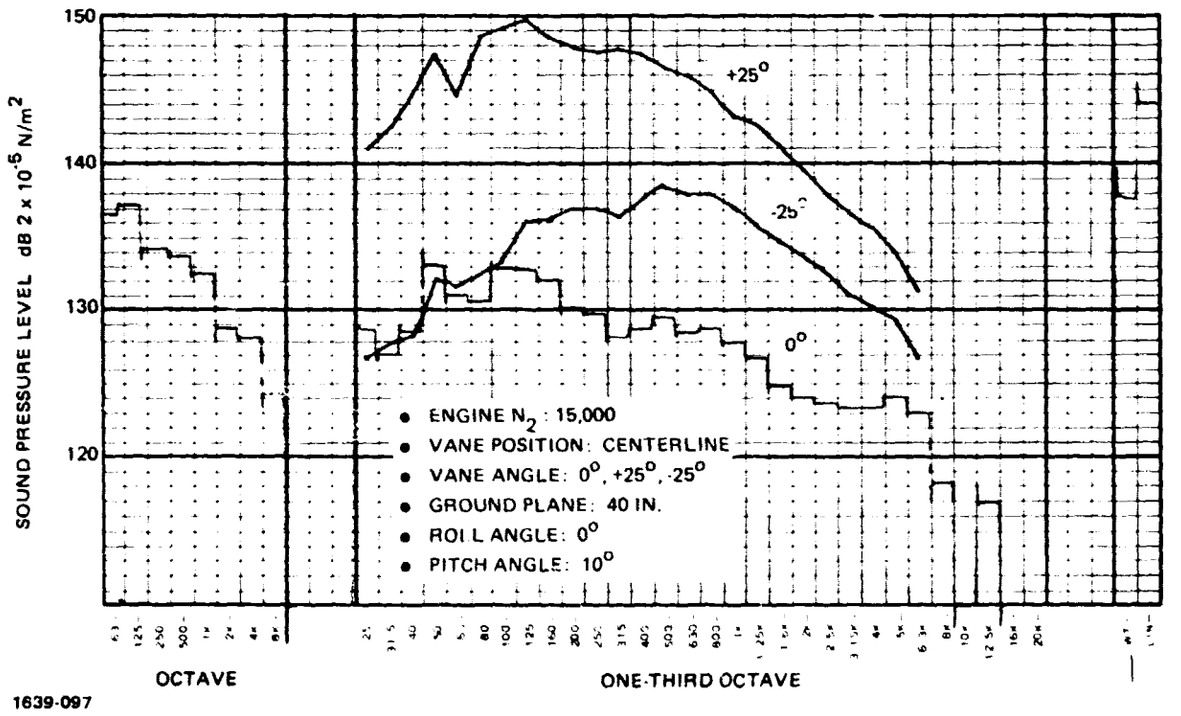


Fig. 4.5-29 Vane Microphone Measurement, Microphone No. 4, Test No. 121

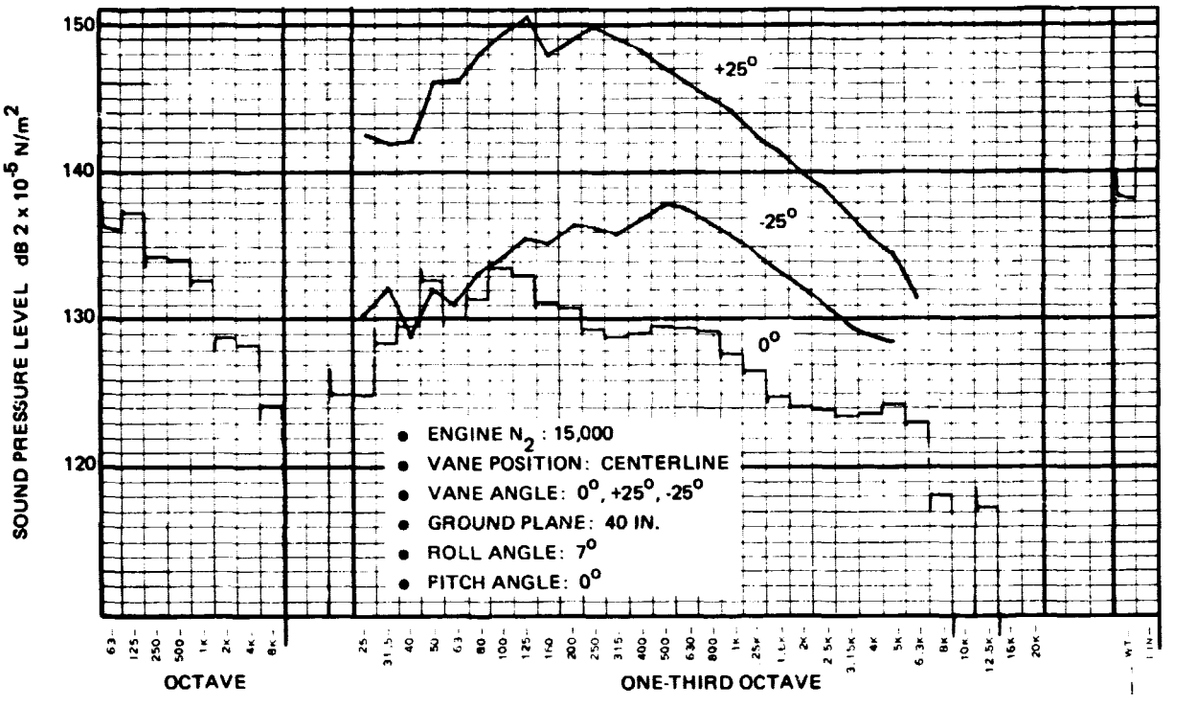


**Fig. 4.5-30 Vane Microphone Measurement, Microphone No. 4, Test No. 122**

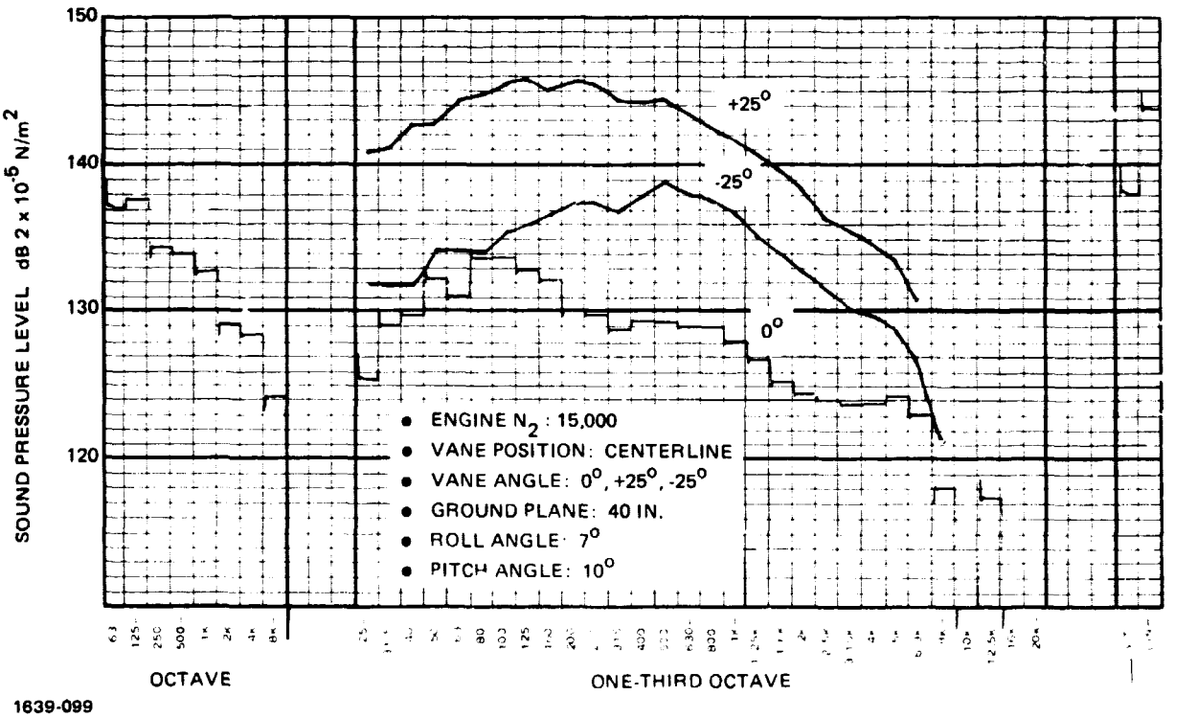


**Fig. 4.5-31 Vane Microphone Measurement, Microphone No. 4, Test No. 123**

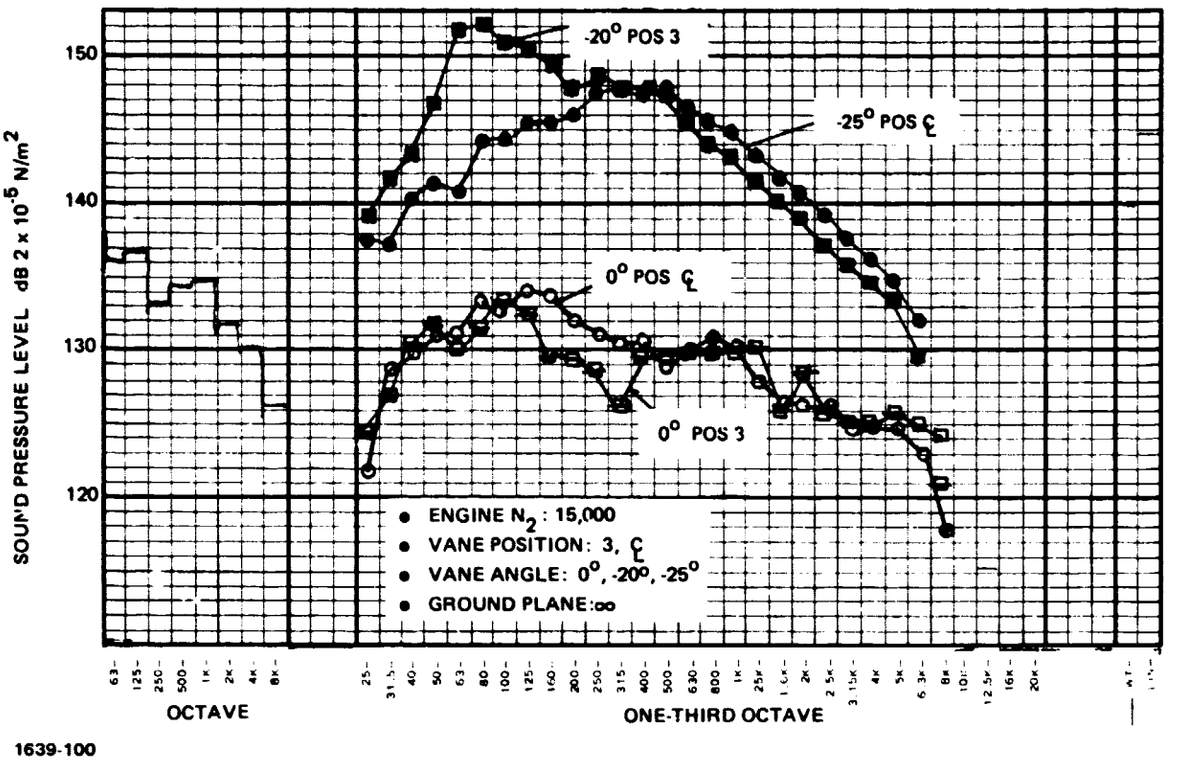


Fig. 4.5-32 Vane Microphone Measurement, Microphone No. 1, Test No. 104, 118

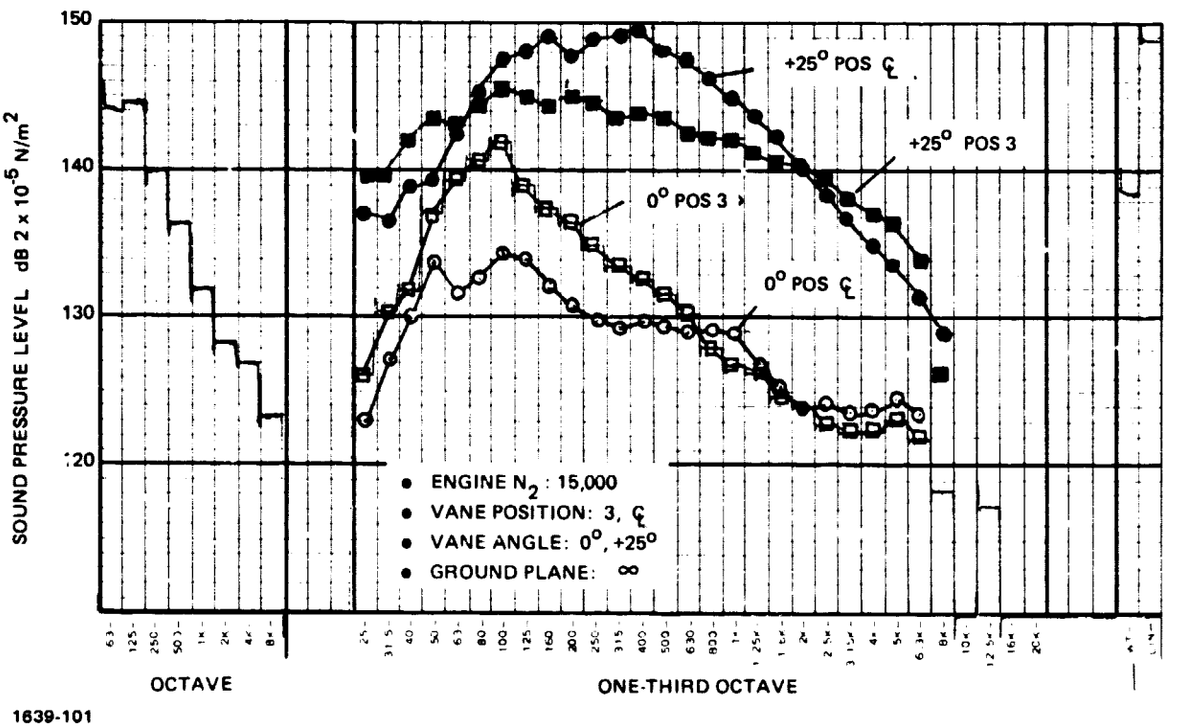


Fig. 4.5-33 Vane Microphone Measurement, Microphone No. 4, Test No. 104, 118

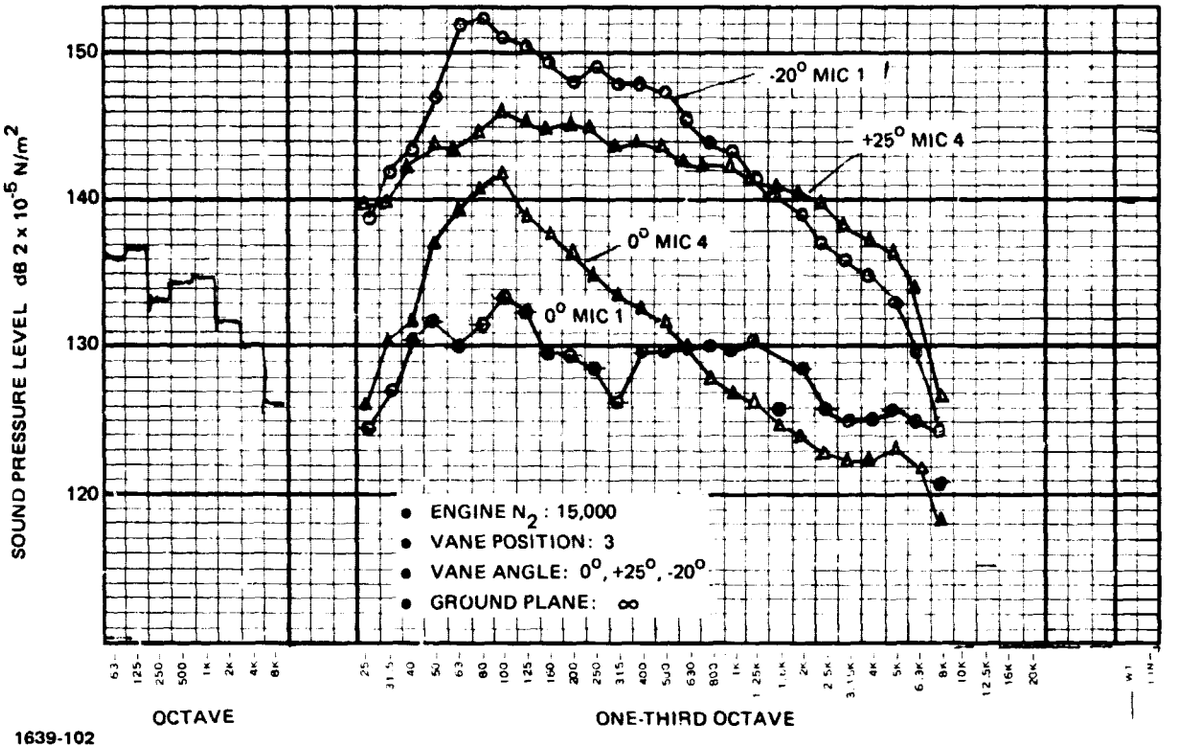


**Fig. 4.5-34 Vane Microphone Measurements, Microphones No. 1 and 4, Test No. 104**

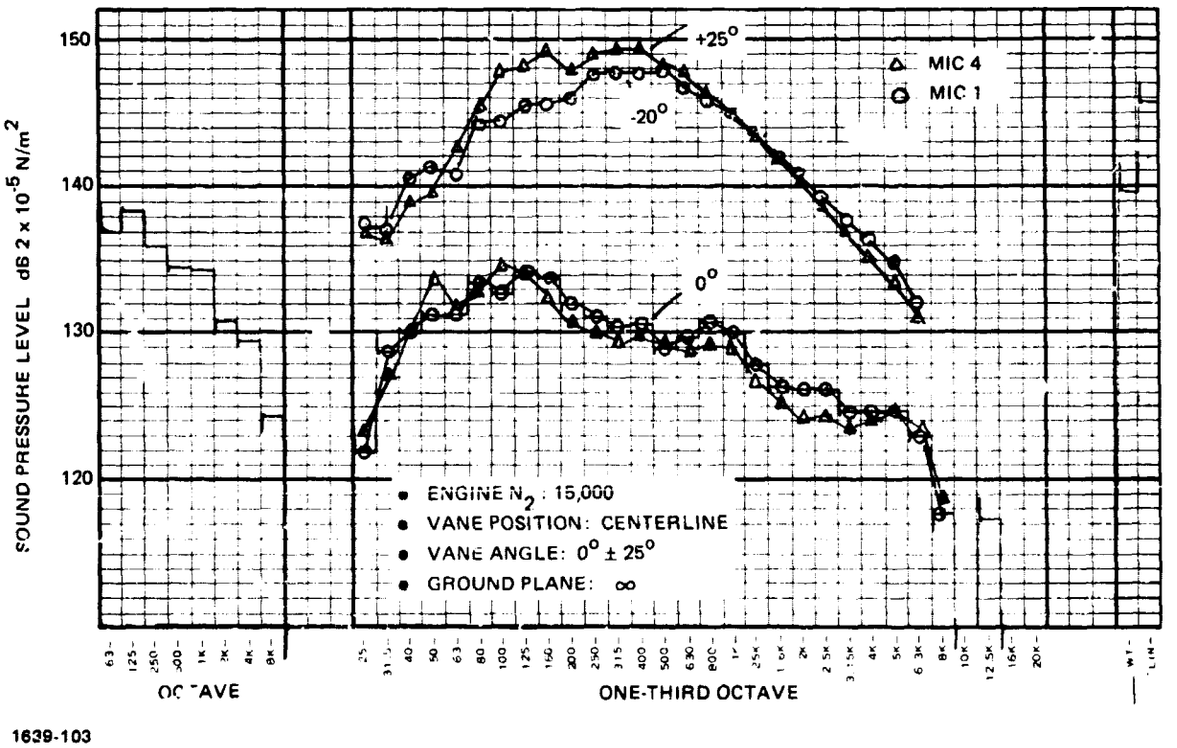


**Fig. 4.5-35 Vane Microphone Measurement, Microphones No. 1 and 4, Test No. 118**

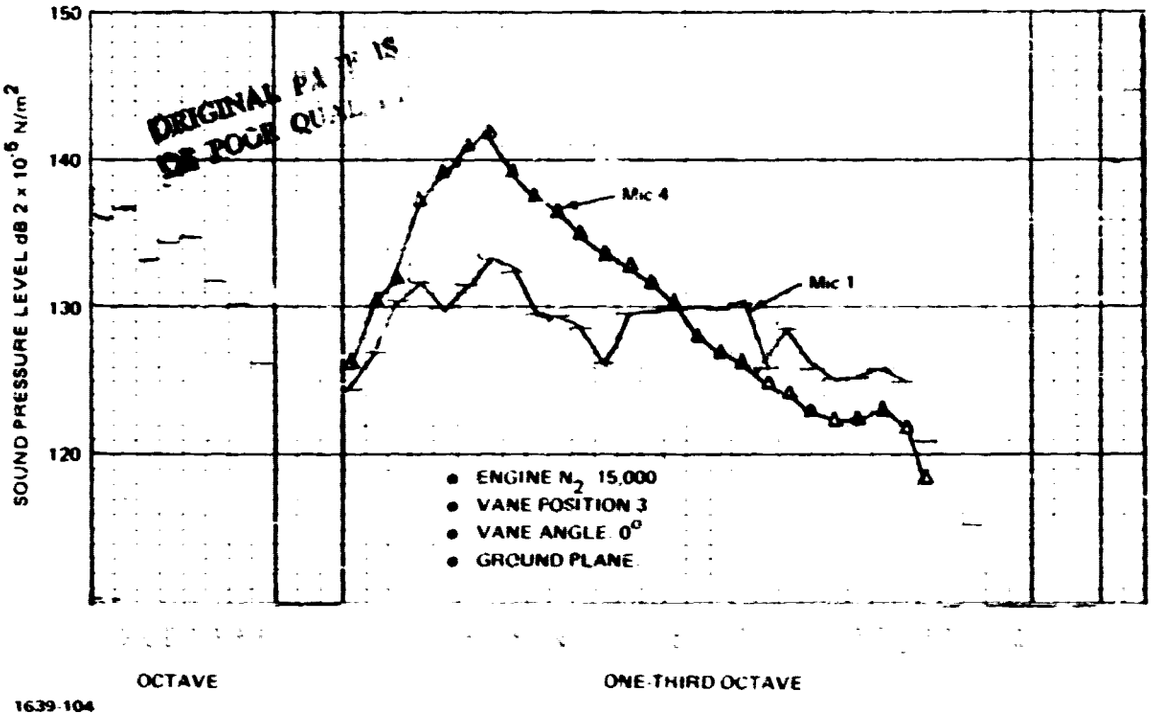


Fig. 4.5-36 Vane Microphone Measurement, Microphones No. 1 and 4, Test No. 104

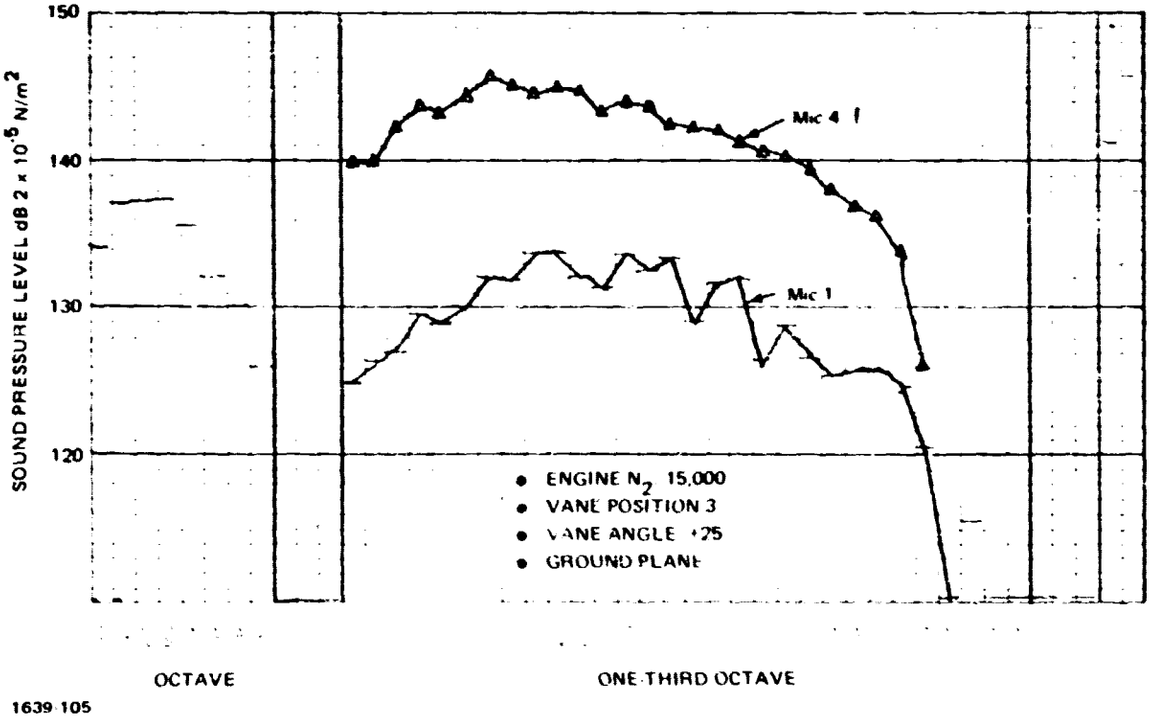


Fig. 4.5-37 Vane Microphone Measurement, Microphones No. 1 and 4, Test No. 104

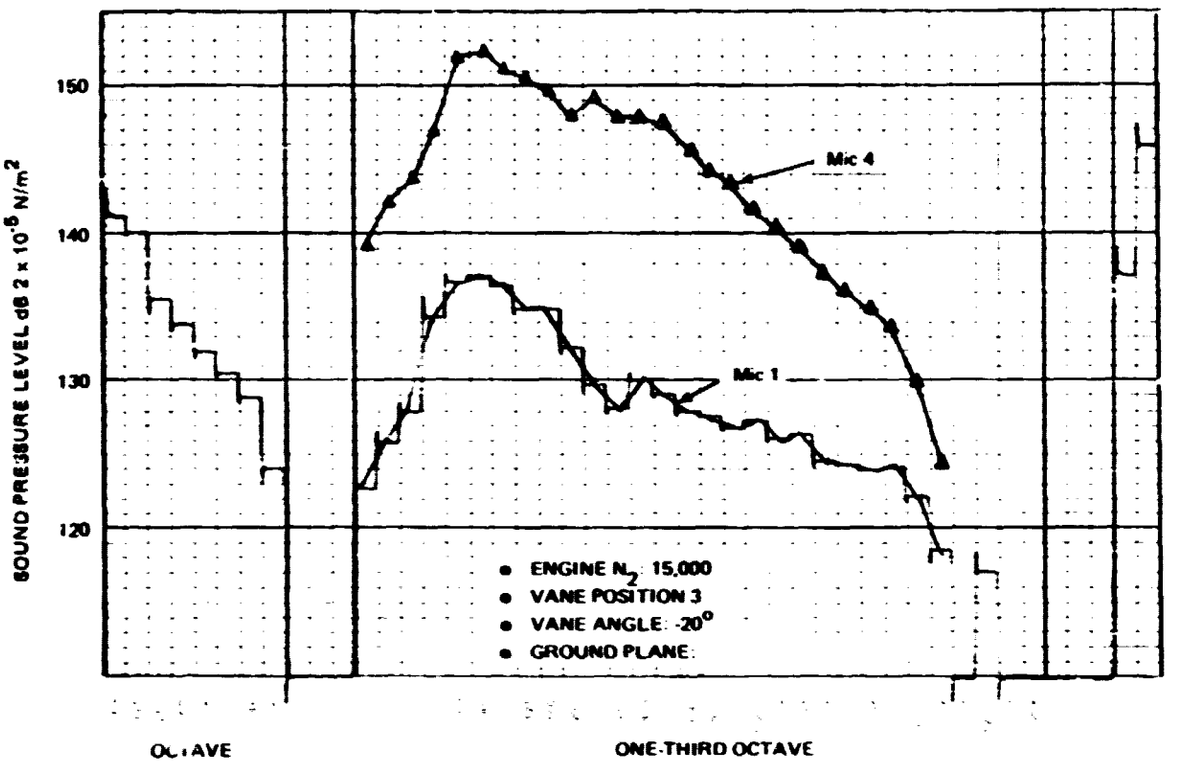


Fig. 4.5-38 Vane Microphone Measurement. Microphones No. 1 and 4 Test No. 104

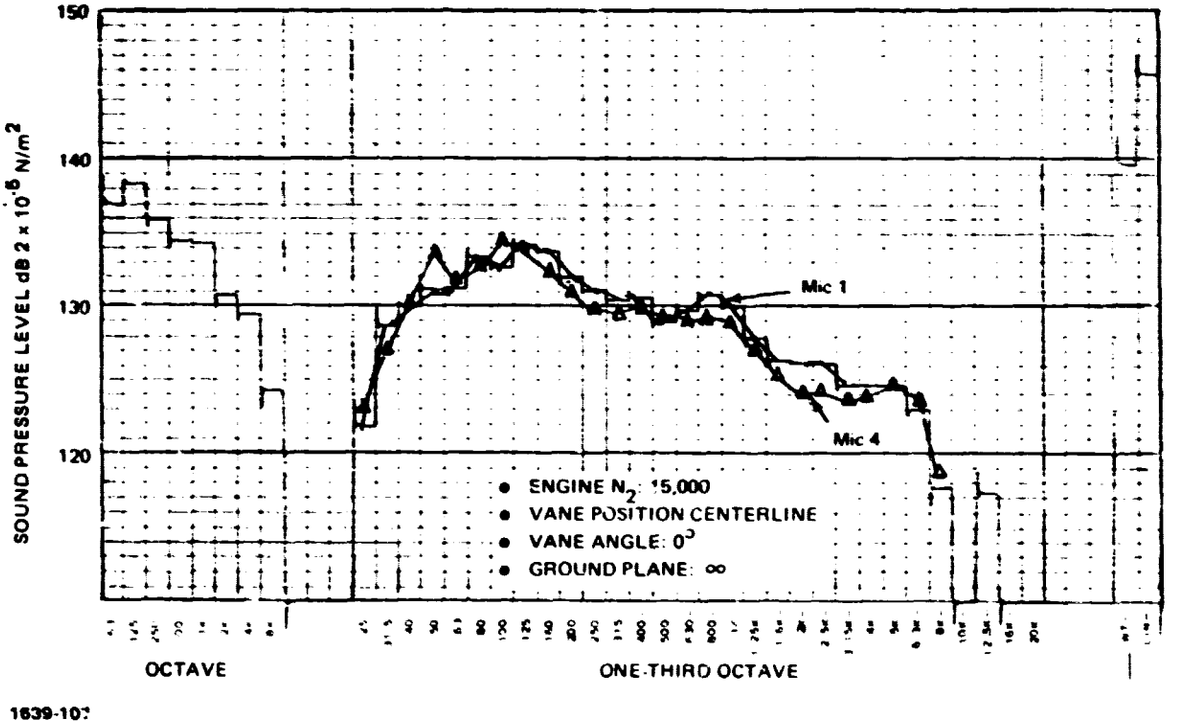


Fig. 4.5-39 Vane Microphone Measurement, Microphones No. 1 and 4, Test No. 118

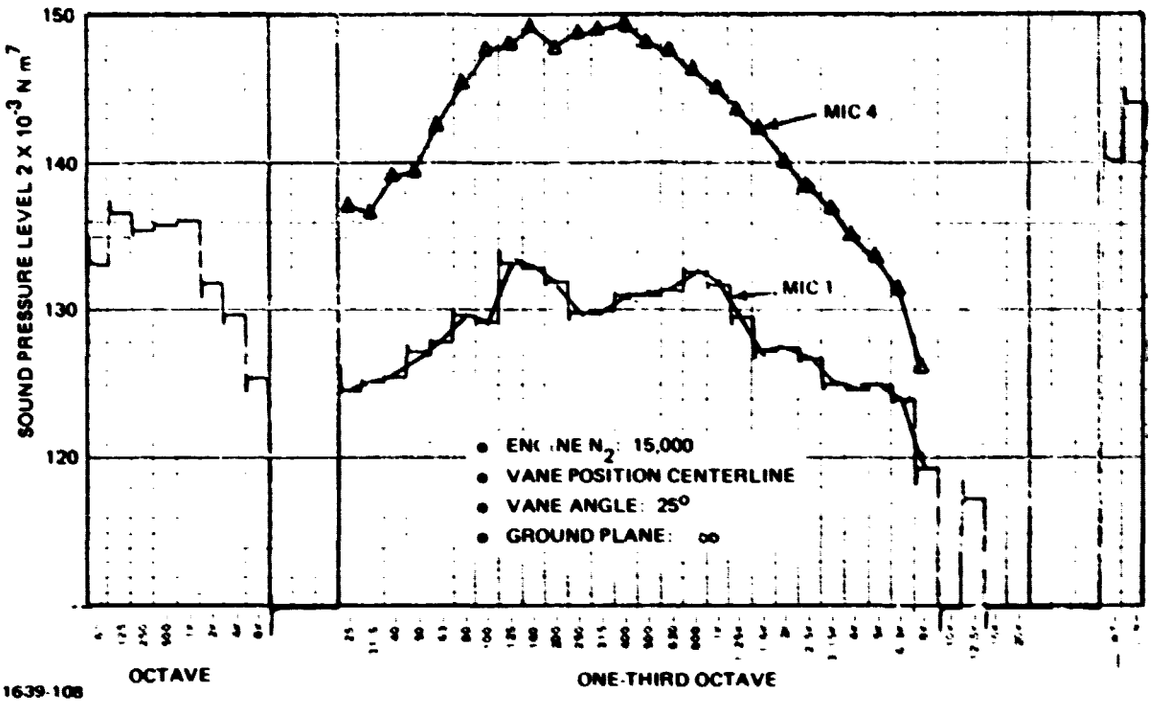


Fig. 4.5-40 Vane Microphone Measurement, Microphones No. 1 and 4, Test No. 118

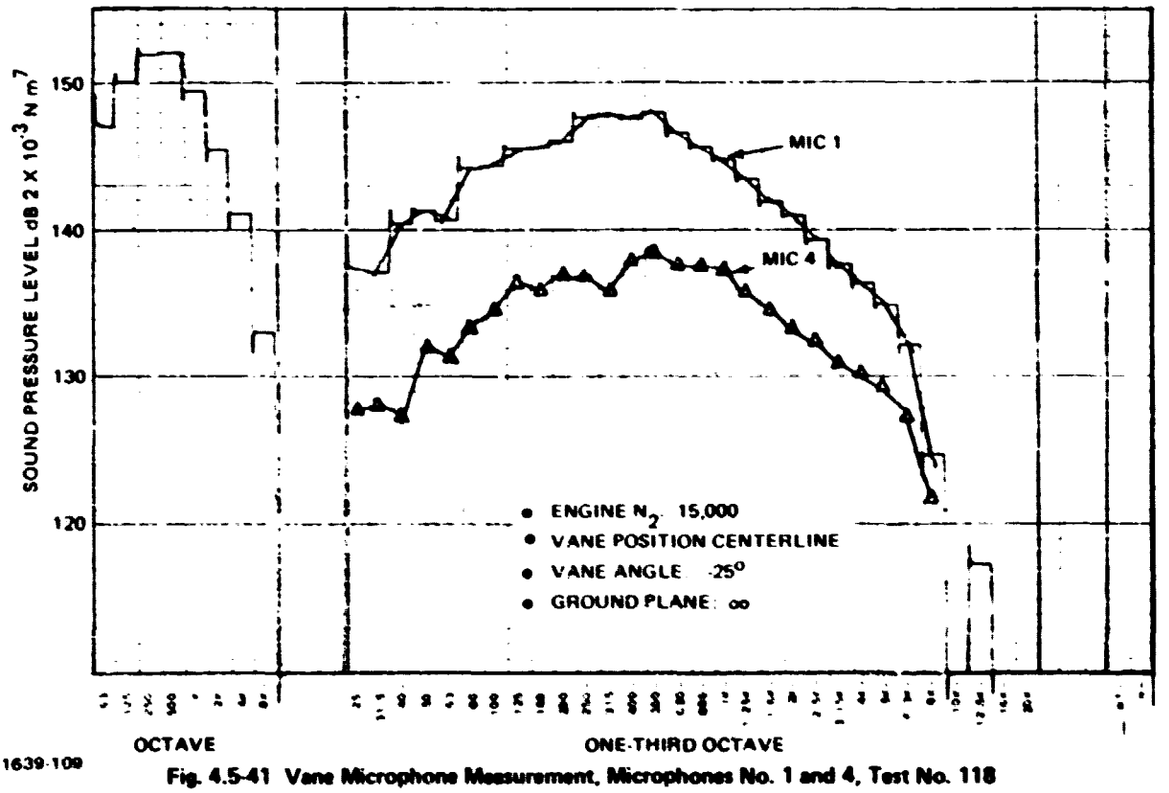


Fig. 4.5-41 Vane Microphone Measurement, Microphones No. 1 and 4, Test No. 118

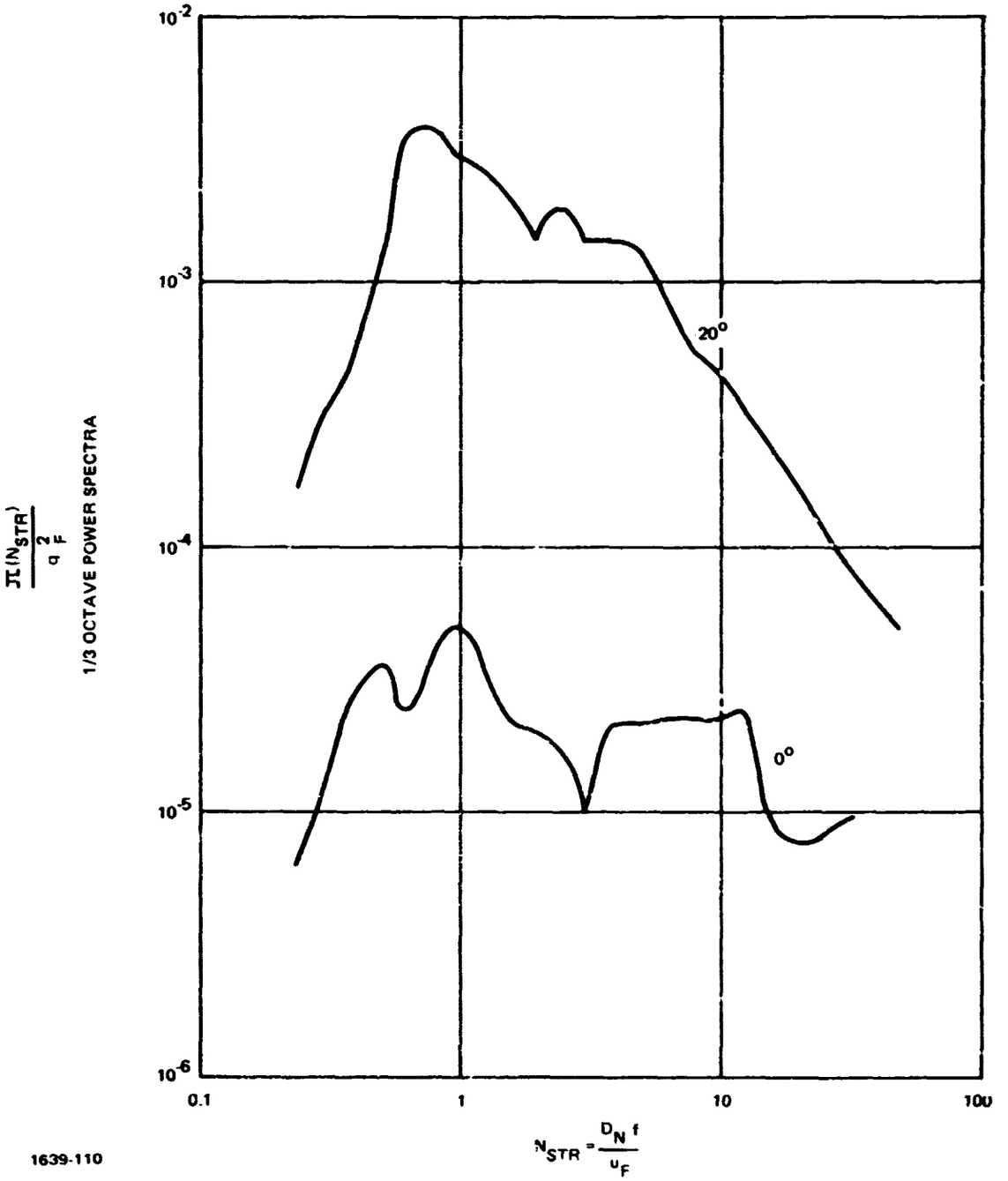


Fig. 4.5-42 Power Spectra of Surface Pressure, Microphone 1, Run 104, Vane Position 3

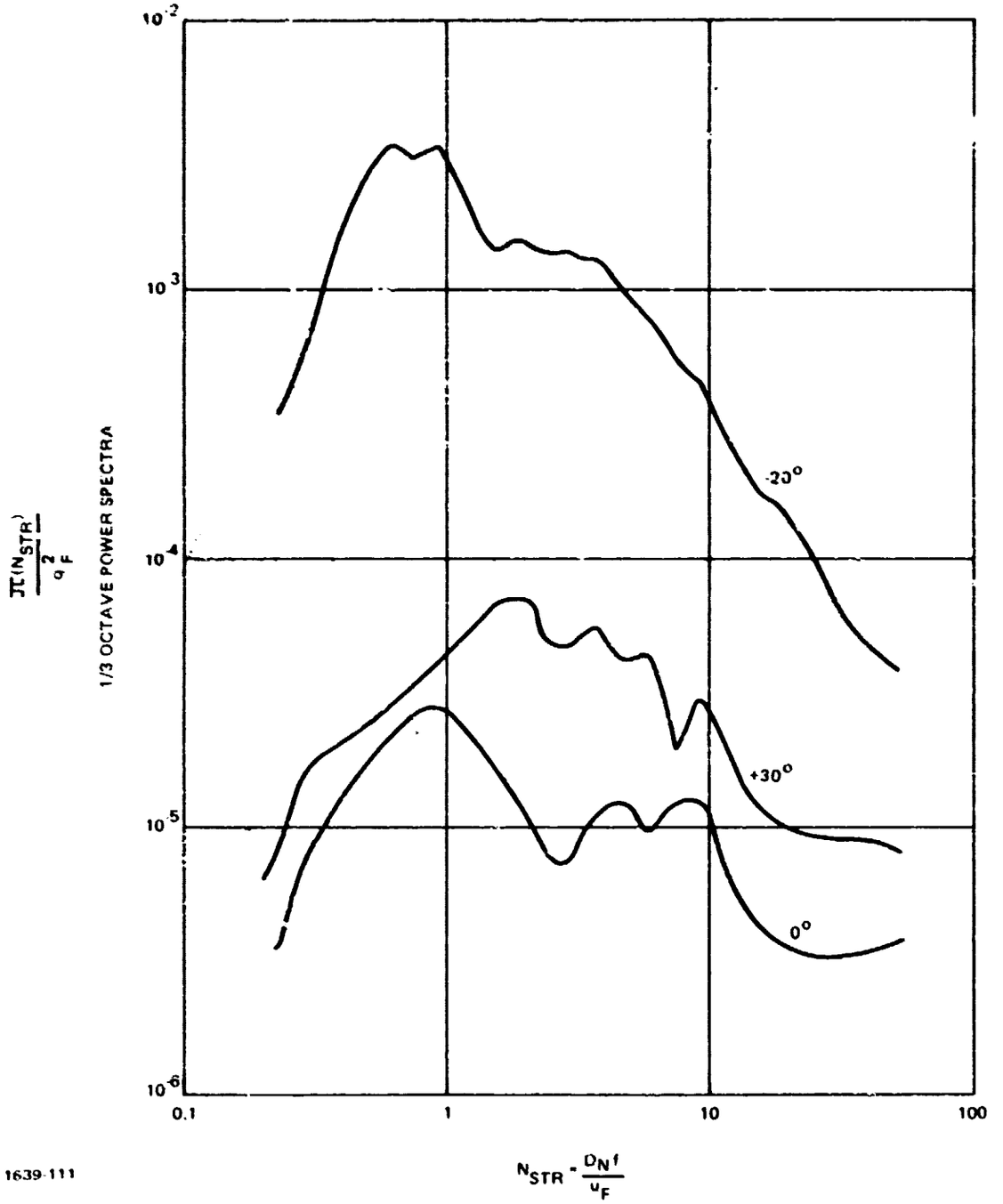


Fig. 4.5-43 Power Spectra of Surface Pressure, Microphone 1, Run 111, Vane Position 3

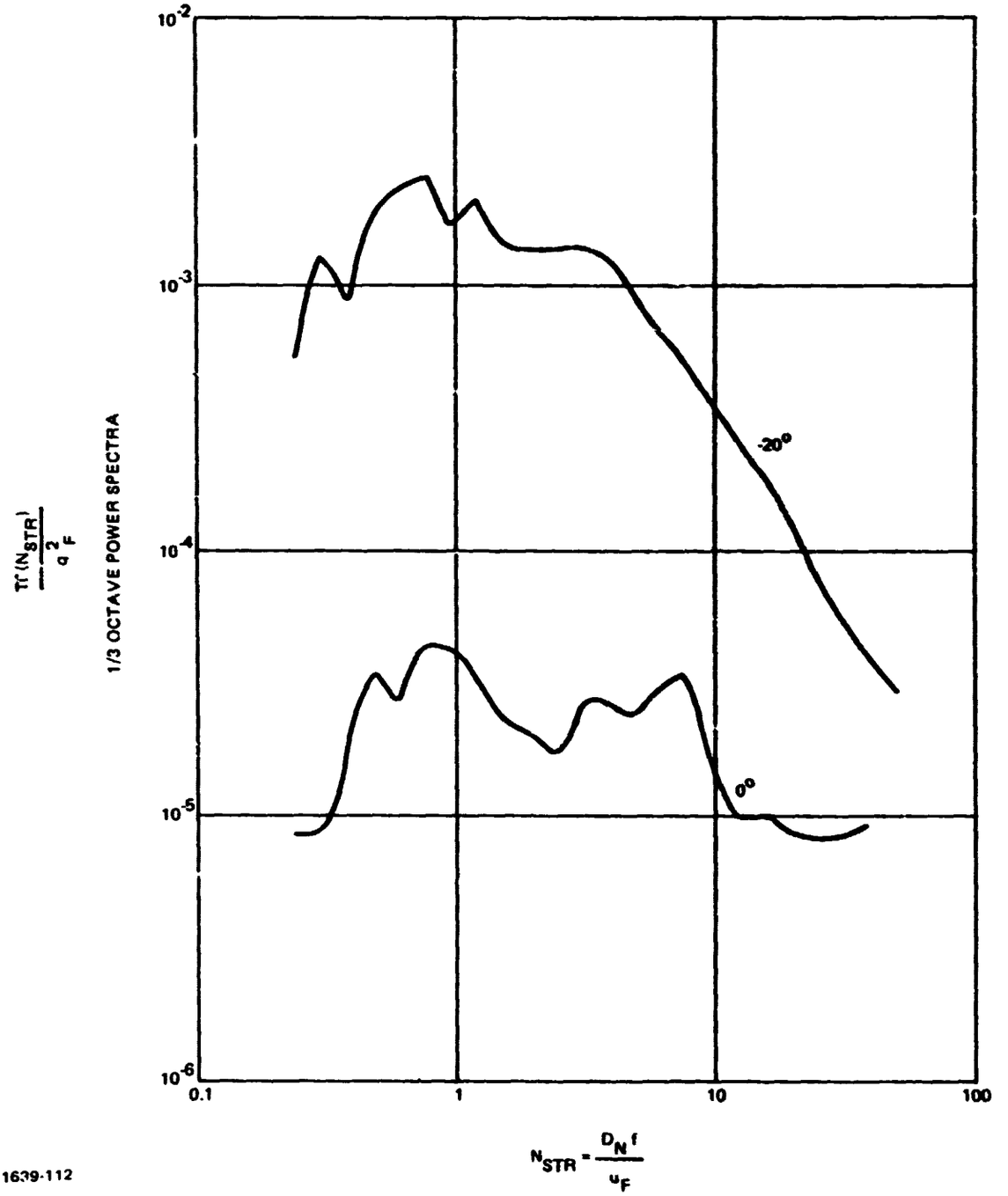


Fig. 4.5-44 Power Spectra of Surface Pressure, Microphone 1, Run 116, Vane Position 3

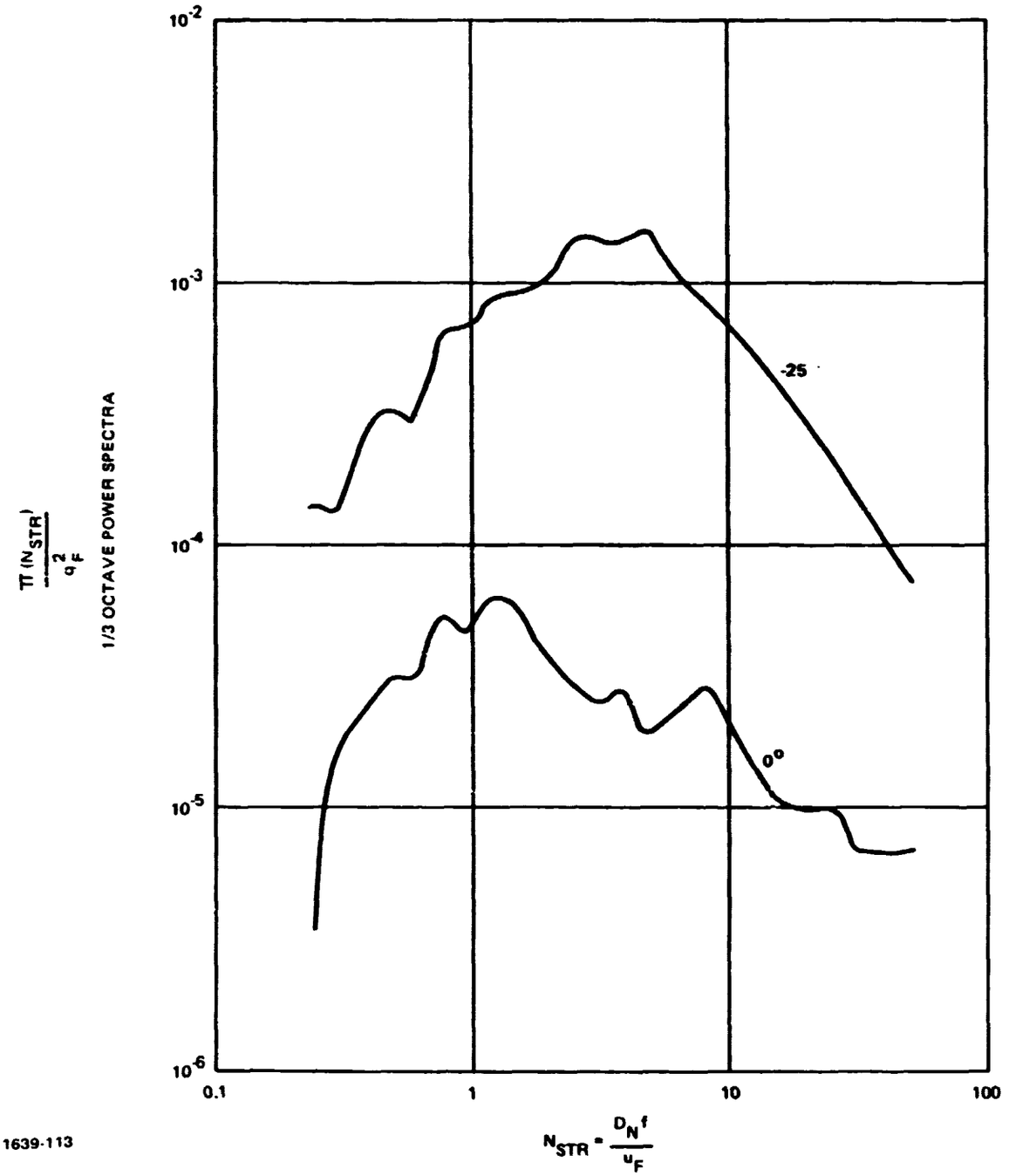


Fig. 4.5-45 Power Spectra of Surface Pressure, Microphone 1, Run 118, Vane Position Centerline

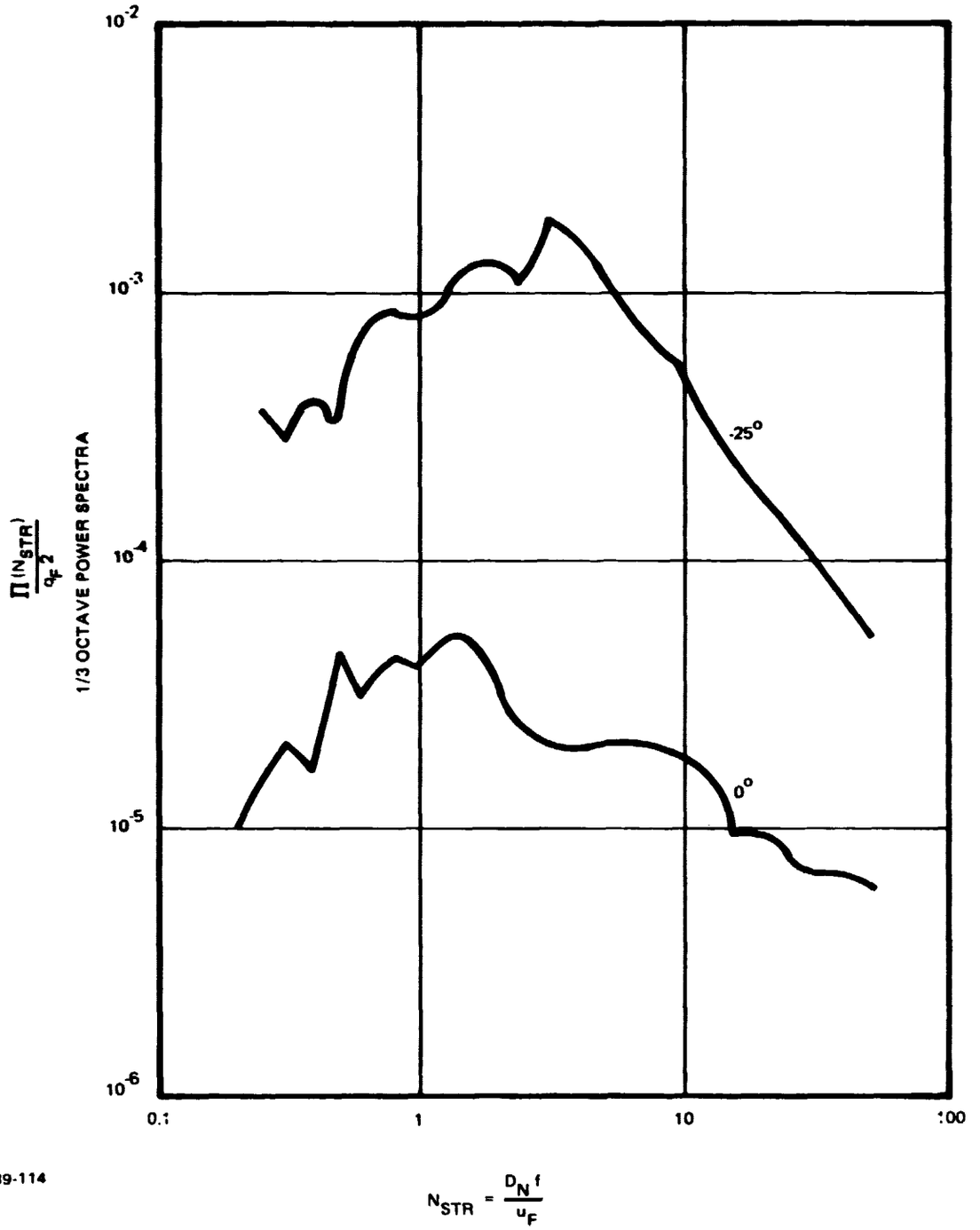


Fig. 4.5-46 Power Spectra of Surface Pressure, Microphone 1, Run 123, Vane Position Centerline

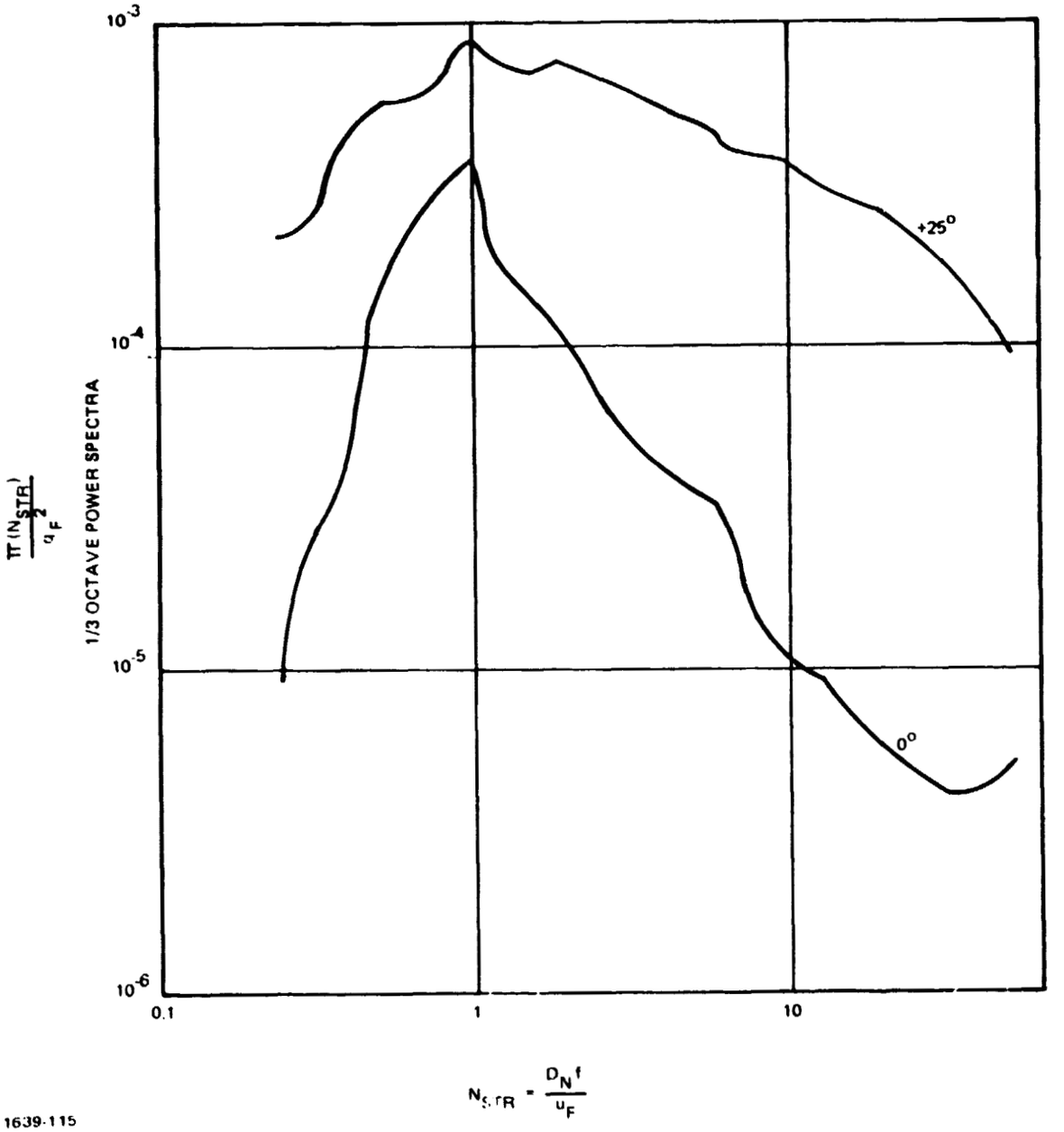


Fig. 4.5-47 Power Spectra of Surface Pressure, Microphone 4, Run 104, Vane Position 3

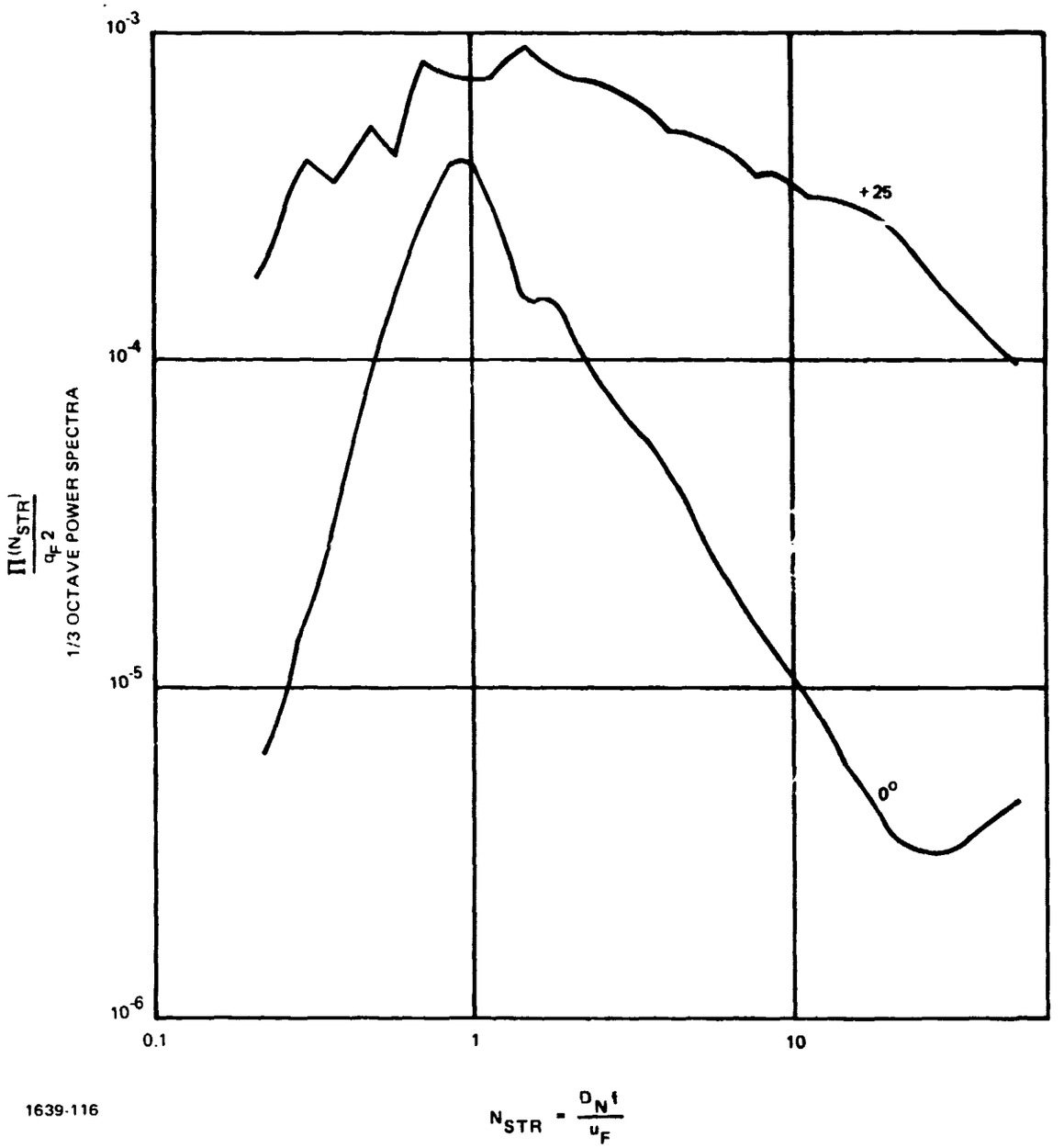


Fig. 4.5-48 Power Spectra of Surface Pressure, Microphone 4, Run 111, Vane Position 3

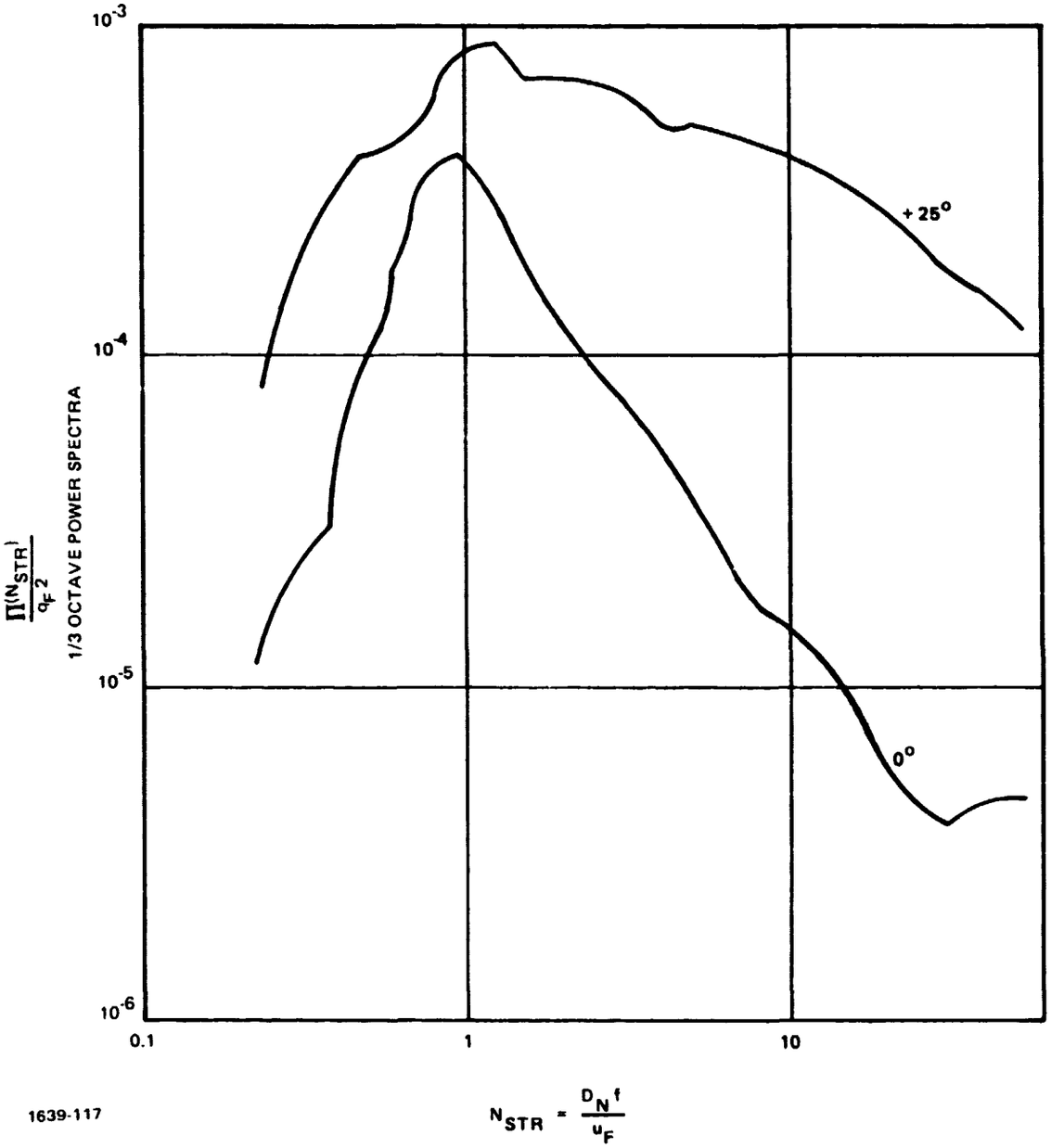


**Fig. 4.5-49 Power Spectra of Surface Pressure, Microphone 4, Run 116, Vane Position 3**

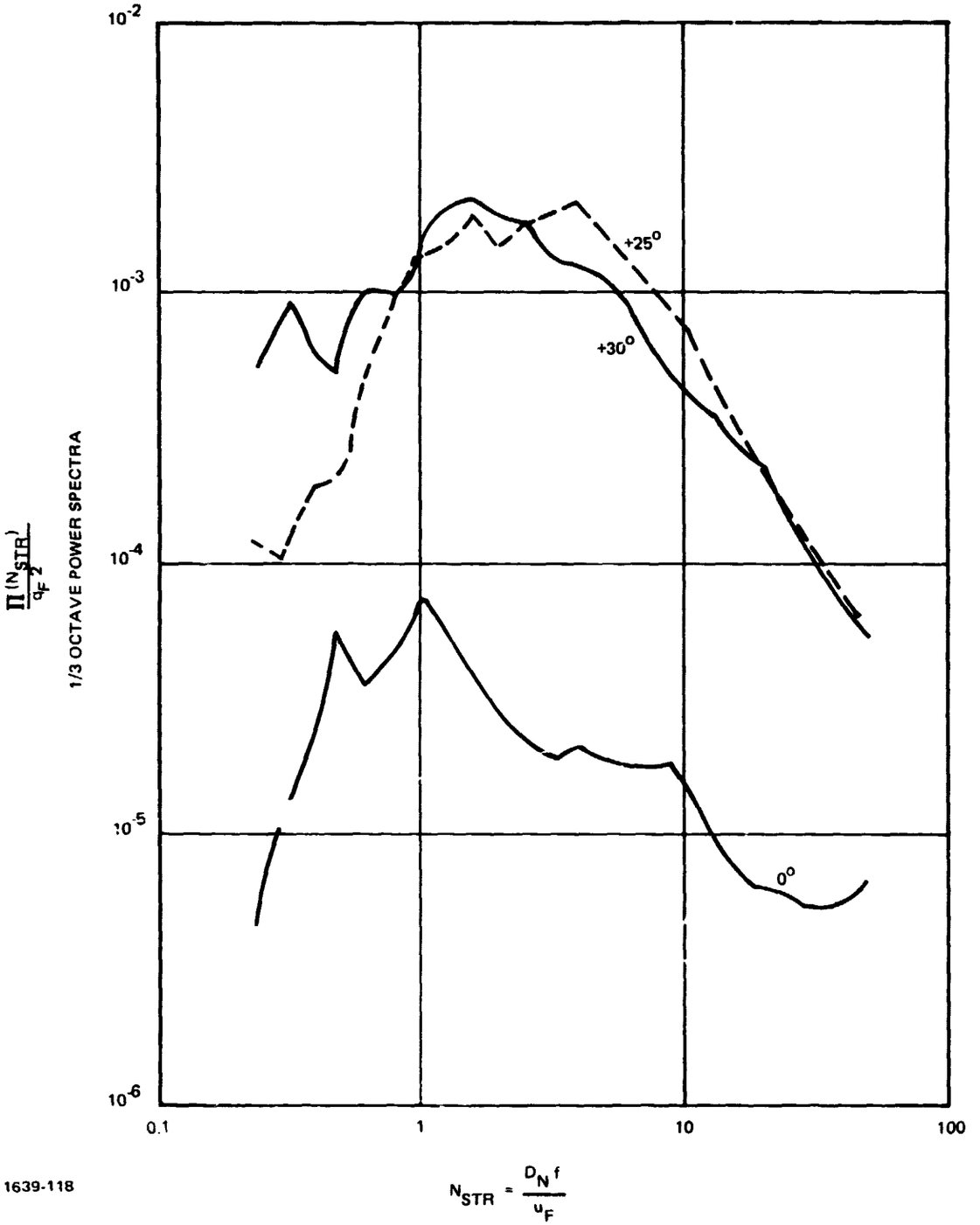


**Fig. 4.5-50 Power Spectra of Surface Pressure, Microphone 4, Run 118, Vane Position Centerline**

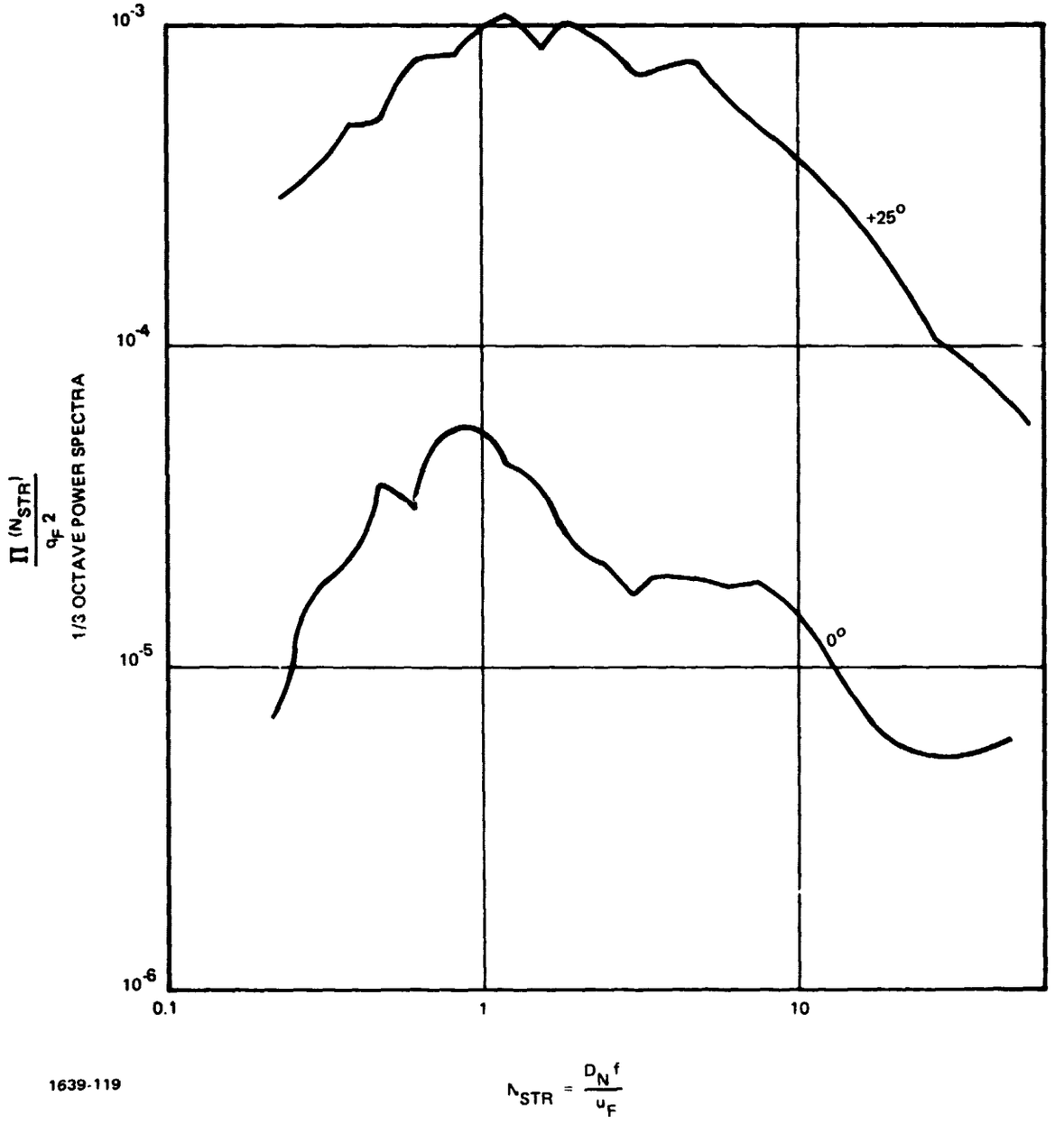


Fig. 4.5-51 Power Spectra of Surface Pressure, Microphone 4, Run 123, Vane Position Centerline

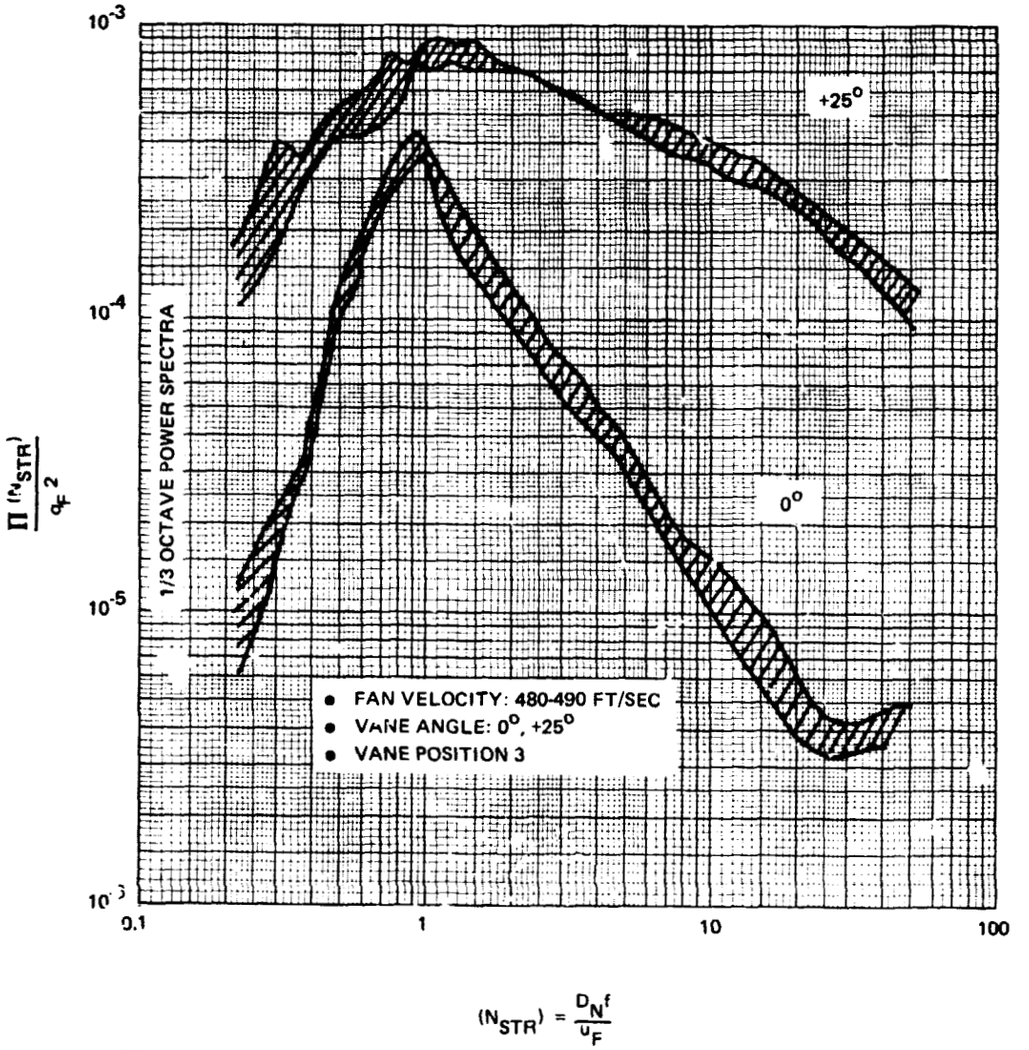




**Fig. 4.5-52 Power Spectra of Surface Pressure, Microphone 4, Runs 104, 111, 116**

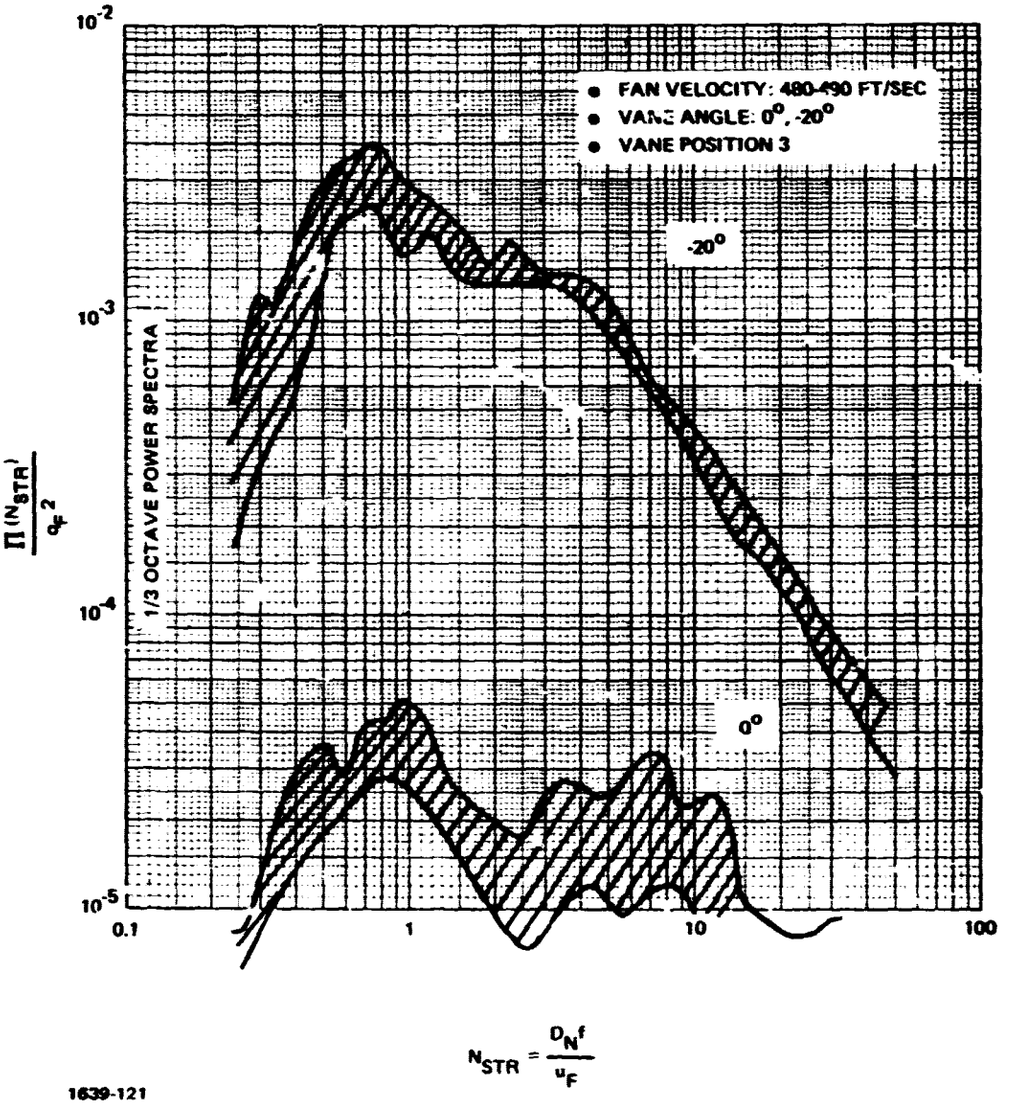


Fig. 4.5-53 Power Spectra of Surface Pressure, Microphone 1, Runs 104, 111, 116

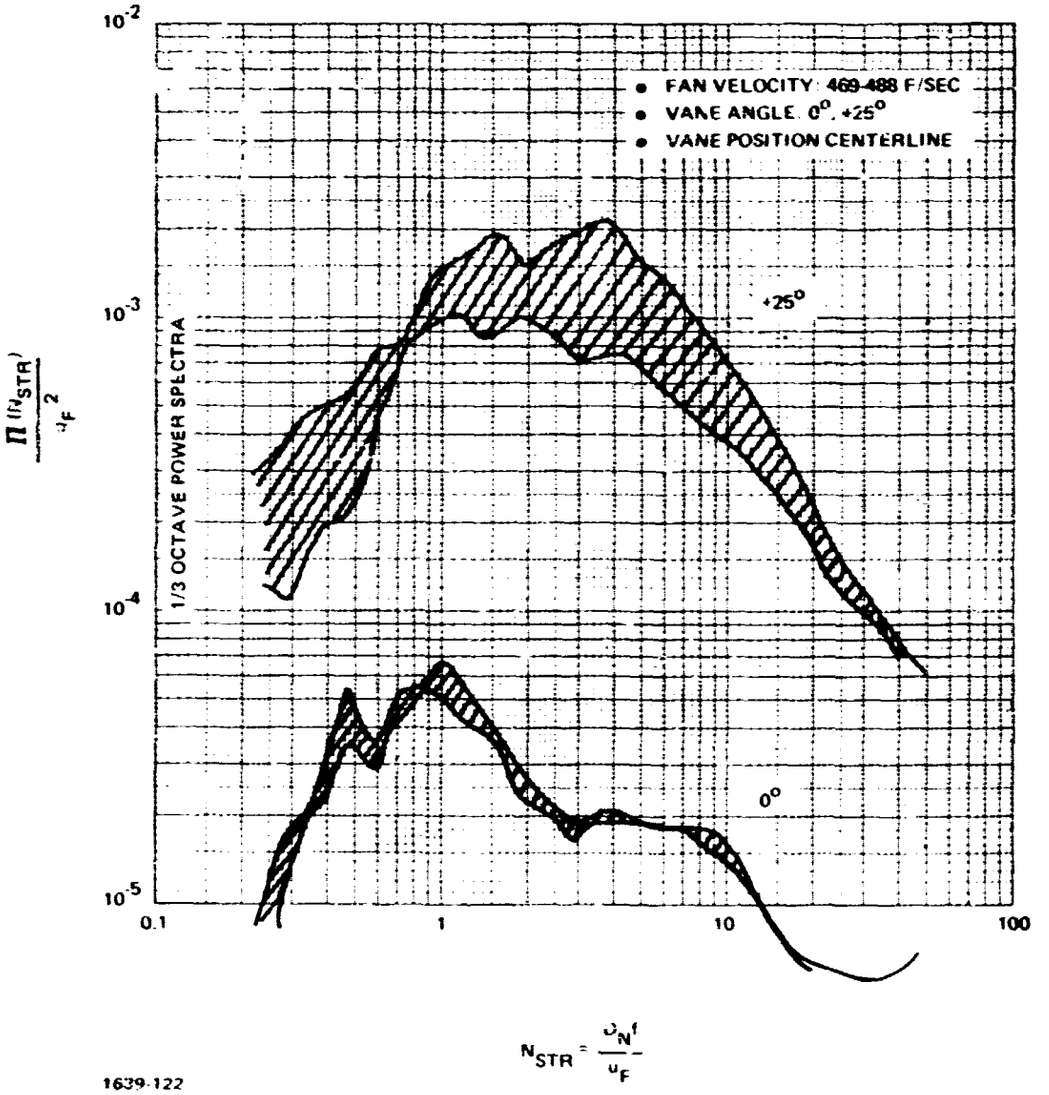


Fig. 4.5-54 Power Spectra of Surface Pressure, Microphone 4, Runs 118, 123

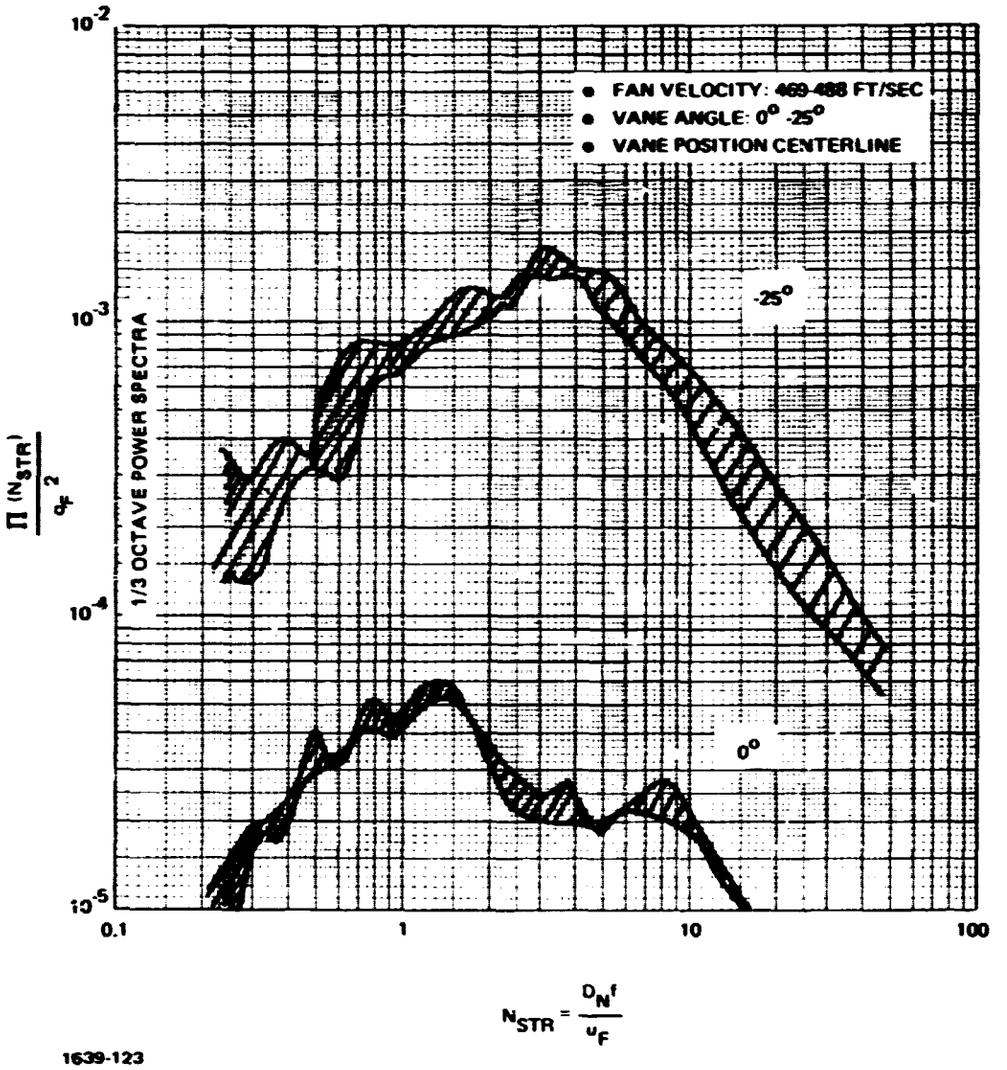




Fig. 4.5-55 Power Spectra of Surface Pressure, Microphone 1, Runs 118, 123

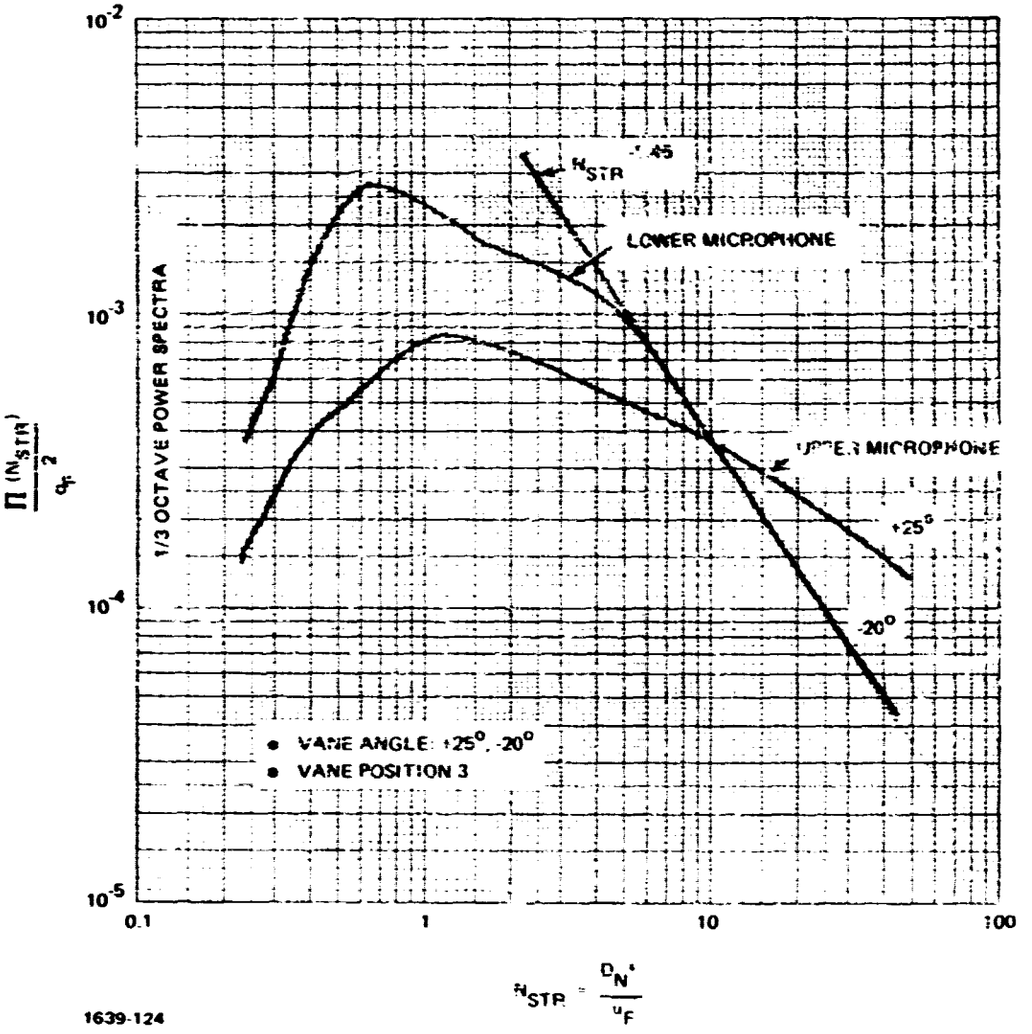


Fig. 4.5-56 Power Spectra of Surface Pressure, Microphones 1 and 4

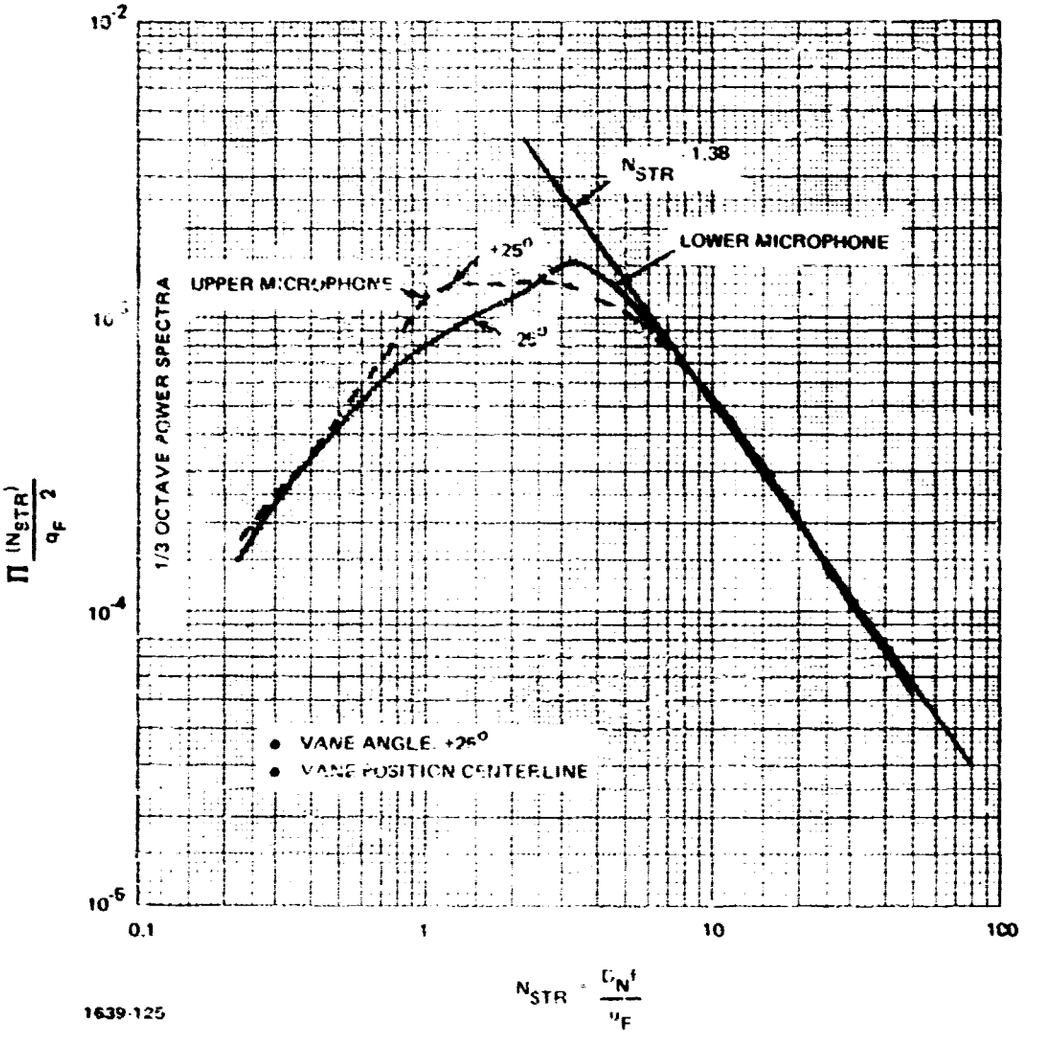




Fig. 4.5-57 Power Spectra of Surface Pressure, Microphones 1 and 4

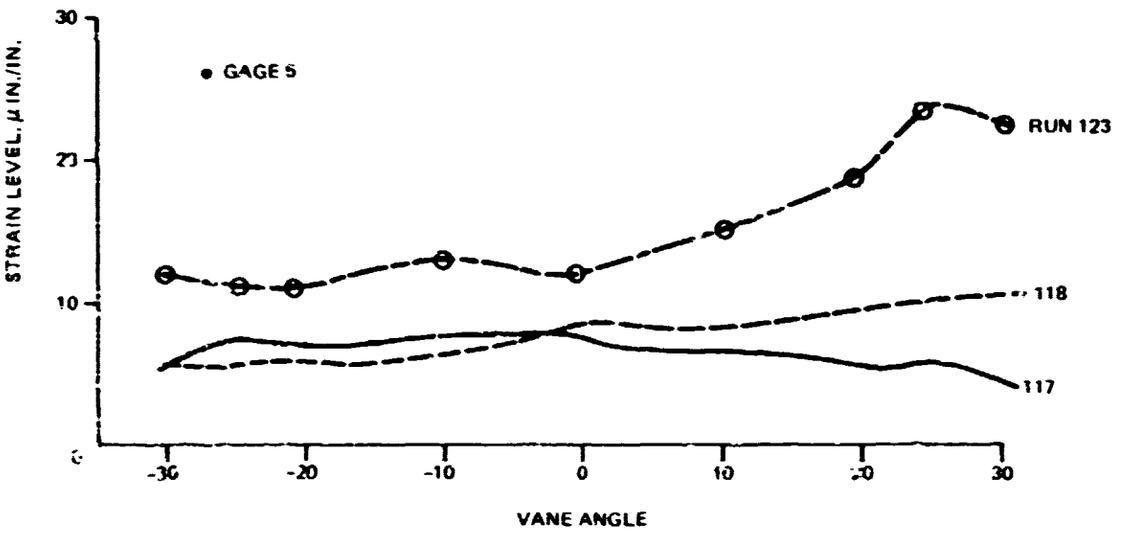


Fig. 4.5-58 RMS Strain Level vs Vane Angle for Several Typical Runs

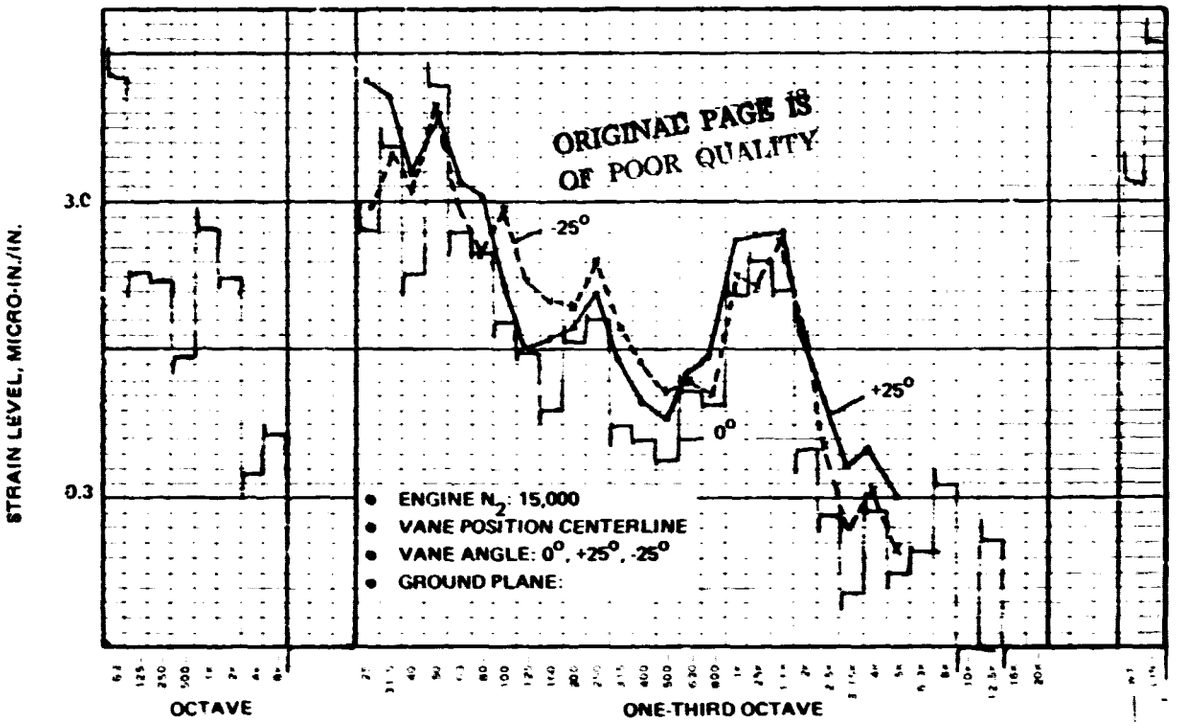


Fig. 4.5-59 Vane Dynamic Strain Measurement, Gage 1, Test 118

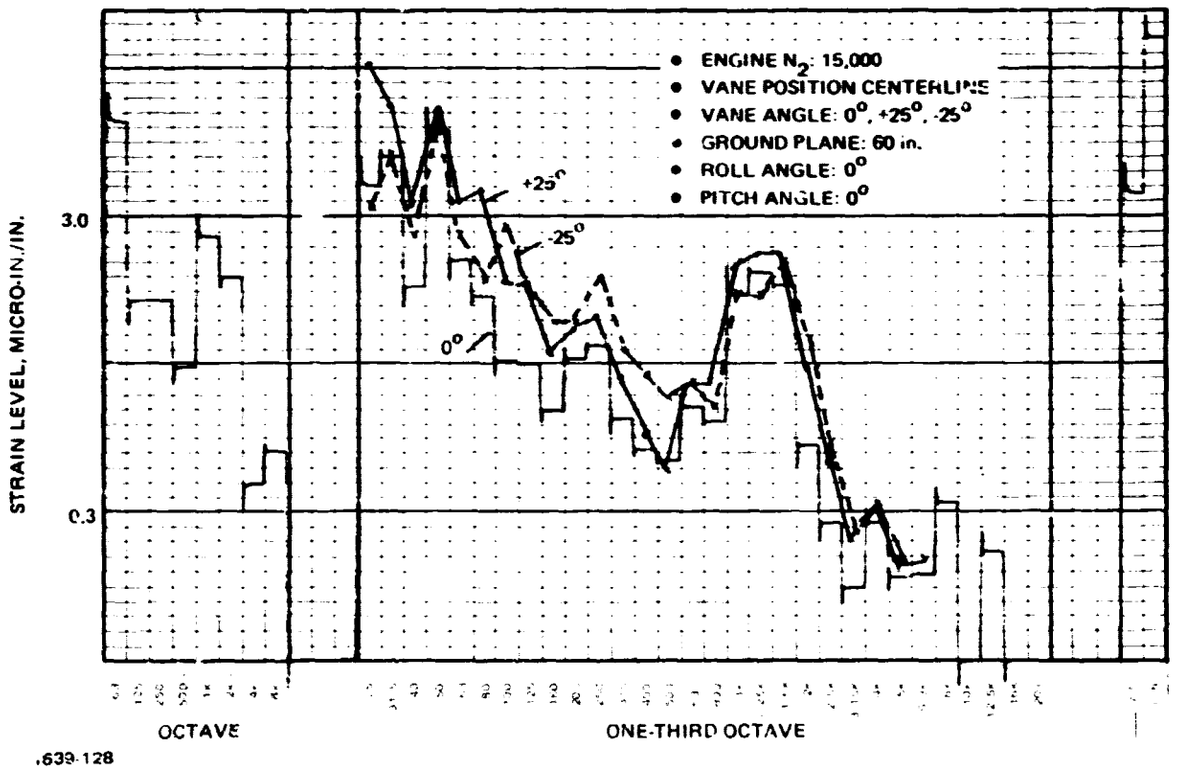


Fig. 4.5-60 Vane Dynamic Strain Measurement, Gage 1, Test 119

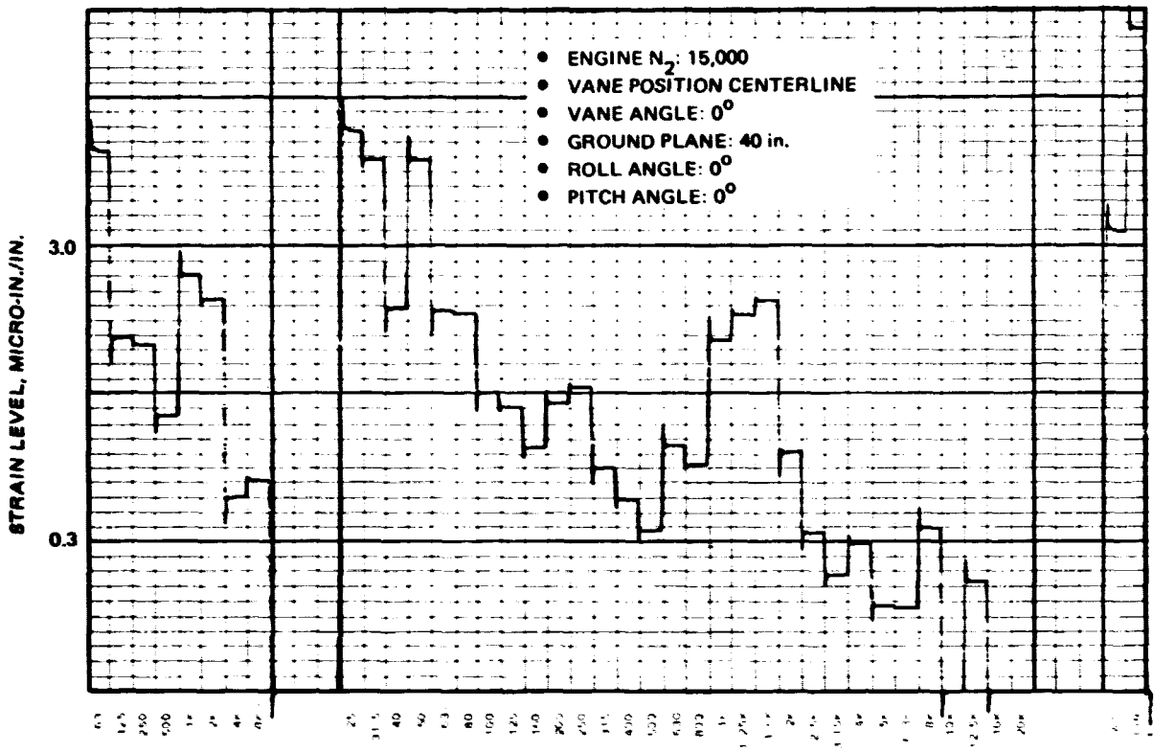


1639-129

**Fig. 4.5-61 Vane Dynamic Strain Measurement, Gage 1, Test 120**

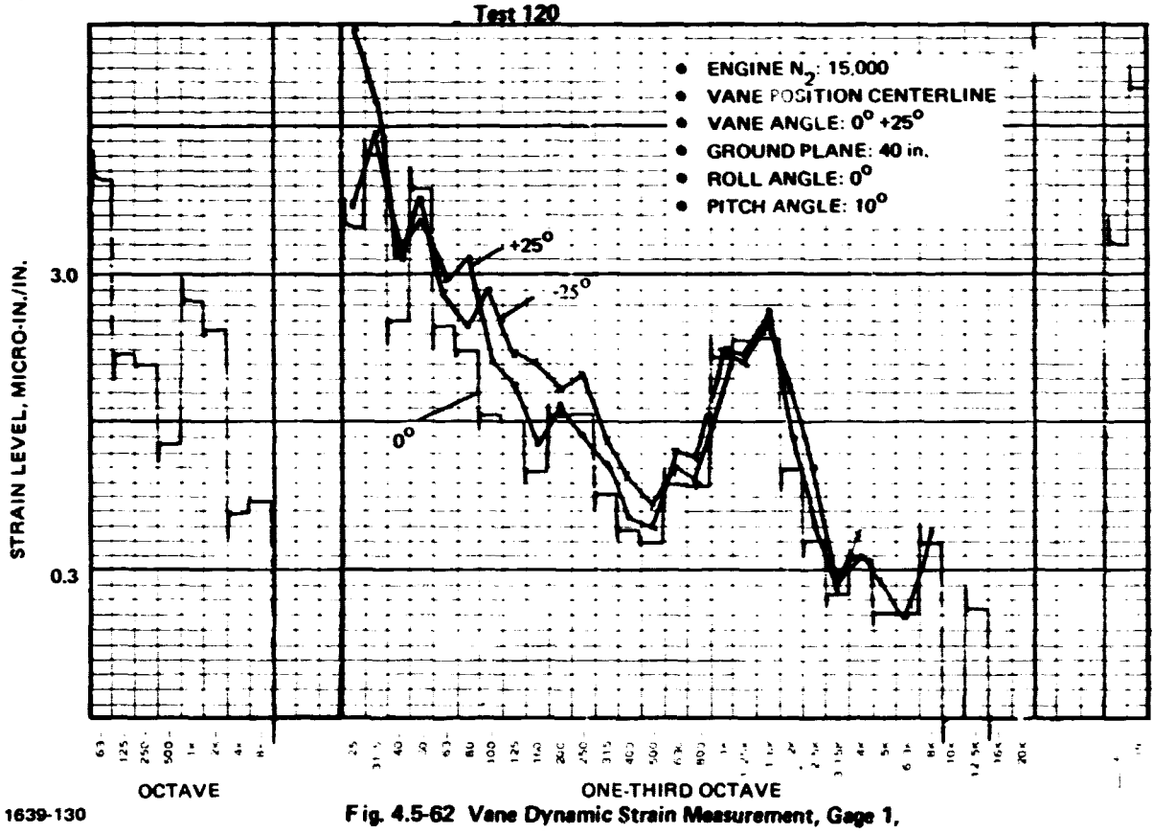


1639-130

**Fig. 4.5-62 Vane Dynamic Strain Measurement, Gage 1, Test 121**

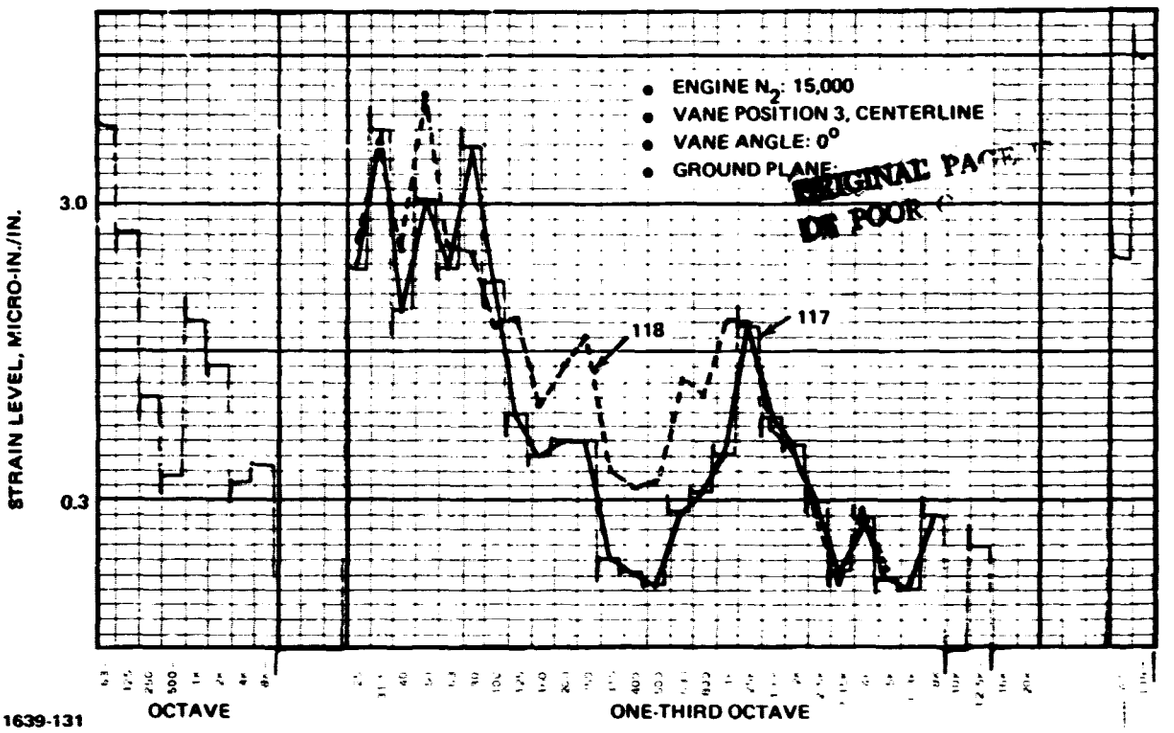


Fig. 4.5-63 Vane Dynamic Strain Measurement, Gage 5, Test 117 vs 118

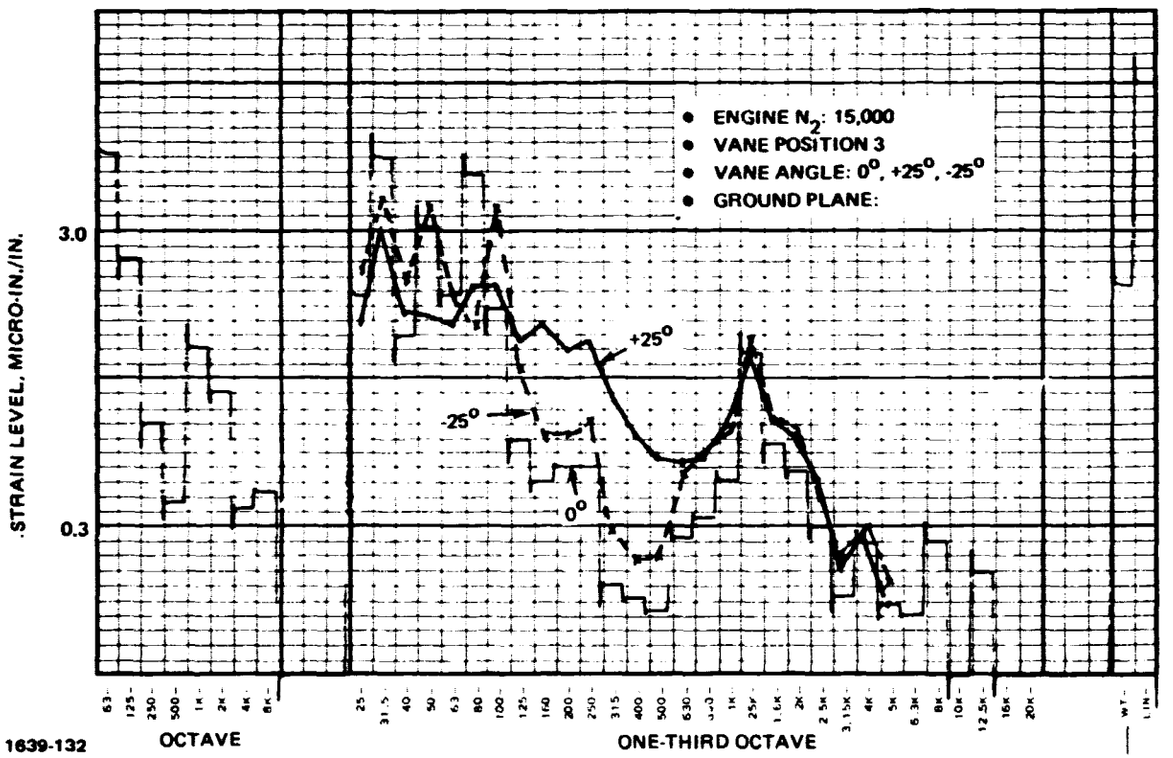


Fig. 4.5-64 Vane Dynamic Strain Measurement, Gage 5, Test 117

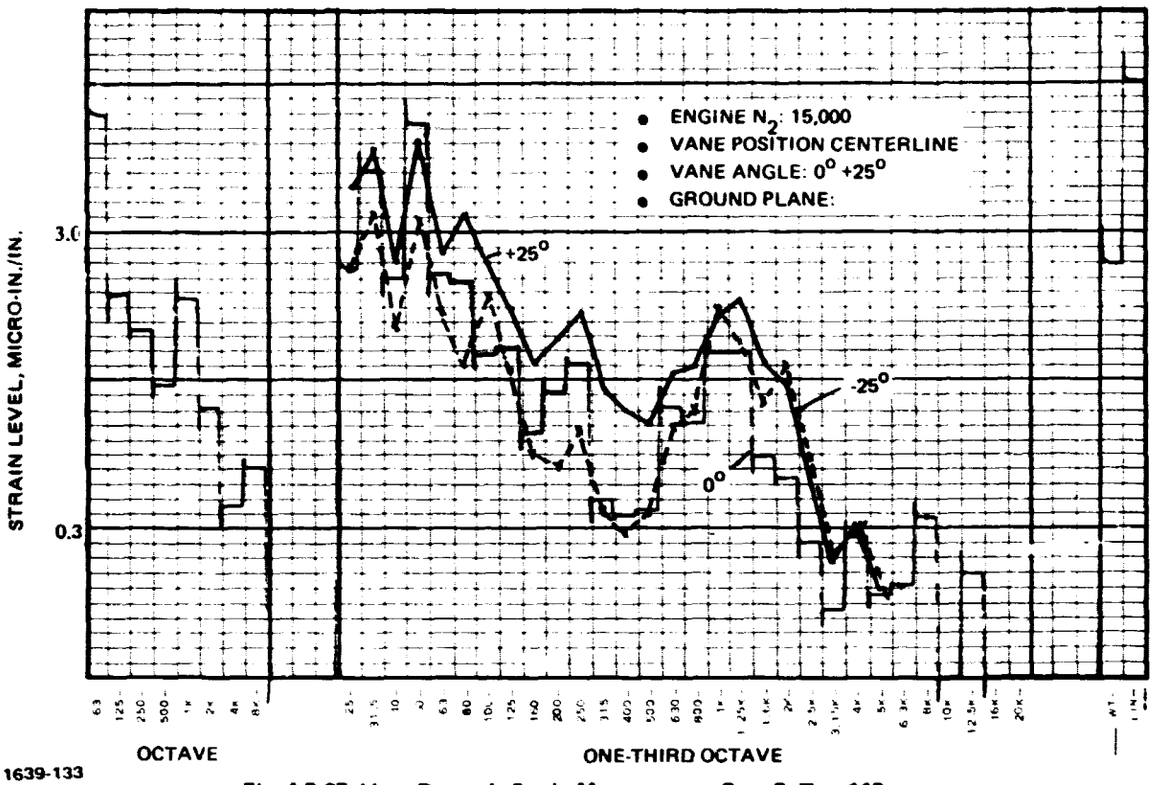


Fig. 4.5-65 Vane Dynamic Strain Measurement, Gage 5, Test 118

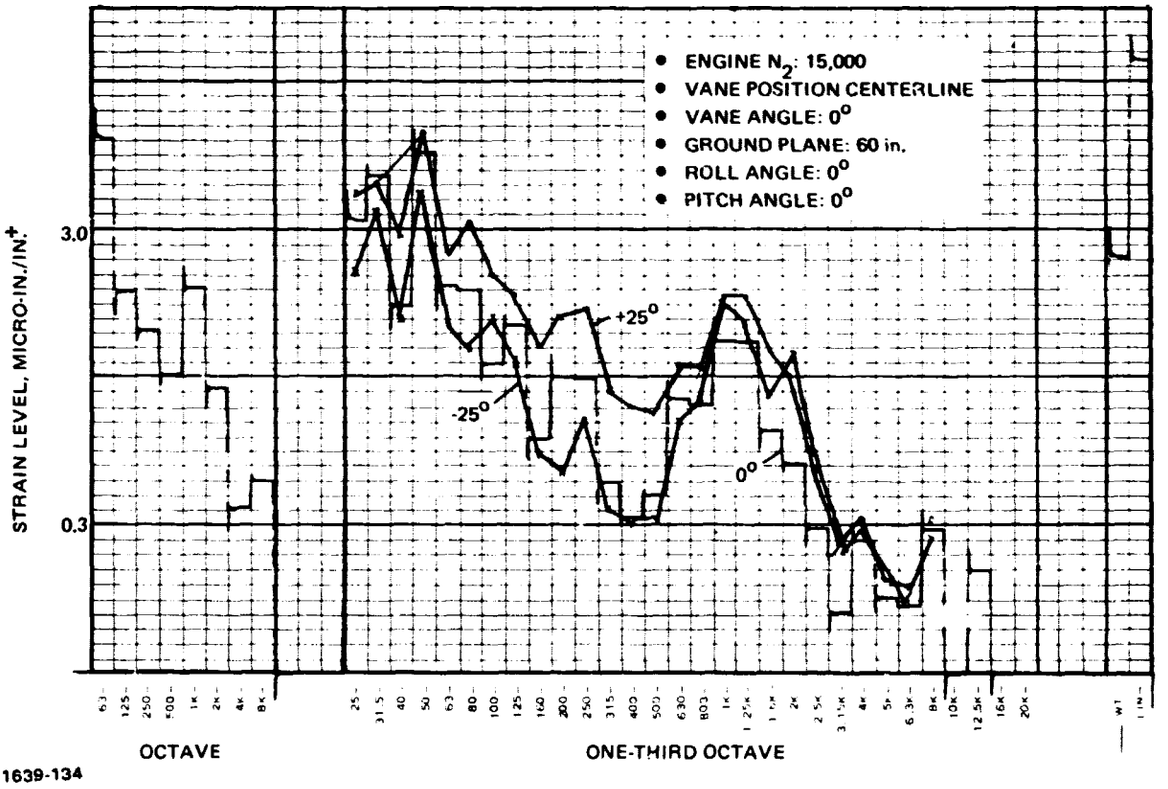


Fig. 4.5-66 Vane Dynamic Strain Measurement, Gage 5, Test 119

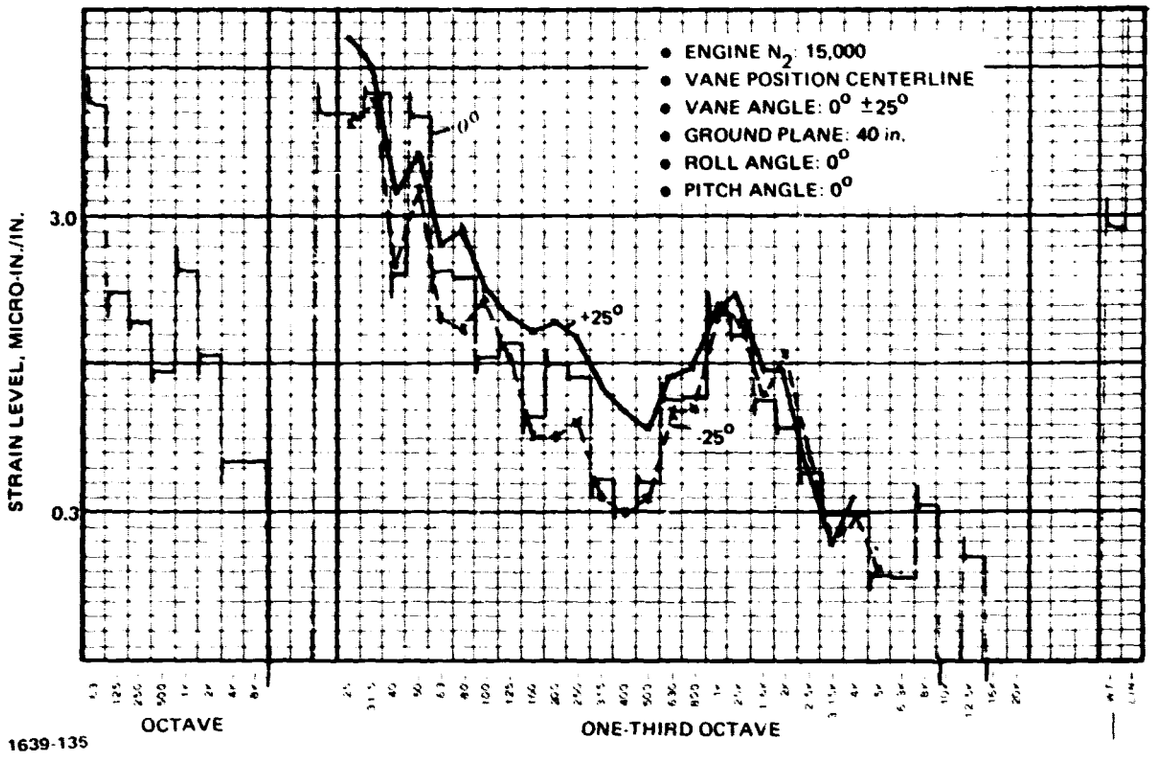


Fig. 4.5-67 Vane Dynamic Strain Measurement, Gage 5, Test 120

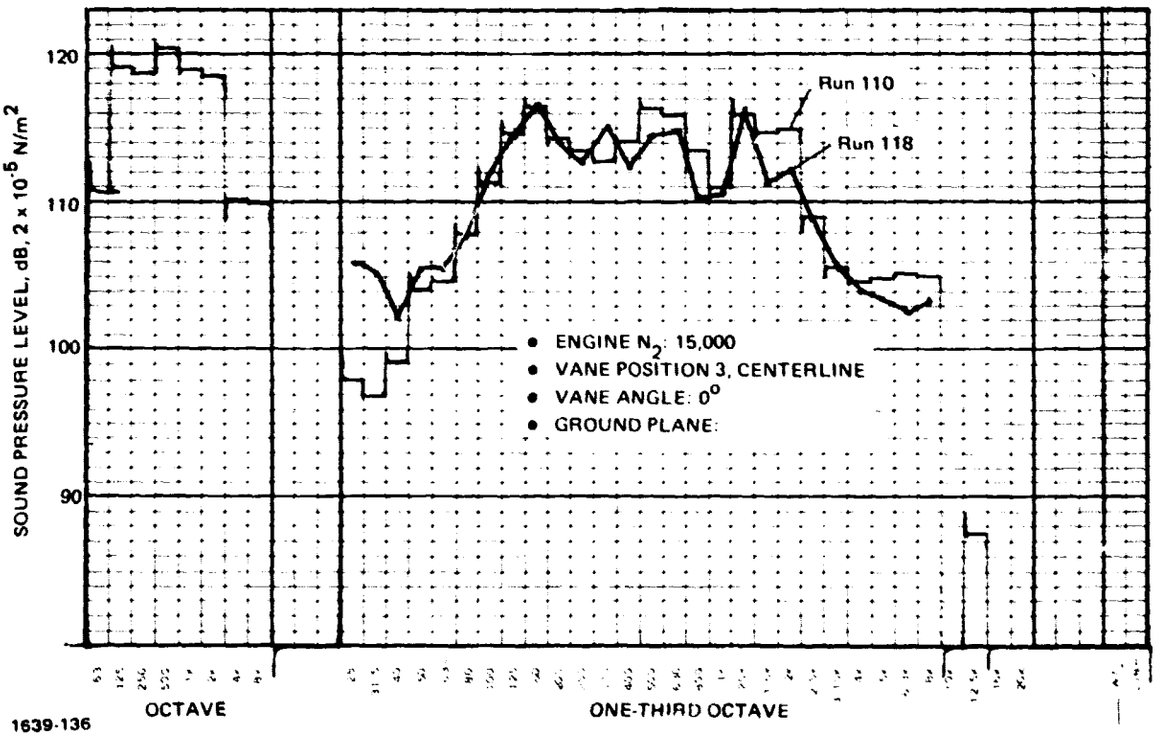


Fig. 4.5-68 External Microphone Measurements, Test 110 vs 118

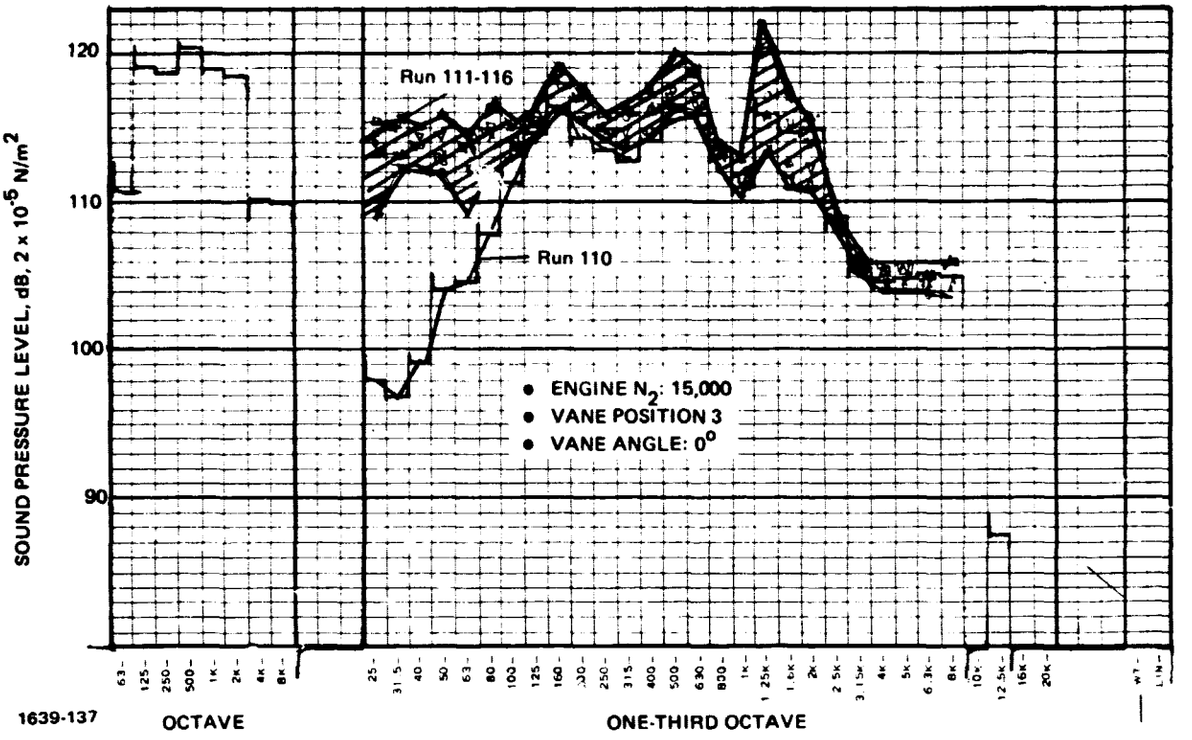


Fig. 4.5-69 External Microphone Measurements, Test 110 vs 111-116

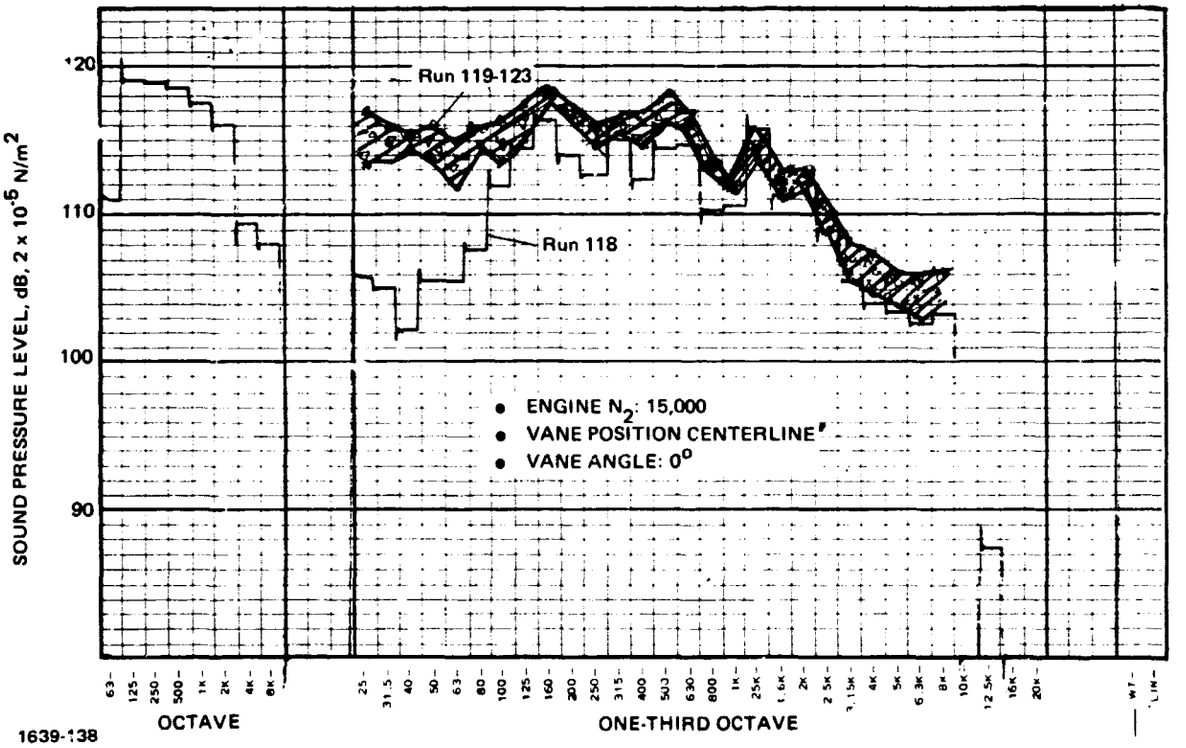


Fig. 4.5-70 External Microphone Measurements, Test 118 vs 119-123

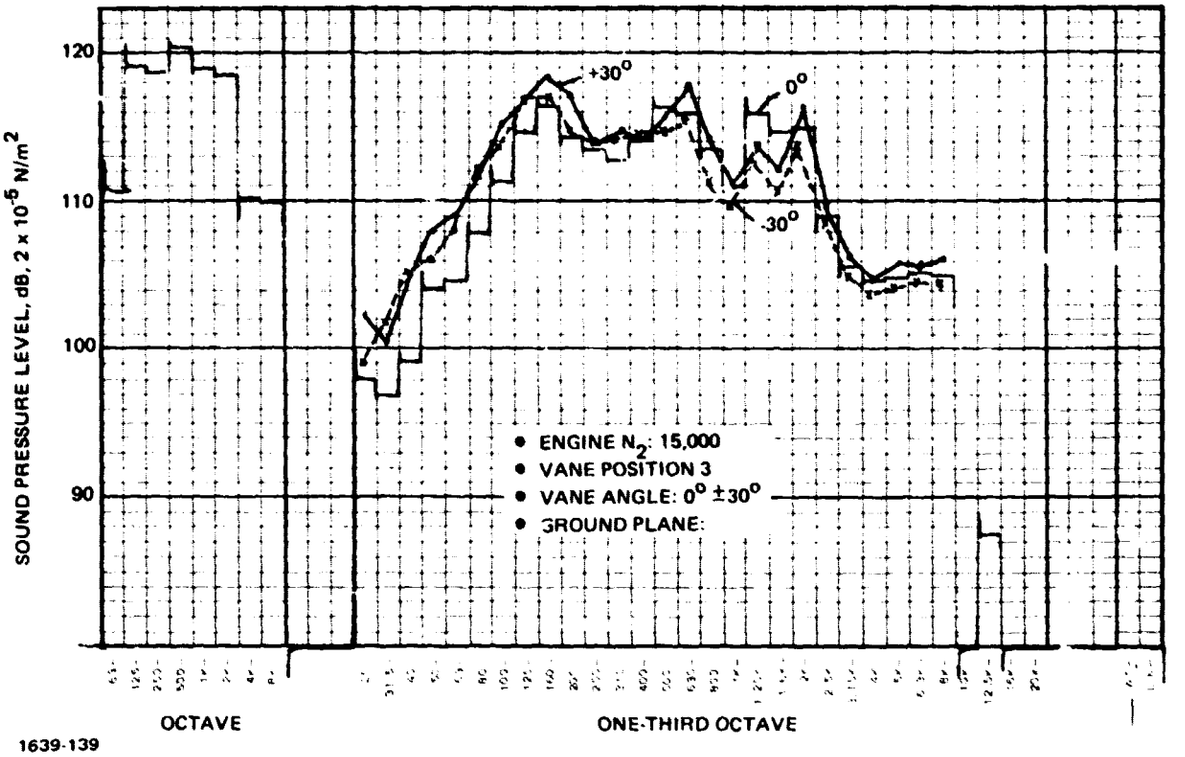


Fig. 4.5-71 External Microphone Measurements, Test 110

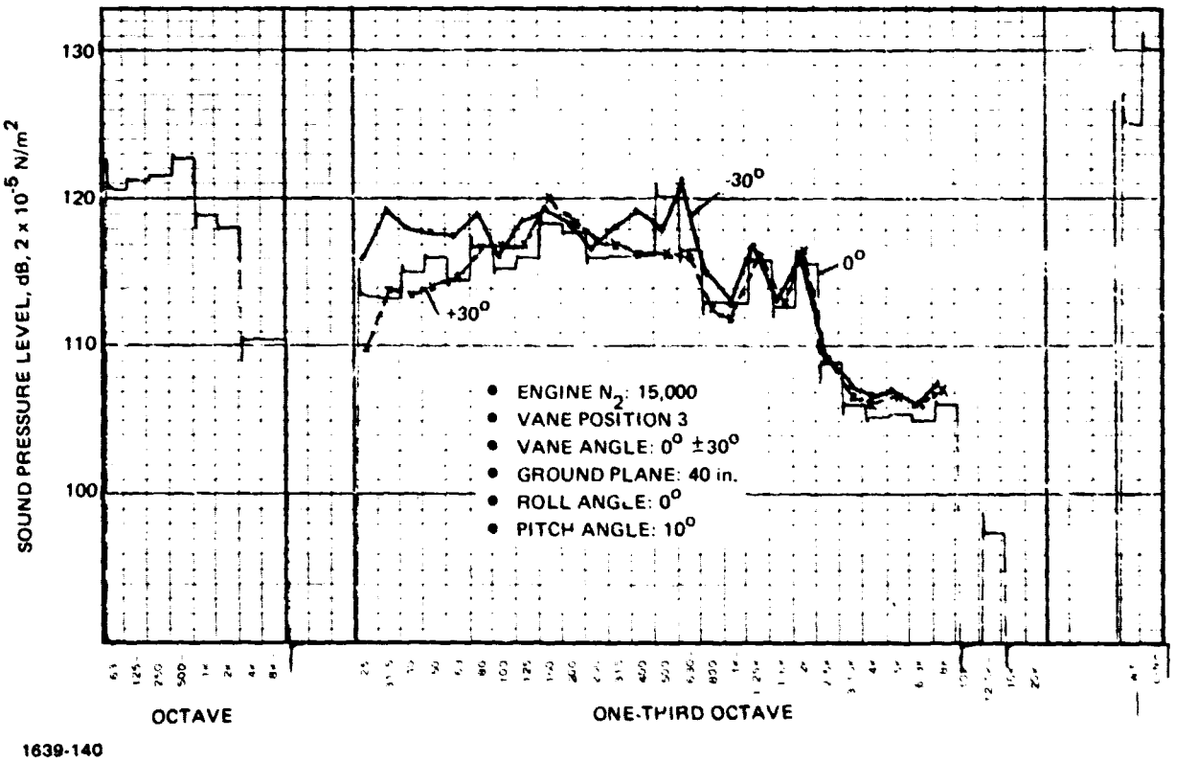


Fig. 4.5-72 External Microphone Measurements, Test 114

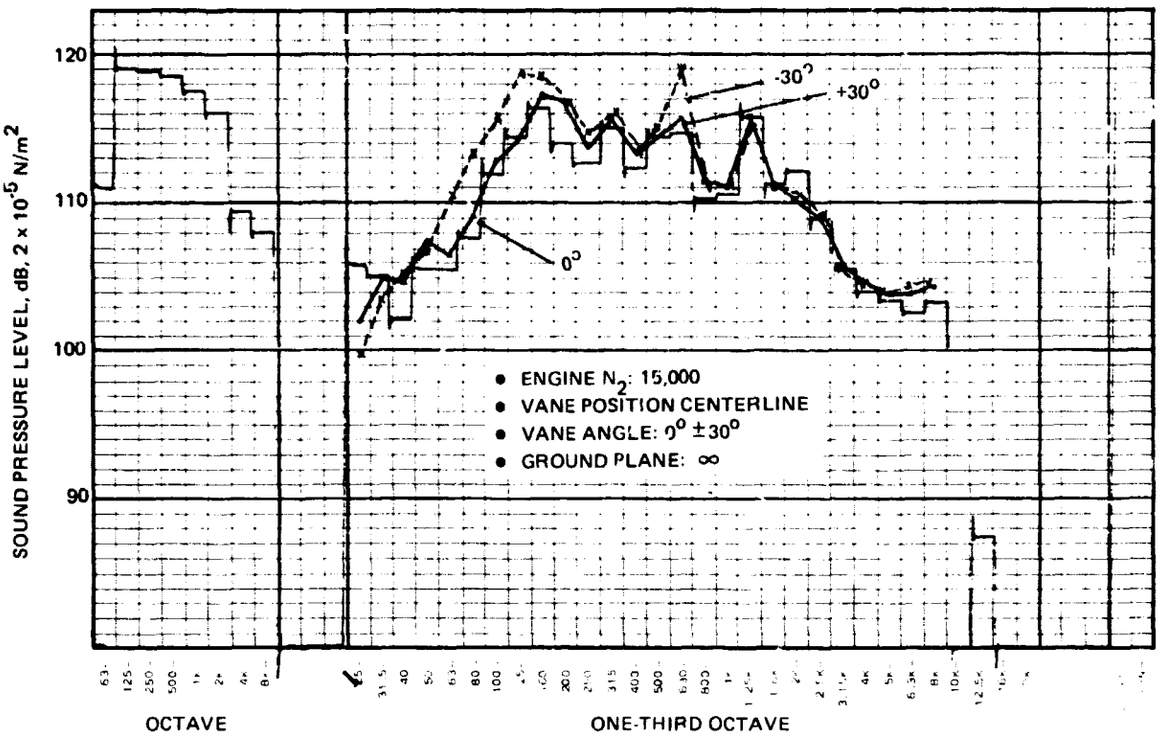


**Fig. 4.5-73 External Microphone Measurements, Test 118**

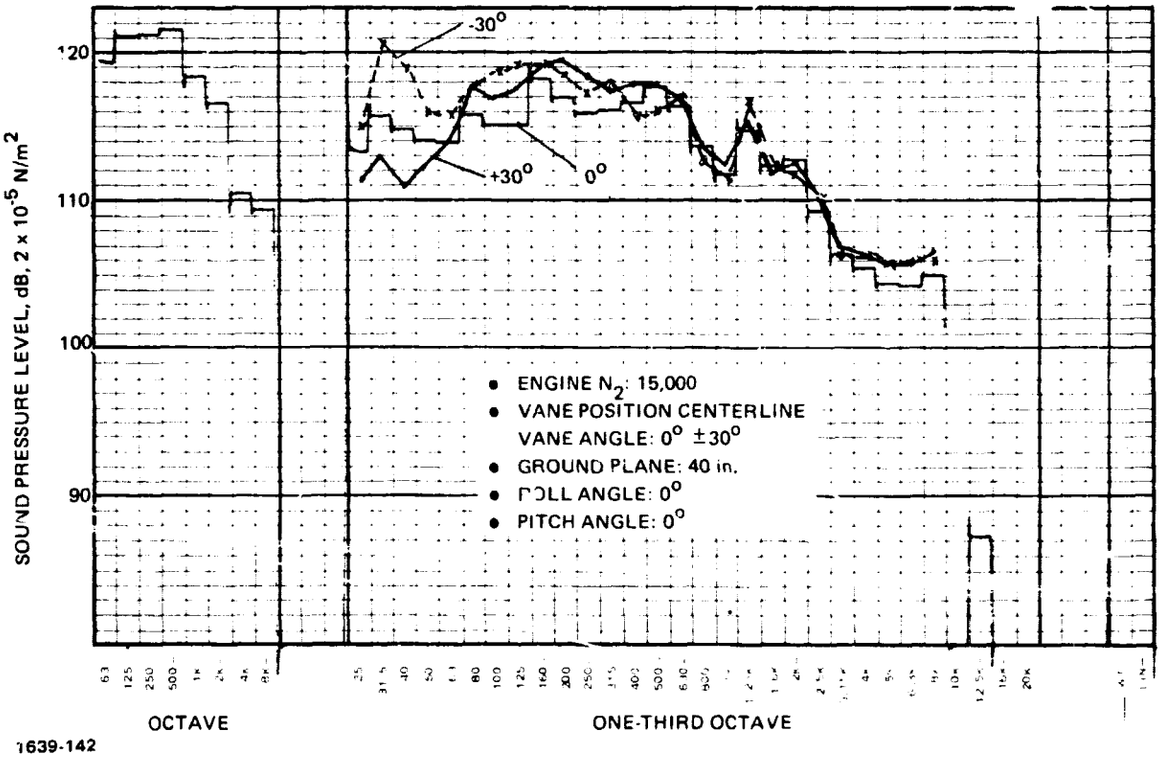


**Fig. 4.5-74 External Microphone Measurements, Test 120**

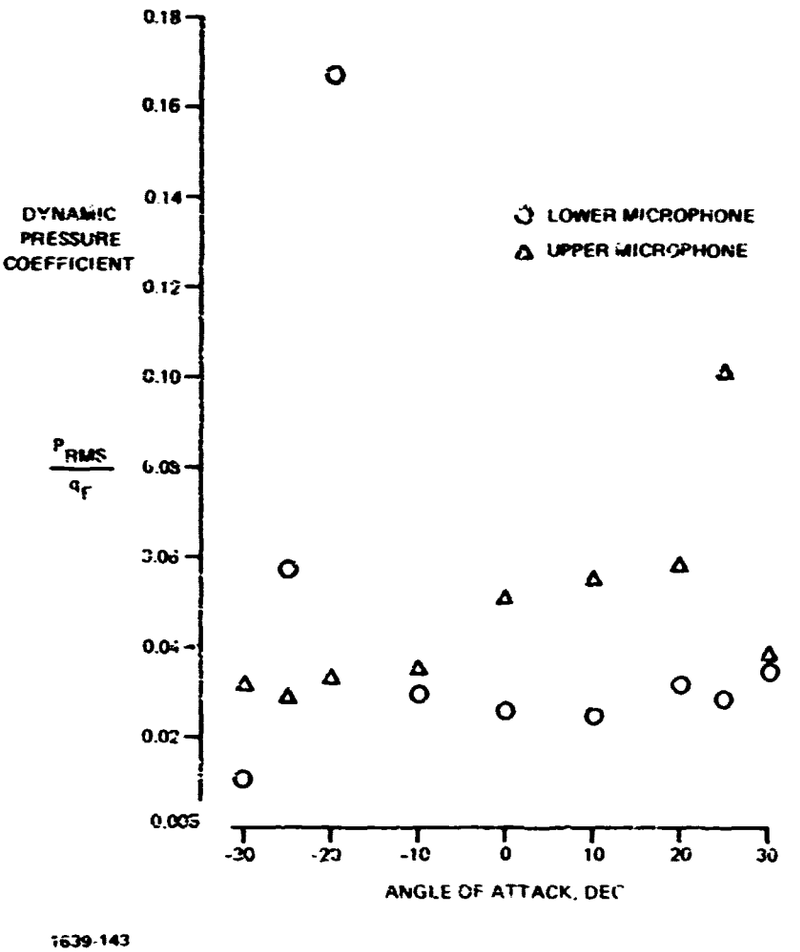


Fig. 4.5-75 Dynamic Pressure Coefficient vs Angle of Attack, Run 116

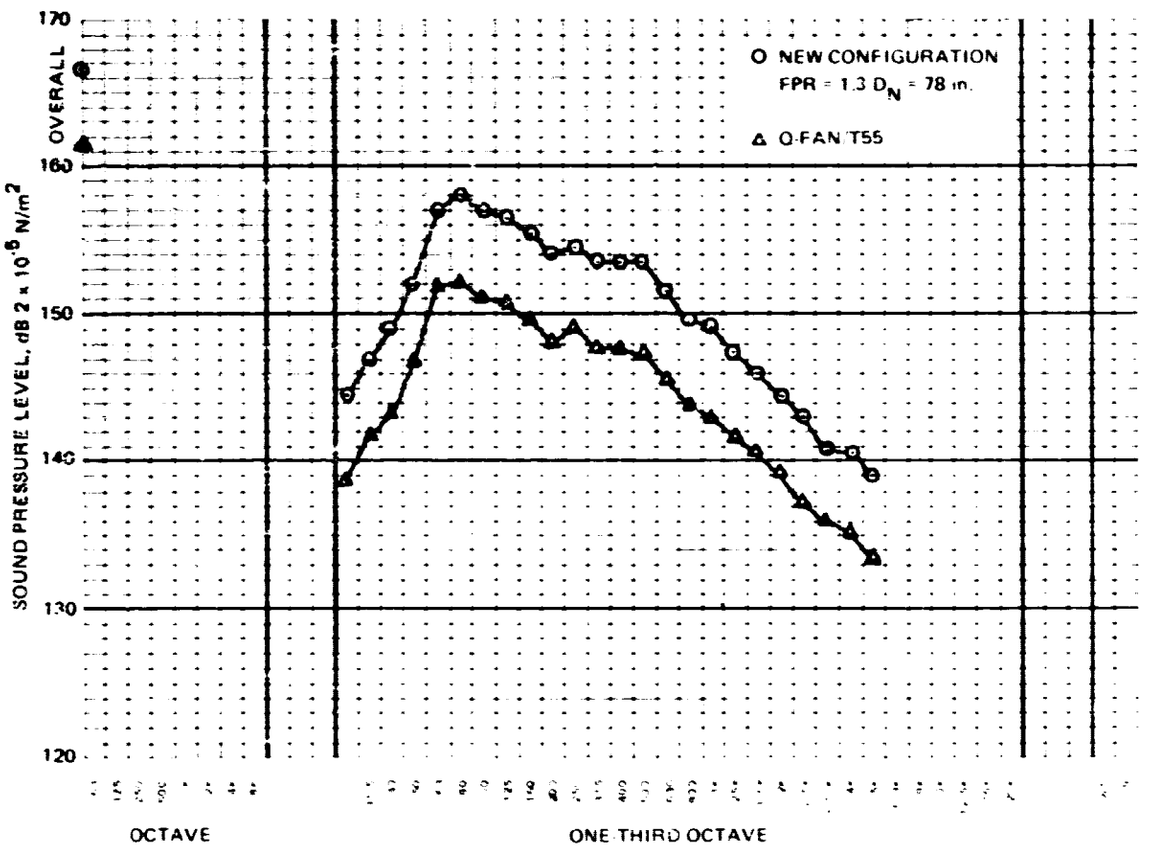


Fig. 4.5-76 Estimated Sound Pressure Level Spectrum for New Configuration Based on Q-Fan/T55 Measurements